On The Application Of Yellowing Inhibitors To Paper Coating: Rheology, Structure, And Numerical Simulation

Haifa El-Sadi

A Thesis

in

The Department

of

Mechanical and Industrial Engineering

Presented in Partial Fulfillment of the Requirements
for the Degree of Doctor of Philosophy at
Concordia University
Montreal, Quebec, Canada

December 2002

ABSTRACT

Haifa El-Sadi, Ph.D.

Concordia University, 2002

The long-term preservation of paper with the same qualities of brightness and color is one of the important requirements for certain paper products. A major problem limiting the wider use of mechanical pulp is the sensitivity of lignin-containing pulps to yellowing induced by ultraviolet (UV) light.

One of the yellowing inhibitor systems contains an Ultra Violet Absorber (UVA) and a Radical Scavenger (RS). The application of this inhibitor system to paper made of mechanical pulps requires the addition of two components, UVA and RS. To Properly understand the use of a paper yellowing inhibition system; it is important to reveal the effect of adding the inhibitors on the global properties of the resulting coating mixture.

We need to optimize the input factors to achieve the longest in time inhibition effect. It is essential to study the rheological properties of the resulting system and the effects provoked by each of the ingredients. Studying the microstructure of the materials sheds more light on the interaction of the additional components with the original formulation. The coating formulation and the inhibition ingredients undergo mixing and transport processes. A study of the effect of

pre-shear adds to the understanding of the system. Numerical simulation of 3D hydrodynamics with non-Newtonian rheology in the vicinity of the coating head creates a powerful tool for investigation of the coating system under these conditions.

Among the operating parameters, the total concentration of inhibitors or total charge proved to have the largest effect of brightness stability or longer in time yellowing inhibition. The rheology of RS is Newtonian. The Ulrta-violet absorber (tin 1130) is an extremely viscous shear-thinning thixotropic material. Water-retention studies show that inhibitors increase water loss, with more water penetrating the paper web. Zeta potential measurements revealed the repulsive forces between pigment and inhibitor particles. RS adsorbs on ground calcium carbonate GCC and disrupts interactions between kaolinite particles. UVA adsorbs on particles of kaolinite and GCC. The inhibitors increase the viscosity, thixotropy, and elasticity of the original coating formulation. A study of pre-shear reveals decrease in viscosity, while inhibitors concentration under pre-shear increases viscosity and elasticity. Transmission Electron Microscopy shows the microstructure of increasing agglomerations with added inhibitors. Numerical 3D simulation of the flow in the coating nip taking inertia forces into consideration depicts vortex formations on the surface of the coater's rolls.

Acknowledgements

I wish to express my gratitude and deep appreciation to my supervisor Dr. Nabil Esmail for his encouragement. Also, I am grateful to him for his support and advice to achieve this work.

I would like to express my special thanks to Dr. Zhiron Yaun, Dr. John Schmidt and Dr. Cyril Heitner from paprican for their assistance and the enjoyment I derived from working with them to do part of my experiments. I would like to thank Dr. Tamal Ghosh from Ciba for his useful discussion.

Special thanks and acknowledgments to Dr. Pierre Carreau from Ecole Polytechnique for his fruitful discussion and his constructive comments and suggestions.

I would like to thank Dr. Van de Van from McGill University, Pulp and Paper center, for experimental assistance and valuable discussion. I wish to acknowledge Dr. Vali Hojatallah and Kelly from Microscopic Center in McGill University for their support using their center facilities. I wish to thank Mr. John Eliot from Concordia University for his assistance. I can't ignore my family support and encouragements. Also, especial thanks to my husband and lovely kittens Omar, Ahmed and Sara.

The financial support of Net Work Center of Excellence (NCE)-Mechanical Wood Pulping, which was provided, is greatly appreciated.

TABLE OF CONTENTS

CHAPTER THREE

METHODOLOGY, INSTRUMENTATION AND EXPERIMENTAL DESIGN

CHAPTER FOUR

OPTIMIZATION OF THE FACTORS AFFECTING THE YELLOWING INHIBITION OF A COATED BTMP PAPER

CHAPTER FIVE

RHEOLOGICAL PROPERTIES OF YELLOWING INHIBITOR

CHAPTER SIX

ON THE CHARACTERIZATION OF THE INTERACTIONS BETWEEN PAPER COATING COLORS AND YELLOWING-INHIBITORS

CHAPTER SEVEN

THE EFFECT OF YELLOWING INHIBITOR SYSTEM ON THE RHEOLOGICAL BEHAVIOR OF PAPER-COATING FORMULATION

CHAPTER EIGHT

THE IMPACT OF PRESHEAR AND TOTAL CHARGE ON THE VISCOELASTICITY OF COATING COLORS

CHAPTER NINE

INFLUENCE OF INHIBITORS ON THE STRUCTURE AND SURFACE MORPHOLOGY OF PAPER COATING COLOR

CHAPTER TEN

SIMULATION OF PAPER COATING COLOR IN THE NIP OF METERING SIZE PRESS

CHAPTER ELEVEN

LIST OF FIGURES

LIST OF TABLES

NOMENCLATURE

G'	Elastic Modulus
G''	Viscous Modulus
G^*	Complex Modulus
δ	Phase Angle
$\dot{\gamma}$	Shear Rate
τ	Stress
L^*	Apercentag e which measures luminance on a scale
a^*	Coordinate s to measure color
b^*	Coordinate s to measure color
k	Absorption Coefficien t
s	Scattering Coefficien t
R_∞	ISO Brightness
RS	Radical Scavengere
UVA	Ultra Violet Absorber
μ	Viscosity
n	Power - Law Index
γ	Strain
w	Frequency
ρ	Density
ω	Rotational vector
v	Velocity
t	Time
ψ	Stream Function
ζ	Vorticity
η_o	Zero - Shear Rate Viscosity
η_∞	Infinite - Shear Rate Viscosity
λ	Natural Time (inverse of shear rate)
a	Index that controls the transitio n from Newtonian to Non - Newtonian
M	Mass Matrices
K	Stiffness Matrices
X	Unkn own Vector
F	Volumetric Forcing Function
X^p_{n+1}	Predicted Value
X_{n+1}	Correct Value
ε	Relative Tolerance

d_{n+1}	Maximum Relative difference Between the Predicted and corrected value
f(s)	Evolution Function
t_i	Initial Time
t_n	Discrete set of times
u	Velocity Component in x-direction
w	Velocity Component in z-direction
x,y,z	Cartesian Coordinates
P	Pressure
SC	Solid Content
T	Extra Stress Tensor
D	Rate of Deformation
θ	Scalar Parameter
N	Normal-Stress
H	Damping Function

Chapter One

INTRODUCTION

In the design of new materials for specific purposes, many of the physical or chemical characteristics can be determined by suitable deformation prototype. Once a process has been determined, there is quite often a need to optimize performance and solve a problem in the line by a rheological audit of the process.

Coating is a process, which is a treatment or application of pigment, polymers, or other materials to the surface. Products of surface-coating industries are essential for the preservation of all types of architectural structures, including factories, from ordinary attacks of weather. Industrial finishes are applied to a wide variety of materials, such as metal, textiles, rubber, plastics and paper as well as wood. Our interests in this work will concentrate on paper coating.

1.1 Paper Coating Process

Coating improves the printing properties of paper. In paper coating industry, an aqueous suspension called coating color is applied to one or both sides of paper. After application of the required amount, the coating is dried and finished. In finishing, the coated paper achieves its smoothness and gloss potential.

1. 1.1- Coating Formulation

The coating components usually consist of three categories of compounds, the pigment, the binder, and additives or rheology modifier besides water. Pigments form the major fraction of the coating color. They are materials such as kaolin clay, delaminated clays, which produce low sheet gloss but high ink gloss [1], ground calcium carbonate, titanium dioxide, and silica.

Another important component of the coating colors is the binder. The main purpose of binder is to bind pigment particles to base paper and to cement the pigment particles firmly to the surface and to each other. This creates a porous structure of pigment particles cemented together at their points of contact. If too much binder is used, the voids begin to fill in and some light scattering capability is lost [2].

The binders are classified as natural binders or synthetic binders. The natural binders include starch, carboxylated and soy protein. Synthetic binders include styrene-butadiene rubber latex, polyvinylacetate latex. Latexes are used in paints, and many coatings are really much like paints. The binder affects the rheological properties of coating and water retention of the coating color. A thickener can also have good binding properties, and then it is called co-binder such as long chain polymers including carboxymethyl cellulose (CMC) and polyacrylates [3].

Beside pigments and binders, a coating color usually contains various additives, which have different functional roles. These are, e.g. additives, which aid in dispersing of pigment, adjust pH, act as lubricant or cause optical brightening.

Water is an essential component of a coating color. Water makes it possible to mix the components of coating color. For example it achieves separation of pigment particles, which is impossible in dry state. Water also makes it possible to transport the color elsewhere and apply it on the base paper so that the coating color remains uniformly dispersed. Eventually, as water evaporates from the coating layer, the coating layer consolidates while the binder forms bridges between pigment particles and base paper.

1. 1.2 Mixing and Dispersion in Coating

Coating is a unit operation common to the coating industry, and it is one of the primary operations carried out during the preparation, blending, and storage of coating materials and coating color. Mixing operations may be classified as agitation, mixing, or dispersion. Agitation is the process of setting up flow patterns and turbulence in a tank so as to prevent the settling, sedimentation, or stratification of the material in the vessel.

Mixing is the blending of multiple materials, which may be miscible or immiscible with each other, to the point where the concentration of each ingredient is constant throughout the tank.

Looking at mixing operation, velocity gradients within the fluid are higher than those developed for pure agitation, and the impellers are usually designed for shear as well as nominal agitation. However, the material in the vessel or tank is homogeneous, the mixing equipment might be used as an agitator to maintain the uniformity of the material until the mixture is released from the vessel.

Dispersion is used to describe the process of incorporating very finely divided particles of a solid into a fluid at high concentration such that the final product is stable to sedimentation and viscosity variation.

There are three stages in the dispersion process: a) wetting of pigment powder, which involves the displacement of the air from the internal surfaces between particles in the pigment, b) disruption of the pigment (agglomerates), c) stabilization. The mechanically dispersed particles at high solids content have a natural tendency to re-agglomerate owing to irreversible collision and electrostatic attractive forces, unless a chemical additive, a dispersant, is present [1].

In coating systems, the shaft-mounted impeller system is the most widespread. The purpose of the impeller is to generate motion in the surrounding fluid through the transfer of momentum [1]. Proper equipment, adequate power, and the use of chemical dispersants are all needed to accomplish satisfactory dispersion.

1. 2- Coating Methods

Most coater designs incorporate the following features: uniform application of color to the surface, metering the coating layer to control its weight or thickness, and smoothing and evening the surface [2]. Coatings are applied at the size press or with air knife. The basic principle of air knife coater is applying an excess of coating mix to the base and then meter off the portion that remains mobile by means of air. The most common method is blade coaters, which come in a number of types; usually described by the form of the blade [4].

Another method for applying the coating is the size press, which is the most common on machine coater. Its main function is to apply non-pigmented, film forming materials such as modified starches, SCMC, etc.

The rod or bar coater is referred to as a metering bar coater. The metering bar can either is stationary or slowly rotating and there are a number of bar designs all developed to apply a more even coating layer [5].

Roll coating is a process whereby liquid flows into a narrow gap between two rotating cylinders, the surfaces of which move either in the same direction (forward) or opposite directions (reverse). Some of the liquid passes through the gap and splits downstream into two thin films, each coating one of the rolls.

1. 3- Surface Application of Yellowing Inhibitor

The traditional market of high-yield pulps is newsprint and short life advertising papers. Paper made from mechanical pulp has attractive optical and printing properties. Advances in pulping and bleaching technology have made it possible to produce high yield pulps with suitable strength and brightness. However, rapid light-induced yellowing of mechanical and high-yield pulps remains a significant problem in their use.

Much of the discoloration is due to photochemical reactions of lignin [6-10]. Many methods of inhibiting the yellowing of mechanical pulp have been attempted, and can be generally classified into two main groups: 1) lignin modification [11-18]; 2) addition of chemicals that either stop the photochemistry or redirect the subsequent reactions to avoid colored products [14-24].

Paprican and Ciba Specialty Chemicals have developed a novel yellowing inhibition system that gives unprecedented light stability to lignin-containing papers [25]. Yellowing inhibitors are compounds used to inhibit light-induced yellowing of lignin-containing papers.

1. 4- Rheological Properties

The rheology is the science of the deformation and flow properties of matter. The overall aim of rheology in processing and development is to understand the relationship between microstructure of dispersion and its rheology throughout its history. This knowledge can then be used to manipulate the rheological properties as desired via calculated structural changes. The rheology of coating suspensions must be controlled so that the coating can be easily pumped and also must perform adequately under the high shear conditions of the coating application system. Because of their potential impact on coating system design and development, it has been necessary to quantify the flow behavior and properties of a wide class of dispersions.

1. 5- Statement of the Problem

A yellowing inhibition system consists of two ingredients, radical scavengers (RS) and ultra-violet absorber (UVA). To improve the quality of the paper product, the raw paper must be treated by this system. The most optimal way for this treatment is the addition of these ingredients to the usual coating treatment, which is applied to the raw paper. This addition will entail many changes in the structure and mechanical properties of the resulting mixture. These changes will affect many aspects of the coating operation.

The objective of the research is to study the global properties of the inhibitor ingredients, their combined properties, and the properties of the mixture of inhibitors and coating formulation, to help understand the effect of the added ingredients on the coating operation.

A novel yellowing inhibition system, which gives unprecedented light stability to lignin-containing papers, is the subject of the research. This inhibitor system contains an Ultra Violet Absorber (UVA) and a Radical Scavenger (RS). The UV absorber absorbs most of the UV light. The radical scavengers eliminate the production of most of the remaining free radicals.

We need to optimize the input factors to achieve the longest in time inhibition effect. It is essential to study the rheological properties of the resulting system and the effects provoked by each of the ingredients. Studying the microstructure of the materials sheds more light on the interaction of the additional components with the original formulation. The coating formulation and the inhibition ingredients undergo mixing and transport processes. A study of the effect of pre-shear adds to the understanding of the system. Numerical simulation of 3D hydrodynamics with non-Newtonian rheology in the vicinity of the coating head creates a powerful tool for investigation of the coating system under these conditions.

The objective of the research is to study:

- The factors: total charge, coat weight and the Ratio of Radical Scavenger and UV absorber affecting the yellowing inhibition and paper initial brightness through a statistical approach.
- The changes in the rheological properties of the coating mixture as a result of adding the yellowing inhibition system using rheological measurements of mixture components and the inhibitors.
- The consolidation of coating color after the addition of inhibitors to the suspension using water retention measurements.
- The interaction between coating color and the inhibitors using zeta potential measurements for ground calcium carbonate and kaolinite particles with inhibitors.
- The microstructure of coating suspension including inhibitors using freeze etching technique and Transmission Electron Microscopy.
- The numerical 3D simulation of the flow in the application nip. Considering inertia and non-Newtonian effects at high speeds of operation ~ 20 m/s.

Chapter Two

LITERATURE SURVEY

Paper coating is a process to treat the surface of paper and paperboard to improve their optical and printing characteristic. Coating is a complex multi-disciplinary matter, comprising aspects of wetting, fluid mechanics, rheology, and mathematics.

2.1 Pulp and Papermaking

There are two main types of pulping- chemical and mechanical and they produce different fiber characteristics. The choice of a pulping process depends upon the wood species available and the end application for the pulp produced. In many papermaking operations, a combination of different chemical and mechanical pulping processes is used in order to obtain the desired paper characteristics for a reasonable cost.

A chemical pulping process dissolves out the lignin, which binds the cellulose fibers together. The resultant fibers are longer, more flexible and considerably stronger than the mechanical pulp fibers. The chemical pulps can be used in the unbleached state for such items as linerboard, wrapper or bag paper and they can be bleached to a substantially higher brightness for use in a wide variety of products. The bleached brightness is considerably more stable than what can be obtained from the mechanical pulps.

Mechanical pulp has certain desirable properties that make it useful in many grades of paper. Because of the mixed nature of the particles in the pulp, and because the lignin has not been removed, the pulp has properties which render it desirable for use in certain papers.

These properties are a small average particle length, a relatively stiff fiber that prevents packing, and therefore tends to give a sheet of paper with high bulk and good opacity. The final accepted pulp might have to be bleached, depending upon the brightness of the pulp and the desired brightness of the paper in which the pulp will be used. Because mechanical pulp retains wood's original lignin, papers containing the pulps tend to turn yellow when it exposed to light [26].

2.2 Yellowing Inhibitor Application and Mechanism

A major problem limiting the wider use of mechanical fiber in high-value furnishes is the sensitivity of lignin-containing pulp to yellowing induced by ultraviolet (UV) light. Cockram [27] has suggested that, if the mechanical pulp could be made color stable for six months under ambient light exposure, its use in value-added applications could expand significantly.

Many methods of inhibiting the yellowing of pulp can be classified into two main groups: 1- modification of the reactive functional groups of lignin, 2- addition of chemicals that either stop the photochemistry or redirect it to colorless products [28]. Proposals for the modification of lignin include borohydride reduction of aromatic carbonyl groups [29,30] to remove the possibility of absorbing UV light.

Many chemical additives have been added to paper in order to stem the photo yellowing of lignin [31-32]. The most successful compound classes are ultraviolet light absorber (UVAs) and radical scavengers. UVAs are widely used to stabilize paints, varnishes, automotive coatings and plastics. These additives preferentially

absorb the damaging UV light, and dissipate the energy harmlessly as heat. While UVAs will inhibit yellowing of mechanical pulps [33, 34], they are much less efficient than when used in synthetic polymers.

Radical Scavengers can trap the radicals formed during irradiation. This is essentially the function of an antioxidant. Lignin is in fact in efficient antioxidant [35-38], so any effective radical scavengers must be better antioxidants than lignin. Thiols [39,40] and ascorbic acid [41] have both been shown to inhibit light induced yellowing but, as with UVAs, the amounts required are too high. Also, when stored in the dark for several months, thiols lose some of their efficacy due to slow air oxidation [42].

In polymer stabilization, combinations of two or more inhibitors that act synergistically are the norm. Several authors have attempted to apply this principle to mechanical pulps by combining an UVA with a thiol radical scavenger [43-45]. While improvement over the use of a single inhibitor was apparent, claims that the performance improvement was greater than the sum of the effects of the individual inhibitors are barely supported by the evidence provided [44].

The mechanism of light-induced yellowing and its inhibition shown in Figure 2.1 is useful in summarizing the process of light-induced yellowing and inhibition [46].

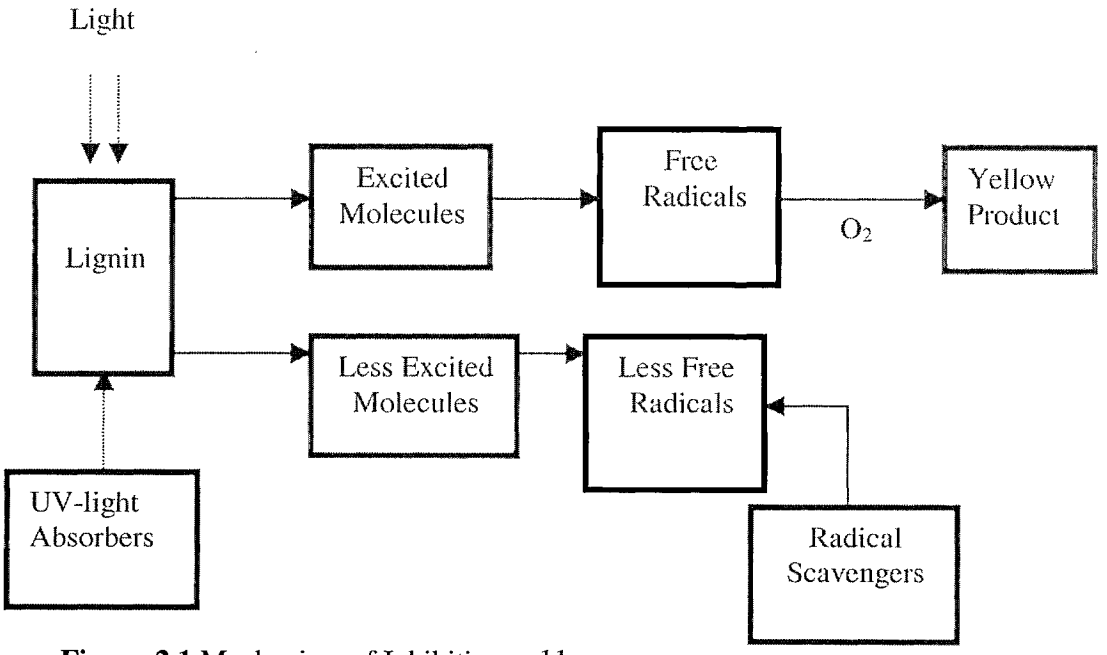

Figure 2.1 Mechanism of Inhibition 11

UV light is absorbed by lignin, creating high-energy excited states. The absorbed energy is sufficient to break chemical bonds, generating free radicals (species having unpaired electron).

The radicals critical to yellowing of mechanical pulps are shown in Figure 2.2.

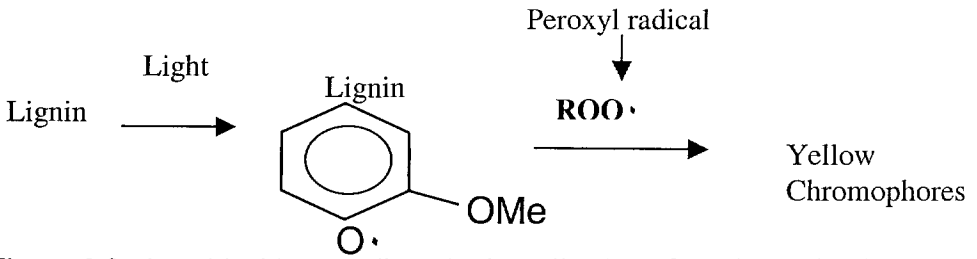

Figure 2.2 The critical intermediates in the yellowing of mechanical pulps.

The addition of ultraviolet absorber (UVA) will absorb the light; therefore will create less excited molecules and then fewer radicals. Radical scavenger will be added to trap the radicals; therefore we will reduce the yellowing and increase the brightness. The brightness, color and opacity of papers are all affected by coating structure. Addition of structuring pigments or chemicals can enhance coating optical scatter, providing higher brightness.

2.3- Materials and Operations

The development in the paper industry has during the past 10-20 years been towards ever-higher quality: higher brightness, better opacity, better smoothness and

printability. The traditional way of achieving this has been to coat the paper. Coating is a powerful tool in paper improvement, but it has some drawbacks too. One of the major disadvantages is the relatively high cost.

Coating colors have had to be modified to improve their runnability in order to keep pace with these new technological developments. The runnability of coating colors is affected by a variety of factors as show in Figure 2.3 [80].

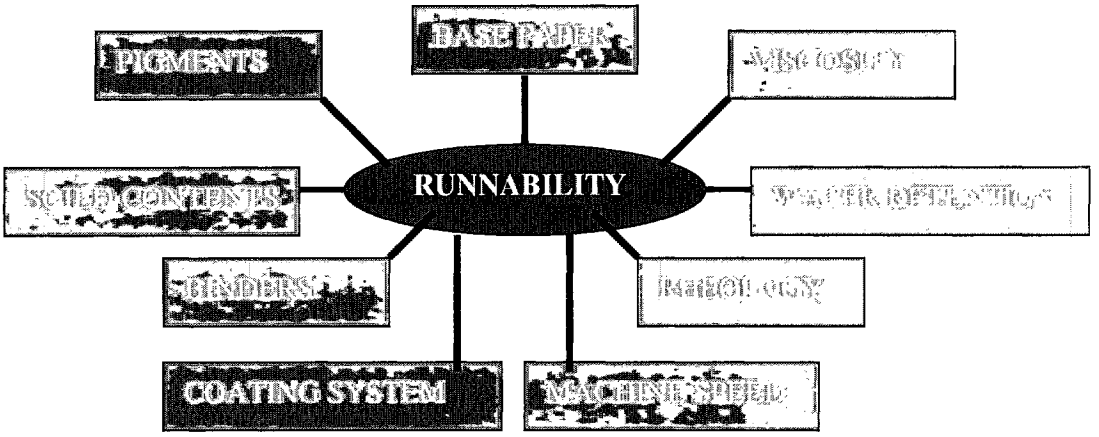

Figure 2.3. Factors influencing runnability

2.3.1 Wet Coating Structure

Paper coating colors are mixtures of dispersed colloidal pigment and latex binder particles along with soluble co-binder species. These different components can associate with each other to generate different types of "wet coating structures."

Typical wet coating formulations consist of pigment particles (clay, CaCO3, TiO2, etc), latex particles (styrene/butadiene, vinyle acetate, styrene/acrylate, etc.) and a

water-soluble co-binder polymer (starch, carboxy-methylcellulose (CMC), protein, polyvinylalcohol (PVA), etc.).

The final structure of the coating can be described as a network of pores with a distribution of sizes. The shape of the pores reflects the shape of the pigment at low binder level. The pores in plate-like clay coatings are elongated while those in a carbonate coating are more isomeric. A basic requirement is the formation of an interface between binder and pigment. With soluble binders, the process starts with adsorption of the polymer molecules onto pigment and fiber surfaces, while the remaining unadsorbed binder accumulates at the cross- over points when water finally leaves [3].

Malik and Kline [47] reported that the use of polymer co-binders influenced water loss rate, viscosity and immobilization. Carboxymethylcellulose (CMC) is derived from cellulose, a natural polysaccharide which is a chain-like molecule consisting of several hundred anhydroglucose units. Each of these units has three reactive hydroxyl groups. When high molecular weight ionic polymers are added to aqueous dispersions containing mineral particles, viscosification is produced by the combination of aqueous phase thickening and particle-particle bridging. This is brought about by the capacity of the polymer chains to adsorb onto the pigment particles by various mechanisms, such as electrostatic-mechanism owing to charge differences; physical-hydrogen bonding or van der Waals forces. CMC is reported to be best for the control of binder migration, while Polyacrylate gave coatings with the lowest water loss rate [47].

Synthetic polymers are derived from petrochemical sources and most of the available commercial products are manufactured by using the additional polymerization technology of acrylic monomers.

The pigment / latex interparticle interaction was reported to depend on pH, latex type and level, and the acid-base characteristics of the latex and pigment particle surfaces. Various researchers have shown that there is adsorption of co-binder polymer on clay and /or latex and formation of network structure in suspension [4]. The adsorption of co-binder to latex surface varied with molecular weight of co-binder and surface functionality of the latex [5].

Thickeners play the most important role in controlling both the flow properties and the dewatering rate of coating colors during the application process and the subsequent film immobilization [48].

A thickener may be added to the coating color to modify its rheology and water retention. The thickener can also have good binding properties, and then it may be called co-binder. Carboxymethyl cellulose (CMC), Starch and Hydrophobically modified ethoxylated urethane can be used as thickeners in the paper coating industry [49].

Many researchers reported on the interaction between latex binders and co-binders such as CMC, PVA, etc.[5, 50-52]. Depending on the type and level of co-binder used, the level of latex destabilization can vary. The destabilization of latex is often

confirmed by particle size analyses, cryo-scanning electron microscopy, and shear thinning characteristics.

The destabilization of latex was argued to occur as a result of electrostatic interaction or depletion flocculation, due to high molecular weight nonadsorbing co-binder polymers. The adsorption of co-binder to latex surface varied with molecular weight of co-binder and surface functionality of the latex [53].

Interaction of pigment particle and water-soluble co-binder depends on (a) co-binder chemistry, (b) co-binder polymer configuration at the aqueous particle interface, (c) co-binder specific adsorption to and interaction with the pigment surface. The impact of co-binder on the stability of pigment particles depends on the co-binder/pigment ratio. The amount of co-binder polymer initially adsorbed per unit area of pigment particles rises rapidly and reaches a plateau with increasing concentration of the polymer.

Wet coating structure is characterized by determining the steady shear and dynamic rheological flow [54,55]. The magnitude of yield point, plastic viscosity, and stress relaxation time obtained from steady shear and visco-elastic measurements are used to estimate the strength of interparticle attraction at rest, floc size etc.

2.3.2 Rheological behavior of paper coating formulation

Rheology is a powerful tool for characterizing the interactions between the different components of a paper coating formulation and speeding up the design of new coating formulations. Paper coating formulations have complex time dependent rheological behavior, which is a key factor influencing runnability and water retention.

Viscosity is one of the most important determinants choices in the selection of liquid products. The simplest way of measuring viscosity is by obtaining the shear stress and shear rate in liquid flow. For all practical purposes this comes down to two simple geometries: a concentric-cylinder apparatus, the second possible geometry is the cone-and plate set-up where a cone is brought into contact with a plate onto which the liquid to be measured is poured [56].

A high viscosity implies high concentration, while too high viscosity will give anticipated problems in mixing and in determining stability for some products. The viscosity of a suspension varies with particle concentration and shear rate. At low shear rates, the viscosity remains close to constant or Newtonian.

The viscosity then begins to drop off at higher shear rates in a shear-thinning region. Then, at high shear rates, the viscosity begins to rise again in a shear-thickening region [57]. It is known that colloidal interactions between the components of the color have a profound effect on the viscosity of the color in the low shear-rate region. Adsorption of water-soluble components on the pigments surfaces and aggregation of the pigment particles are examples of factors, which have been reported to affect the rheological properties in the low shear rate regime. As the shear rate increases, hydrodynamic effects become more important for the rheology [58].

The solids content is one of the most important factors determining the magnitude of the viscosity. With increasing solids content the viscosity increases [59]. The particle size and the particle-size distribution of the pigment have a substantial effect on the shear rate dependence of the viscosity [60]. On the other hand, the viscosity that

starch gives the coating color is of great importance for its behavior before and during the coating process.

The yield stress or yield point is the minimum stress necessary to cause a fluid to flow. The yield stress is a useful rheological parameter to characterize particle-particle interactions in suspensions [61]. Above this yield stress the material flows readily. Concentrated suspensions of solid particles in Newtonian liquids often show a yield stress followed by nearly Newtonian flow. These materials are called visco-plastic or Bingham plastics. An important feature of plastic behavior is that if the stress is not constant over a body. Parts of it may flow while the rest acts like a solid [62].
Thixotropy is the change of viscosity with time of shearing rather than rate of shearing [63]. If a thixotropic material is sheared at a constant rate after a period of rest, the structure will be progressively broken down and the viscosity will decrease with time. The rate of breakdown of structure during shearing at a given rate will depend on the number of structural linkages available for breaking and must therefore decrease with time. A state of dynamic equilibrium may be reached when the rate of build up of structure equals the rate of breakdown [64].

Characteristically, a high level of thixotropy and shear thinning are desirable to avoid occurrence of the turbulent pattern at low speeds. Coatings with a poor performance are characterized by small amounts of thixotropy, high high-shear viscosity and a tendency toward dilatancy [96]. The area enclosed between the up and down curves quantifies thixotropy. In the flow curve the "up curve" is no longer directly underneath the "down curve". The hysteresis now encountered between these two curves surrounds an area "A" that defines the magnitude of the thixotropy. This area

has the dimension of energy related to the volume of the sample sheared which indicates that energy is required to break down the thixotropic structure.

2.3.2.1 Paper Coating Visco-elasticity

In a Newtonian fluid the shearing stress is proportional to the rate of shear. In most materials, under appropriate circumstances, effects of both elasticity and viscosity are noticeable. If these effects are not further complicated by the time-dependent behavior, we call the material visco-elastic. When describing visco-elastic behavior, of concern are the relationships between stress, strain, and time.

Visco-elastic materials have distinctive rheological properties that define their fluid like (viscous) and solid like (elastic) behavior upon deformation. Like viscosity, which is defined as the resistance of a material to flow, visco-elastic material constants describe the ability of the material to recover from deformation. In purely viscous flows, the material deforms as long as there is stress applied. When the stress is being removed, flow ceases. For a purely elastic behavior, the material deforms instantly upon the action of stress, the deformation spontaneously reverses when the stress is removed.

For the case of visco-elastic materials, the response to deformation is complex. While the stress transmitted by a purely viscous fluid is related to the rate of deformation (shear rate), the stress transmitted by visco-elastic fluids is a function of the amount of deformation (strain).

The problems associated with instabilities in the process can be overcome by performing oscillatory measurements. In a dynamic test oscillating stresses are applied to the test sample to measure the storage modulus G' and the loss modulus G". The storage modulus represents the elastic response of the sample, which indicates that the stress energy is temporarily stored during the test but it can be recovered afterwards. The loss modulus represents the level of viscous response, which indicates the energy, which has been used to initiate flow. This energy is irreversibly lost having been transformed into shear heat. The complex modulus G* represents the total resistance of a substance against the applied strain, it can be calculated from:

$$G^* = G' + iG''$$

For visco-elastic materials both the complex modulus and the phase angle δ are frequency dependent. Their phase angle is positioned between $0 < \delta < 90^{o}$. When the phase angle is less than 45°, it is an indication that the elastic character of the material is more pronounced than the viscous character. When the phase angle is more than 45° the material is more elastic than viscous. When the phase angle is 45°, we can say that the viscous and elastic characters are equal.

The response of visco-elastic materials depends on the time scale of deformation in relation to the characteristic time it takes for the material to relax after deforming. In addition to the amount of deformation, characteristic visco-elastic parameters depend on the rate at which a material sample is being deformed.

An important feature of visco-elastic fluids, in contrast to Newtonian or purely viscous fluids, is that they exhibit normal stresses even in steady shearing flows. An implication of the existence of these significant normal stresses is that visco-elastic fluids may exhibit elastic or viscous behavior depending on the magnitude of a dimensionless number called the Weissenberg number. Weissenberg number (We) is given by the ratio of the difference between the two normal stresses and the shear stress. When We is large, elastic effects dominate the rheological behavior of the material. Many of the unusual macroscopic flow phenomena observed with visco-elastic fluids, like climbing up a rotating rod and die swell, are attributed to their normal stresses. In addition to deformation rate, these material parameters also depend on the characteristic time of the flow. The characteristic dimensionless number, which describes the significance of the elastic stresses in process flows, is the so-called Deborah number (De). This number is the ratio of a characteristic relaxation time of the fluid to the characteristic residence time in the flow field of a process. When De is greater than 1, the fluid behavior is predominantly elastic, and when De is less than 1, the fluid behavior is predominantly viscous. Therefore, both the normal stress and viscosity describe the rheological behavior of visco-elastic fluids in processing flows [65].

The reaction of visco-elastic fluids to sinusoidally-imposed shear stresses is related to the mobility of molecules and volume elements within such a sample. This mobility, also characterized by the relaxation time, is related to the type of the major fluid component but also to the type and percentage of all other ingredients of a particular material.

The elastic and viscous moduli and their position in the frequency domain vary and differentiate to specific regions. The viscous or terminal region is the region where elastic modulus predominates and viscous behavior prevails. All materials have such a region, even solids. The transition to flow region is so called because, when viewed from higher frequencies, the loss modulus, describing viscous or flow behavior, becomes significant. The rubbery or plateau region is where elastic behavior dominates. A leathery or higher transition crossover region is seen, where, due to high frequency relaxation and dissipation mechanisms, the viscous modulus rises, this time faster than elastic modulus. Glassy region is seen at the highest frequencies, where viscous modulus again predominates and continues to rise faster than elastic modulus.

The particular regions mentioned above depend on the longest relaxation time (τ_{max}) of the material which is given by G'/(G"w). If $w\,\tau_{max} > 1$, then often only the plateau region where elastic behavior dominates is seen. There is always an increase in G' with frequency (w). If $w\,\tau_{max} \sim 1$, then the viscous and transition to flow regions can be seen. On the other hand, for many materials, $w\,\tau_{max} < 1$, and viscous modulus always predominates [66]. The wet coating structure exhibits a visco-elastic behavior at very low shear rate [67], and time dependence and viscous behavior at high shear rate [92].

Previous rheological studies indicate that coatings with clay and/or calcium carbonate pigments, latex, and various types of co-binders are visco-elastic at low shear [69]. Pigmented paper coatings exhibit visco-elastic properties arising from formation of structure in suspension.

2.3.3 Consolidation Behavior of Coating Color

It is well known that the properties of the coating layer and thus also the properties and the quality of the coated product are to a large extent governed by the structure of the coating. The structure of the dry layer is in turn determined by the colloidal interactions between the components of the coating color and the course of the consolidation of the layer. Consolidation is the process by which the liquid phase leaves the coating layer by evaporation and the layer transforms from a fluid to a dry porous, rigid structure.

The consolidation process has a strong influence on the final coating structure in the dry state. The structures, which form in the wet color, may be broken down by the capillary forces exerted on the structure during the consolidation process [70]. The effect of the water-soluble polymer on the consolidation behavior appears not to have been studied in any great detail although it is known that certain polymers can cause an expansion of the pigment network provided that the amount of polymer is not too high [71,72]. The effect of water-soluble polymers on the water retention characteristics, which can have some relation to the consolidation behavior, has been extensively investigated over the years [73,74].

Water retention is a significant property of the coating color that allows it to retain water while the coating color is in touch with the paper surface. There can be runnability problems if the color suffers excessive water loss prior to the film splitting region in metered size press coating. Use of water-soluble thickeners can ensure that dewatering is slowed, but they also lead to reduction in sheet quality. Clearly there is an advantage for pigments, which have a natural water retaining ability. It is generally

known that water retention is worse with GCC than with kaolin. In the case of kaolin, water simply has to go a longer way through the platy packing and the particle size distribution becomes narrower. Various forces acting at the interface between the base paper and the freshly applied coating color influence the rate at which water released from the coating color penetrates into the base paper.

Water is forced into the base paper as the result of the capillary pressure of the base paper and the hydrodynamic pressure in the nip between the roll and the blade. The osmotic pressure within the coating color is the only factor that prevents excessive dewatering. Work by Beazley and Climpson [75] and Windle [76] clearly illustrated the likely migration of the fluid phase from coating colors under applied pressures.

The concentration and the chemical structure of the dissolved thickener and the temperature mainly determine the osmotic properties of the coating color, on which its water retention depends [77-79]. If the water retention is good the solid content of coating formulation is stable [80]. The influence of CMC and starch on the consolidation of the coating layers can be characterized by the gloss technique, the coating layers shrink in the thickness direction and that the final gloss level of the layer is inversely related to the shrinkage during the consolidation [81].

The right solids content of pigments is especially important because pigments alone form the biggest portion in the coating color recipe. If the solids content of the coating color is too high or too low, its effects will be seen immediately with coating amounts and runnability of coating units [80]. Heiser and Cullen [82] and Krishnagopalan and

Simard [83] showed that coatings having high solids content were far less prone to binder migration than coatings having low solids content.

The coating solids content is the most important factor affecting the binder migration in paper coating processes. Because coating colors of high solids content contain less liquid, less total dewatering will result in less binder migration into the base paper [84].

Nissan [85] suggested four mechanisms for water transport in paper: (a) water transport through the pores by capillary action, (b) vapor phase transport through the porous structure, (c) surface diffusion in the pores, and (d) water diffusion through fibers.

In paper coating processes, binder may migrate along with movement of the aqueous phase of paper coating colors toward the base paper and the coating surface. This migration of binders may cause non-uniform binder distributions in the final coating. Thus, binder migration is defined as a differential movement of a binder or binders with respect to pigment particles leading to non-uniform binder distributions in coated paper.

The migration of binders can occur toward the base paper during drainage of the aqueous phase what may affect coating adhesion to the paper, and toward the coating surface during evaporation at the coating surface. On the other hand, binder migration toward the coating surface may significantly influence coating surface properties such as surface porosity and coating optical, especially gloss and brightness [86].

2.3.4 The Stages of Coating Application

The purpose of paper coating is to improve the optical properties of a paper sheet by applying onto it a thin and uniform pigment suspension by using a metering size press. A typical metering size press is composed of a set of contra-rotating transfer and backing rolls, both of which are covered with an elastomer layer to reduce the risk of clashing, to allow the metering of thinner and more uniform films and to reduce coating instability [92]. The deformation of the roll cover alters the shape of the boundaries of the coating flow. That flow generates pressure and viscous stresses that in turn affect the deformation of the roll cover.

The paper substrate is fed into the application nip and picks up the coat that has been applied onto the transfer roll in the metering nip. In the metering nip, the shape of the transfer roll and hydrodynamics of the process depend on each other. The soft roll deforms owing to the stresses imparted by the fluid flow, which in turn is altered by the deformation. This process goes on until some equilibrium is reached. Such equilibrium is influenced by a lot of factors: size of the rolls, speed of the rolls, nip gap size, and fluid rheology.

2.3.5 Coating Defects

Roll coating is a process whereby liquid flows into a narrow gap between two rotating cylinders, the surfaces of which move either in the same direction (forward) or opposite directions (reverse). Some of the liquid passes through the gap and splits downstream into two thin films, each coating one of the rolls. In recent years as coating speeds have increased beyond 3500 ft/min several runnability problems have

risen. These include visual defects such as spraying, misting, spitting and scratching of the coating.

Making progress in preventing coating defects and irregularities is important in order to obtain high quality coated surfaces. Surface tension forces, body forces, flow adsorption into the base sheet, drying and rheological behavior influence the coated surface. The uniformity of the coating layer is critical in determining the quality of the final paper coating. The ribbing instability of roll coat applicator produces systematic regions of thick and thin coating layers. Huang [93] identified that the dewatering of the coating and rheological properties of coating color are the major cause of blade scratches.

Streaks in the coating, loss of coat weight profile control and poor runnability are increasing with increasing machine speed, therefore the coating color composition and rheology are necessary to eliminate the runnability problems [94]. The film-splitting process consists of three different stages: (a) an immobilization stage, (b) a filament formation and breakup stage as a result of the surface tension, (c) a coating leveling stage. Film splitting of the coating color occurs in metered film coaters at the exit of the application nip. This may lead to misting and/or orange peel formation, which is characterized by the extension of the coating in the outgoing nip into longer filaments until the surface tension forces break them up to small misting droplets. These are the two dominant runnability and quality issues in high-speed film coating that limit its applicability [95].

Nick and Malcolm [96] revealed that a specific problem due to film splitting at the premetering or transfer nips could be manifested in the form of misting. Another problem is a non-uniform pattern transferred to the web, creating the orange peel defect. Onset and control of misting and orange peel depend on equipment operation, coat weight, properties of the substrate, and the flow characteristics, including solids of the coating.

2.4 Interfacial Properties of Coating Color

At an interface or phase boundary between two dissimilar materials, there exists a surface electrical potential that reflects differences in the electronic makeup of the two phases.

Because almost all surface-active materials have a polar head group, when the molecules adsorb at the surface, the dipole moments of those groups become at least partially oriented with respect to the interface. As a result of the orientation of the dipoles (or charges), the potential difference across the interface will be altered [87].

The contribution of particle-particle interactions is particularly significant. The colloidal interactions involve electrostatic, polymeric steric, dispersion and depletion forces [88]. The electrostatic and polymeric steric repulsive forces, which determine the stability of coating colors, are primarily affected by the surface charge of particles, dispersants and thickeners.

The rheological properties of coating colors are affected by the nature of the thickener used and depend on its chemical structure and molecular weight. However, its role is not clearly understood yet [89,49].

The formation of pigment networks due to polymeric bridging between particles has been proposed as a possible mechanism for the coating colors thickened with associative thickeners (ATs) such as hydrophobically modified ethoxylated urethane [90]. Since both pigment and latex particles are negatively charged [91], it is not expected that latex will interact with pigments strongly.

2.5 Paper coating quality and Properties

Coating quality involves, e.g., smoothness, gloss, and ink absorption. These depend on the coating structure, by which is meant the spatial arrangement of the main components-pigment and binder in the coating layer as well as the air. It has been explained earlier that the coating layer is porous, which is why air should also be considered a component of the coating layer. Paper quality depends on the coverage. Coverage indicates how well the coating is able to hide the base paper under it. A coating layer of as constant thickness as possible has good coverage.

2.5.1 Calendering

Calendering is a general term meaning pressing with a roll. Several different types of calendering operations are carried out over paper such as: machine calendering, super calendering, friction calendering and brush calendering. The most common operation, called machine calendering, is the passage of paper through one or more nips formed by a set of iron rolls, and is the principle calendering operation that is always carried out on machine.

Calendering of paper is a mechanical operation by which the web is compacted and the surface properties are improved. Calendering action comprises three elements:

pressure, allied deformation in both paper and filled rolls, and temperature. Coated-paper properties are the sum of the internal properties of the paper itself plus the external properties of the coating. The objectives of calendering are to reduce sheet thickness to the desired level, and impart desirable surface properties, primarily smoothness [2].

2.5.2 Brightness

Brightness is the reflectivity of a sheet of pulp or paper measured under standardized conditions; used to indicate the degree of whiteness [2]. Whiteness is a comprehensive term used to express the visual impact of near white surfaces by means of the single value. Numerous equations have been developed, by CIE (Commission international de l'eclairage). Whiteness is used to denote a more comprehensive expression of color by use of the CIE color coordinate L*, a*, and b*. Positive figures for a* express redness, negative figures greenness, and positive figures for b* express yellowness, negative figures blueness. L* is a percentage which measures luminance on a scale where black is zero and pure white is 100%. One can measure color coordinates as well as brightness with the same instrument.

Brightness and whiteness properties are highly dependent on the coating composition, pigment type, and coating amount. Optical brightening agents may also be used to enhance whiteness by increasing "optical activity" when exposed to ultraviolet light. The pigments used in pigmented coatings for printing papers are white and opacity. Since the visible light travels in a matrix of refractive index 1.5 (typical of paper coatings formulated with pigments of low refractive index such as clay or Calcium carbonate), the optimum size of the voids should be about 0.3-0.5 microns. Typically,

pigments have a size distribution so that the voids, as well, have a size distribution [3]. Ground calcium carbonate influences the brightness and opacity of the coating layer. Therefore, high-brightness carbonate used in coating formulations at a high percentage can improve the brightness of coated papers.

2.5.3 pH and bacteria level

The normal coating color pH is between 8 and 8.5 because the pigment depends on the pH. The pigment source of coating is mainly kaolin, a hexagonal plate-like shape pigment with negatively charged faces and charges on the edges. The edges are positively charged at low pH and become negative as pH is increased [97]. Van Olphen assumed that at low pH the electrostatic interaction between opposite charges faces and edges leads to the formation of a "house of cards-type" or three-dimensional network [98].

A high bacteria level of coating color chemicals can influence the machine's runnability but, if the coated paper will come in contact with food, it is extremely important that the bacteria level is low. The Easicult Combi test can be used to count the bacteria level of material [80].

2.6 Microstructure of Wet Coating

A procedure was reported for high-magnification freeze-fracture cryo-scanning electron microscopy to visualize directly wet microstructures in suspensions of coating components. Mechanisms of colloidal interactions and their relevance to paper coatings were discussed previously by Whalen-Shaw [99].

In 1944, Williams and Wykoff developed a freeze-drying technique in combination with metal shadowing. The specimens investigated with this technique, e.g. skin surfaces, yielded high quality micrographs and reproducible results. Soon afterwards, C.E. Hall [102] and H.T. Merryman [103] designed, independent of one another, a device with which they produced replicas of frozen specimens by coating them with silicon oxide. The replicas were then investigated in the electron microscope. However, Merryman and Hall were only successful with the investigations of crystals. R.L.Steere [104] modified the technique of Hall and Merryman. He froze suspensions and fractured the resulting ice blocks in a special cold box.

Detailed models of how colloidal particles may interact, aggregate, and form volume-filling networks under various conditions have been proposed [125-126]. The corresponding models are based on the physical-chemical properties of the suspensions and on the morphological features of the individual colloidal particles and their aggregates.

There are hardly any EM observations that give reliable information about the amount and kind of aggregation, which a colloid displays, in the dispersed state since the aggregations shown in some EM studies may be artifacts formed during specimen preparation. When water is removed from colloidal clay solutions in the course of the EM preparation, rearrangements of the mineral particles are to be expected. Air-drying must be considered as totally unsuitable for the study of particle interactions. Even the consistent observation of units with specific dimensions and shapes on dried specimens is no proof of their preexistence in the suspension. Freeze-drying, critical

point drying, and substitution techniques can overcome the deleterious effect of the surface tension.

The above techniques may be sufficient for the investigation of specimens with low water content and for work with limited resolution on the scanning electron microscope. They are not suitable for studying the distribution and association of dispersed particles in dilute colloidal solutions with high confidence and accuracy. Therefore, advanced techniques of very fast cryofixation have been applied. The specimens frozen in this way were then processed by freeze-etching [127-128].

Since High-Magnification Cryo-SEM requires freezing, freezing fixes water-based coating suspensions that are unstable in the vacuum of an SEM. Fast-freezing suppresses ice crystal formation and prevents segregation of sample components at grain boundaries [100]. Sheehan [101] has demonstrated with cryo-SEM that the microstructure of latex in suspension depends on both ionic strength and water-soluble polymers and on how freeze-fracture Cryo-SEM provides the visual link between wet and dry microstructures.

2.7 Brief Review of Numerical Simulations for Coating process

Roll coating is a technique commonly used in the coating industry to meter a thin fluid film on a moving substrate. During the film formation, the fluid is subjected to very high shear and extensional rates over a very short period of time. The fluid domain changes as a function of the hydrodynamic pressure within the nip as a result of the deformable cover usually used on one of the rolls. The free surface also adds more complexity to the flow due to the force equilibrium in the fluid gas interface.

Last of all, the rheological behavior of the coating fluid is usually non-Newtonian, so the metering flow hydrodynamics is finally very difficult to describe.

Over the last few years, researchers have used the lubrication theory as well as Navier Stokes equations (CFD models) to investigate reverse roll coating flows [105-111]. For the lubrication theory, the main hypothesis is that inertia effects are minimal and therefore neglected. The flow can be represented by $dP/dx = \mu (\delta^2 \upsilon_x/\delta y^2)$ [105]. Greener and Middleman [105], using both vanishing pressure and pressure gradient as boundary conditions, predicted the coating thickness on the transfer roll for a relatively narrow range of metering rod to transfer roll speed, although the flow rate deviated from the predictions of the model due to some flow recirculations upstream from the nip.

Coyle et al. [107] showed that the metered nip flow deviates from the lubrication theory predictions at high-speed ratios and capillary numbers. The dynamic wetting line moves towards the nip center, the nip length shrinks, and the film thickness passes through a minimum. Most of previous studies of forward roll coating focused on the simple case of two rigid rolls separated by a narrow gap [112-114]. In many cases, one of the rolls is rubber covered, and an external load W presses both rolls against each other. The coating thickness is thus governed by the operating parameters (speeds and loading), mechanical properties of the solids and the mechanical properties of the fluid. Coyle [115] described the general features of roll coating operations involving a deformable roll.

Chapter Three
METHODOLOGY INSTRUMENTATION AND EXPERIMENTAL DESIGN

3. 1- Materials

An uncalendered paper made from a peroxide-bleached softwood thermo-mechanical pulp (BTMP) was obtained from an eastern Canadian mill. The BTMP paper was made from a mixture of approximately 70% black spruce and 30% balsam fir. It had a 57 g /m^2 grammage (OD), 78% ISO brightness and 0.4 CIE b* value. The inhibitor system contained an UV absorber (UVA), an alkylene oxide substituted hydroxyphenyl benzotriazole, and a radical scavenger (RS), a hydroxylamine (4-hydroxy-2,2,6,6-tetramethyl-N-hydroxypiperidine) salt.

The main components of the coating colors studied in this work were a commercial clay, Astraplate (70% of delaminated clay mixed with water), and ground calcium carbonate, Covercarb, used as the pigments as shown in Table I. The pigments were mixed using Stir-Pak heavy duty mixer, at high shear rate with speed of 900 rpm. Starch (Penford Gum 280) was added to the suspension and used as binder. The additives were AcronalS728, which provides paper coatings with excellent sheet and is ideally suited as a cobinder for paperboard coating and KZCote, SterocollBL which is viscous and thixotropic and off-white liquid used as a cross linking agent to bind the starch.

The coating colors were prepared using different concentrations of inhibitors, 0.1-1%. The pH- value was adjusted to 8-8.8 using 50% NaOH aqueous solutions. The solid content of the coating colors was 55%.

Table 3.1 Coating Color Components.

Chemical name	Purpose of chemical	Solid Content (%)	Parts/ 100 of pigment
Covercarb	**Pigment (ground calcium carbonate)**	**71.6**	**80**
Astraplate	**Pigment (delaminated clay, Kaolinite)**	**70**	**20**
Penford Gum 280	**Binder (Starch)**	**20**	**6**
Acronal S728	**Cobinder (Latex)**	**49.4**	**12**
KZCote	**Cross Linking agent (Additives)**	**100**	**0.5**

3. 2- Laboratory Film Applicator

The coating formulation was delivered at 4, 6, or 8 g/m^2 per side onto the machine-made 100% BTMP paper with a laboratory film applicator (Figure 3.1), where coat weight = weight of paper before coating + ((coat weight/solid content)/57 g/m^2).

The laboratory film applicator consists of a grooved metal metering roll, a soft transfer roll, a hard backing roll and a temperature controlled feeding pan. A thin film of coating color is metered onto the surface of the transfer roll. The paper is coated on one side when it passes between the transfer roll and the backing roll with the support

of a Mylar sheet. The required pickup was obtained by mainly adjusting the web speed, the nip pressure between the metering and transfer roll, and finally the solids content of the formulation. The samples were dried by a STFI sheet dryer at 105°C, and then treated on the other side. The solids content of the coating formulation was around 30%. The total pickup was determined by the weight difference before and after surface treatment under standard conditions (50% R.H. and 23 °C).

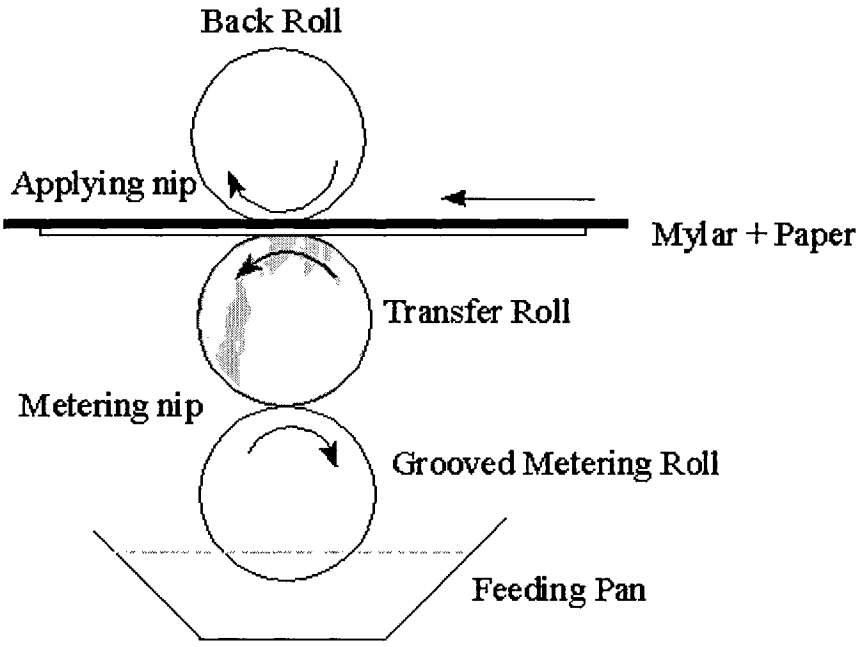

Figure 3.1 Laboratory film applicator

3. 3- Calendering

Coated and dried samples were calendered by a laboratory hard nip calender to get the required caliper of about 110 μm. The calendering has been done under the following conditions:

Target= 110 μm, Speed = 50 m/min, Roll Temperature = 50 °C, width = 3 inches.

Sheets were calendered at 40 KN/m because the average thickness 109.3 is close to 110. The following Table shows the different thickness of the sheet. Figure 3.2 shows target 110 μm can be obtained at nip load 40 KN/m.

Table 3.2. The Coating thickness on the sheet.

Load (kN/m)	**Thickness (μm)**					**Average**
0	167.0	158.1	158.8	162.6	159.6	161.2
40	125.7	115.0	107.9	103.5	94.6	109.3
50	109.9	103.3	99.1	93.0	89.9	99.0
60	111.3	108.1	103.8	96.6	89.8	101.9
70	94.6	92.8	92.5	88.7	86.1	90.9

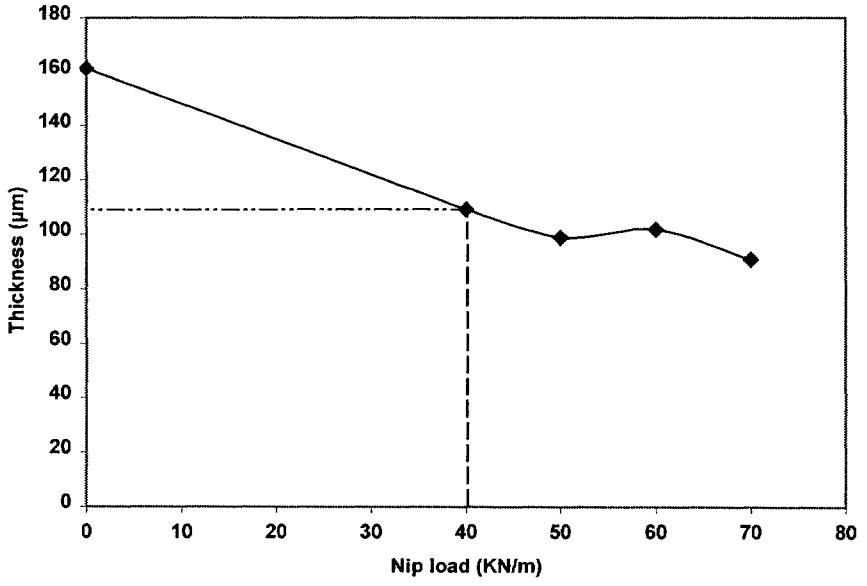

Figure 3.2 shows the relation between the thickness and nip load.

3. 4- Brightness Stability Test

The effect of yellowing inhibitors on paper light stability was examined under accelerated light exposure conditions in a metal box (Luzchem Research Inc.) with eight, 8W cool-white fluorescent lamps positioned 19 cm above the samples. The box was ventilated so that the temperature inside the box remained at about 30 °C during the exposure period. The light intensity inside the box was approximately 1100-foot candles. Yellowing inhibition was monitored by the decrease in paper brightness and the increase in post color number (PC number). The ISO brightness was determined according to PAPTAC Standard Testing Method E.1 using a Technidyne Micro TB-1C reflectometer. Since brightness is a non-linear function of chromophore concentration, it is sometimes difficult to interpret brightness changes for papers with different initial brightness in terms of the underlying changes in chromophore concentration. In many cases, a satisfactory solution to this problem is to convert the brightness to PC number according to the following two equations:

$$PC = ((k/s)_{after} - (k/s)_{before})*100 \quad (1)$$

$$k/s = (1-R_\infty)^2 / 2\,R_\infty \quad (2)$$

Here k and s refer to the absorption and scattering coefficients, respectively, and R_∞ is the value of ISO brightness expressed as a fractional value. The smaller the PC number, the less the paper has yellowed.

3. 5- Rheological Measurements

The rheological measurements were carried out using a Haake rheometer RheoStress RS100. This rheometer has several operating test modes. It has a universal controlled rate (CR) mode, a controlled stress (CS) mode, and an oscillation (OSC) test mode. In

the CR-mode, shear stress is applied to a test sample by extremely low inertia. The drive shaft of the RS100 is centered by an air bearing to ensure an almost frictionless transmission of the applied stress to the test fluid. The resulting deformation of the sample is detected with a digital encoder that processes 10^6 impulses per revolution. This resolution makes it possible to measure small yield values, strains, or shear rates.

The computer-controlled rheometer can be easily switched between both the CS and CR modes, and it can provide oscillating stress inputs. A controlled variable lift speed is used to position the cone on the plate. A thermal gap size is controlled to compensate for any of the sensor-generated heat. The software package "Haake" controls both test routines and data evaluation. For the completeness of the study, it was important that RS100 rheometer could test visco-elastic fluids. The rheometer is equipped with a cone and plate sensor. Hercules DV-10 viscometer was used to measure the viscosity at very high shear rate up to 180001/s with temperature controller and concentric cylinders.

3. 6- Water Retention Measurements

The water retention property of coating colors was measured using a Gravimetric Water Retention Meter. A piece of pre-weighted blot paper was first placed on a rubber supporting plate. Then, a polycarbonate-based membrane with a pore size of 5 μm was placed on the top of the blot paper followed by placing a sample holder. Two mL of coating colors was transferred to the sample holder. A pressure of 15 psi was applied as a function of the time. Finally, the blot paper was weighed again and the

weight difference of the blot paper before and after absorbing water was taken as the water loss of the sample.

3. 7- Zeta Potential measurement

All the zeta potential measurements were conducted using Zeta-meter 3.0+, which is a microprocessor-controlled instrument. Zeta-meter 3.0+ can measure electro-phoretic mobility and zeta potential. Zeta potential measurements are manufactured using a technique called micro electrophoresis. A high quality stereoscopic microscope is utilized to detect colloidal particles within a chamber called an electrophoresis cell. Electrodes situated in each end of the chamber are connected to the zeta meter 3.0+ and an electric field is generated across the chamber. Charged colloids move in the field and their velocity and direction are associated to their zeta potential (shown by video display). The Zeta-meter determines the specific conductance of the sample and helps choose the appropriate voltage to exert. The final solid concentration of the diluted samples was 0.025% and the final pH was around 8.

3.8- Photo Correlation Spectroscopy (PCS) Measurements

The Photon Correlation Spectroscopy (PCS) technique is used in photon-correlation spectrometer to measure sub-micron particle sizes, diffusion coefficients and viscosities. The PCS method is composed of calculating the velocity of particles movement by measuring dynamic fluctuations of the amount of scattered light. The diffusion coefficient can be calculated by fitting the measured correlation function to a single exponential function.

The diffusion coefficient of the particles is inversely proportional to the decay time of light scattering fluctuations. The decay time is found from the time-dependent correlation function of the scattered light. The particle size can be calculated using Stokes-Einstein formula by relating the particle size to the diffusion coefficient and viscosity.

3.9- Transmission Electron Microscopy (TEM) Measurement

The surface microscopy of different coating formulations including inhibitors was examined on high-resolution replicas by TEM. A drop of the suspension is placed on a commercial, 3mm-sized gold specimen carrier for freeze-etching and dropped into liquid propane then to liquid nitrogen. Figure 3.3 shows the preparation steps of freeze-etching.

3.9.1 Fracturing

In order to present the internal structures of the specimens, as the specimens consist of brittle ice, the samples cannot be cut, but must be fractured. This is carried out on a cooled specimen with the aid of liquid nitrogen. The layer (the layer which exhibits the internal structure) is gradually advanced after it disintegrates from the sample until the finest possible fracture surface is obtained.

3.9.2 Etching

In addition to the fracture-faces arising during fracturing, which reveal the main structures of the specimen, a few detailed structures remain hidden just underneath a thin layer of ice. The removal of ice from the fractured surfaces to a depth of a few

nm, is sufficient to present further, otherwise concealed details, above all membrane surfaces. For sublimation, the vapor pressure of the sample must be greater than the water partial pressure under vacuum. Otherwise the result would be condensation of water (ice) on the sample.

3.9.3 Shadowing

The specimen structures revealed by fracturing and etching can be reproduced with the aid of a thin platinum/carbon (95Pt/5Cwt% and 1-2 nm thick). Since the replica should determine the finest possible details for shadowing, which produces the actual replication, only metal such as platinum, which forms well contrasting, and fine-grain coated films can be used. Pure carbon is suitable as a supporting-film.

Platinum melted into a carbon rod, is evaporated at an angle of 45° with an electron beam gun. The platinum replica is strengthened by additional coating of carbon at an angle of 90° (so-called supporting film). The film thickness of the coating can be very accurately adjusted. The combination platinum/carbon has also proved to be mechanically and chemically stable during the subsequent cleaning process.

3.9.4 Cleaning of the Replica

The specimen grid with the adhering sample and the replica is removed from the freeze-etch apparatus. By immersing the plate obliquely in water, the replica can easily be peeled of the sample. Due to the surface tension, replica and adhering residues of the specimen float on the water surface. In order to clean the replicas completely, they are transferred to acid baths (10% HF solution and HCL). After the

cleaning time, the replica is washed in distilled water and then placed on a narrow-mesh specimen grid.

3.9.5 Transmission Electron Microscopy Observation

When observing the replicas in the TEM, the replicas must be protected as much as possible during microscopic observation in order to avoid subsequent formation of artifacts.

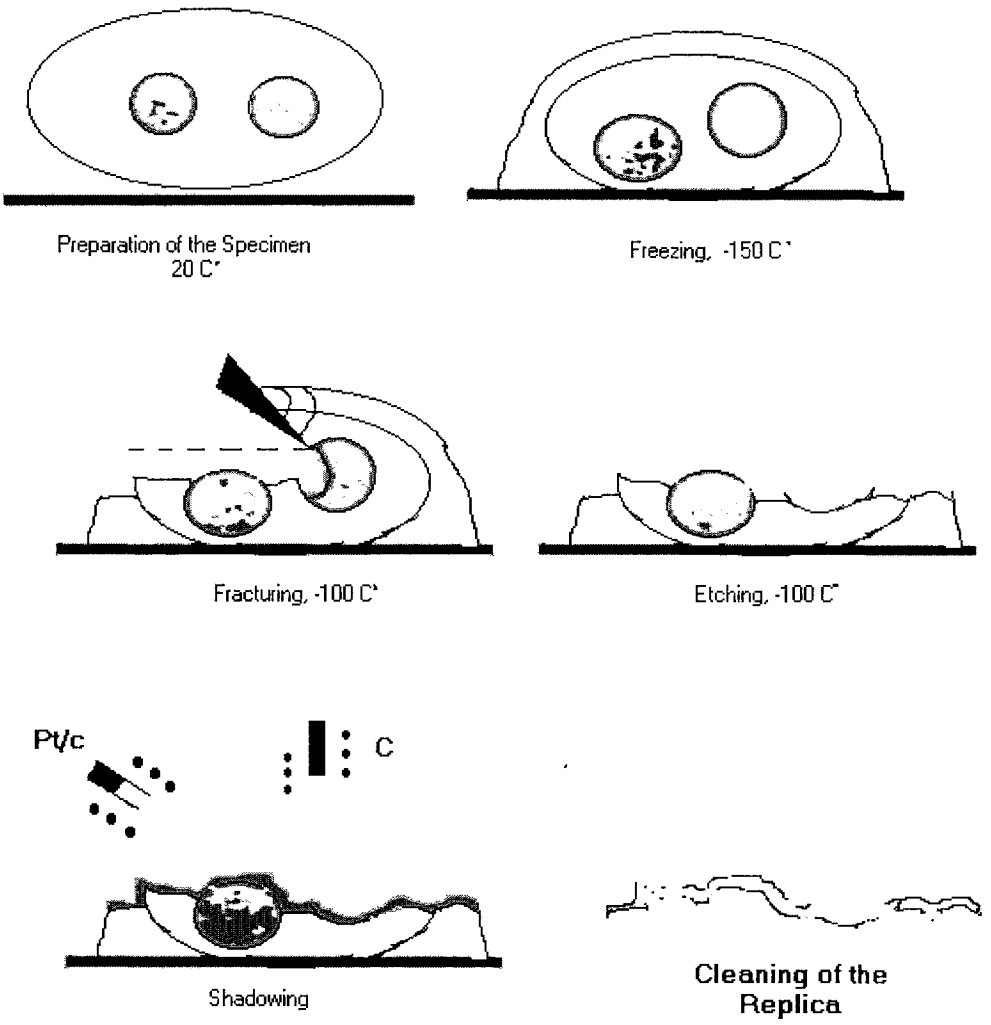

Figure 3.3 The preparation steps of freeze-etching.

3. 10- Experimental Design

A factorial experimental design (Box-Behnken) was used in this study to minimize the number of experiments required to provide a robust description of the chosen variables on the yellowing inhibition of the above-coated paper. Total charge of inhibitors (RS+UVA), coat weight per side of paper, and weight ratio of radical scavenger over UV absorber (RS/UVA) were the three variables chosen for this study. Their ranges are shown in Table 3.2.

The design required fifteen experiments, of which three were duplicates as shown in Table 3.3. The range of coat weight used was of interest to an eastern Canadian mill from which the paper was obtained. The ranges of inhibitor charge and ratio were designed to provide a wide range of yellowing inhibition for this coated paper. Statgraphics® Plus was used to analyze the experimental data and to generate the response equations.

Table 3.3 Experimental variables and their range

Variable	Designation	Lower limit	Higher limit
Total charge (% on o.d. fiber per side)	X1	0.2	1
RS/UVA ratio	X2	0.25	7.75
Coat weight (g/m^2 per side)	X3	4	8

Table 3.4 shows the different concentrations of yellowing inhibitors, which have been obtained from the experimental design

Table 3.4 Shows the different concentration of yellowing inhibitor

Tc %	RS/ UVA	C. W.	Tc.BW. SC	WT OF INH.	UVA%	RS%	UVA, PPH	RS, PPH	RS CH	UVA CH
1	4	4	0.52	17.9	20	80	3.58	14.3	0.8	0.2
0.6	4	6	0.31	10.1	20	80	2.03	8.10	0.48	0.12
0.6	0.25	8	0.31	10.1	80	20	8.11	2.03	0.12	0.48
0.6	7.75	4	0.31	10.1	11.428	88.57	1.16	8.97	0.531	0.068
1	4	8	0.52	17.89	20	80	3.58	14.32	0.8	0.2
0.6	4	6	0.31	10.13	20	80	2.025	8.10	0.48	0.12
0.6	7.75	8	0.31	10.13	11.428	88.57	1.157	8.97	0.531	0.068
0.2	4	8	0.11	3.19	20	80	0.639	2.55	0.16	0.04
0.2	0.25	6	0.11	3.19	80	20	2.55	0.64	0.04	0.16
0.6	0.25	4	0.31	10.13	80	20	8.10	2.03	0.12	0.48
0.2	4	4	0.11	3.19	20	80	0.64	2.55	0.16	0.04
1	7.75	6	0.53	17.89	11.43	88.57	2.05	15.85	0.885	0.12
0.6	4	6	0.32	10.13	20	80	2.03	8.11	0.48	0.12
1	0.25	6	0.53	17.89	80	20	14.32	3.58	0.2	0.8
0.2	7.75	6	0.11	3.19	11.43	88.57	0.365	2.828	0.18	0.023

Tc: total charge, RS: radical scavengers, UV:ultra violet, C.W.:coat weight, B.W.:base weight of paper (57 g/m^2), SC: solid content of the paper (92%), WT. OF INH:weight of inhibitor, CH:charge

Sample calculation

Weight of inhibitor = total mass (pph) (total charge*base weight of paper*solid content of paper) / (coat weight – (total charge*base weight of paper*solid content of paper))

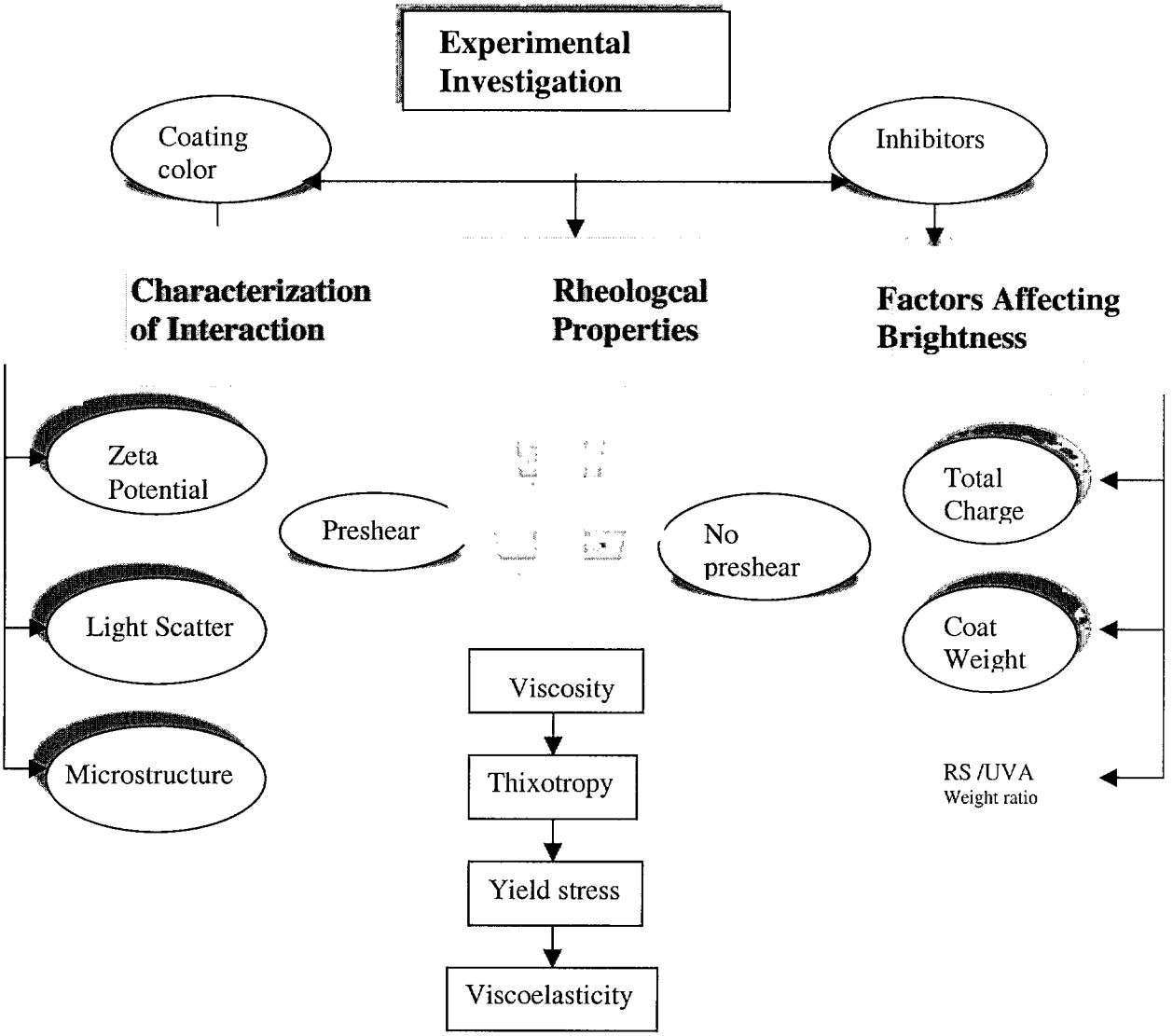

Theoretical CFD investigation

Schematic Diagram for Experimental Program

Chapter Four

OPTIMIZATION OF THE FACTORS AFFECTING THE YELLOWING INHIBITION OF A COATED BTMP PAPER

Yellowing inhibitors significantly improved the brightness stability of a paper made from 100% peroxide-bleached thermo-mechanical pulp (BTMP), when incorporated into a pigmented coating formulation. In this work, we tested this yellowing inhibition system on a paper made from 100% peroxide-bleached thermo-mechanical pulp (BTMP) using a laboratory film coater.

The inhibitors were applied onto the dry paper surface as part of a pigment coating formulation. Preliminary experiments showed that coat weight, total inhibitor charge, and ratio of RS/UVA significantly affected yellowing inhibition of this BTMP paper. Therefore, the objective of this study was to systematically examine how these three factors affect the yellowing inhibition and paper initial brightness through a statistical approach.

4.1 Application of Yellowing Inhibitors

The yellowing inhibitors (RS+UVA) were incorporated into the coating formulation as additives, as shown in appendix A. The simple scheme shown in Figure 2.1 is summarizing the mechanism of light induced yellowing, and to classify the various

approaches to yellowing inhibition. The coated samples were calendered, conditioned, and then subjected to brightness reversion test. Table 4.1 lists the ISO brightness of the coated samples before and after light exposure.

Table 4.1 Experimental conditions and brightness of the coated samples before and after 12 days of accelerated photolysis.

Inhibitors		Coat weight (g/m^2)	ISO brightness (%)	
Total charge (%)	RS/UVA ratio		Before	After
0.2	4	8	80.9	72.8
0.6	7.75	8	80.5	75.6
1	4	8	80.0	75.8
0.6	0.25	8	80.6	77.0
0.2	7.75	6	80.2	72.0
1	0.25	6	79.3	74.6
0.6	4	6	79.1	72.0
1	7.75	6	78.4	71.2
0.2	0.25	6	79.8	67.6
0.6	4	6	79.5	71.2
0.2	4	4	80.3	68.2
0.6	0.25	4	80.6	72.8
0.6	7.75	4	79.6	71.4
1	4	4	78.8	71.3
0.6	4	6	79.5	70.8
0	0	4	80.5	60.8
0	0	6	80.7	62.4
0	0	8	81.4	66.9

Figure 4.1 shows the effect of coat weight on the yellowing inhibition of BTMP paper without inhibitor. Coat weights of 4, 6 and 8 g/m^2 per side were tried. A coat weight of $4g/m^2$ resulted in a very small gain in paper brightness, even with the high-brightness mixture of GCC and clay. At coat weight of $6g/m^2$ the gain was insignificant comparing to coat weight $4g/m^2$.

However, coat weight of 8 g/m^2 demonstrates a high brightness gain. It is apparent from the results that increasing the coat weight of paper sheet increases the brightness gain. While the emergence of the film press has enabled the papermaker to use high coat weights. Therefore, the expected gains in brightness are more acceptable by adding inhibitor than by increasing coat weight.

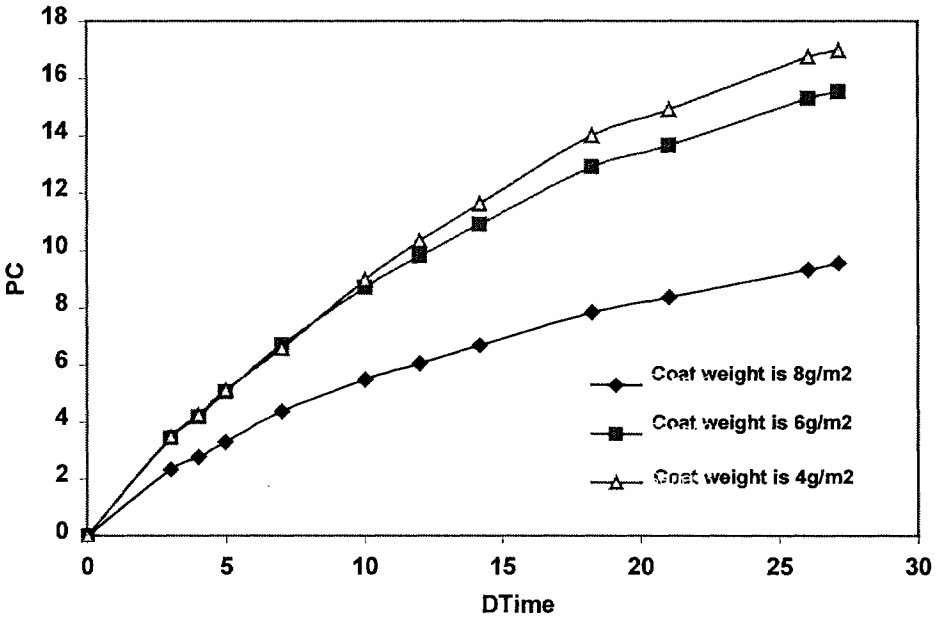

Figure 4.1 Effect of coat weight on PC without inhibitor.

Figures 4.2a, 4.2b and 4.2c plot ISO brightness against irradiation time for control and inhibited samples, coated with 4, 6 and 8 g/m^2 per side, respectively. To eliminate the difference on paper initial brightness at various coat weights and inhibitor treatments, PC number was plotted against irradiation time in Figures 4.3a, 4.3b and 4.3c. The smaller the PC number, the less the paper has yellowed. PC increased with irradiation

time, while paper brightness decreased with irradiation time as more chromorphores were produced in paper upon light exposure.

Increase in coat weight improved the brightness stability of the control samples, but to a limited extent. The incorporation of yellowing inhibitors into the formulation significantly increased the paper brightness stability. For example, after 12 days of accelerated irradiation, the sample treated with 0.6% inhibitor at a RS/UVA ratio of 0.25 had a PC number of 2.7, compared with 10.3 of the control sample that had the same coat weight of 4 g/m^2 per side. With the same inhibitor charge and ratio, an increase in coat weight to 8 g/m^2 further decreased the PC number to 1.1 over the same irradiation period.

Whiteness is one of the optical properties and it is a comprehensive term used to express the visual impact of near white surfaces by means of the single value. Since the subject of whiteness is beyond the scope of study, it will not be mentioned in details. However, some measurements were investigated, and the reader is referred to Appendix A for more details.

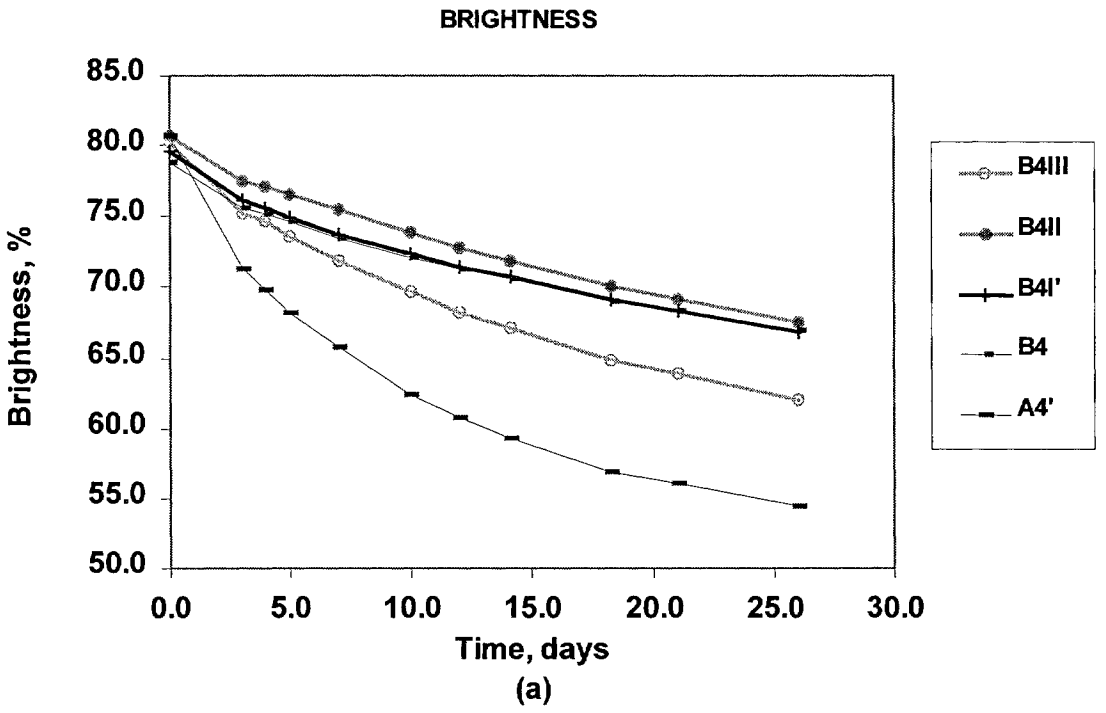
BRIGHTNESS
85.0
80.0
75.0
70.0
65.0
60.0
55.0
50.0
Brightness, %
0.0
5.0
10.0
15.0
20.0
25.0
30.0
Time, days
B4III
B4II
B4I'
B4
A4'

(a)

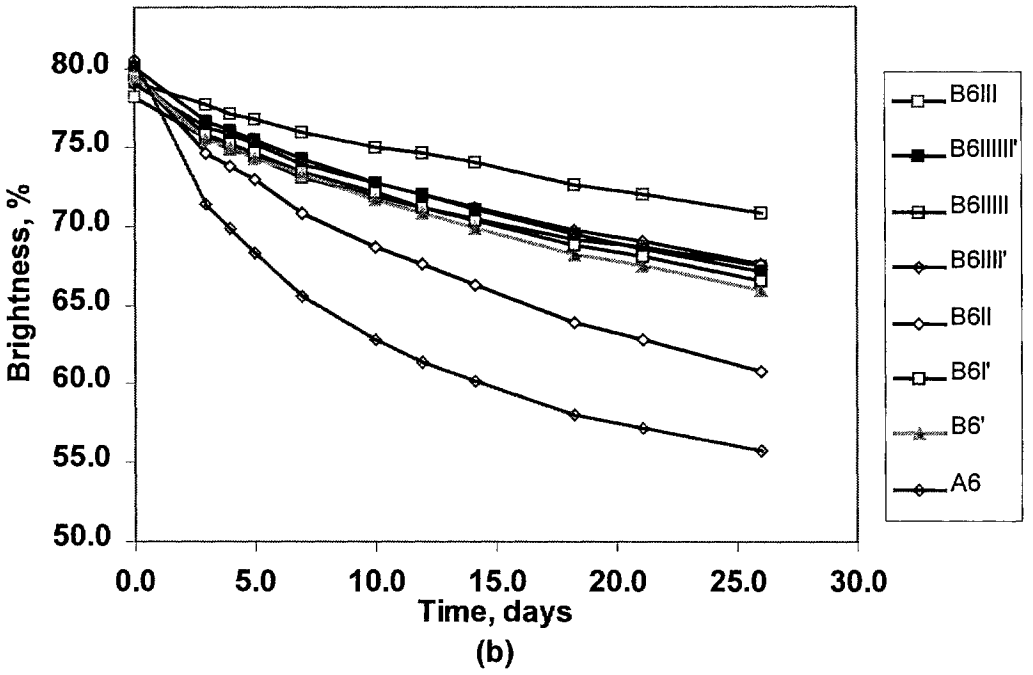
80.0
75.0
70.0
65.0
60.0
55.0
50.0
Brightness, %
0.0
5.0
10.0
15.0
20.0
25.0
30.0
Time, days
B6III
B6IIIIII'
B6IIIII
B6III'
B6II
B6I'
B6'
A6

(b)

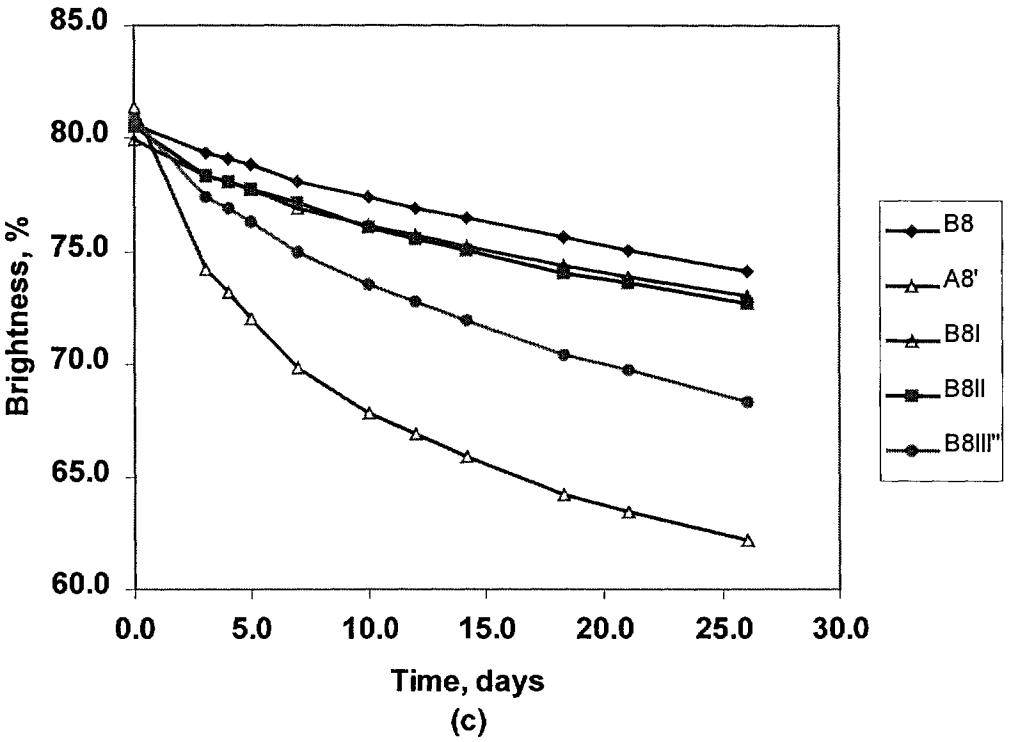

Figure 4.2 Brightness stability of BTMP paper under accelerated light exposure conditions: a) coat weight 4g/m^2, b) coat weight 6g/m^2, c) coat weight 8 g/m^2.

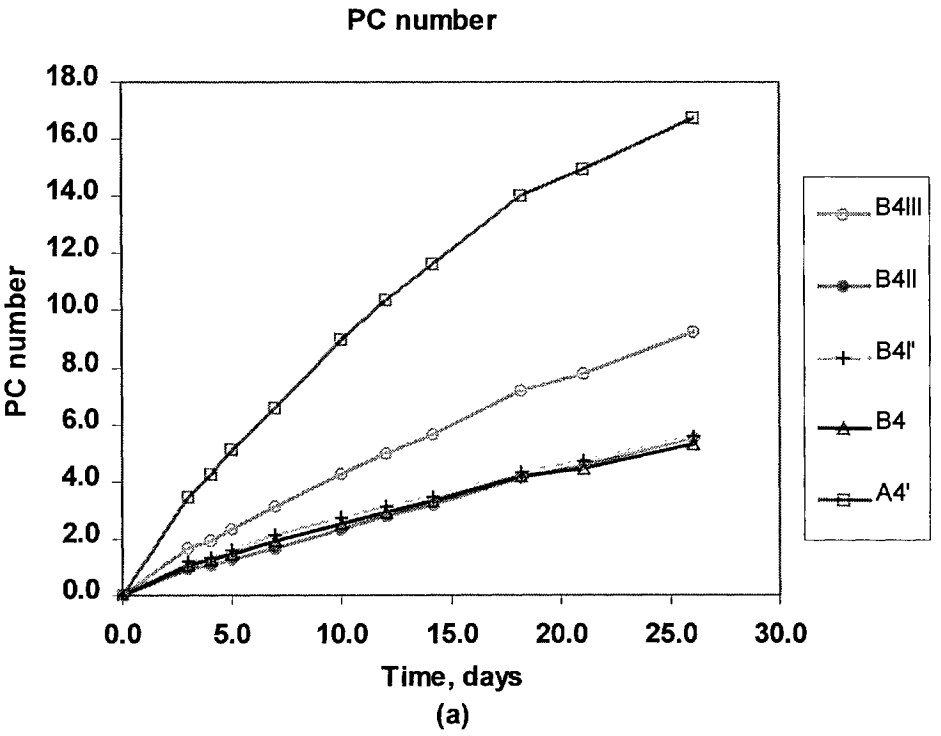
PC number
18.0
16.0
14.0
12.0
10.0
8.0
6.0
4.0
2.0
0.0
PC number
0.0
5.0
10.0
15.0
20.0
25.0
30.0
Time, days
B4III
B4II
B4I'
B4
A4'

(a)

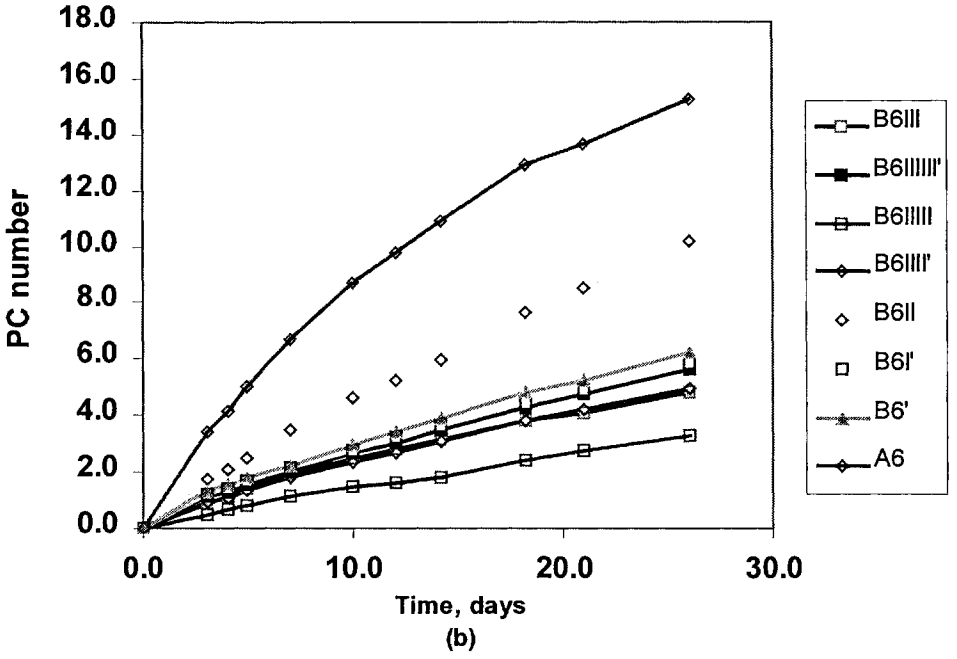
18.0
16.0
14.0
12.0
10.0
8.0
6.0
4.0
2.0
0.0
PC number
0.0
10.0
20.0
30.0
Time, days
B6III
B6IIIIII'
B6IIIII
B6IIII'
B6II
B6I'
B6'
A6

(b)

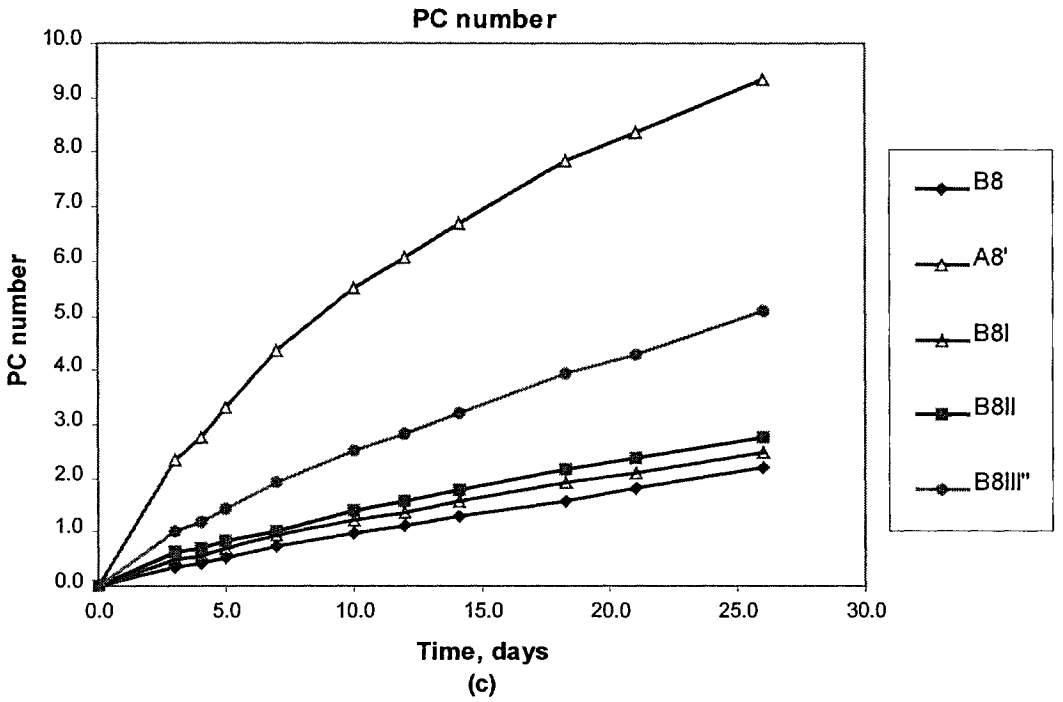

Figure 4.3 The change in PC number of BTMP paper under accelerated light exposure conditions: a) coat weight 4g/m^2, b) coat weight 6g/m^2, c) coat weight 8g/m^2.

The results of the experiment are interpreted based on our estimates of how each of the experimental factors affected the response (measure of process performance). The statistical analysis provides estimates of these effects. The effect of each factor is the difference in the response value associated with going from low to high setting of the factor. In this study, the initial paper brightness and PC number after 12 and 24 days of accelerated irradiation as shown in Table 4.2.

Table 4.2 Data file of Fifteen Run Experiment.

Total charge [%]	RS/UVA ratio	Coat weight [g/m^2]	PC number for 12 days (response)	PC number for 24 days (response)
1	4	4	2.93	4.95
0.6	4	6	3.41	5.82
0.6	0.25	8	1.12	2.0
0.6	7.75	4	3.1	5.24
1	4	8	1.36	2.30
0.6	4	6	3.19	5.41
0.6	7.75	8	1.58	2.59
0.2	4	8	2.82	4.75
0.2	0.25	6	5.21	9.43
0.6	0.25	4	2.77	5.13
0.2	4	4	4.97	8.65
1	7.75	6	2.78	4.49
0.6	4	6	2.69	4.65
1	0.25	6	1.59	3.11
0.2	7.75	6	3	5.26

4.2 Statistical Model

A statistical model has been developed to predict the PC number as a function of total charge, RS/UVA ratio and coat weight. This statistical model provides a prediction of the best settings of factors, which should produce the optimum value of PC.

The results in Table 4.2 were used to obtain the response equations using a computed regression analysis as shown in Table 4.3. These equations describe the relationships between the responses (paper initial brightness and PC number) and the variables (total charge, RS/UVA ratio, and coat weight). They are a second order polynomial model. The output shows the results of fitting a multiple linear regression model as shown in Table 4.4 to describe the relationship between PC and independent variables. Here the initial brightness refers to the brightness after coating and before the exposure to light.

Table 4.3 Response equations obtained from the factorial design using a computed regression analysis.

Response	Equation	Coefficient (r^2)
PC number (after 12 days)	$3.8 - 7.74X_1 + 2.83X_1^2 + 0.512X_1X_2 - 0.0384X_2^2 - 0.137X_3^2 + 1.22X_3$	0.95
PC umber (after 24 days)	$6.4 - 13.45X_1 + 5.16X_1^2 + 0.779913X_2X_1 - 0.065X_2^2 - 0.25X_3^2 + 2.25X_3$	0.91
Initial Brightness	$86.28 - 2.28\ X_3 + 0.195\ X_3^2 + 0.024\ X_3X_2 - 0.34\ X_1\ X_2$	0.9
Variables are defined as:	X_1= Total charge, X_2 = RS/UVA, X_3 = Coat Weight	

Table 4.4 Multiple Regression Analysis for samples kept for 12 days in light box.

Dependent variable: PC			
Parameter	Estimate	Standard Error	T Statistic
Constant	3.8257	1.59259	2.40219
Tcharge	-7.74112	1.38816	-5.57655
Tcharge*Tcharge	2.83257	1.09728	2.58145
Tcharge*RSUVA	0.512072	0.0947359	5.40526
RSUVA*RSUVA	-0.0384538	0.00748473	-5.13764
Coat weight*Coatweight	-0.137322	0.0438912	-3.1287
Coat weight	1.21724	0.530072	2.29637

Since the P-value in the Table 4.5 is less than 0.01, there is a statistically significant relationship between the variables at the 99% confidence level. This model generates a response surface plot for PC.

Table 4.5 Analysis of Variance

Source	Sum of Squares	Degree of freedom	Mean Square	F-Ratio	P-Value
Model	18.1184	6	3.01974	26.43	0.0001
Residual	0.913934	8	0.114242		

The R-squared value provides a measure of how much of the variability in the observed response values can be explained by the experimental factors. The R-squared value is always between zero and one. A value of one indicates that the

statistical model explains all of the variability in the data. A value of zero indicates that none of the variability in the response can be explained by the experimental factors. The R-squared value in this experiment is 0.95198.

There are several additional diagnostic plots to consider when evaluating the goodness of the reduced statistical model. These are the predicted versus observed plot. The predicted values are calculated from the statistical model. The observed values are the actual values of the response. Figure 4.4 shows the points on the predicted versus observed plot lie close to a line with slope of one which passes through the origin. This indicates that the model successfully predicts the responses. More details in statistical results can be found in Appendix A.

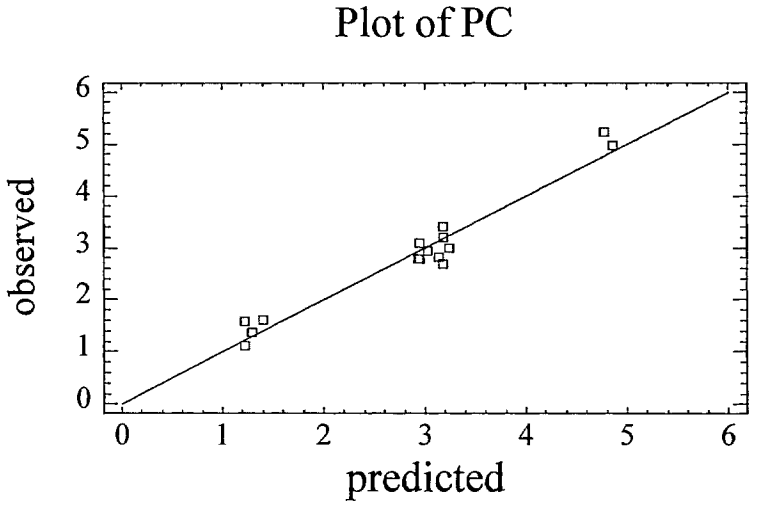

Figure 4.4 Plot of predicted versus observed values for the reduced model

Figure 4.5 is the standardized pareto chart for PC number which shows that all variables have a direct impact on the paper brightness stability with the influence

decreasing in the following order: total charge > coatweight > RS/UVA ratio. There are also strong interactions between total charge and RS/UVA ratio. The Pareto chart shows each of the estimated effects in decreasing order of magnitude. The length of each bar is proportional to the standardized effect, which is the estimated effect divided by its standard error. This is equivalent to computing a t-statistic (The t-value measures how large the coefficient is in relationship to its standard error, the t-value is obtained by dividing each coefficient by its standard error) for each effect. The vertical line can be used to judge which effects are statistically significant. Any bar which extend beyond the line correspond to effects which are statistically significant at the 95% confidence level. In this case, 4 effects are significant.

Pareto chart suggests that only a few factors are responsible for most of the changes in the yellowing inhibition. Total charge has the largest effect on yellowing inhibition, coat weight and combination of total charge and RS/UVA ratio, also seem to be important factors. In a fractional factorial design, the effect of each factor is the difference between the average of measurements (PC) made at high level of the factor and the average PC made at low level of the factor.

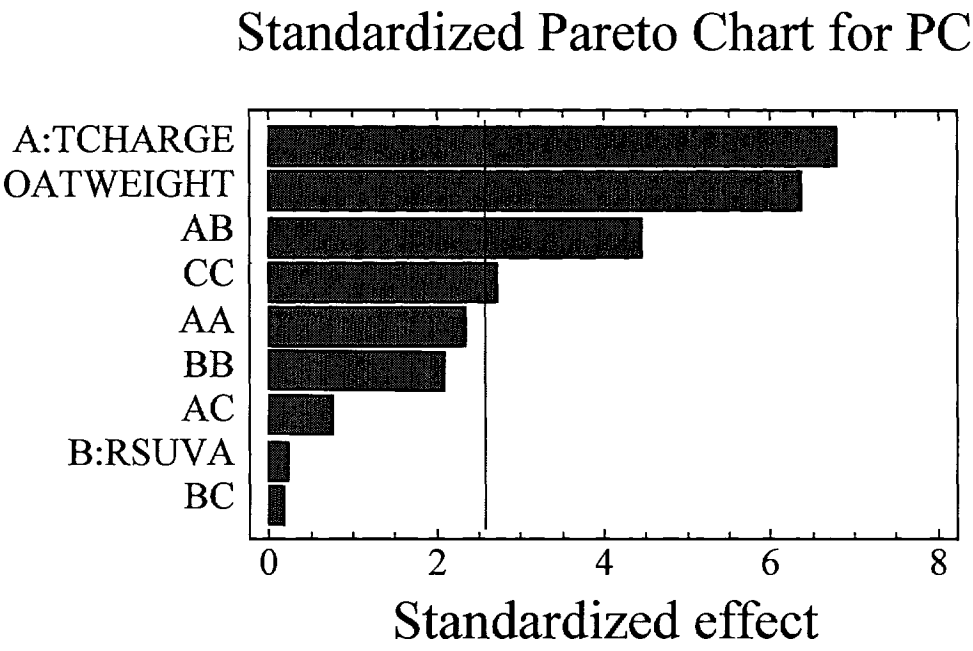

Figure 4.5 Standard Pareto chart for PC number after 12 days of accelerated irradiation.

To confirm the model obtained, the BTMP paper was treated with yellowing inhibitors at a coat weight of $8g/m^2$, but at arbitrarily chosen inhibitor charges and RS/UVA ratios. Table 4.6 compares the experimental and model predicted response for these samples (initial brightness and PC number after 12 days of accelerated irradiation). As we can see, the model has a good prediction of both the initial brightness and PC number.

Table 4.6 Comparison of experimental and predicted response for samples treated with various inhibitor charge and RS/UVA ratio at a coat weight of 8 g/m^2.

Sample	Total charge	RS/UVA	Initial brightness (%ISO)		PC number	
	(%)	ratio	Experimental	Predicted	Experimental	Predicted
1	0.3	1.75	80.7	80.5	2.2	2.8
2	0.5	3.5	80.9	80.9	1.8	2.0
3	0.8	5	80.7	81.1	1.4	1.5

The data in Table 4.7 are presented the correspondence between PC number and paper brightness and to show the initial brightness drop while PC number is increasing.

Table 4.7 Correspondence between PC number and paper brightness for coat weight 4 g/m^2, total charge 1% and RS/UVA 4.

Brightness	**PC number**
78.83	0.0
75.62	1.09
75.15	1.27
74.62	1.47
73.48	1.94
72.11	2.55
71.3	2.93

4.2.1 Effect of coat weight on paper brightness stability

Figure 4.6 (a) shows the effect of coat weight on the PC number at (a) a fixed RS/UVA ratio of 4; (b) a fixed total charge of 0.6%. Both Figure 4.6(a) and 4.6(b) show that PC number decreased with increasing coat weight. The curve shape was similar at all total inhibitor charges or RS/UVA ratios. A coat weight increase from 6 to 8g/m^2 per side lead to a larger decrease in PC number than from 4 to 6 g/m^2.

Figure 4.6(a) also shows that at fixed coat weights and a RS/UVA ratio of 4, yellowing inhibition increased at a higher total inhibitor charge. An increase in total charge from 0.2 % to 0.6% significantly decreased the PC number. However, further increase from 0.6% to 1.0% only slightly lowered the PC number.

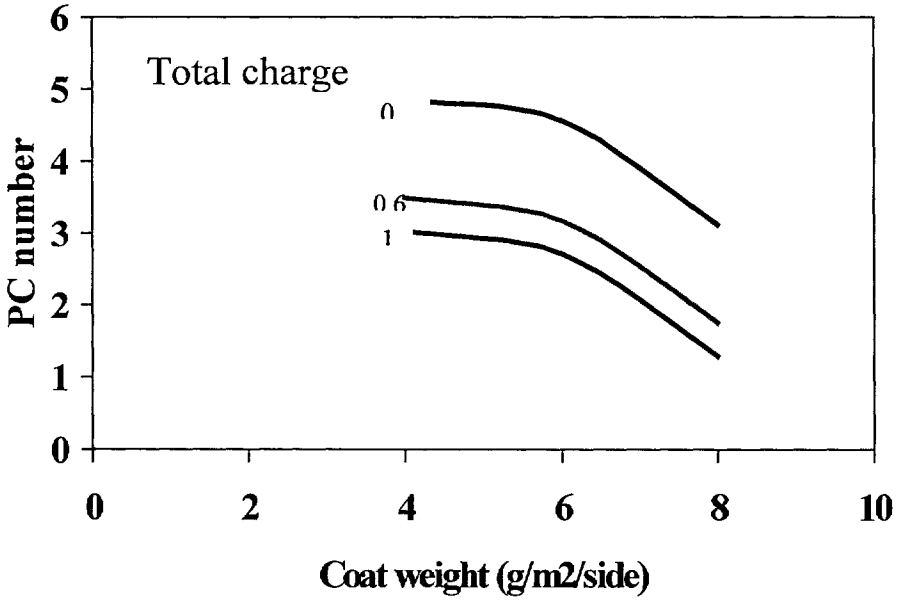

(a) At RS/UVA of 4

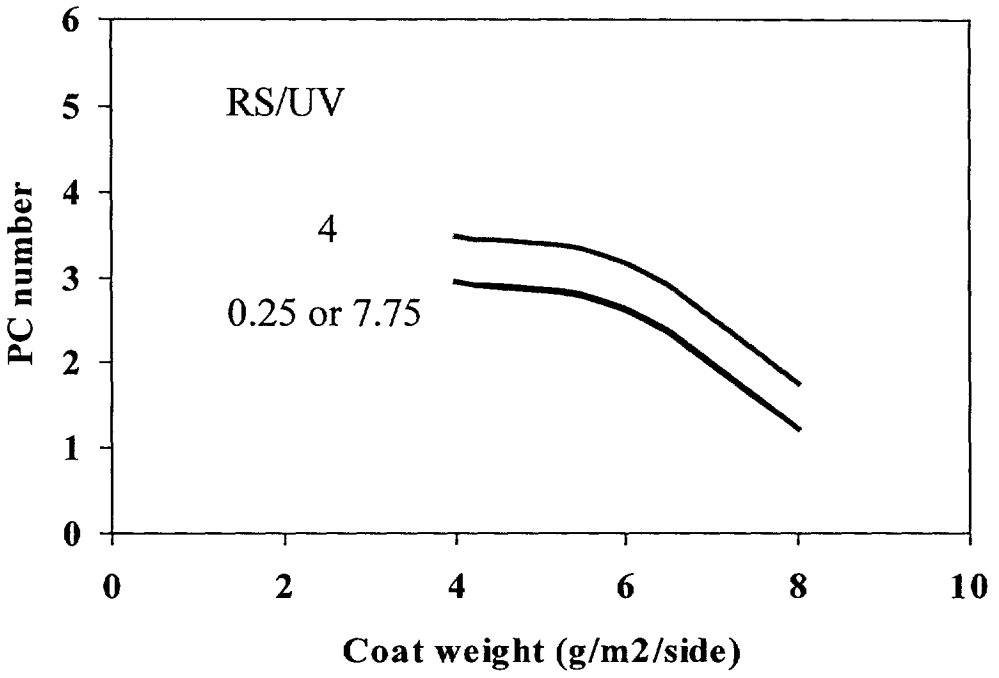

(b) at total charge of 0.6%

Figure 4.6 Effect of coat weight on PC number at: (a) a fixed RS/UVA ratio of 4; (b) a fixed total inhibitor charge of 0.6%

To obtain the same brightness stability, the BTMP paper can be treated with various combinations of coat weight, total inhibitor charge, and RS/UVA ratio. To maintain a PC number of 3 after 12 days of accelerated irradiation, for example, the BTMP paper could be treated with either 1% total inhibitor charge at a coat weight of 4 g/m^2, or with 0.6% charge at a coat weight of 6.3 g/m^2 both at the same RS/UVA ratio of 4 (Figure 4.6(a)).

Figure 4.6(b) shows that at a fixed total charge of 0.6%, the same yellowing inhibition could be obtained at a RS/UVA ratio of 0.25 or 7.75. With the same coat weight, the worst inhibition was obtained at a RS/UVA ratio of 4.

4.2.2 Effect of total charge on paper brightness stability

Figure 4.7 shows the effect of total inhibitor charge on PC number at (a) a fixed RS/UVA ratio of 4; (b) a fixed coat weight of 4g/m^2 per side. Yellowing inhibition increased at a higher total inhibitor charge, and the same trends were observed at various coat weights from 4 to 8 g/m^2. However, Figure 4.7(b) shows that the dependence of yellowing inhibition on total charge varied with the RS/UVA ratio. This is due to the strong interaction between the total charge and RS/UVA ratio, as seen in Figure 4.5. The actual RS and UVA charges are determined by both the RS/UVA ratio and total inhibitor charge.

The effect of total charge on yellowing inhibition was greater at a lower RS/UVA ratio. An increase in total charge from 0.2% to 0.6% decreased the PC number by 3.1 units at a RS/UVA ratio of 0.25, compared with only 0.6 drop at a RS/UVA ratio of 7.75. Further increase in total charge above 0.6% at a RS/UVA ratio of 7.75 had a negligible improvement in inhibition. Figure 4.7(b) also confirms the conclusion from Figure 4.6(b) that the same inhibition can be obtained at 0.6% with either 7.75 or 0.25 RS/UVA ratio.

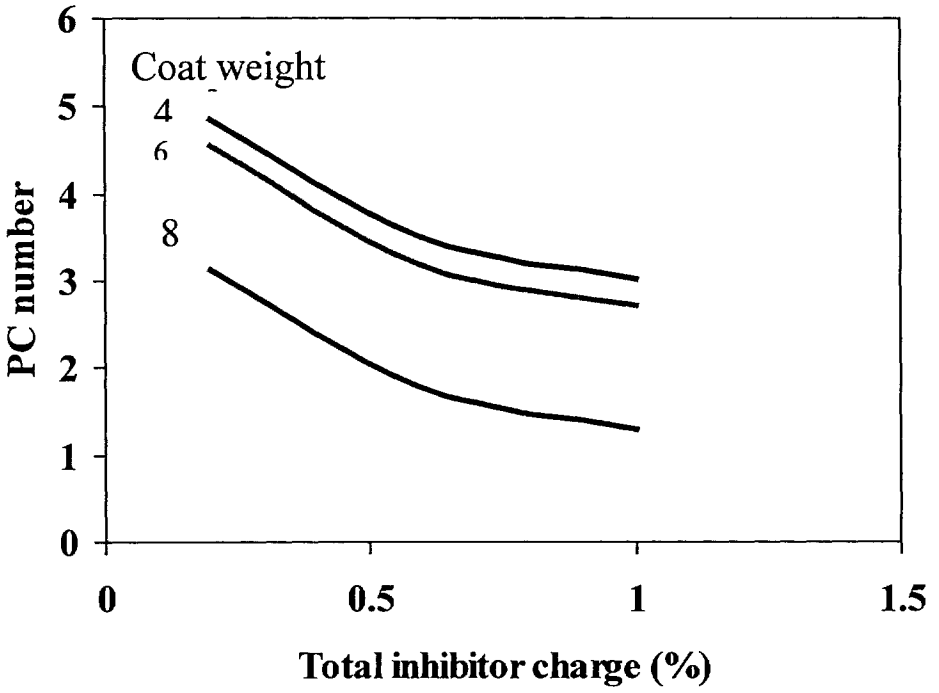

(a) At RS/UVA of 4

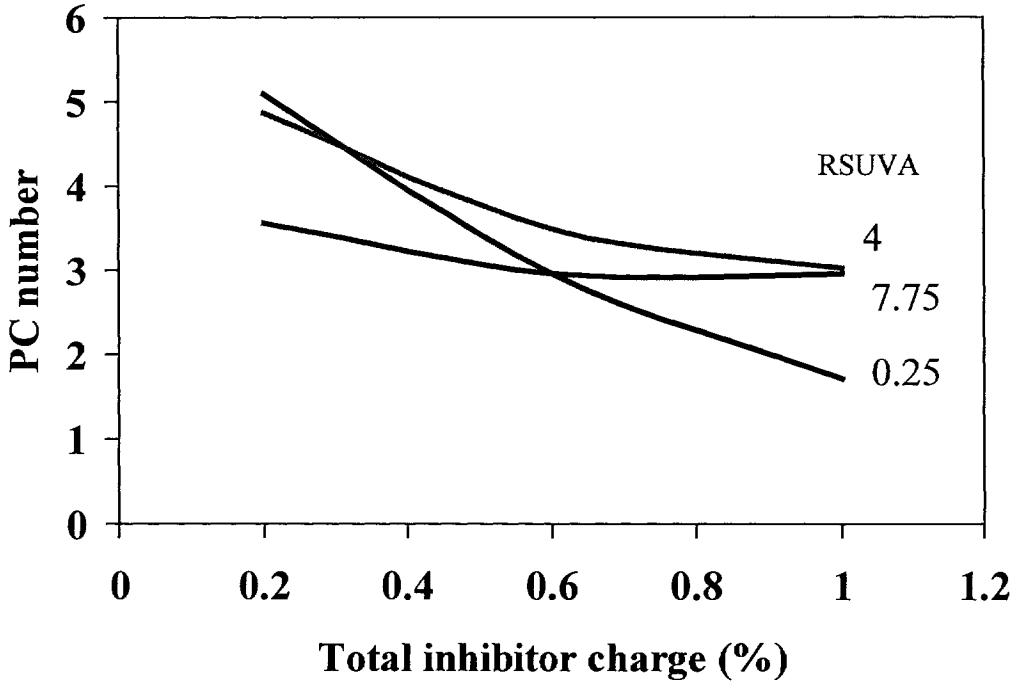

(b) At coat weight of 4 g/m^2

Figure 4.7 Effect of total inhibitor charge on PC number at: (a) a fixed RS/UVA ratio of 4; (b) a fixed coat weight of 4 g/m^2.

At a total charge below 0.6%, a higher RS/UVA ratio of 7.75 should be used to get a higher yellowing inhibition; at a total charge above 0.6%, a lower RS/UVA ratio of 0.25 is preferred. Figure 4.7 again shows that various combinations of coat weight, RS/UVA ratio, and total charge could be used to achieve the same yellowing inhibition. For example, to get a final PC number of 3 after 12 days of accelerated irradiation, a total charge of 0.25% or 0.75% should be used respectively on 8 or 6 g/m^2 coated paper at a RS/UVA ratio of 4. Better yellowing inhibition could be obtained by either increasing coat weight or total inhibitor charge. The choice of coat weight and inhibitors mainly depends on the paper end use requirement and the relative cost of radical scavengers and UV absorbers.

4.2.3 Effect of RS/UVA ratio on paper brightness stability

Figure 4.8 shows the effect of RS/UVA ratio on the PC number at (a) a fixed total charge of 0.6%; (b) a fixed coat weight of 4 g/m^2 per side. Figure 4.8(a) confirms that at a total charge of 0.6% and various coat weights, a RS/UVA ratio of 0.25 or 7.75 lead to the same yellowing inhibition while the ratio at 4 gave the worst inhibition. However, Figure 4.8(b) shows that at a total charge of 0.2%, PC number decreased with increasing RS/UVA ratio. For 1% total inhibitor charge, a lower ratio of 0.25% is preferred.

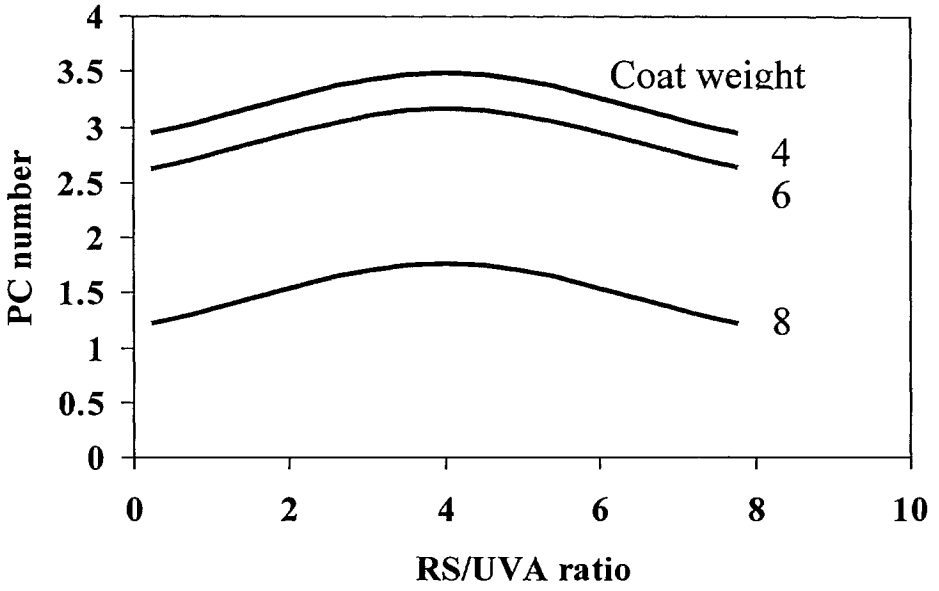

(a) at total charge of 0.6%

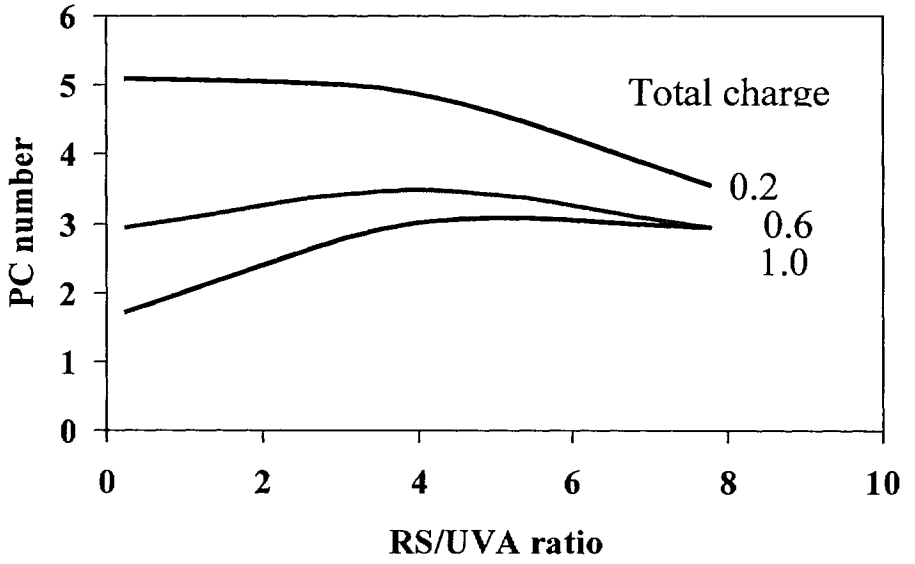

(b) At coat weight of 4 g/m^2

Figure.4.8. Effect of RS/UVA ratio on PC number at: (a) a fixed total charge of 0.6%; (b) a fixed coat weight of 4 g/m^2.

4.2.4 Effect of yellowing inhibitor and coat weight on paper initial brightness

Figure 4.9 shows the effect of yellowing inhibitors on paper initial brightness at a coat weight of 6 g/m^2. At a low inhibitor charge or low RS/UVA ratio, inhibitors had negligible effect on paper initial brightness. However, at a high inhibitor charge, paper initial brightness decreased with the increase in RS/UVA ratio. In other words, initial brightness decreased with the increase of RS charge at a certain total charge. The paper treated with 1% total charge at a RS/UVA ratio of 7.75 had the biggest ISO brightness drop of 2.3%. (78.4% vs. 80.7% for the control).

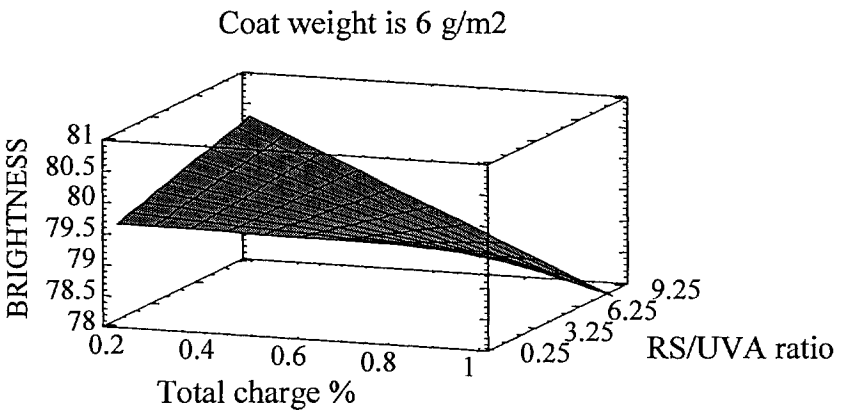

Figure 4.9 Effect of yellowing inhibitors on paper initial brightness at a coat weight of 6 g/m2.

Figure 4.10 shows that initial brightness increased at a higher coat weight. This could be explained by the fact that coating coverage on paper surface increased with increasing coat weight [130]. Figure 4.10 also shows that the initial brightness drop due to inhibitors is less at a higher coat weight.

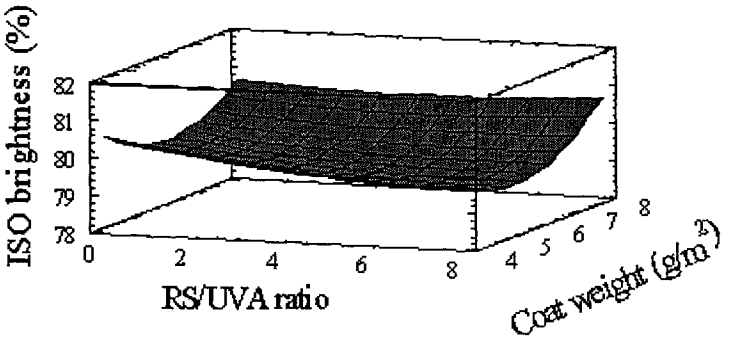

Figure 4.10. Effect of yellowing inhibitors on paper initial brightness at an inhibitor Charge of 0.6%.

The yellowing inhibition was affected by three factors: coat weight, total inhibitor charge, and ratio of radical scavenger and UV absorber (RS/UVA). The response equations describing the relationship between these factors and paper brightness stability were obtained through a statistical approach.

The results presented here illustrate that the total inhibitor charge has the largest effect on the yellowing inhibition, which is independent of the coat weight, but strongly depends on the ratio of RS/UVA. A higher coat weight leads to a better yellowing inhibition. This trend remains the same at various inhibitor charge and ratio.

At a low total inhibitor charge or low RS/UVA ratio, inhibitors had negligible effect on paper initial brightness. However, a high RS/UVA ratio decreased paper initial brightness at a high inhibitor charge. The initial brightness drop due to the inhibitors was smaller at a higher coat weight.

Small amount of additives such as inhibitors increases the complexity of the system. This complexity is clearly illustrated by the difficulties encountered in trying to predict the rheological properties of the coating colors. These properties are very important for the runnability of a coating color during the coating operation.

Chapter Five

RHEOLOGICAL PROPERTIES OF YELLOWING INHIBITOR

In the previous chapter, we studied the effect of a number of parameters on the brightness stability of the final product when the yellowing inhibition system is added to the coating formulation. We studied the effect of adding these components in the particular concentrations, which are amenable to the specific industrial application. Therefore we do understand the limitation of our findings from the point of view of in-depth academic study. However, the results are of extreme importance to the paper coating industry. Since the rheological properties of the coating colors are to an appreciable degree governed by the interaction between coating components and the inhibitor, in this chapter, interest is mainly focused on the rheological properties of inhibitors. There is strong industrial interest in using the inhibitors as additives to the coating color, which is applied on the surface of the paper. However, the device of application is still under study.

5.1 Steady State Flow Study

The flow curve of any sample provides the correlation between the assigned shear rate and the resulting shear stress in CR mode. Our experimental strategy included measurements for the component materials; Radical Scavenger and UV absorber (the structure in Appendix C). First let us discuss the results of testing the inhibition system. The rheological results for each of the inhibitor elements cibafast h (UVA1), PAX (RS) and tin1130 (UVA2) revealed quite different patterns. Figure 5.1a shows the flow curves in terms of viscosity-shear rate for RS and UVA1 for shear rates up to about 700 1/s.

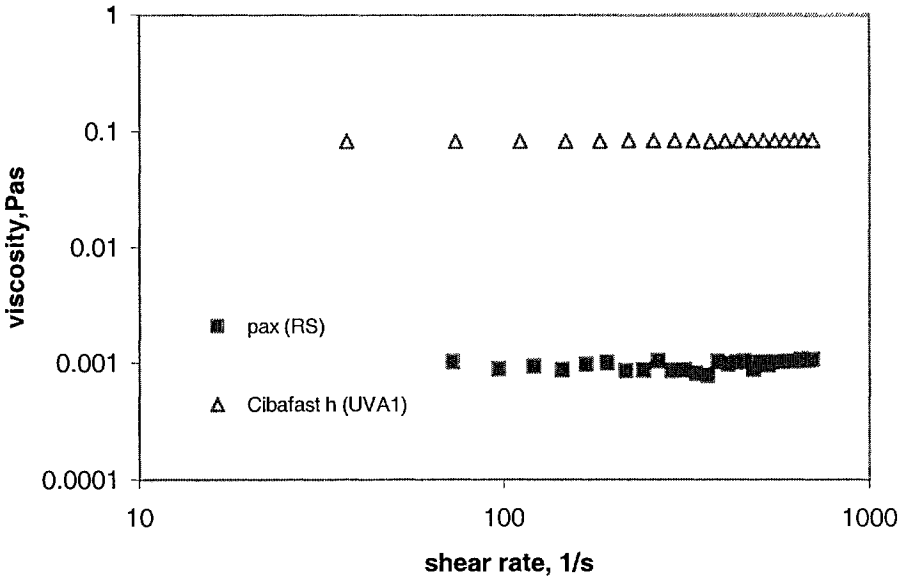

Figure 5.1a Viscosity-shear rate of RS and UVA1

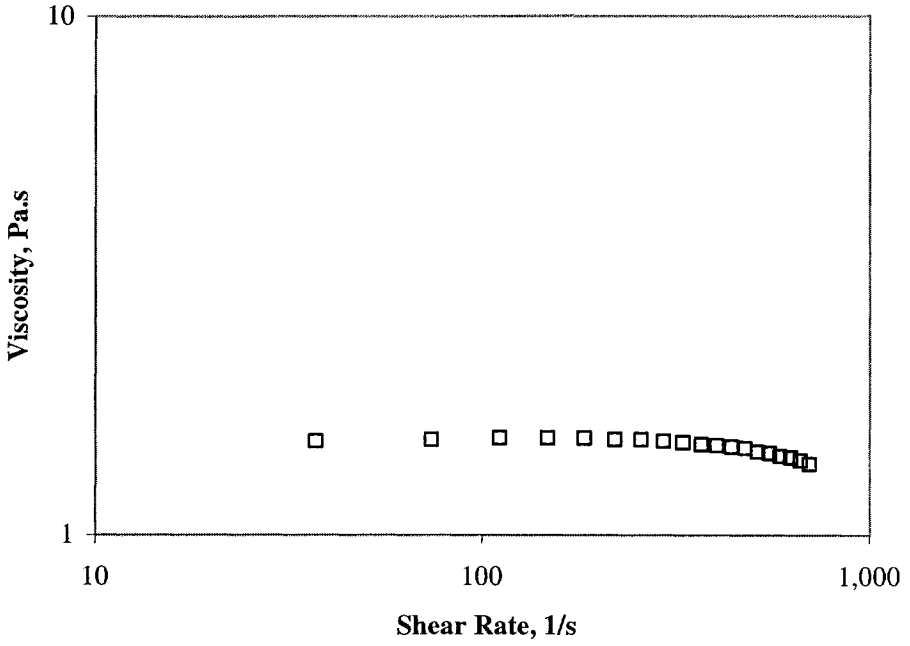

Figure 5.1b Viscosity-shear rate of UVA2

The graphical results show that the viscosity is independent of shear rate. The flow curve of UVA2, Figure 5.1b, reveals shear-thinning behavior for higher shear rates (over 200 1/s). Regression analysis was carried out on the experimental points using different models. The analysis shows that the behavior of RS and UVA1 follows Newton's Equation, which is a suitable model for flow measurements. This can be written as

$$\tau = \mu \gamma,$$

where τ [Pa] is shear stress, γ [s^{-1}] is shear rate, η is the viscosity. The results are shown in Table 5.1.

Table 5.1 Regression coefficients

Material	*η (Pas)*
Cibafast h	0.083
Pax	0.001

Regression analysis in the case of UV Absorber2 (tin1130) showed that it followed the Ostwald-de Waele model. This can be written as: $\tau = k \gamma^n$ where k = 1.8 is consistency as a viscosity related constant, and the exponent (slope of the log-log flow curve) is n = 0.96. The exponent is slightly lower than the Newtonian value of n=1, in agreement with the pattern shown in the flow curve Figure 5.1b. Obviously, the UVA2 is significantly more viscous than the RS and UVA1.

It is observed from Figure 5.2 that the flow curves in terms of shear stress-shear rate for yellowing inhibitors are linear.

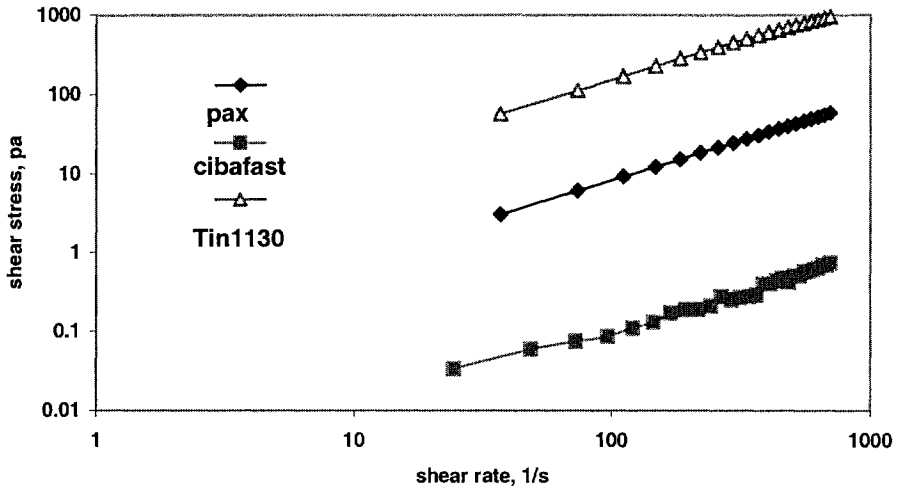

Figure 5.2 Shear stress-shear rate behavior of cibafast, pax and tin1130.

5.2 Transient Shear Stress Response

Transient test was conducted for cibafast h, pax and tin1130, the test was performed for 5 min, for a number of constant value shear rates over a range of 0.6 and 10 s^{-1}. Figure 5.3 shows that at low shear rate = 0.6 s^{-1}, there is no transient effect. Despite increasing the shear rate up to 10 s^{-1} as observed in Figure 5.4, there is no transient effect. Also, it is observed that UVA2 has high viscosity comparing to UVA1 and RS. On the other hand, this test revealed that there is no change in the viscosity of inhibitor under low shear rate.

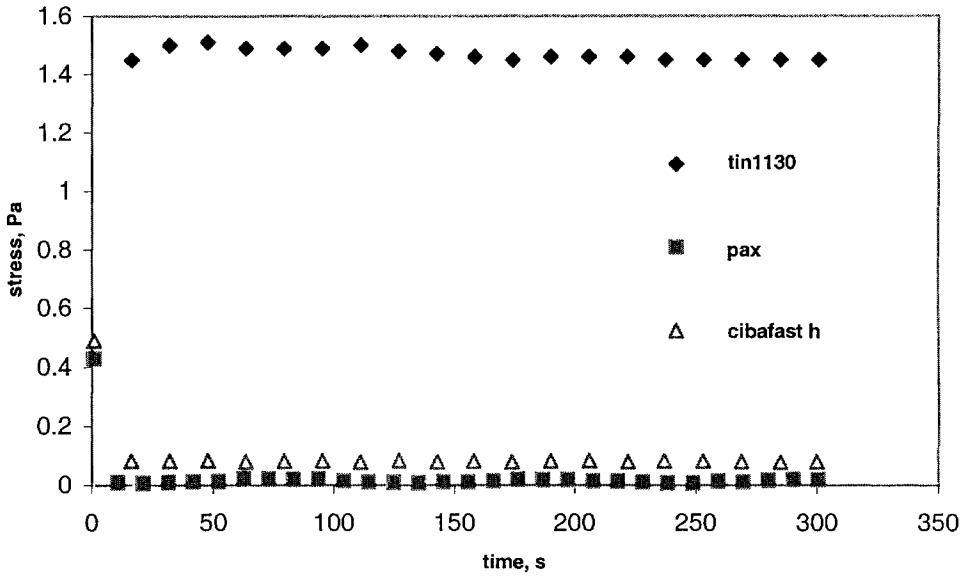

Figure 5.3 Transient shear stress response as a function of shear rate = 0.6 s^{-1}

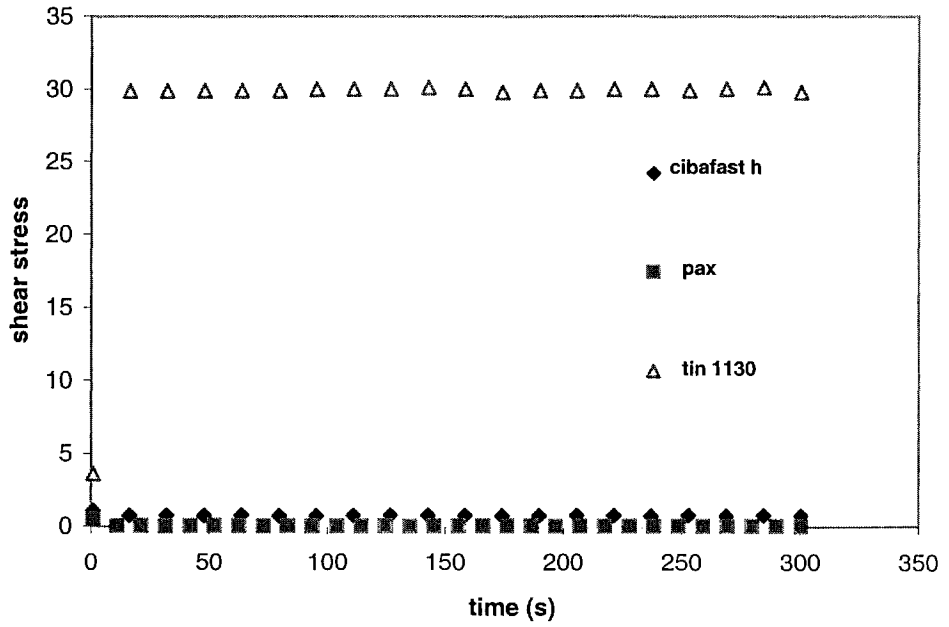

Figure 5.4 Transient shear stress response as a function of shear rate = 10 s^{-1}

Figure 5.5 revealed the yield stress test which was carried out for cibafast h, pax and tin1130. This test employed controlled stress mode to ramp stress until the assigned stress surpasses the yield value and the sample starts to flow. In the first segment, the

assigned stress ramped from 0.09 to 4 Pa to establish the up curve for pax (RS), cibafast h(UVA1) and tin1130 (UVA2). It can be noticed that there is no yield stress for inhibitors, therefore, inhibitors can flow easily without stress.

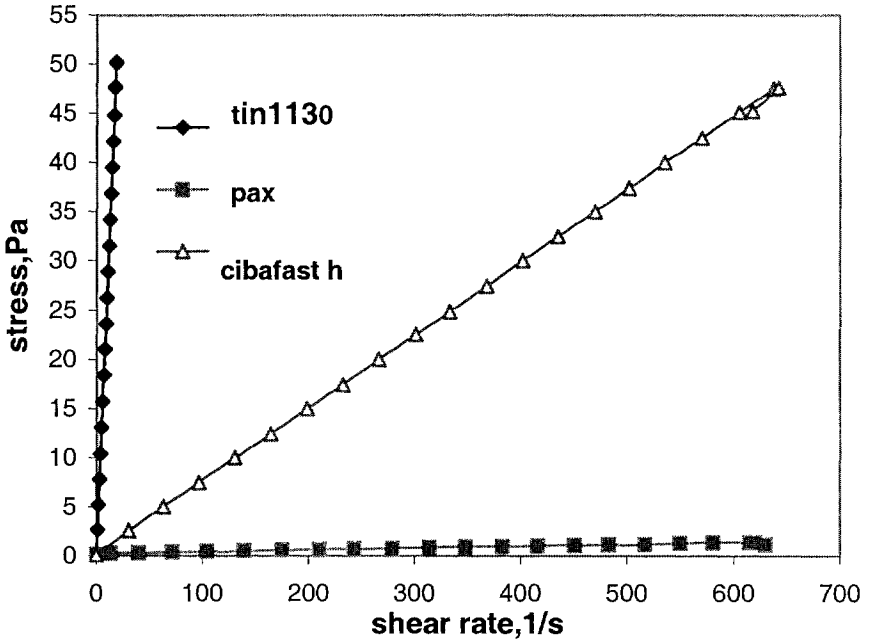

Figure 5.5 Yield Stress response of cibafast h, pax and tin 1130.

Figure 5.6 shows the result of the thixotropic test for RS (pax), UVA1 (cibafast h) and UVA2 (tin1130). The test was carried out for 3 minutes up to 700 1/s. While the RS and UVA1 have shown no thixotropy, UVA2 is clearly thixotropic. The results of these experiments are reported in Table 5.2. This indicates that the viscosity of UVA2 (tin1130) changes with time of shearing, which is related to the change in the microstructure of UVA2.

Table 5.2 Hysteresis Areas (Pa s^{-1}) of tin1130 (UVA2).

Pa s^{-1}	Tin1130
Up curve	580949
Time curve	0.00
Down curve	504510
Total	76439

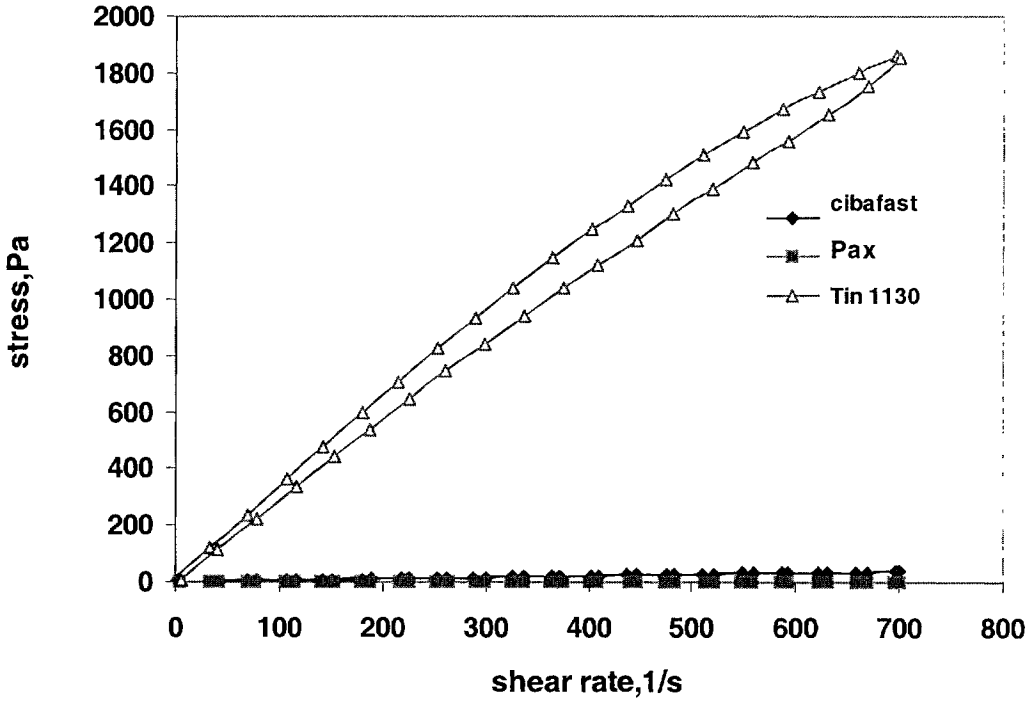

Figure 5.6 Thixotropic behavior of UVA1, UVA2 and RS.

It can be concluded that RS and UVA1 are simple Newtonian liquid, with water-like viscosity, while UV absorber (tin1130), which is hydrophobic polymer is a shear-thinning thixotropic liquid, and is considerably more viscous. Since, small amounts of inhibitors are important components of the color, they increase the complexity of the system. This complexity is clearly illustrated by the difficulties encountered in trying to predict the rheological properties of the coating colors. These properties are very important for the runnability of a coating color during the coating operation.

Studies of the rheology of color containing inhibitors are therefore highly motivated. Detailed understanding of the interaction between coating color ingredients and total charge of inhibitors and resulting rheological behavior is a subject of considerable concern.

Chapter Six

ON THE CHARACTERIZATION of the INTERACTIONS BETWEEN COATING COLORS and INHIBITORS

The properties of paper coatings are related to the coating structure, which is determined for a good part by pigment, pigment-inhibitor and binder-inhibitor interactions. Addition of chemicals into a coating suspension can induce the destabilization of the pigment particles and the formation of agglomerates. In this chapter we study the addition of inhibitor that interacts with clay and binder studied using light scatter and zeta potential.

We also study the interaction between paper coating colors, and yellowing inhibitors, which were added to coating colors to increase the stability of paper brightness. We measure the surface potential of ground calcium carbonate and kaolinite particles. The measurements revealed the influence of adsorption of inhibitors on ground calcium carbonate and kaolinite particles and that it is also related to the changes in the rheological properties.

6.1 Effect of interfacial properties

Coating colors are very complex concentrated suspensions. After the addition of yellowing-inhibitors to kaolin and ground calcium carbonate dispersion, they interact with kaolin and ground calcium carbonate (GCC) particles. This is followed by adsorption of inhibitors onto the surface of kaolinite and GCC particles. Figures 6.1 and 6.2 show the interfacial properties of kaolinite and GCC particles without and with inhibitors. The surface potential of GCC particles increases with RS, UVA and with the combination of UVA & RS. This clearly demonstrates that there is adsorption of inhibitors onto the particle surface. The GCC and kaolin concentration used for measuring zeta potential is 0.025%. Moreover, UVA (polymeric solution) interacts and adsorbs on kaolin particles. Its surface potential is high comparing to RS and combination of UVA & RS, while the addition of RS on kaolin decreases the surface potential. We may deduce that RS maximize the repulsive force between kaolinite particles and disrupts the aggregation.

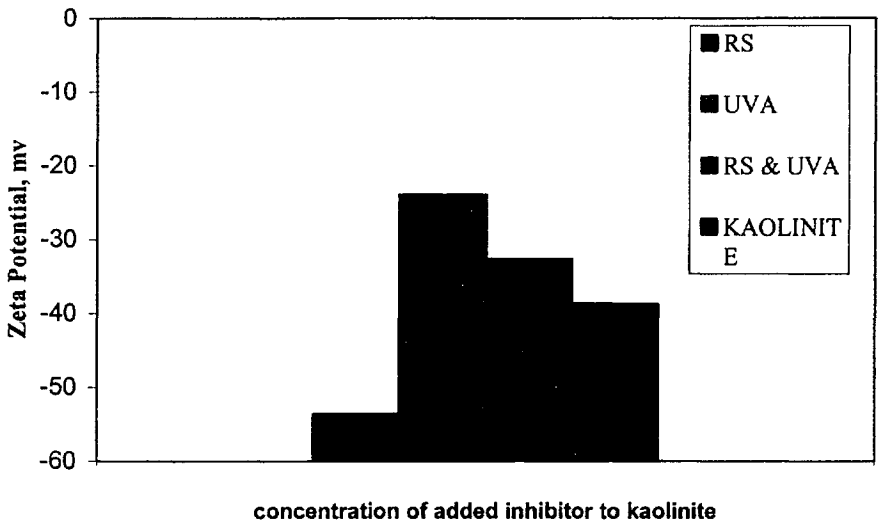

Figure 6.1. zeta potential vs. percentage concentration of added inhibitor to kaolinite.

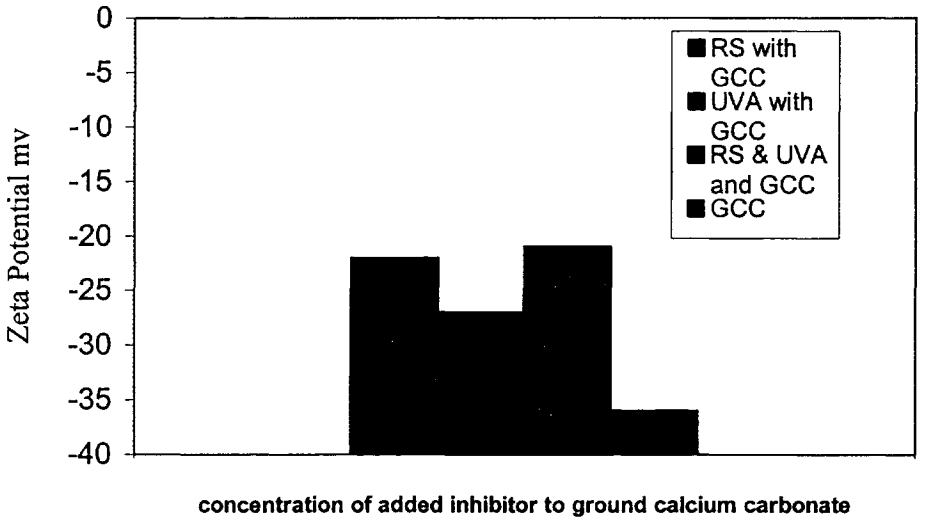

Figure 6.2. zeta potential Percentage concentration of added inhibitor to ground calcium carbonate

In general, aqueous colloidal particles are stabilized by (a) electrostatic repulsion due to coulombic forces, (b) steric repulsion from an adsorbed polymeric layer of co-

binder and inhibitor, (c) depletion forces due to non adsorbing high molecular weight co-binder species. The colloidal stability of coating formulations is usually determined by a combination of the above forces [50]. Therefore, the resulting wet coating structure falls into two major classes: highly flocculated structured (agglomerated pigment particles) or a network structure of pigment and inhibitor.

The above results can be revealed, as the UVA is hydrophobic and thus adsorbed more readily onto the surface of kaolinite and GCC particles, increasing the surface potential and causing aggregation. On the other hand, RS interacts and adsorbs on the GCC particles and causes aggregation.

Figure 6.3 reports the zeta potential of kaolinite and ground calcium carbonate particles as a function of added different concentration of inhibitors at pH 8. It can be seen that the zeta potential of ground calcium carbonate particles decreases with the concentration of inhibitor. Also, the zeta potential of kaolinite particles decreases with the concentration of inhibitors. As we mentioned above, the inhibitors are a combination of radical scavenger and the UV absorber. The ratio RS/UV absorber is 4. Radical scavenger (hydroxylamine salt) is soluble in water when it has been added to kaolinite.

The positive ions of salt interact with the surface of kaolinite producing a negative surface charge. Therefore, it prevents kaolinite from aggregation. The main chain, -$OCH_2C\ H_2$- in UV absorber, as shown in A3, is weakly hydrophilic. After the addition of inhibitor to kaolin dispersion, the UV absorber adsorbs onto the surface of kaolinite particles. It is observed from optical microscope that ground calcium

carbonate particles start to aggregate more than kaolinite particles after the addition of inhibitors. Therefore, the surface potential of ground calcium carbonate particles is higher than kaolinite particles.

The concentration of radical scavenger is 4 times larger than UV absorber. The interfacial properties can be noticed in Figure 6.3. This clearly demonstrates that there is a significant adsorption of inhibitors onto the ground calcium carbonate particle surfaces. The surface potential of kaolinite and ground calcium carbonate particles increases significantly.

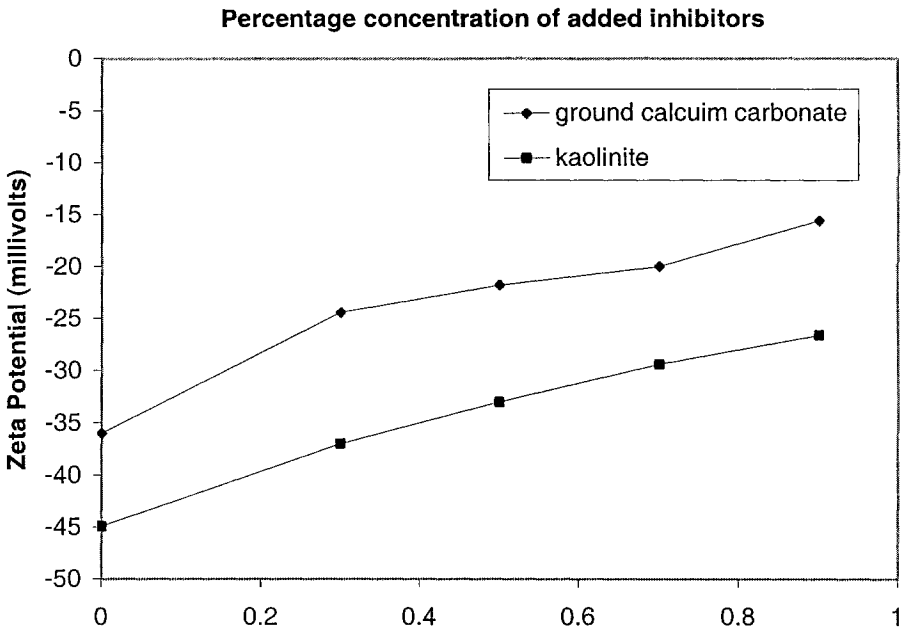

Figure 6.3 Zeta potential of kaolinite and ground calcium carbonate particles vs. concentration of added inhibitors at pH 8.

6.2 Study the Interaction Between Coating Components

Zeta potential can be used to study the interaction between colloidal suspension particles. On the other hand to understand the interaction between non-colloidal materials, we used Photo Correlation Spectroscopy. Also, it can be used for colloidal materials. In this study, Photo Correlation Spectroscopy was used to observe the track of inhibitor in consideration of coating components pigments, starch and polymer separately by laser light scatter.

Figure 6.4 shows the diameter of the particle of pigment (kaolinite and ground calcium carbonate) without inhibitor and with different inhibitors. It is observed that diameter of the particles of pigment decreases with radical scavenger (RS), while the

diameter of the particles of pigment increases with UV absorber and with the combination of UV absorber and radical scavenger. The explanation may be that the agglomerated pigment particles have been broken down by radical scavenger. It was found from the interfacial properties that the radical scavenger broke down the crystal of kaolinite. Since UV absorber adsorbs on kaolinite and ground calcium carbonate particles, therefore the diameter of pigment particles increases with UV absorber. Also, the adsorption of radical scavenger and UV absorber on the ground calcium carbonate can be as a result of increasing the diameter of pigment particles.

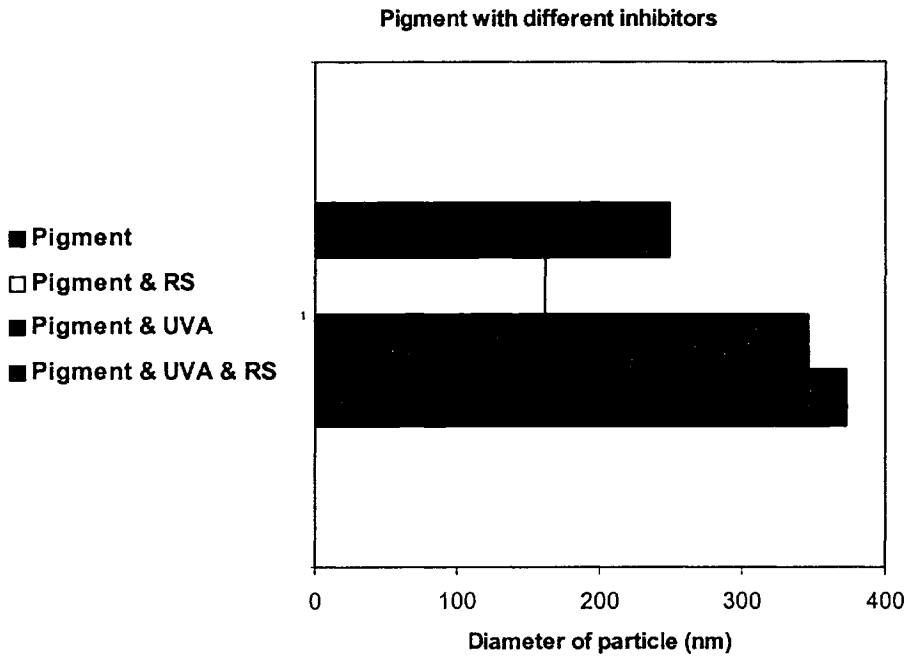

Figure 6.4. The effect of inhibitors on the pigment.

Figure 6.5 describes the interaction between binder (starch) and inhibitors where the interparticle interaction depends on inhibitor type. The addition of radical scavenger and the addition of the combination of radical scavenger and UV absorber have insignificant effect on the starch. While the addition of UV absorber broke down the

structure of the starch. We can conclude that UV absorber acts as a dispersal agent of the starch.

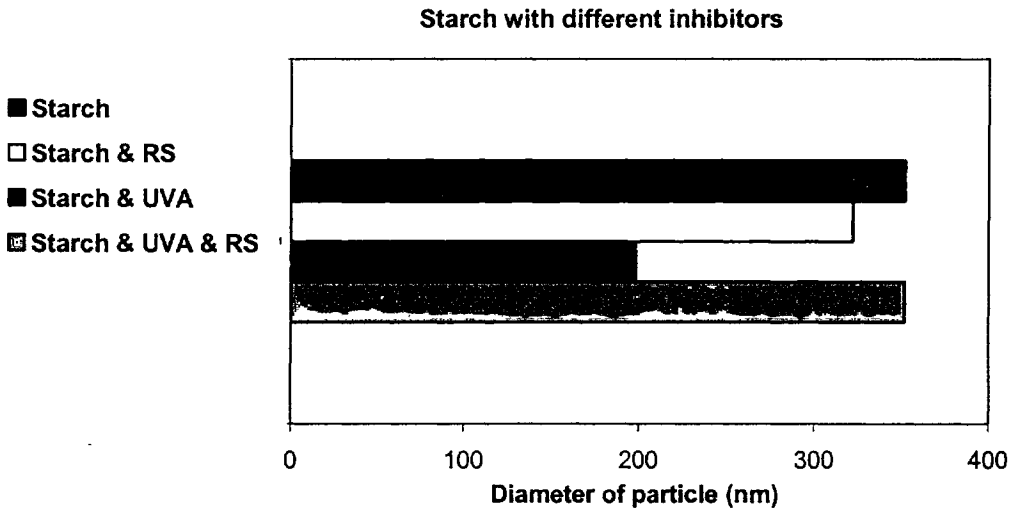

Figure 6.5. The effect of inhibitors on the starch.

Figure 6.6 reveals that the inhibitors have insignificant effect on the combination of additives and latex. It can be concluded that there are several types of interactions having different strengths of association between the different coating components and inhibitors. These include flocculation of pigment particles with each other, as well as interactions between pigment/inhibitor particles, starch/inhibitors as discussed above.

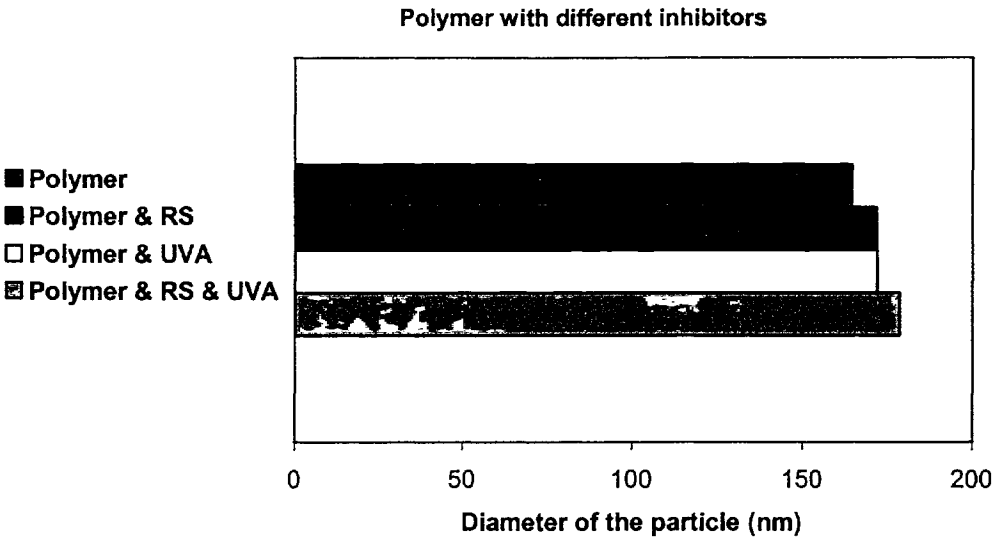

Figure 6.6. The effect of inhibitors on the polymer.

6.3 Effect of water retention properties

Dewatering of coating colors during coating applications affects the coater runnability and the final paper properties. Dewatering of coating colors depends on particle-particle interactions, polymeric additives and the base paper properties. Loss of water between application and metering will lead to a high solids level and cause disruption of flow and increase the defects on coated paper. Therefore, in this work, the effect of the yellowing- inhibitors on water loss has been studied. Figure 6.7 shows that the water loss of coating colors increases with time. The same pressure (15 psi) is used in all experiments.

Some water is involved in the pigment and inhibitor network structure through hydrogen bonding and some remains as bulk water. It is observed that the coating colors with UVA have the strongest water holding capability followed by those paper coating color without inhibitors, with combination of RS&UVA and finally with RS. The radical scavenger is adsorbed onto ground calcium carbonate particles and disrupts the aggregation of kaolinite. Also, ground calcium carbonate weight is four times more than kaolinite weight in this work.

Therefore, water retention of coating color containing radical scavenger is less than other samples. UVA has insignificant effect on the water loss of paper coating color compared to the RS because of the difference in the concentration. We conclude from these results that inhibitors decrease the water retention of coating colors. The explanation may be that the packing of the pigment particles becomes more open for coating containing inhibitor. Because of the more open structure, the water drains faster causing less water retention. This will be observed in the microstructure (chapter 8).

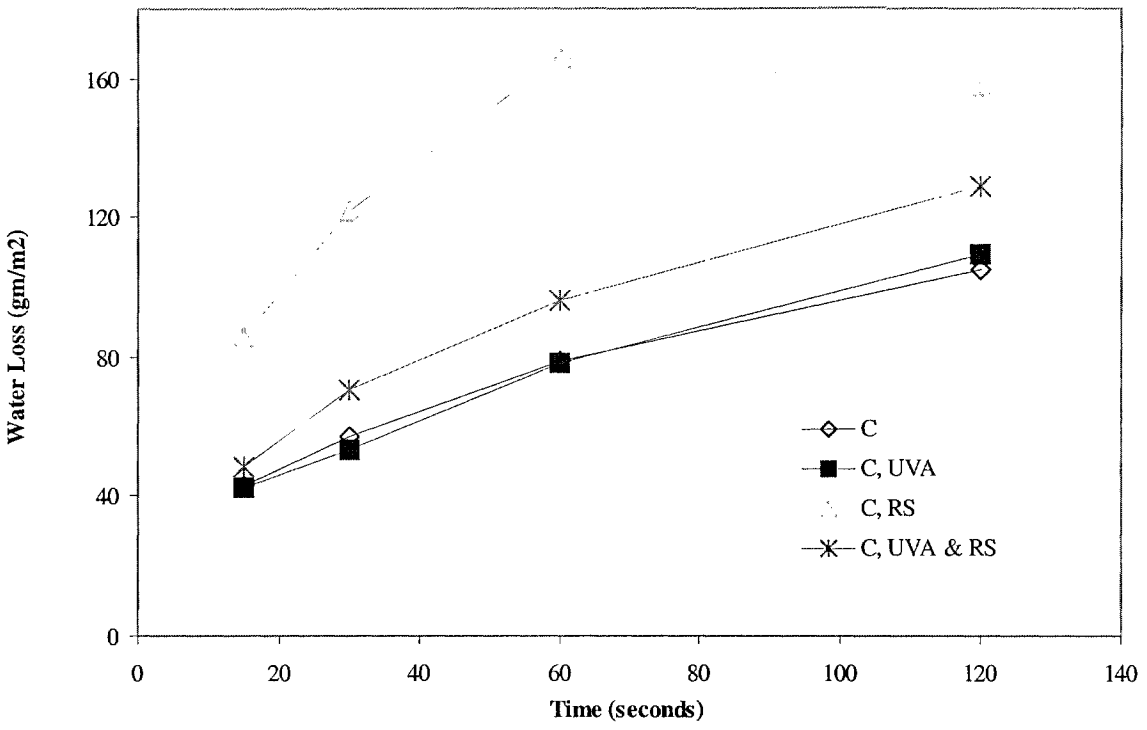

Figure 6.7.water loss of coating dispersion Percentage concentration of added inhibitor.

Figure 6.8 shows measurements taken at various time and total charge of inhibitor. The coating formulation including 1% total charge has the highest water loss. This indicates that the packing of the coating color particles becomes more open at high levels of total charge addition. Addition of 0.6% total charge of inhibitor to the coating formulation resulted in the particles becoming more densely packed than in the case of 0.2% total charge. The coating color with total charge (0.2%) has the strongest water holding capability followed by that with 0.6% and finally with 1%.

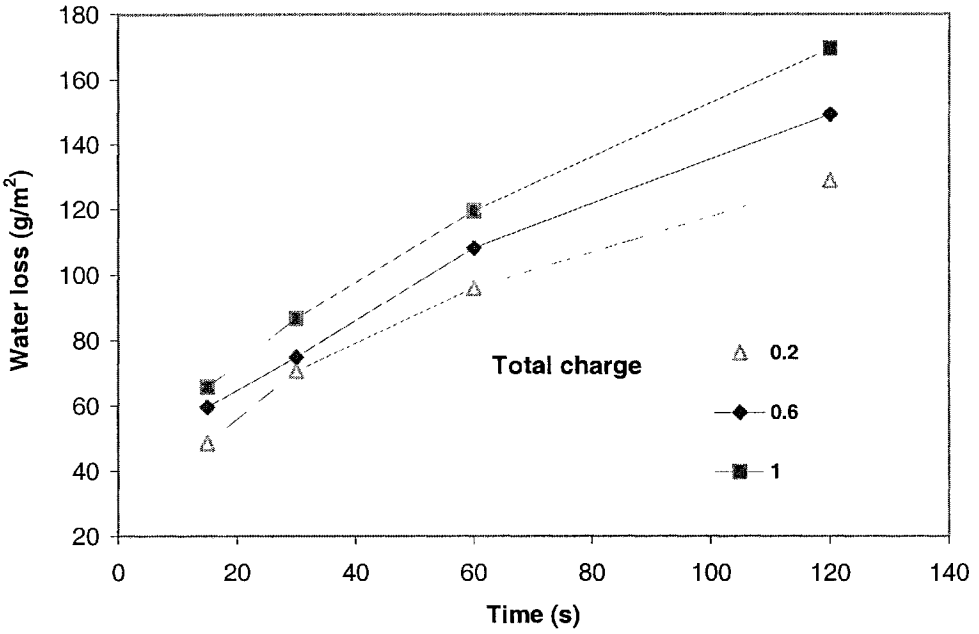

Figure 6.8. Water loss of coating formulation with different total charge.

Paper coating formulations are complex colloidal systems. The different components interact to generate different types of associations which give rise to a "wet coating structure". This structure impacts on the dewatering rate and the coating color rheology. During the coating process there is some breakdown of structure under shear followed by a recovery. It is suggested that the shift in the onset of consolidation could be due to flocculation of the pigment induced by the inhibitor.

The importance of the interactions between the coating color components is a marked effect on the rheological properties. These properties are very important for the runnability of coating color during the coating operation.

Chapter Seven

The Effect Of Yellowing Inhibitor System On The Rheological Behavior Of Paper-Coating Formulation

Coating formulations have complex rheological properties. The rheological properties of different inhibitors are studied to evaluate the impact of inhibitors on the coating colors. The interaction between paper coating colors, and yellowing inhibitors, which are added to coating colors to increase the stability of paper brightness is studied. Moreover, coating rheology affects the quality of coated and printed-papers through their influence on the dynamics of coating color delivery.

7.1 Rheological Properties of Coating Colors

A variation in viscosity is observed as the yellowing inhibitor system changes from one formulation to the other. This test describes the flow behavior of coating formulations including different inhibitors components. In addition measurements were conducted for the coating formulation with RS, the coating formulation with UVA, and the coating formulation with both elements of the yellowing inhibition system RS and UVA as shown in Figure 7.1. Appendix, C, shows the coating color formulations.

It is observed that RS gave the highest viscosity of coating formulation at total charge 0.6% and RS/UVA 7.75, however, UVA and the combination of UVA and RS appear to have slight effect on the viscosity of coating formulations. Figure 7.2 shows the

flow curves in terms of shear stress- shear rate relationships, which are plotted over a log-log scale that includes shear rate from 1 to 749.79 s^{-1}. A consistent nearly linear pattern is recorded for all coating formulation.

Figure 7.3 reveals the yield stress of coating formulations without inhibitor and with different inhibitors. This test employs controlled stress mode, the assigned stress ramp from 0.9 to 4 Pa to establish the up curve. Inhibitors have insignificant effect on the yield stress of coating formulations. In this study, it is observed that all coating formulations with and without inhibitor have yield stress. The sample needs 2.1-2.5 Pa to start to flow despite the difference of degree of interaction between the inhibitor and coating components for each sample.

It is concluded that the coating formulation behavior is shear thinning or pseudo-plastic liquid with yield point that is corresponding toplastic liquid. RS increases the viscosity of coating formulations.

Key properties of the four coatings colors are presented in Table 1

Table 7.1 Key properties of the coating colors

Inhibitor type in coating color	Solid content, wt. %	Density (g/ml)
Without inhibitor	55	1.389
With UVA	55	1.25
With RS	55	1.17
With UVA&RS	55	1.15

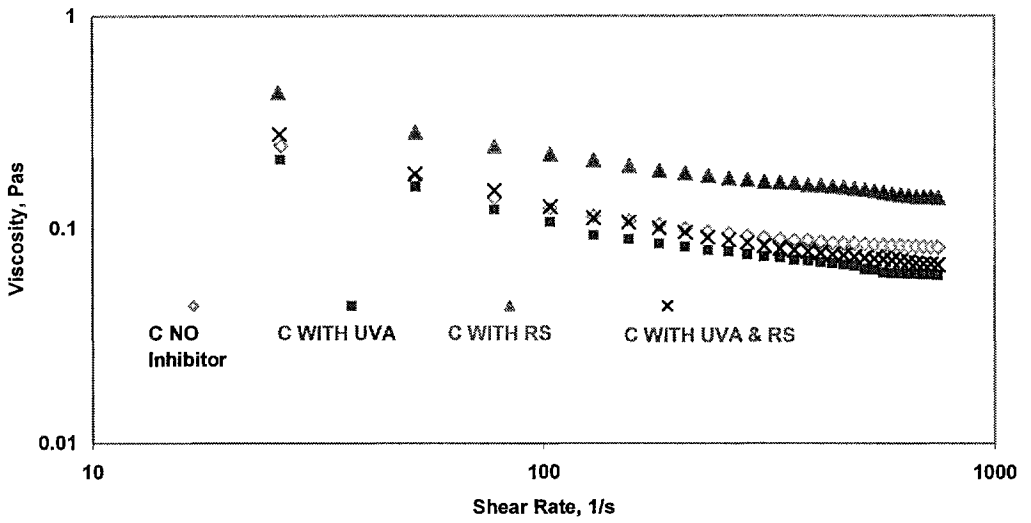

Figure 7.1 Viscosity-shear rate behavior of coating formulation (C), C with UVA, C with RS, C with RS & UVA.

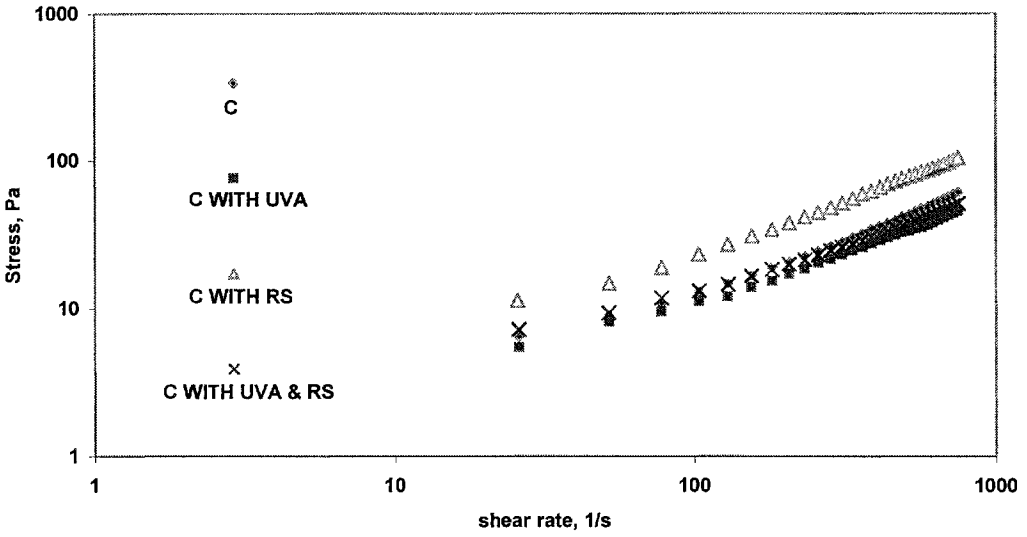

Figure 7.2. Shear stress-shear rate of coating formulation (C). C, C with UVA, C with RS, C with RS & UVA.

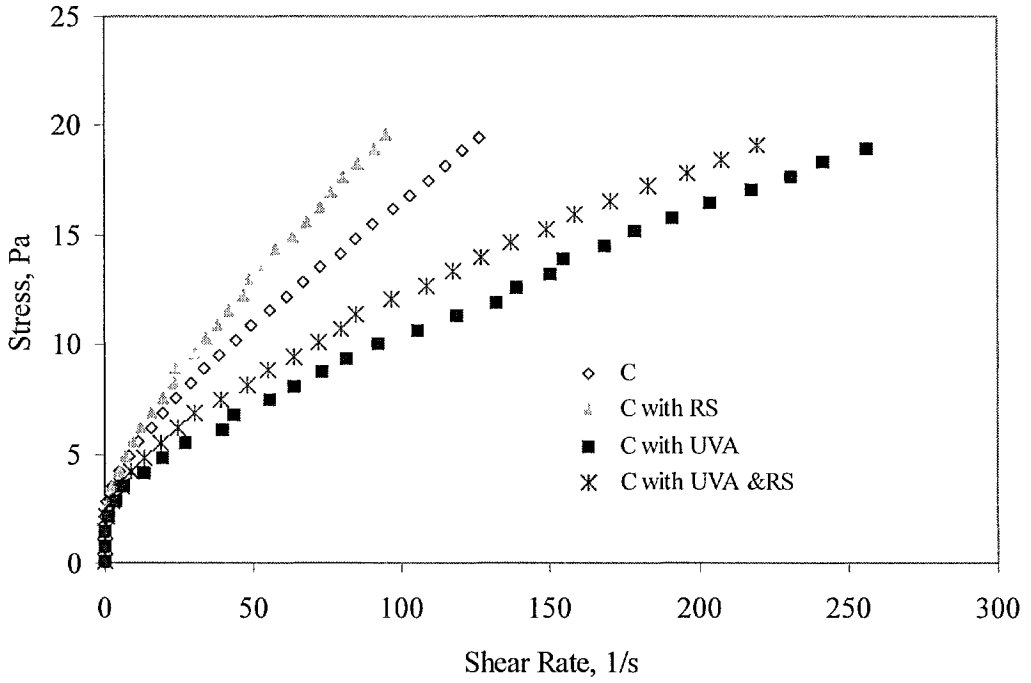

Figure 7.3 Yield stress of coating colors.

7.1.1 Viscosity of Coating Colors Containing Inhibitors at High Shear Rates and Different Temperatures

During the application, high shear rate will create heat in the application nip. Therefore, it is worthwhile to discuss the temperature dependence of coating properties. We ran tests for the coating formulation C, the coating formulation with the UVA additive, the coating formulation with the RS additive, and finally the coating formulation with both, UVA and RS, additives. These tests were conducted in thermally controlled environment, producing results for the following temperatures 25, 45, 60 and 75 degrees Celsius.

Figures 7.4, 7.5, 7.6 and 7.7 show the flow curves in terms of viscosity-shear rate for the tested samples. The range of shear rates in these tests extended from 0.015 to 18,000 s^{-1}. Increasing the temperature from 25 to 75 C° reduces the viscosity of paper-coating colors. The coating formulation behavior is shear thinning till the shear rate is high enough. The increase in viscosity followed by decrease of viscosity with increasing shear rate is seen for all coating formulations. This is because the particle ordering will break down and clumps of particles are formed. The formation of these clumps is temporary across the flow. This disruption is an increase in viscosity followed by sharp decrease in viscosity for all the samples. The viscosity of coating colors containing RS, hydroxylamine salt, is high compared to other coating colors followed by coating color containing UVA and finally with the color containing the combination of UVA and RS. The above results can be explained by the degree of

interaction between RS and the ground calcium carbonate and coating components to form flocs. It is concluded that the viscosity is decreasing with increasing the temperature, till specific shear that is high enough to thicken the sample to cause shear thickening, which followed shear thinning.

One may argue that viscous heating may be a strong factor in these tests. All coating colors were tested under the same conditions. The differences between all tests are the additives. If viscous heating were a significant factor in comparison to the influence of the additives, the similar viscous heating effects would have led to the same results regardless of the additives. Since this is not the case, it is realistic to associate the difference in viscosity to the type and the concentration of inhibitor.

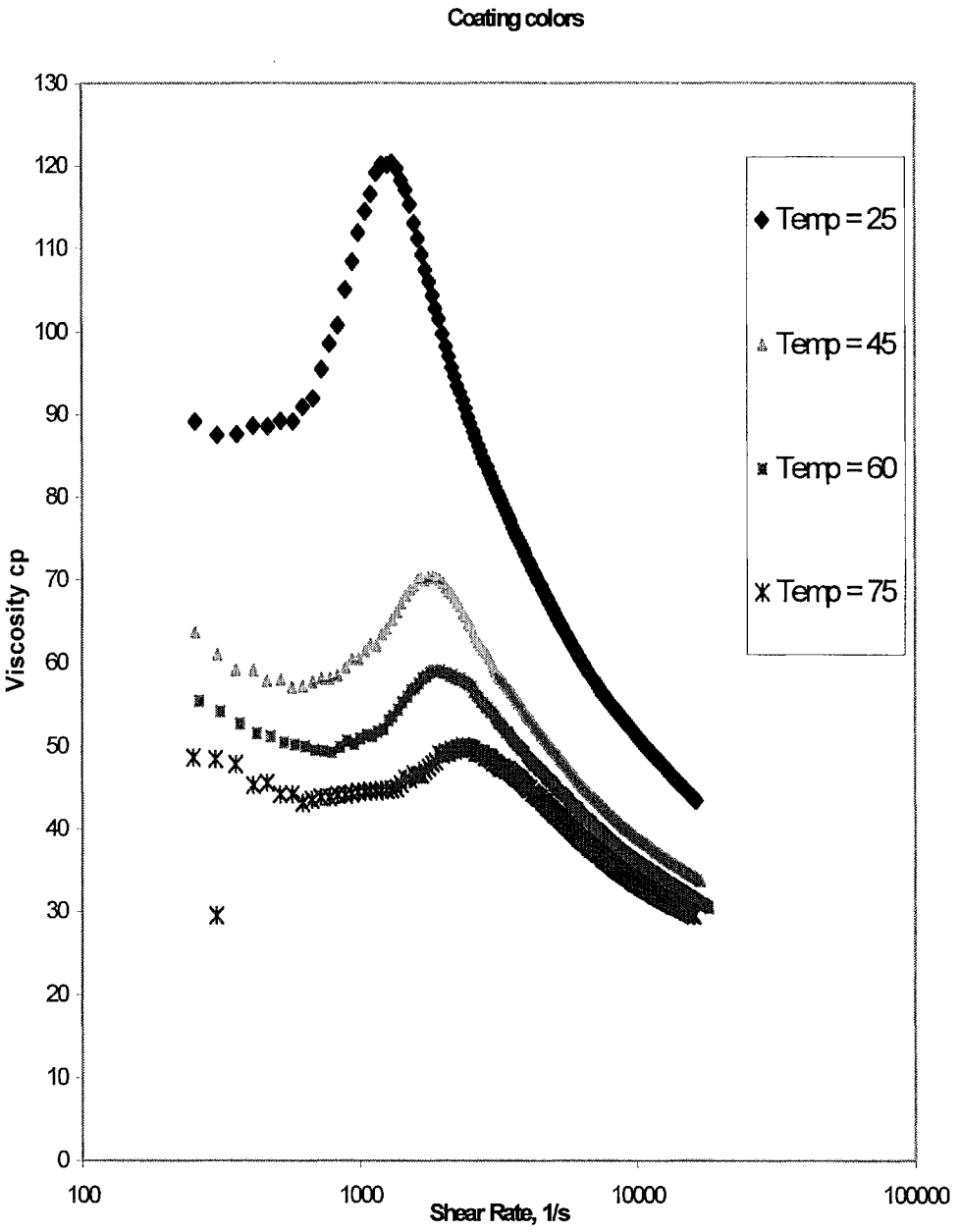

Figure 7.4 Viscosity as a function of shear rate for coating color at different temperatures.

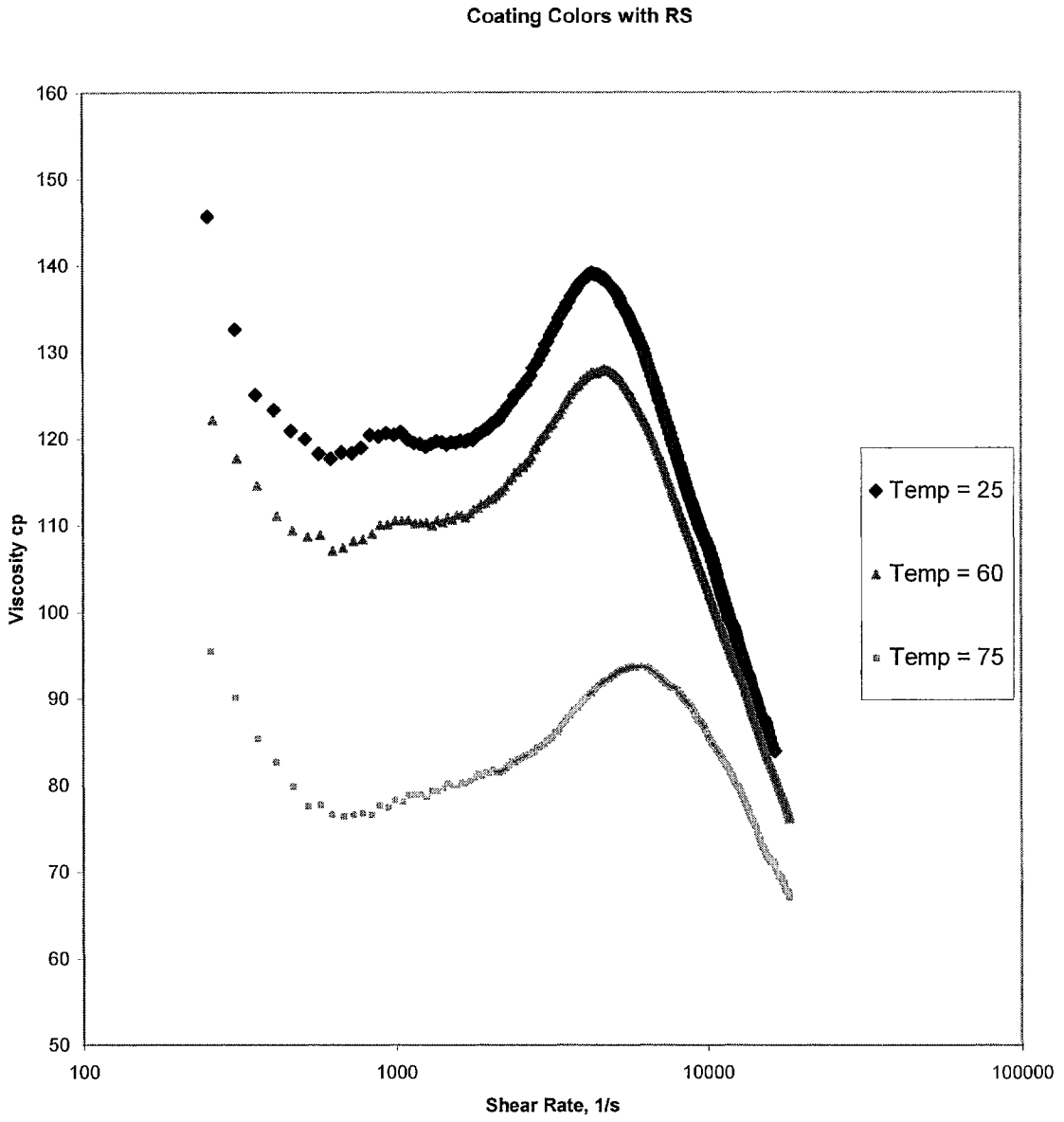

Figure 7.5 Viscosity as a function of shear rate for coating color containing RS at different temperatures.

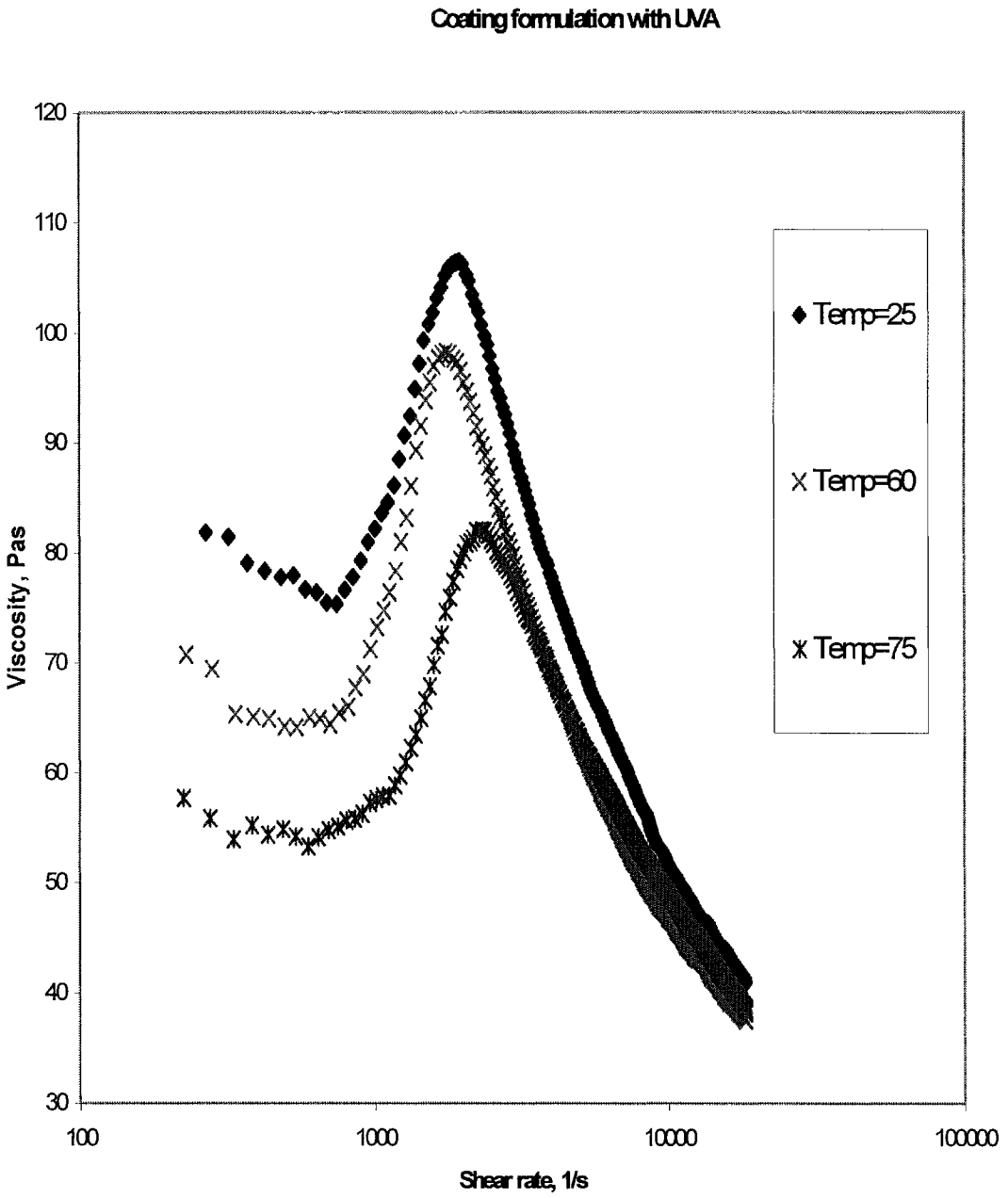

Figure 7.6 Viscosity as a function of shear rate for coating color containing UVA at different temperatures.

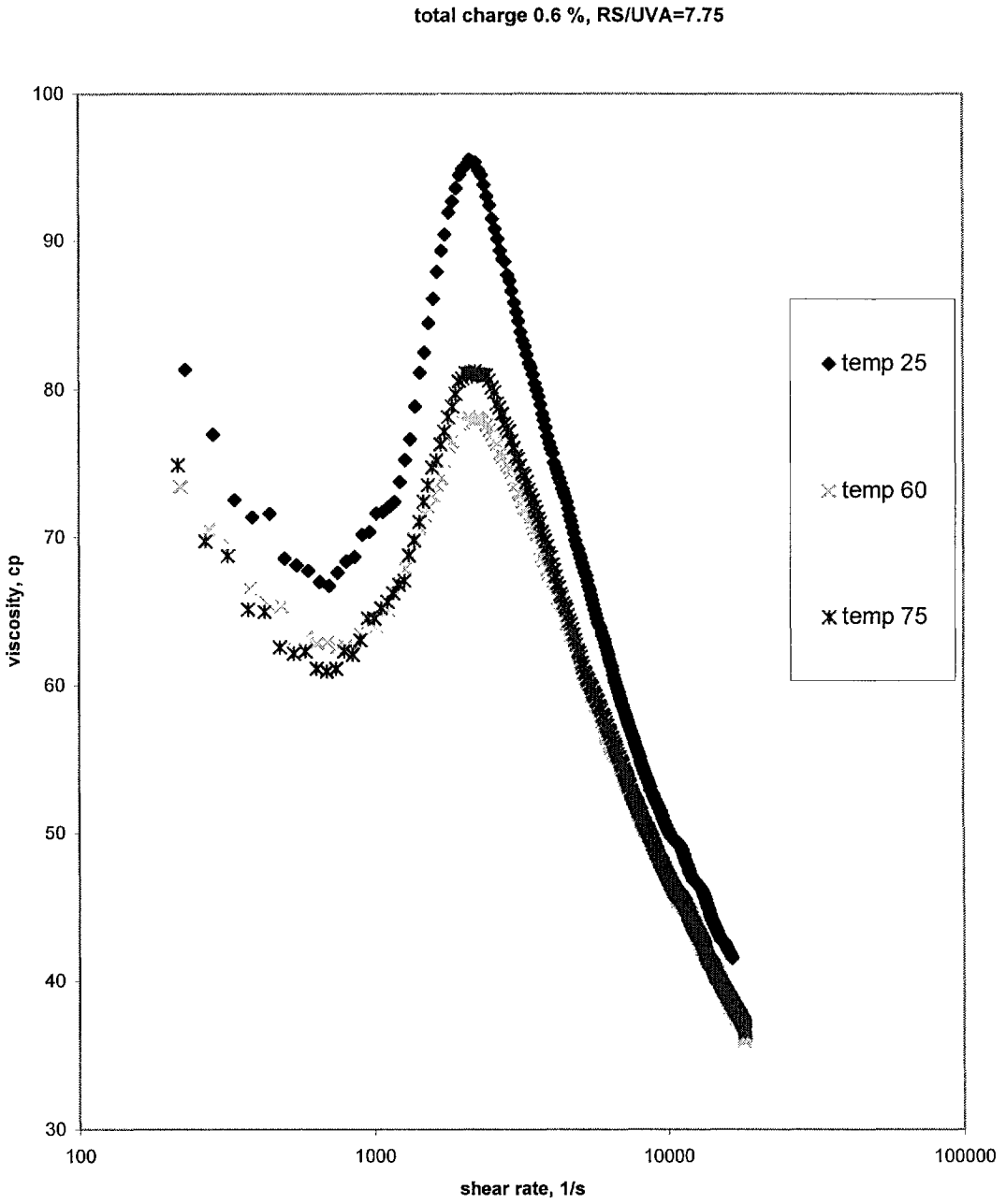

Figure 7.7 Viscosity as a function of shear rate for coating color containing UVA and RS at different temperatures.

The explanation may be that the paper-coating color containing RS (Figure 7.5) needs more shear rate than other paper-colors to increase the particle sizes from very small to quite large, which are responsible for the onset of shear thickening.

7.1.2 The Influence of Inhibitors on the Thixotropy

The thixotropy test was conducted under the controlled rate CR mode. The stresses and the shear rates of flow were recorded. The resulting up curve was obtained in the process of gradually increasing the shear rate. After reaching the assigned maximum rate, a gradual decrease gives the down curve, which should be identical to the up curve for time-independent rheological behavior. The down curve of thixotropic solutions is different from the up curve.

The curves form a hysteresis process that encloses an area A. It has the dimensions of energy over volume, the energy required to break down the thixotropic structure of the solution. Tests were carried out for coating formulations including different types of inhibitors. In this test, 180 seconds periods were used for the single cycle of upward ramped shear rate from 0.15 to 749.79 s^{-1}, constant 749.79 rate, and downward ramped rate from 749.79 to 0.15 s^{-1} as shown in Figure 7.8.

The maximum shear rate reached over the time curve corresponds to change in the structures of the coating formulations, and also corresponds to the highest shear rate in a real process. The results of this test are reported in Table 7.2

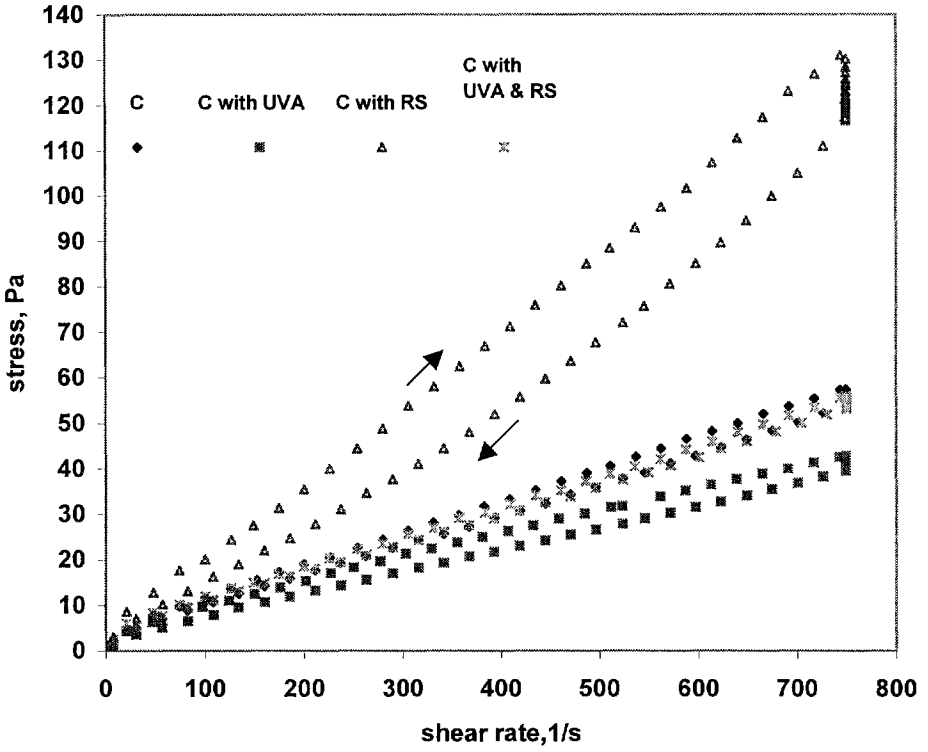

Figure 7.8. Thixotropic response of coating formulations (C). C with UVA (tin1130), C with RS, C with RS & UVA.

Table 7.2 Hysteresis Areas (Pa s^{-1}) of coating color.

Samples	**Up** Hysteresis area J/M^3s	**Down** Hysteresis area J/M^3s	Enclosed Hysteresis area J/M^3s
Coating Formulation, C	22,926	21,040	1,886
C with UVA	17,746	15,550	2,196
C with RS	48,924	39,475	9,449
C with UVA &RS	22,159	21,108	1,051

Characteristically, a high level of thixotropy and shear thinning are desirable to avoid occurrence of the pattern at low speed.

Small amounts of thixotropy, high shear viscosity and a tendency toward dilatancy [133] are usually associated with poor performance coating process.

7.1.3 Transient Shear Stress Response

Transient tests were conducted for coating formulations with UVA, RS, combination of UVA & RS and without inhibitor components consequently. The tests were performed for 450 seconds each for shear rate of 0.5 1/s. Figure 7.9 shows no transient effect for all coating formulations including those with different inhibitors. However, the stress increases with increasing the time for coating color, which includes radical scavenger. This is related to the change in viscosity at low shear rate.

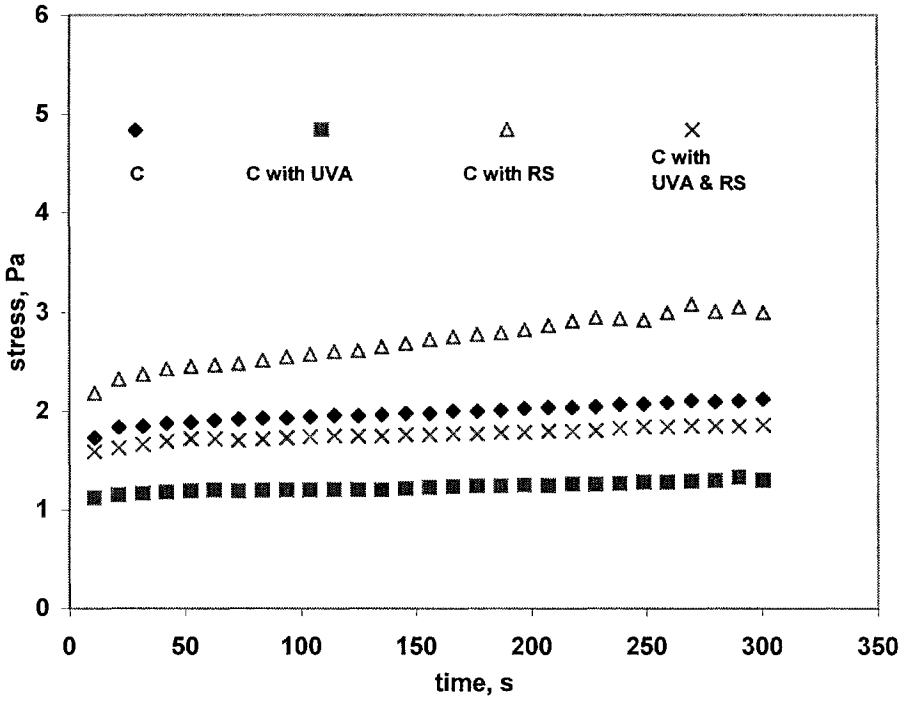

Figure 7.9. Transient shear stress response as a function of shear rate 0.5 1/s for coating formulation (C).

7.1.4 Visco-elasticity of Coating Color

Application of a steady shear flow to the samples inevitably breaks down its structure, giving rise to shear thinning behavior. Moreover, for many high visco-elastic fluids due to the onset of plug flow, melt fracture and other instabilities. These problems can be overcome by performing oscillatory measurements. In a dynamic test oscillating stresses are applied to the test sample to measure the storage modulus G' and the loss modulus G". The storage modulus represents the elastic response of the sample. The loss modulus indicates the level of viscous response. The complex modulus G* represents the visco-elasticity of the sample, it can be calculated from:

$$G^* = G' + iG''$$

A frequency sweep test was carried out at the stress value 10 Pa. Figure 7.10 shows the complex modulus G* which represents the total resistance of a substance against the applied strain. It is observed that the inhibitors decrease the visco-elasticity of coating formulations. For visco-elastic materials, both the complex modulus and the phase angle δ are frequency dependent.

Figure 7.11 reveals a decline of a δ/frequency-curve within its full range from 0 to 90°. The corresponding phase angle is less than 30°, which indicates that the elastic character of the color including inhibitors is more pronounced than the viscous character.

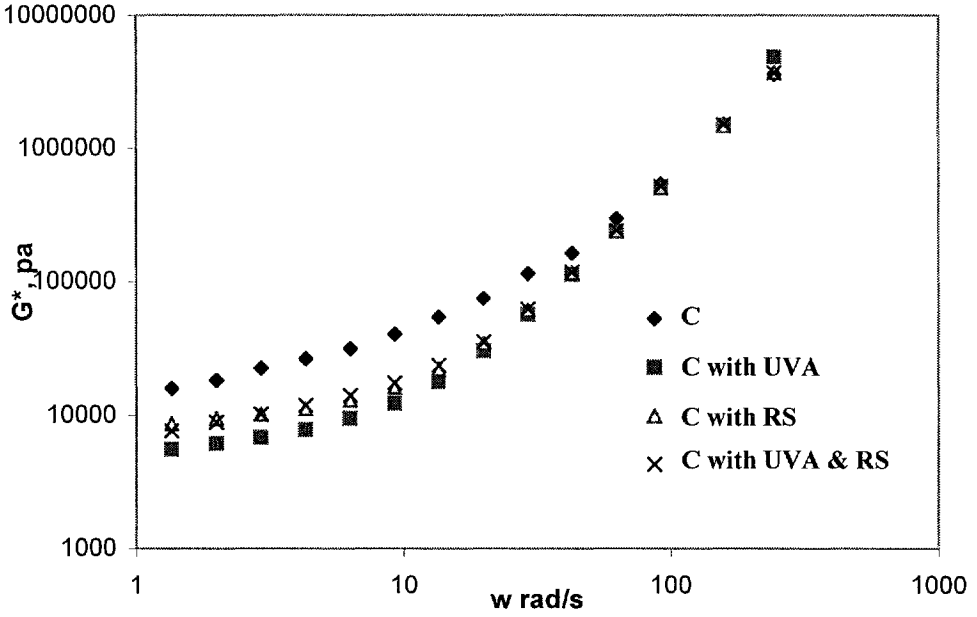

Figure 7.10. G* versus frequency for coating formulation (C). C with UVA (tin1130), C with RS and C with RS & UVA.

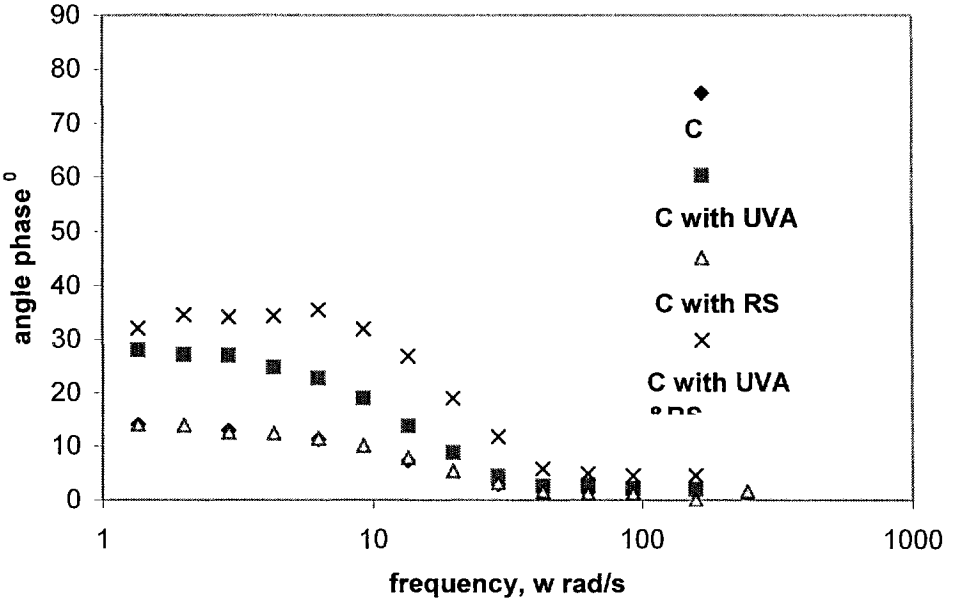

Figure 7.11. phase angle versus frequency for coating formulation (C). C with UVA, C with RS, C with RS & UVA.

Visco-elasticity arises in coating mixtures from flocculation of its components. Therefore, at zero frequency more of the energy will be stored in the elastic structure of coating color. Also, the elastic moduli will be larger than viscous moduli and the yield stress will be high. We focus in this study on the linear visco-elasticity range because in this range the sample deform and return back to its original structure. However, when the sample is deformed to the point that the internal temporary bonds of molecules or of aggregates are destroyed, a major part of the energy is irreversibly lost as heat, and the rheological behavior is called nonlinear visco-elasticity.

In Figure 7.12, the elastic and loss moduli (G' and G") of coating colors are plotted as functions of the frequency. It shows that the coating colors without inhibitors and with Hydroxylamine (RS), UV absorber and the combination of RS and UV absorber have a similar dynamic behavior in the frequency range investigated. Once a specific frequency is reached all coating colors with and without inhibitors increase with frequency for all the samples. Also, it is observed that the elastic modulus is significantly larger than the loss modulus.

The coating color with Hydroxylamine (RS) and the combination of RS and UV absorber have a significant higher elastic modulus compared to those without inhibitor and with UV absorber. The above behavior of coating colors may be related to the microstructure change since the elastic modulus is sensitive to the build-up of microstructure. On the other hand, the elastic modulus of coating colors is a function of the strength of bonds in network formed. Because of the strength of the interaction

between the radical scavenger and the ground calcium carbonate as explained in interfacial properties, the coating containing RS has high elastic modulus.

The elastic modulus and the viscous modulus of coating formulations including inhibitors are related to the increase in suspension network with increasing the frequency.

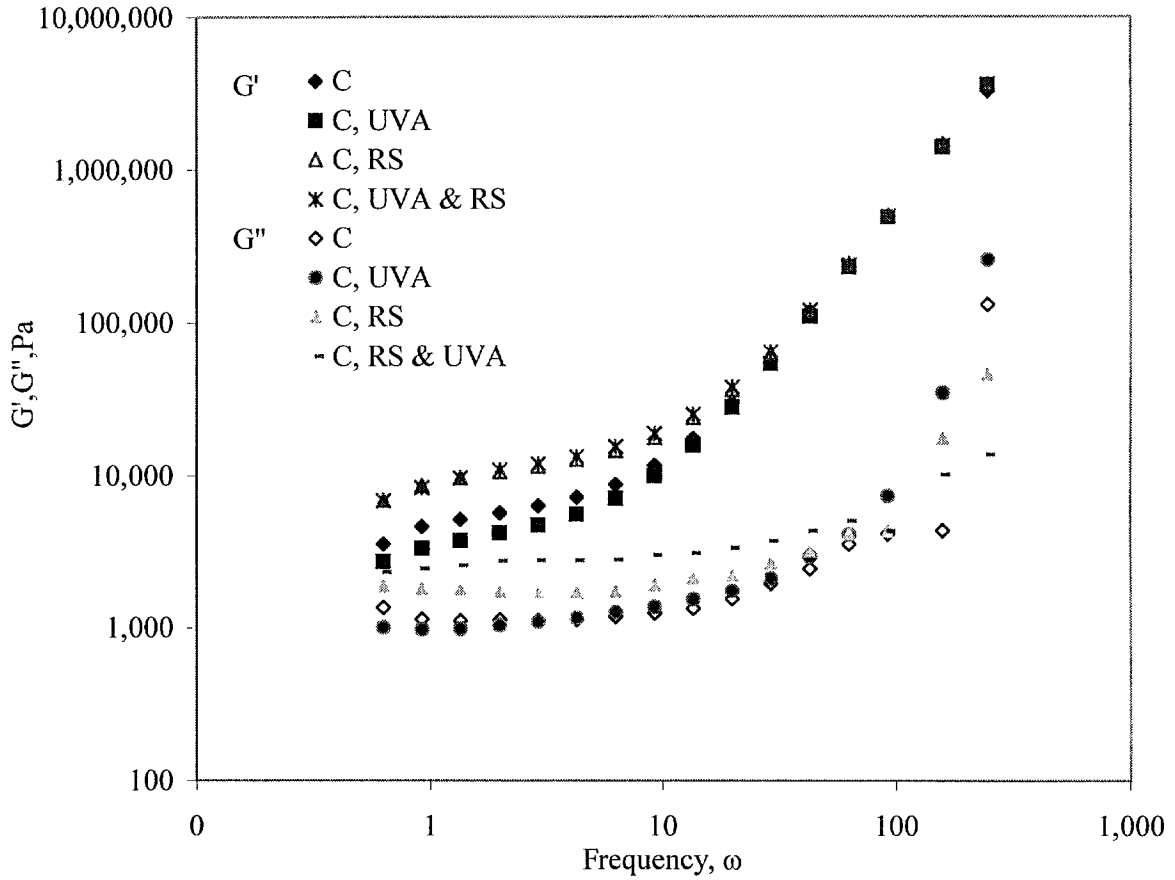

Figure 7.12. Viscous and elastic modulus as a function of frequency for coating formulation.

7.1.4.1 The Oscillatory Response of Coating Colors

Time sweep test has been done under 10 Pa and for a single frequency 0.1 1/s. The test was performed for 600 seconds. Figure 7.13 reports the variations of the elastic

modulus with time for coating formulations without inhibitor and with UVA, RS and combination of RS and UVA. For the coating formulation including RS, the elastic modulus gradually increases with time till 6 min and then experiences a sharp increase.

The elastic modulus increased with time according to a power-law relation: $G' \alpha t^n$ and no equilibrium was reached up to 10 min. For the coating formulation including inhibitors, the exponent n depends on the type of inhibitor as shown in Table 7.3. However, the exponent n is high for coating formulations including inhibitors comparing to the coating formulation without inhibitor.

Table 7.3 Coating formulation with different inhibitors and their exponent n.

Coating formulation with	Exponent n	
No inhibitor	0.134412	
UVA	0.238581	
RS	0.19	1.6
	t = 0-6 min	t = 6-10
RS &UVA	0.30279	

The explanation may be that there is no rebuilding of the coating color microstructure of the sheared system for a short period of time. However, there is more agglomeration in the structure of the coating color containing RS at certain time. This can be noticed from the sharp increase in the elastic modulus as shown in Figure 7.13. We can conclude that there is no rebuilding of coating color with or without

inhibitor for a short period of time and that the structure of coating color changes directly proportional with the time.

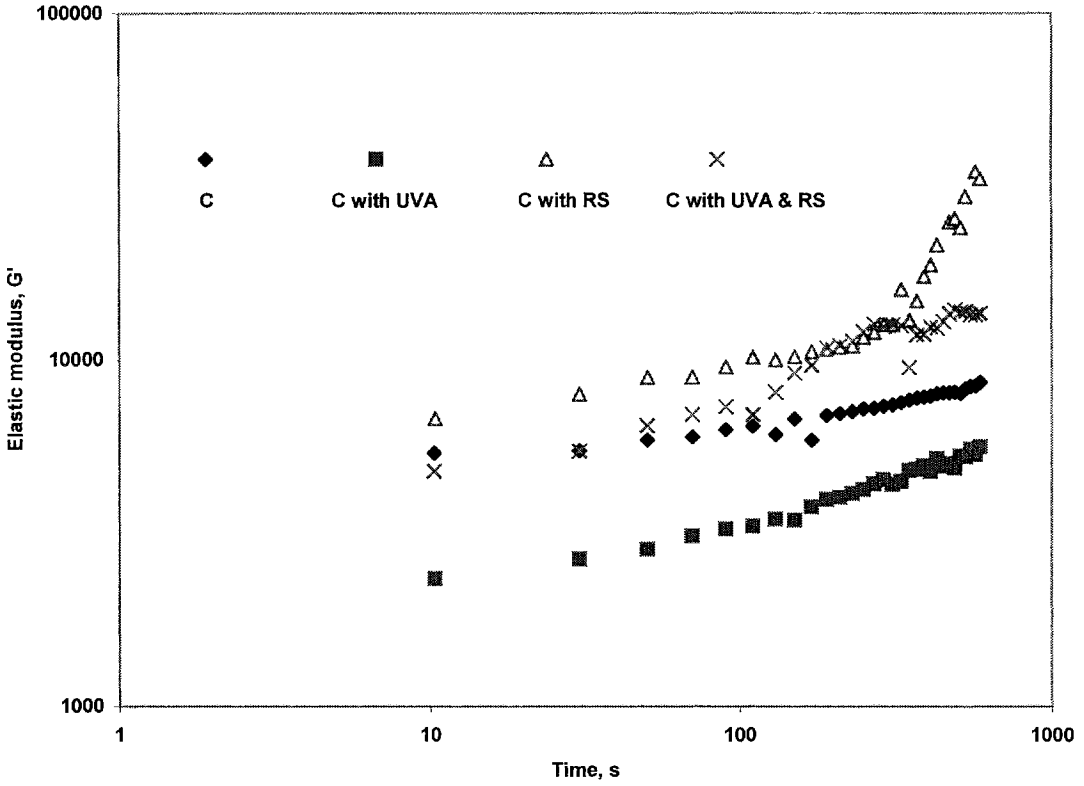

Figure 7.13. Elastic modulus vs. time of coating formulation (C).

Figure 7.14 shows the relaxation time as a function of frequency for different coating formulations containing inhibitors. The relaxation time is related to the type of the major fluid component but also to the type and percentage of all other ingredients of a particular material. Therefore, the coating formulation without inhibitor has the longest relaxation time (the longest time required for the material to relax) (5.4 s). The lowest value of relaxation time (2.7 s) occurred with UVA or with the combination of UVA & RS.

The exact values of the moduli and their position in the frequency domain will vary. But the indicated overall qualitative behavior is usually seen if data is available over a wide-enough frequency range and is differentiated to number of specific regions. These regions depend on the longest relaxation time, τ_{max} [12]. If $w\,\tau_{max} > 1$, then within the plateau region where elastic behavior dominates, there is always an increase in G' with frequency. It is concluded that the elastic modulus dominates for all coating formulations containing inhibitor.

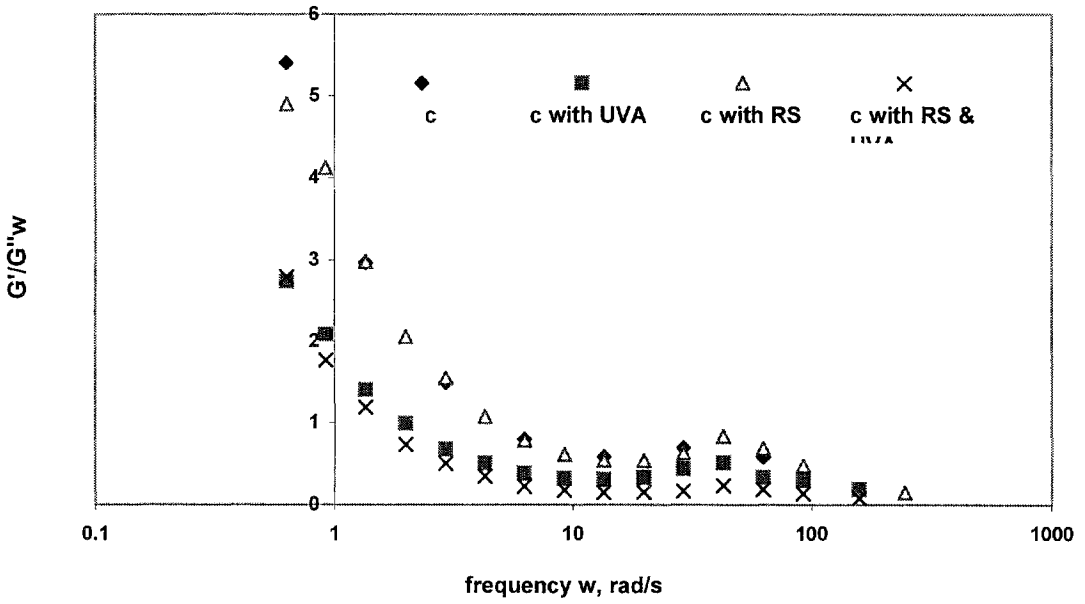

Figure 7.14. relaxation time versus frequency for coating formulations (C). C with UVA, C with RS, C with RS & UVA.

7.2 Study of Different Total Charge Contributions to the Rheology

The rheological response of coating colors to deformation is a result of the synergistic interplay of pigments, latex, starch and inhibitors. In this study, we explore the effect of total charge of inhibitor on the rheological properties of coating color. Total charges of inhibitor affect the viscosity of coating colors.

The viscosity of the color increases with increasing the total charge. This is shown in Figure 7.15 for coatings containing different total charge. The viscosity as a function of the shear rate in the range 0.15 – 749.9 s^{-1} for a color containing 0.2, 0.6 and 1 % inhibitor's total charge, decreases with increasing the shear rate. An apparent shear thinning of the coating color is observed. A very sharp drop in viscosity is noticed at high shear rate for coating colors including high concentration of inhibitors while the same is not observed for other colors. Therefore, this behavior is related to the increase in inhibitor concentration not to the viscosity heating.

Figure 7.16 illustrates that the viscosity decreases with increasing the shear rate. Therefore the behavior is shear thinning. Above a critical shear rate, the viscosity increases. Collins et al. [10] have noted that a large distribution of particle sizes can suppress shear thickening. Finally, we observed that above specific shear rate, the viscosity began to decrease. While at high total inhibitor charge 1%, the behavior is shear thinning; the viscosity decreases at high shear rate.

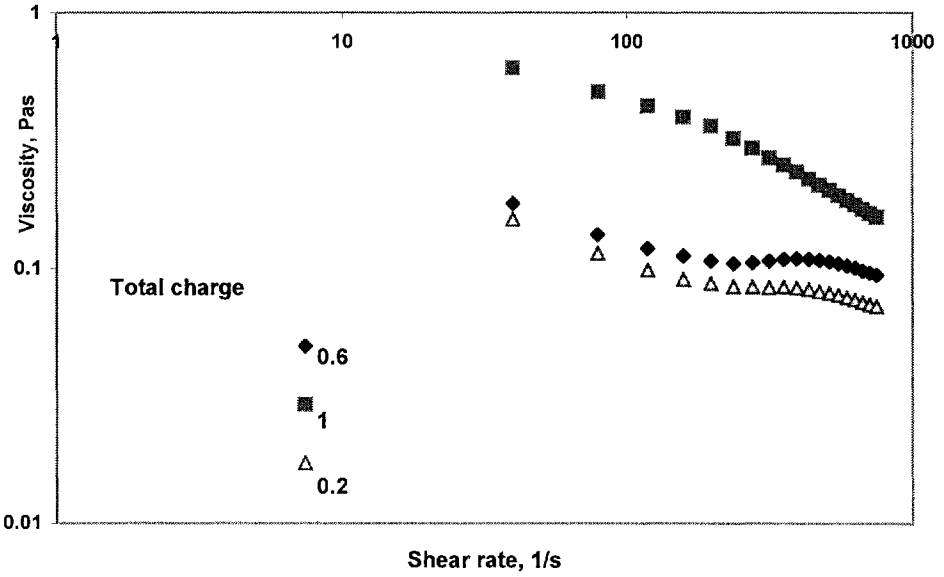

Figure 7.15. The viscosity as a function of shear rate for different total charge (rheometer HAAKE).

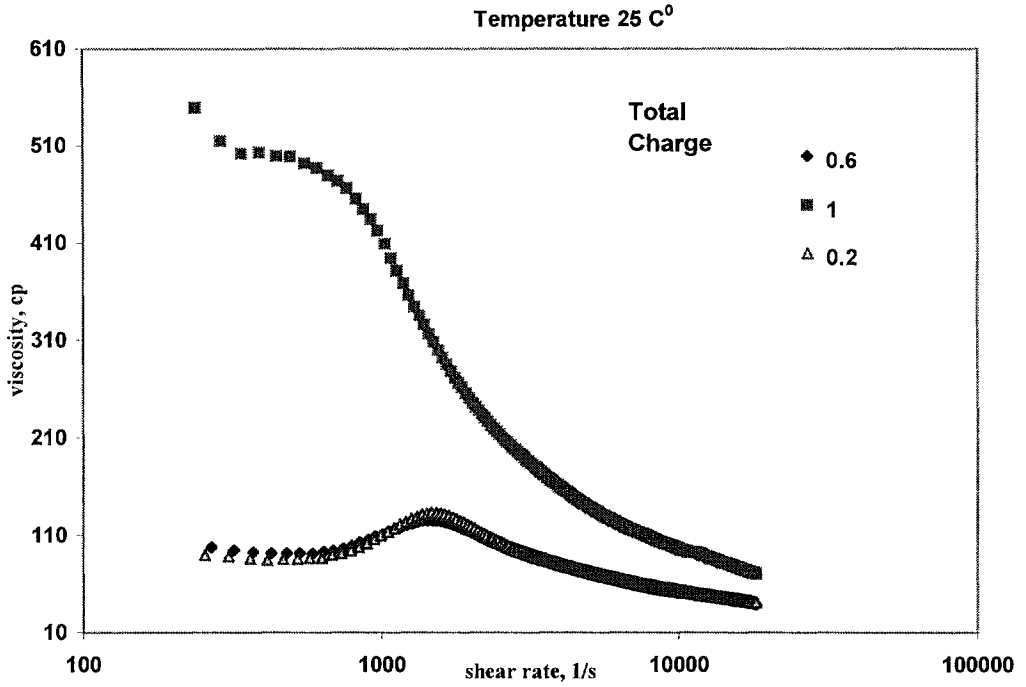

Figure 7.16. The viscosity as a function of high shear rate for different total charge (Hercules DV-10 Viscometer).

7.2.1 The Effect of Total Charge on the Thixotropy

Thixotropic materials are those whose consistency depends on the duration of shear as well as on the rate of shear. A state of dynamic equilibrium may be reached when the rate of build up of structure equals the rate of breakdown [11]. Thixotropic measurements were conducted under the controlled rate CR mode. The stresses and the shear rates of flow were recorded. The resulting up-curve was obtained in the process of gradually increasing the shear rate. After reaching the assigned maximum rate, a gradual decrease gives the down-curve, which should be identical to the up-curve for time-independent rheological behavior.

The down-curve of thixotropic solutions is different from the up-curve. The curves form a hysteresis process that encloses an area A. The hysteresis area A of a sample that reached its sol structure is a measure of its thixotropy. It has the dimensions of energy over volume, the energy required to break down the thixotropic structure of the solution. Tests were carried out for different coating formulations, which have different total charge of inhibitor such as 0.2, 0.6 and 1%.

Table IV shows the thixotropic areas, which were obtained in these tests. Figure 7.17 shows that the total charge 1% has the highest thixotropic behavior of the coating formulations. On the other hand, the thixotropic behavior is increasing with increasing the total charge.

Table 7.4 Hysteresis Areas (Pa s^{-1}) of coating formulation with different total charge.

Total charge %	0.2	0.6	1
Up curve Pa s^{-1}	20090	28069	65651
Time curve Pa s^{-1}	0	0	0
Down curve Pa s^{-1}	17126	24406	34635
Total Pa s^{-1}	2964	3662	31016

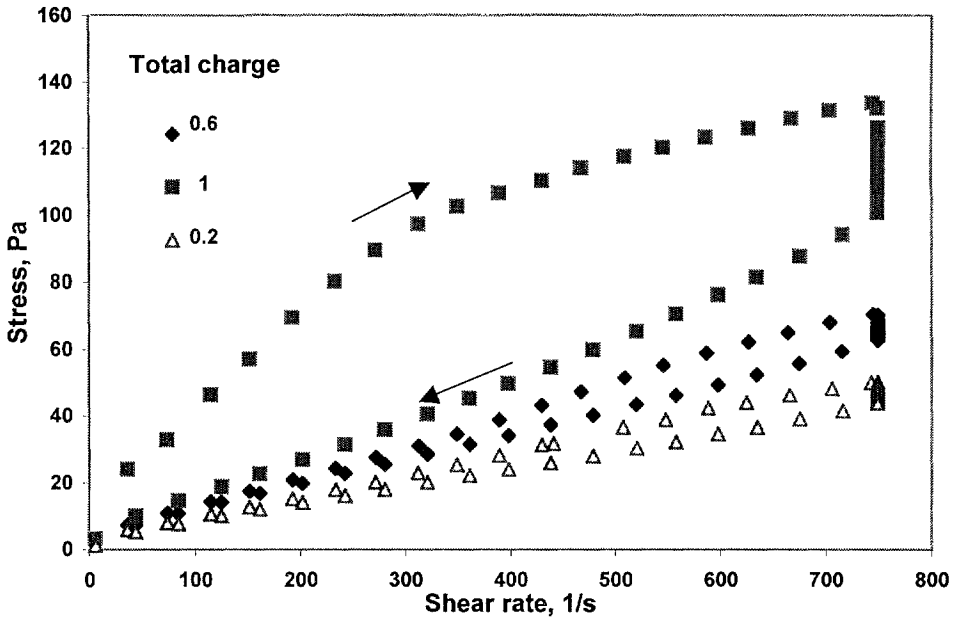

Figure 7.17 Thixotropic of different total charge of coating formulation.

Figure 7.18 shows the yield stress of coating formulations with different total charge. It is observed that the coating colors with 0.2% and 0.6% of inhibitor require the same stress to flow. While increasing the concentration of inhibitor to 1% requires more stress to flow. The explanation may be that the interaction between coating structures is controlled by the composition of the coating suspensions and by the formation of denser structures when the concentration of inhibitor increased.

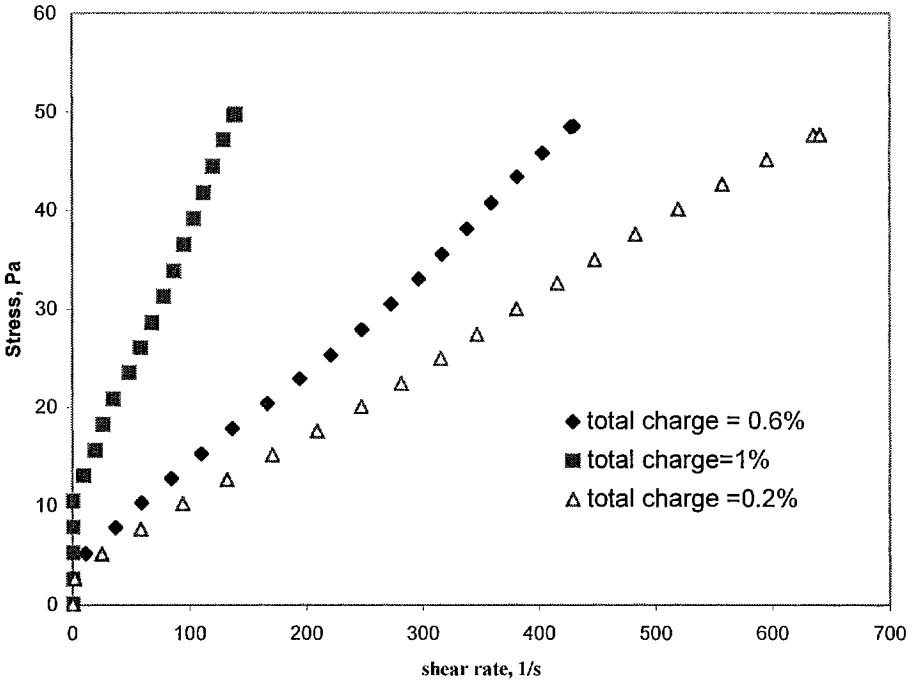

Figure 7.18 Yield stress of different total charge of coating formulation.

7.2.2Visco-elastic Behavior of Different Total Charge

Visco-elastic materials have distinctive rheological properties that define their fluid like (viscous) and solid like (elastic) behavior upon deformation. The creep and recovery measurement introduces the response time to the stress dependency of both the viscous and the elastic behavior of solids and fluids. During the creep test of visco-elastic fluids the stress applied will cause a transient response that cannot be broken up clearly into the overlapping elastic and the viscous contribution. The higher the compliance, the easier the sample can be deformed by a given stress.

For creep and recovery tests, constant shear stress 0.5 Pa were applied for 150 s to the sample. Following this period of time, the applied stress was brought instantaneously to zero. The response of deformations was recorded over a total period of 300 s. The stress in the recovery phase of this test must be set to zero for full recovery to reach a final permanent strain level. Figure 7.19 shows that the creep deformation for total charge 1, 0.6 % is approximately the same or higher than creep deformation at low total charge.

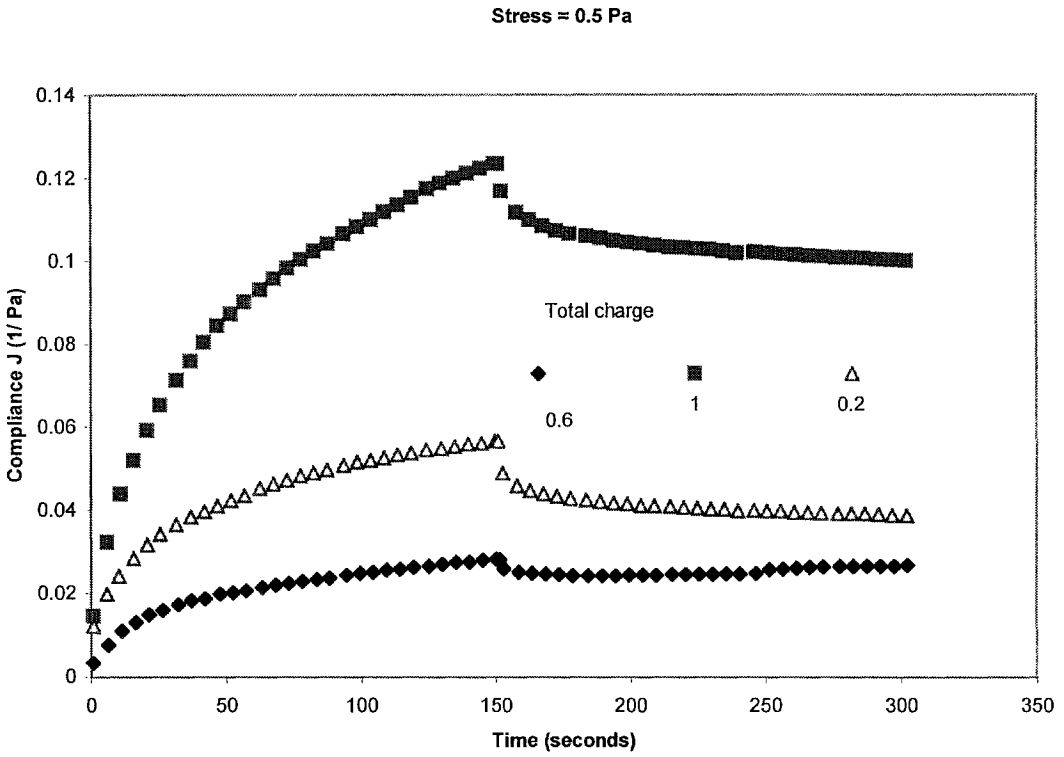

Figure 7.19. Creep curves for coating formulation of different total charge, at stress 0.5 Pa.

The variations of the elastic moduli with frequency for different total weight inhibitors are presented in Figure 7.20. The measurements were carried out at stress

10 Pa for coating colors. Figure 7.20 shows that the elastic modulus increases with frequency at stress 10 Pa, the coating formulation of high 1% and low 0.2% total charge have the same elasticity.

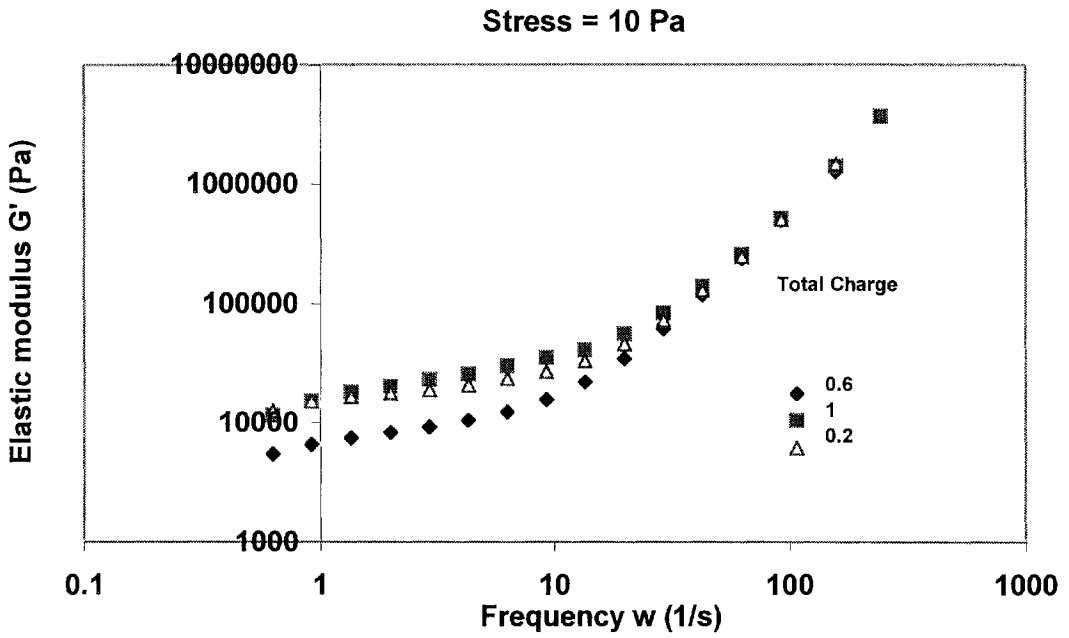

Figure 7.20. Elastic modulus curves for coating formulation of different total charge at stress 10 Pa.

Figure 7.21a demonstrates that the total charge of coating formulation has no effect on the complex modulus at high frequency (10 1/s). It is noticed that the complex modulus is constant; therefore, the visco-elasticity is linear. It is observed, Figure 7.21b, that at low frequency (0.1 1/s), there is variation in complex modulus of coating formulations with the total charge of inhibitor. The complex modulus increases with increasing the stress amplitude. The linear visco-elastic range is

limited to that stress amplitude range for which complex modulus is constant. Moreover, the stress has no effect on the compliance and the storage modulus within the range of linear visco-elasticity.

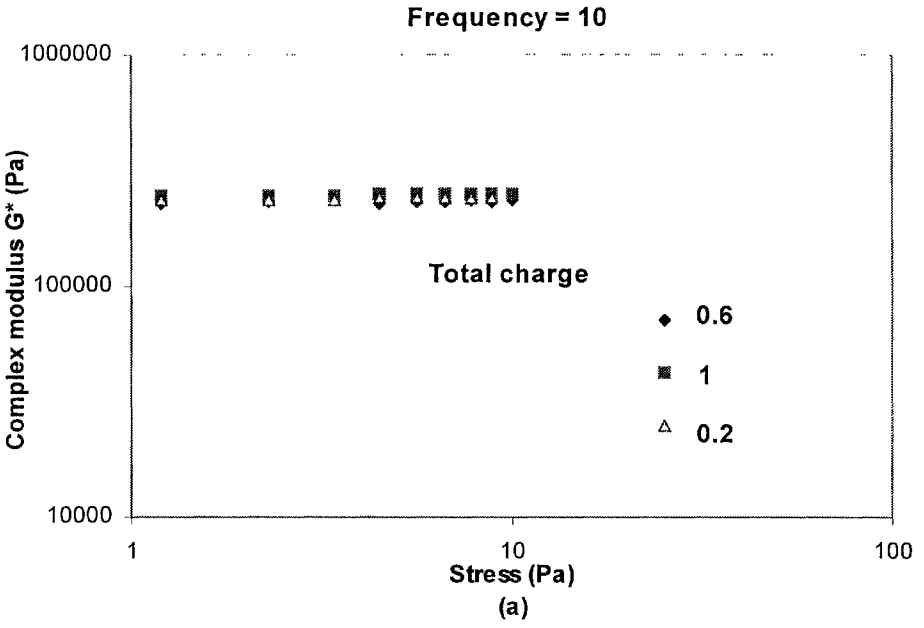

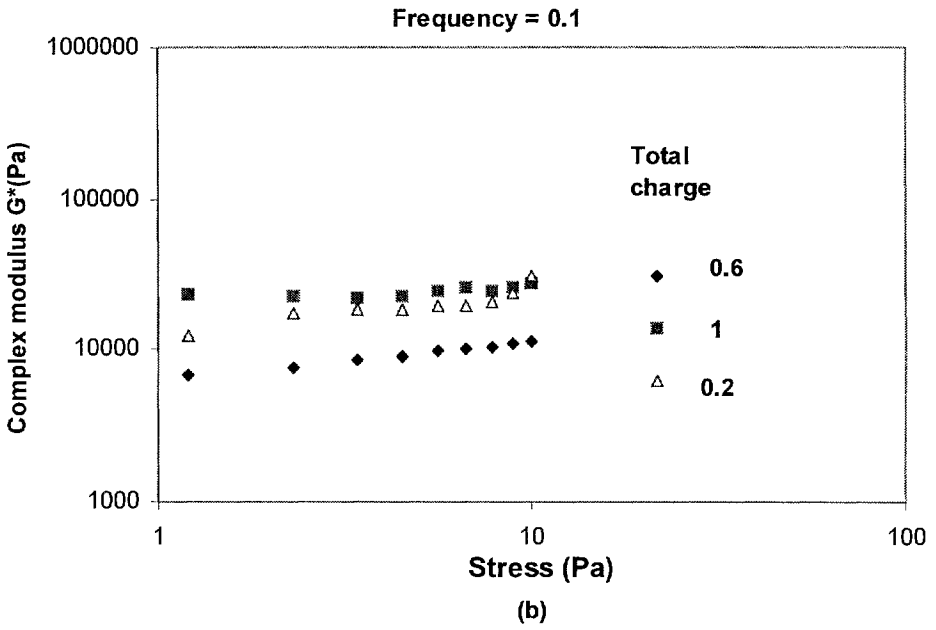

Figure 7.21. Visco-elasticity of coating formulation with different total charge (a) at frequency 10HZ (b) at frequency 0.1HZ

Rheological measurements were conducted using oscillatory and steady shear tests. Utilizing the resulting rheological data, the effect of total weight charge on the potential for interactions was studied. High total charge increases the thixotropy of coating formulation. The viscosity increases with increasing total charge, however, the complex modulus is independent of total charge at high frequency 10 1/s. Coating formulations are very complex materials, therefore it is important to study the history of coating color behavior before its application.

Chapter Eight

The Impact of Preshear and Total Charge on the Visco-elasticity of Coating Colors

Evaluation of the rheological properties of coating colors used in the paper industry reveals that such colors have a visco-elastic character. The elastic components are associated to the interaction between the inhibitor and polymer (in the aqueous phase) and the solid particles (pigment and latex) of the color. Preshear is the history of the coating colors when they flow through pipes, pumps, and filters from the coating kitchen to the pre-metering head-box. Here we will focus on the two points. The first point is the effect of preshear on the viscosity of coating color. In the second point we will show that the visco-elastic character depends on the concentration of inhibitor in color formulation.

8.1 The Effect Of Preshear On The Viscosity Of Coating Color

Figure 8.1 shows the steady shear viscosity curves attained for coating formulations with different concentration of inhibitors, 0.1%, 0.3%, 0.5%, 0.7%, 0.9% and without inhibitor. Appendix D shows the coating color formulations. It can be seen that all the coating colors have about the same steady shear behavior. It is observed that the decrease of viscosity with shear rate is due to the deformation and break down of structured pigment, which depends on the concentration of inhibitors.

The viscosity of coating color increases with increasing the concentration of inhibitors. That may be due to charge interactions between inhibitors and coating components. Figure 8.2 shows the viscosity of pre-shear coating colors with different concentrations of inhibitor and without inhibitor. It can be noticed that the viscosity of coating color is high comparing to the viscosity of pre-shear coating color. For example, the viscosity of coating color containing 0.9% of inhibitors is 1.37 Pas. However, the viscosity after pre-shear the coating color is 0.93 Pas. It is obvious that the pre-shear has an effect on the structure of coating color.

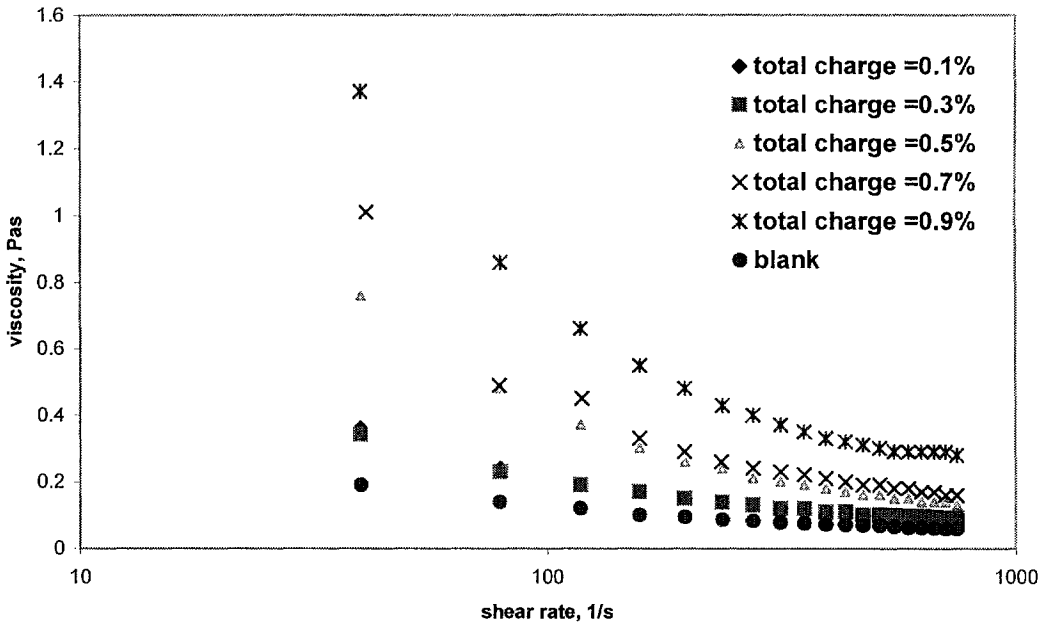

Figure 8.1. Steady shear viscosity as a function of the shear rate for the industrial coating color with different inhibitors and blank (color with no inhibitor).

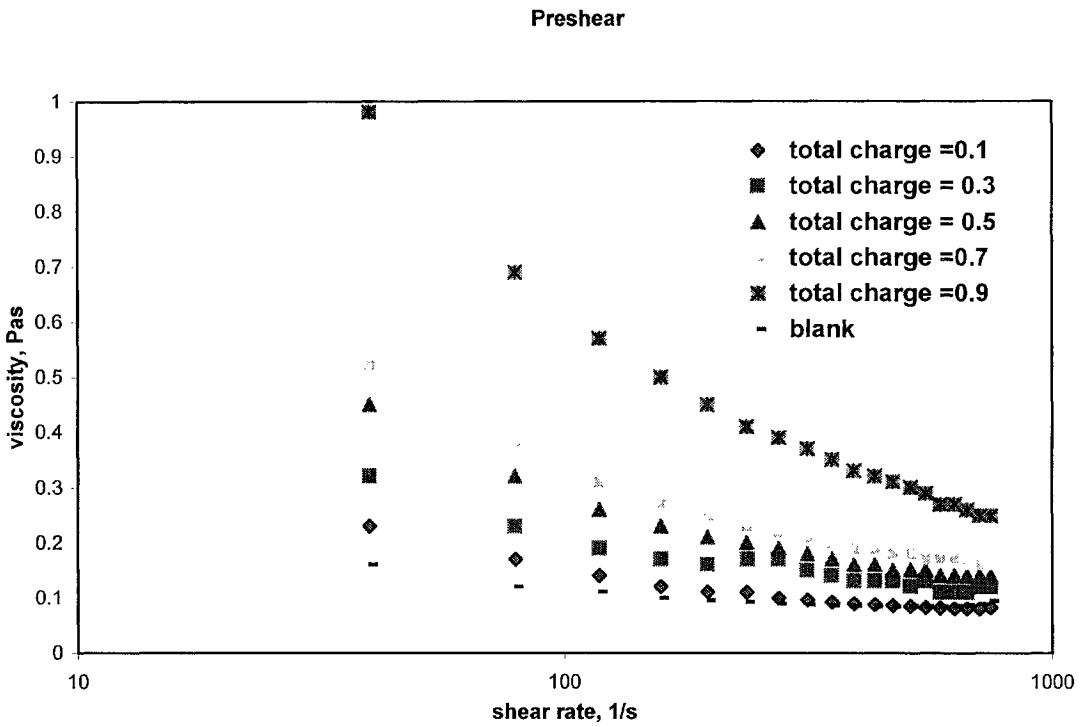

Figure 8.2. Pre-shear coating color with different inhibitors and blank (color with no inhibitor).

It will be shown that a relatively low pre-shear (30 s^{-1}) can be sufficient to provide a structural breakdown in coating color using the minimum yield stress of coating color as shown in Figure 8.3. The preshear was recorded over the period of 180 s.

Therefore, such a level of shear rates may be exerted on coating colors when they flow through pipes, pumps, and filters from the coating kitchen to the pre-metering head-box.

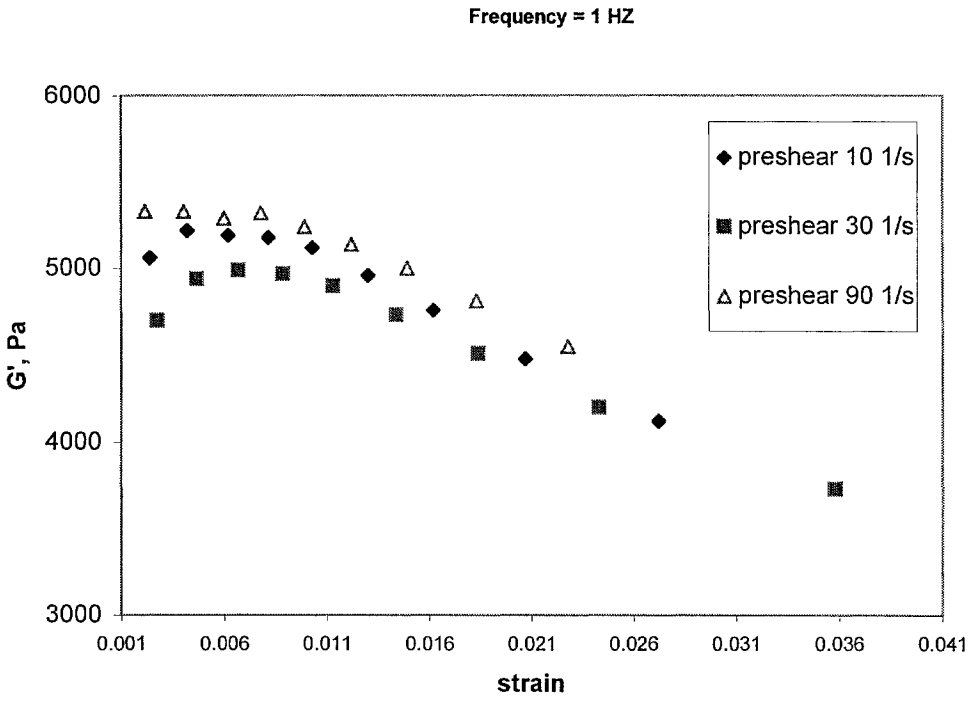

Figure 8.3 the elastic modulus of coating color as a function of the strain.

The yield stress of coating color can be calculated as follows: τ (yield stress) = $\dot{G}\,\gamma_c^{\circ}$ (Bingham model), $\dot{G}$ is the elastic modulus and γ_c° is the critical strain.

8.2 The Impact Of Inhibitors Concentrations On The Visco-Elasticity

In Figure 8.4a and b, the storage and loss moduli (G' and G") of coating colors are plotted as functions of the frequency, for different concentrations, 0.3%, 0.5%, 0.7%, 0.9% of inhibitors and without inhibitor. We notice that the storage modulus is larger than the loss modulus, and both moduli increase with inhibitors concentration. The storage and loss moduli are constant at low frequency and increase significantly at higher frequencies. Also, it is observed that the storage modulus of coating color with different concentrations of inhibitors coincides and increases sharply at a specific

frequency. This is related to the increase in the interaction between coating components and hence, the increase in agglomeration.

Therefore, the coating suspensions at low deformation behave as visco-elastic gels. This is the typical behavior observed for coating colors [68]. The elastic modulus of coating colors is a function of the strength of bonds in the network formed [49]. The hydrophobic ends of UV absorber are adsorbed onto the surface of kaolinite and ground calcium carbonate particles followed by particle-particle interaction to form a network.

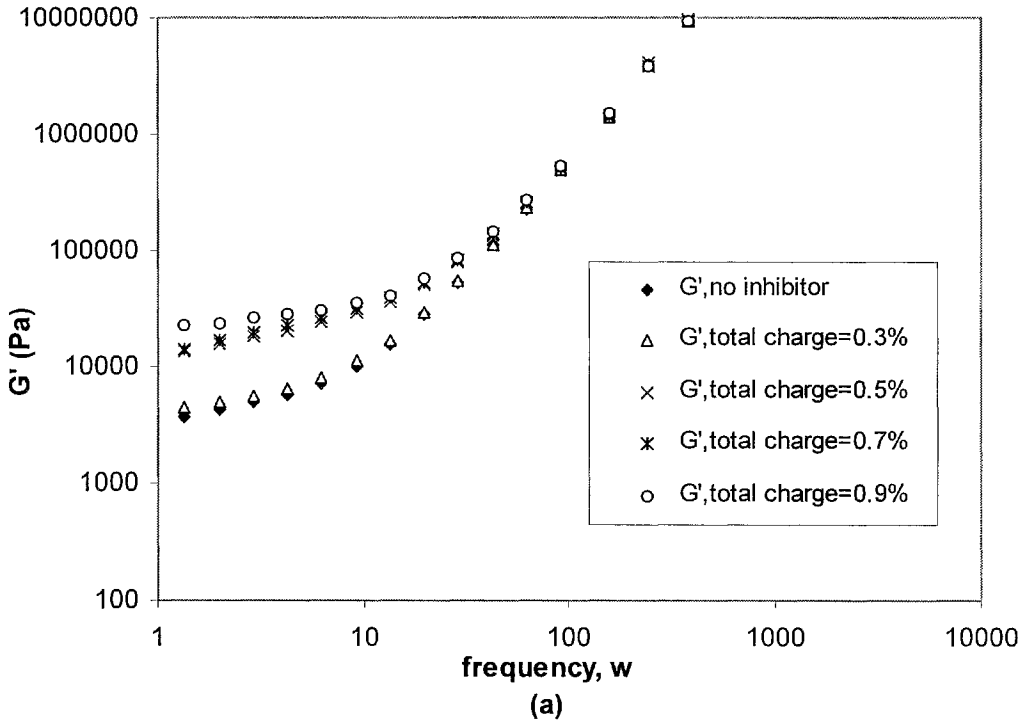

(a)

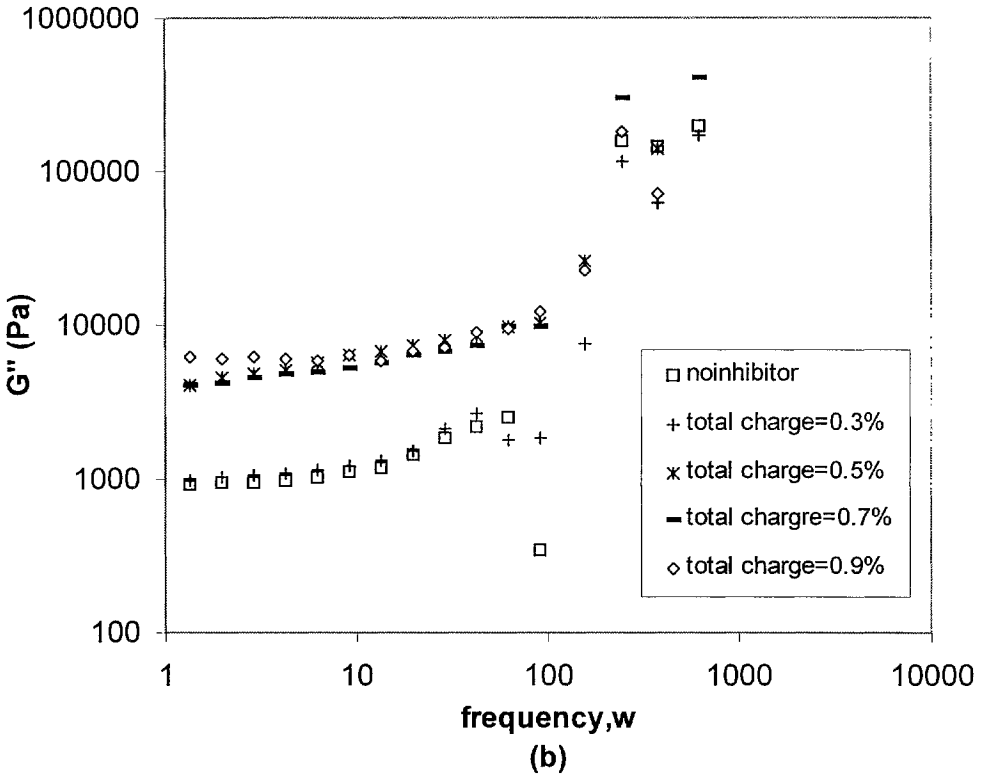

Figure 8.4. a) elastic modulus as functions of the frequency for coating colors with different inhibitors and blank (no inhibitor). b) viscous modulus as functions of the frequency for coating colors with different inhibitors and blank (no inhibitor).

Figure 8.5 shows the storage modulus for coating colors with different concentration of inhibitors as a function of strain amplitude. The storage modulus is constant at low deformation and decrease as the deformation increases. This behavior is due to microstructure changes induced by flow. At low deformation, the storage modulus G' is constant with increasing the strain where the domain is linear. The limit of the linear domain is related to critical deformation, γ_c. It has been shown that a relatively low pre-shear (30 1/s) can be sufficient to provide a complete structural breakdown in coating color.

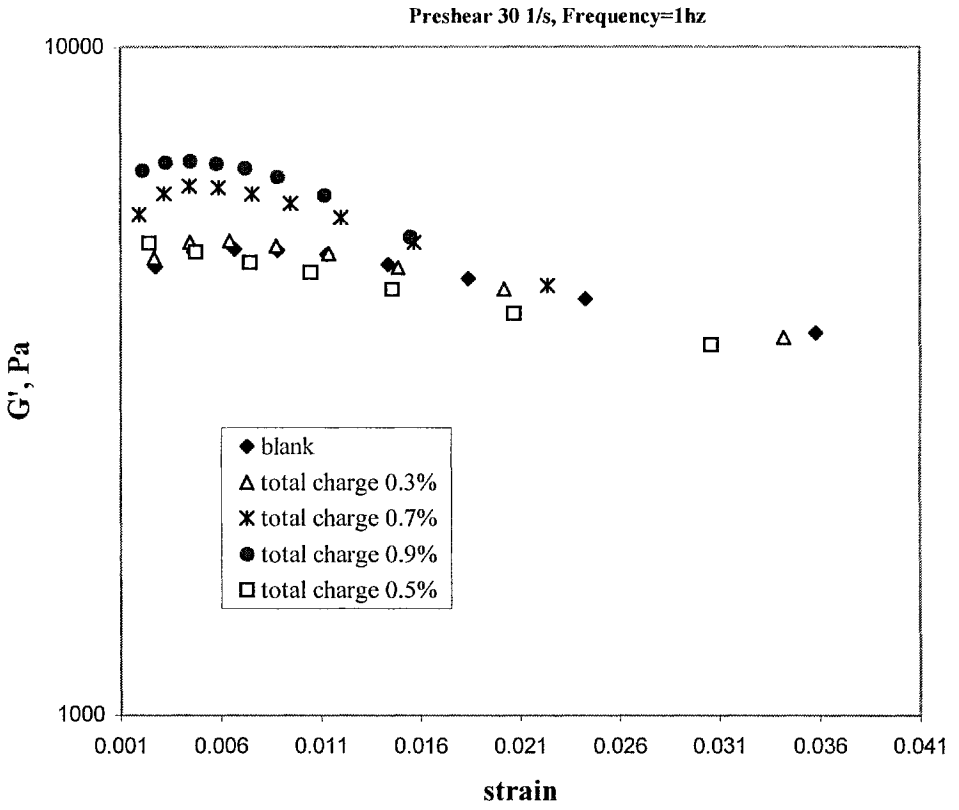

Figure 8.5. Elastic modulus as a function of the strain for coating colors with different inhibitors.

Figure 8.6 reports the storage and loss moduli as function of the time for coating colors for different concentrations of inhibitor and without inhibitor at frequency 0.1 HZ. We observe that the storage modulus is close to the loss moduli. The moduli

increase with increasing inhibitor concentration. However, the modulus is increasing slightly with the time for coating color containing 0.7% and 0.3% of inhibitor, while, for coating color containing 0.5% of inhibitor is decreasing with the time. This can be explained by the absence of rebuilding of the coating color microstructure of sheared system for short period of time. We can conclude that the variation in coating color structure of sheared system for short time is independent of the inhibitor concentration. It is observed that the storage modulus of coating color in Figures 8.6 and 8.4 is high comparing to the storage modulus of coating color in Figure 8.5. It may be explained that the samples in Figures 8.4 and 8.6 have been investigated under constant stress 20 Pa. While the samples in Figure 8.5 have been investigated under stress between 1 to 50 Pa. Since the storage modulus is related to the microstructure of coating color and the degree of interaction between the coating components, the stress (stress = elastic modulus *strain), which was exerted on the sample during the test, affects the microstructure of coating color.

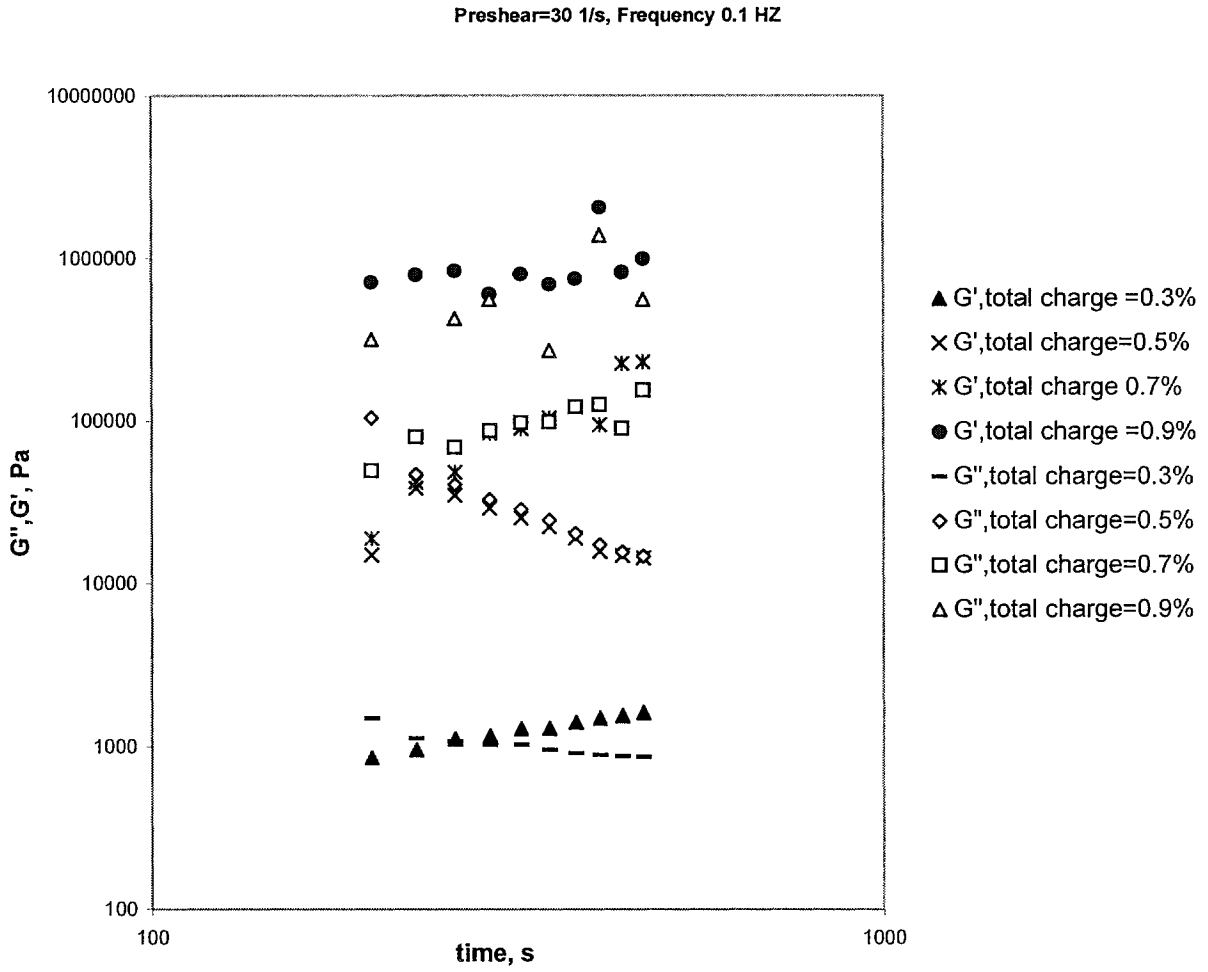

Figure 8.6. Dynamic modulus as functions of time for coating color with different Concentration of inhibitors.

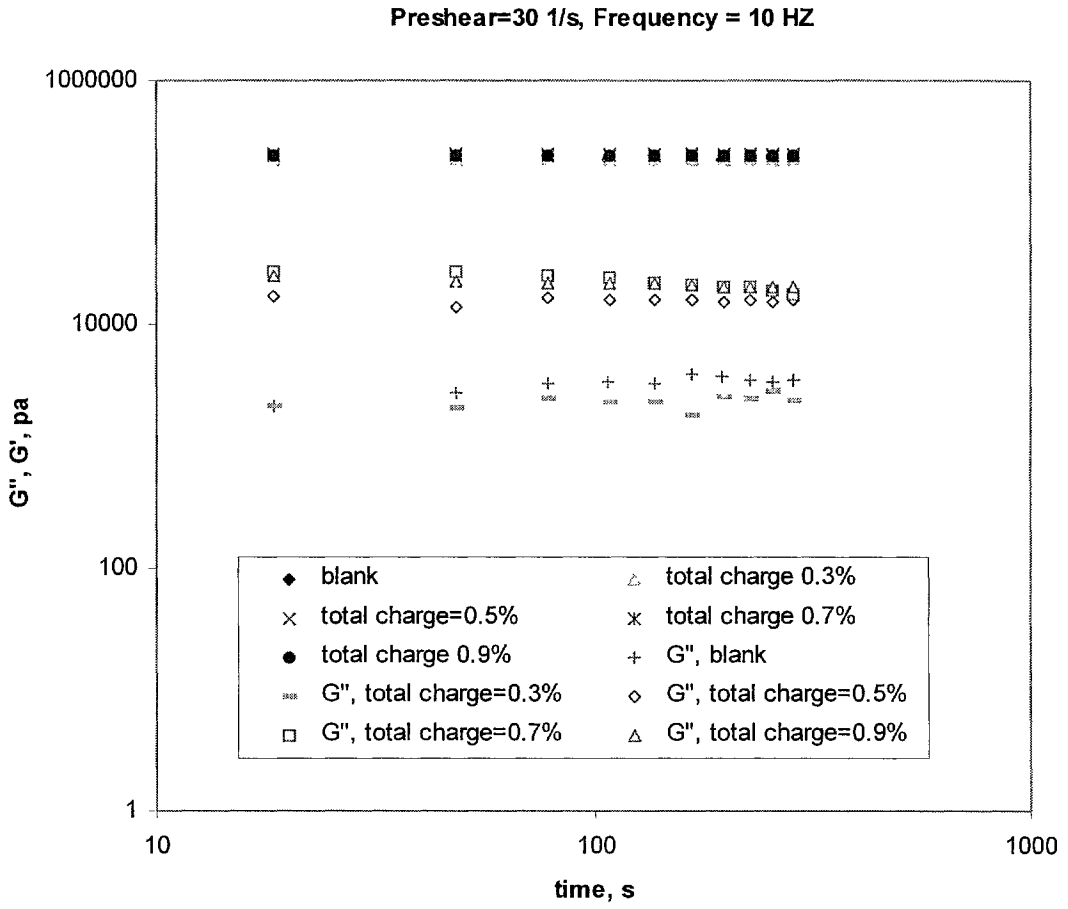

Figure 8.7. Dynamic modulus as functions of time for coating color with different Concentration of inhibitors.

Figure 8.7 shows the storage and loss moduli as a function of the time for coating colors for different concentrations of inhibitor and without inhibitor at frequency 10 HZ. We observe that the storage modulus is independent of the concentration of

inhibitor at high frequency (10HZ). Also, the elastic modulus is higher than loss modulus. However, the concentration of inhibitor affects the loss modulus at high frequency 10 HZ. On the other hand, elastic and viscous moduli are independent of time. Since the elastic modulus and the viscosity represents the internal structure of the coating color, our focal point for the next step is to study the microscopic structure and the surface morphology of the coating color.

Chapter Nine

Influence of Inhibitors on the Structure and Surface Morphology of Paper Coating Color

The ultrastructure of colloidal coating color dispersion is the result of complex interactions between the submicroscopic plate-like and aragonite mineral particles and the medium. The flow behavior of the suspensions is one of the most sensitive indicators for this particle interaction, which can be drastically changed by even small variations in the composition of the medium. These include the concentration and valency of the ions and organic additives [116-119].

In the case of clays, the dimensions, shape, and structure of the individual particles are determined by electron microscopy (EM) and by selected area electron diffraction [120-124]. Freeze-etching, shadowing, high magnification, and transmission electron microscopic are used to visualize directly components in a concentrated coating color without inhibitor and with different concentration of inhibitors in order to deduce component interactions. We have examined pigments, pigments with binder (starch) and coating color. The key to high resolution is where each frozen sample is fractured, etched, shadowed and coated with Pt (platinum)/C (carbon) and then transported to TEM for examination.

9.1 Microstructure Of Ground Calcium Carbonate And Kaolinite

Figure 9.1 shows the microstructure of aqueous suspension of 70% w. delaminated kaolinite (clays) that is delivered in coarse and fine particle size less than 2 μm. The image reveals the presence of faces on some particles, plate-like, labeled "E". When faces of particles are not clearly distinguishable, the perimeter can be seen to display hexagonal shapes, as seen from Figure 9.1 on the particle labeled "F". Also, it can be noticed the agglomeration between the clay particles. Edge to edge, edge to face and face to face associations are seen in the sample (Figure9.1).

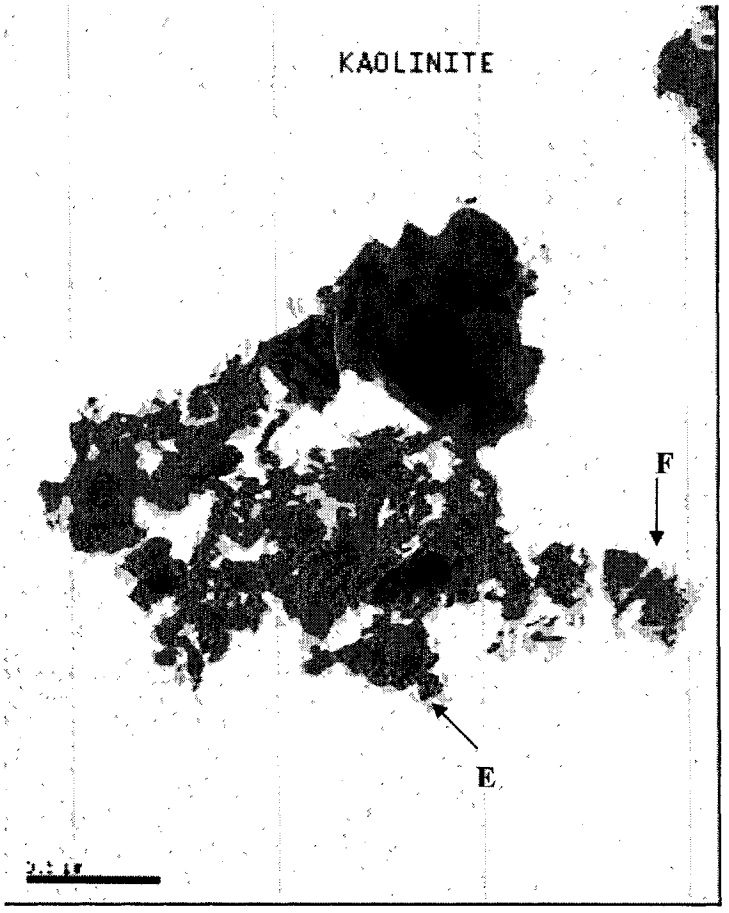

Figure 9.1 Microstructure of 70% w. delaminated kaolinite.

Figure 9.2 reveals the microstructure of delaminated clay and ground calcium carbonate. The image reveals the presence of aragonite crystals, labeled "GCC" as shown in Figure 9.2. High crowding and substantial parallel crystals alignments are plain.

Figure 9.2 Microstructure of delaminated clay and ground calcium carbonate.

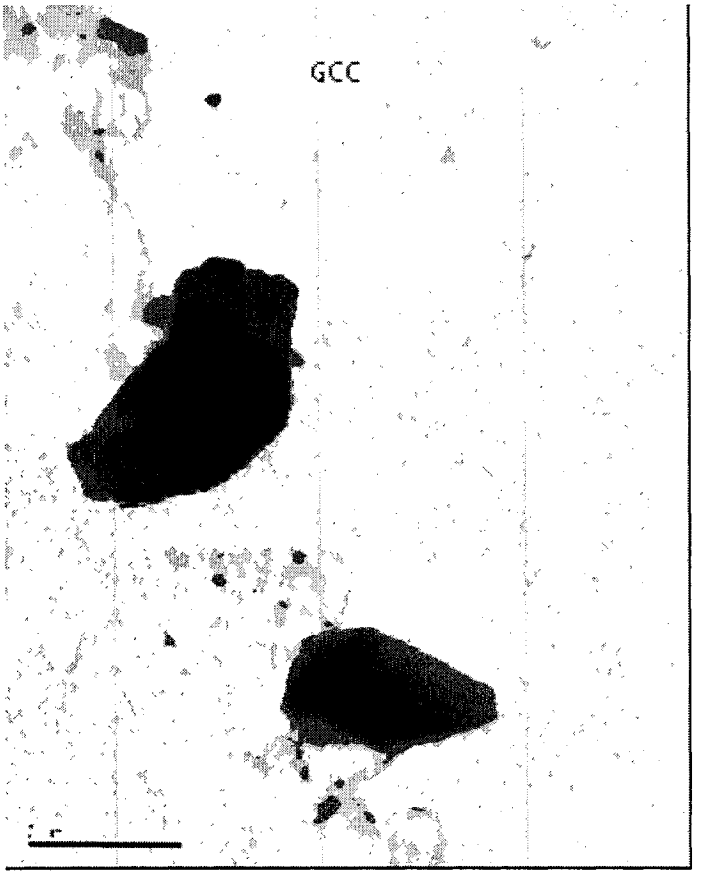

Figure 9.3 Microstructure of ground calcium carbonate.

Figure 9.3 reveals the microstructure of ground calcium carbonate. The image reveals the presence of aragonite crystals, labeled "GCC".

Frozen samples in Figures 9.1 and 9.3 were examined without freeze etching and shadowing while other samples were investigated using freeze etching, shadowing by TEM. The TEM images reveal the presence of clear evenly size- distributed particles in high magnification.

The high magnification image (Figure 9.4) is used to visualize the ground calcium carbonate, delaminated clay and starch. The synthesis of the starch particles was based on a cross-linking. On the other hand, starch is dissolved in water, but it is not possible to form stable suspensions or to obtain colloidal systems from native starch. Figure 9.4 indicates crowding of ground calcium carbonate crystals, clay platelets and starch cross-linking particles.

Figure 9.4 Microstructure of delaminated clay, ground calcium carbonate and starch.

9.2 Microstructure of coating color without inhibitor

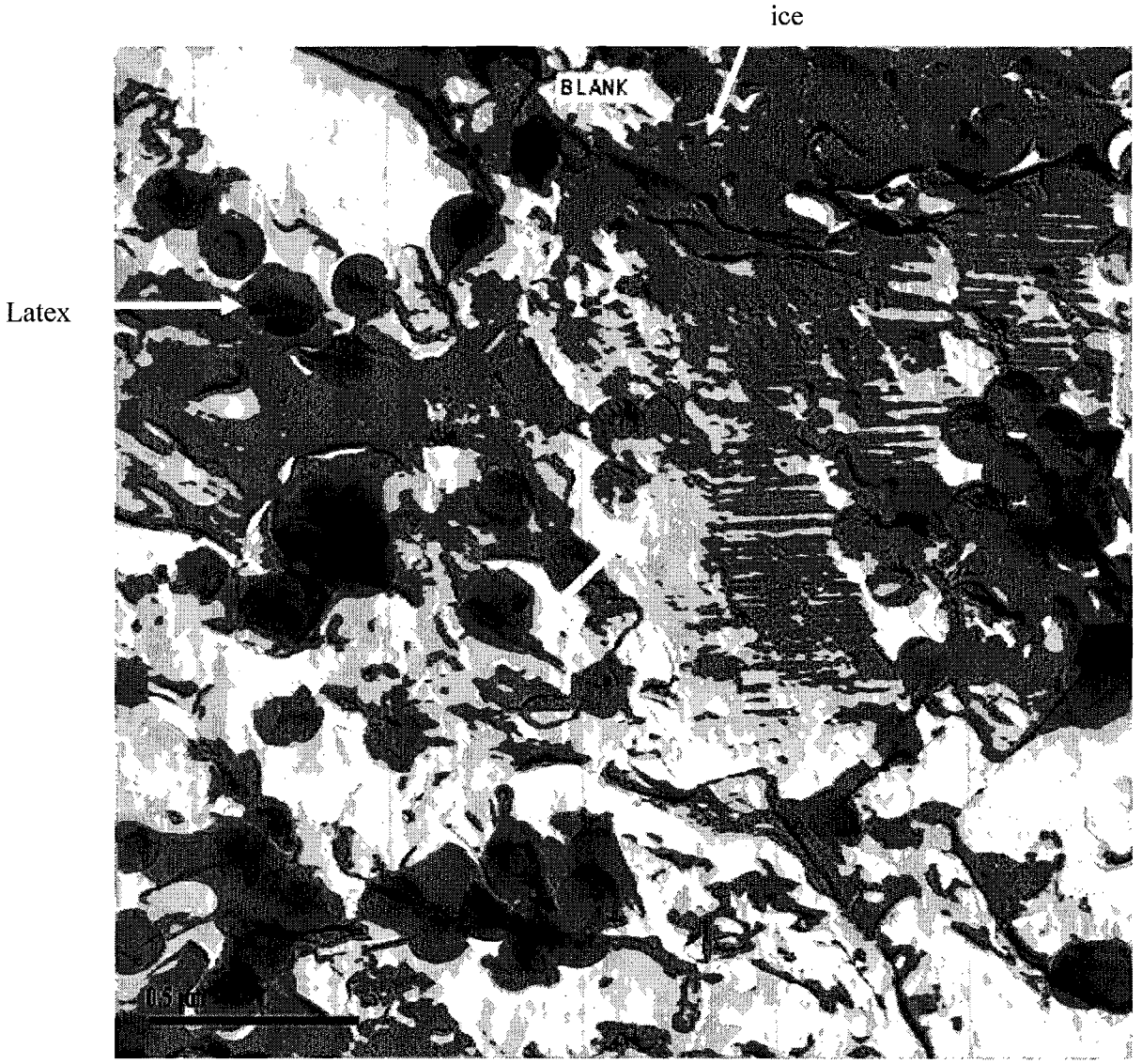

Figure 9.5 Microstructure of coating color without inhibitor.

Figure 9.5 shows the surface microstructure of wet coating color without inhibitor. It was noticed that the water was entrapped in the voids between coating components (marked ice). This can be due to the hydrogen bonding with pigment surface (Si-OH on clay) and water.

On the other hand, the interaction of starch (binder) with pigment, additives and water can form a network structure. The TEM image reveals the presence of pigment crystals. The latex has mostly monomodal spheres. Many particles are bridged with water and other coating components. There are clusters of many spherical latex particles (marked Latex). High magnification transmission electron microscopic (TEM) pictures were used as a qualitative indication of the extent of interparticle structuring and for comparison with the rheological measurement. Note that the ice surface is visible.

9.3 Microstructure Of Coating Color With Different Concentration Of Inhibitors

The microstructure of the coating color with low concentration of inhibitors, 0.1%, 0.2% and 0.3% of UV absorber and radical scavenger is illustrated in Figures 9-6, 7, 8. The surface of the coating color appears more densely packed in comparison to the coating without inhibitor and the particles come close to one another and the gap between them is quite small.

From the interfacial properties, the location of inhibitor can be identified on the image. UV absorber should adsorb on the kaolinite and GCC particles, while radical scavenger should adsorb on GCC crystals.

The absence of ice in micrograph of coating suspension with inhibitors has three explanations. First, excessive etching left only GCC crystals, kaolin platelets spherical latex with no ice. Second, metal coating that is too thick,

required to differentiate between ice and pigment particles. Third, high crowding between coating components and inhibitors made ice invisible. The yellow arrow in Figure 9.6 points to particles oriented perpendicularly to freeze-etched surface and parallel to direction of shadowing, (note: shadows are white). Most of the particles were distinctly aggregated. The thickness of these particles (ex. Figure 9.6) is small up to 1 μm.

Figure 9.6 Microstructure of coating color with 0.1% of total charge of inhibitor.

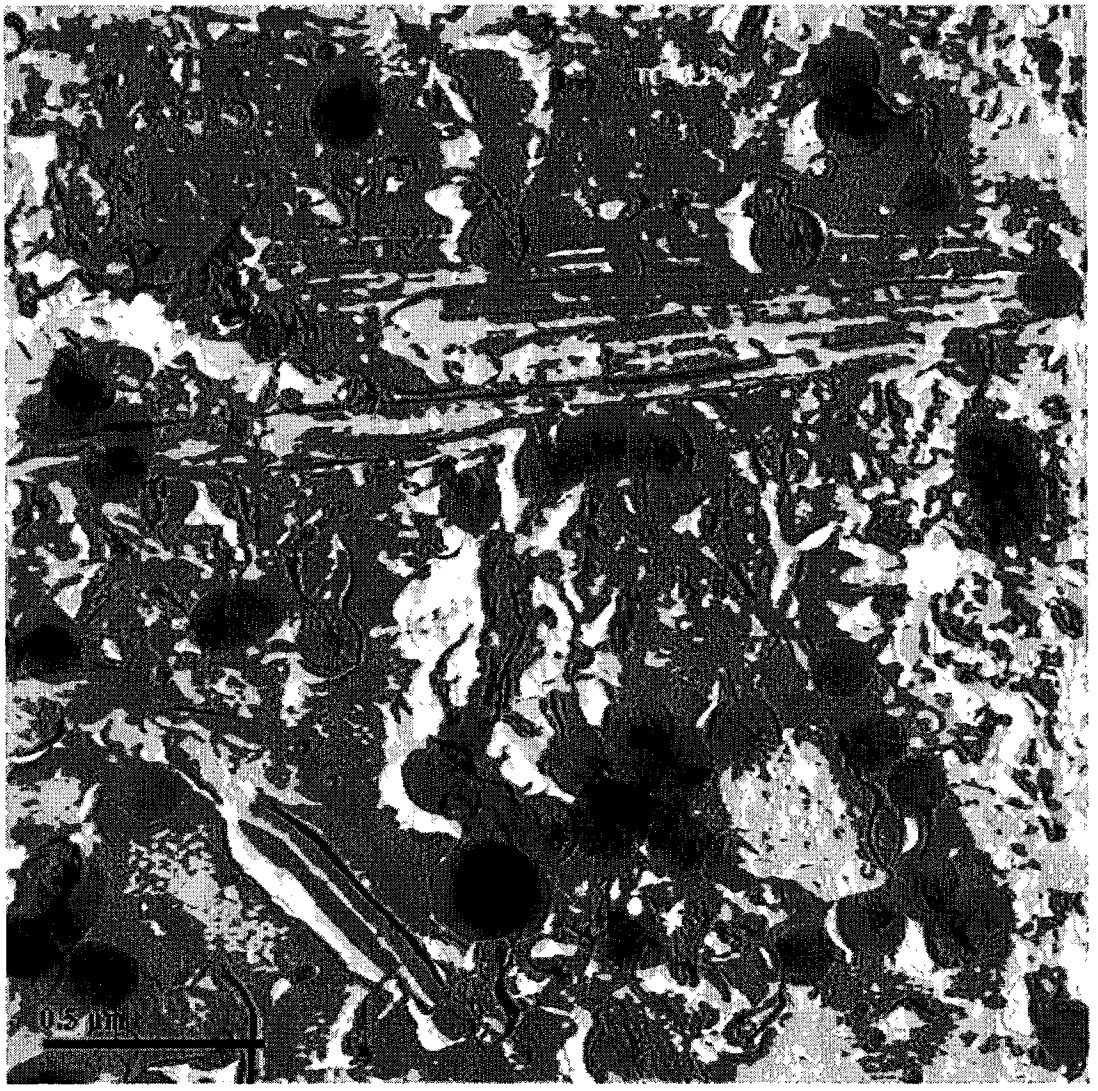

Figure 9.7 Microstructure of coating color with 0.2% of total charge of inhibitor.

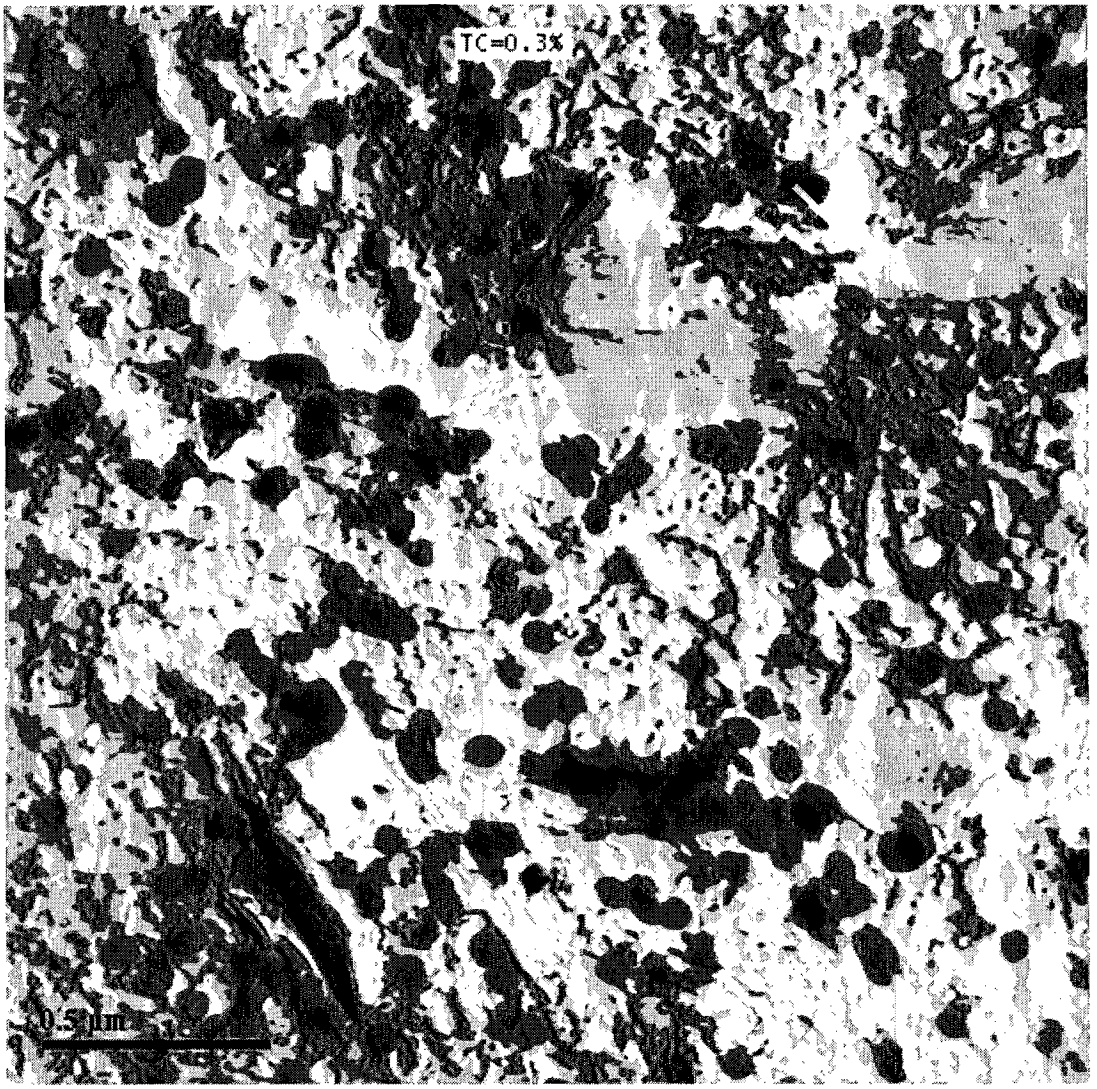

Figure 9.8 Microstructure of coating color with 0.3% of total charge of inhibitor.

Figures 9-9 and 9-10 show the images of coating color with 0.6% and o.7% of total charge of inhibitors. The increase in the concentration of inhibitor leads to increase in the crowding of coating components and therefore the ice became invisible. As a result, less porous coating structure forms. According to this micrograph, it is clear that the concentration of inhibitor is more predominant than aggregation effect. The overall effect is that the two particles are pulled together. This pull can be so strong that it exceeds any repulsive forces, and with addition of the van-der-waals force, it can produce flocculation of the particles. All these kinds of interactions lead to increase in the aggregation.

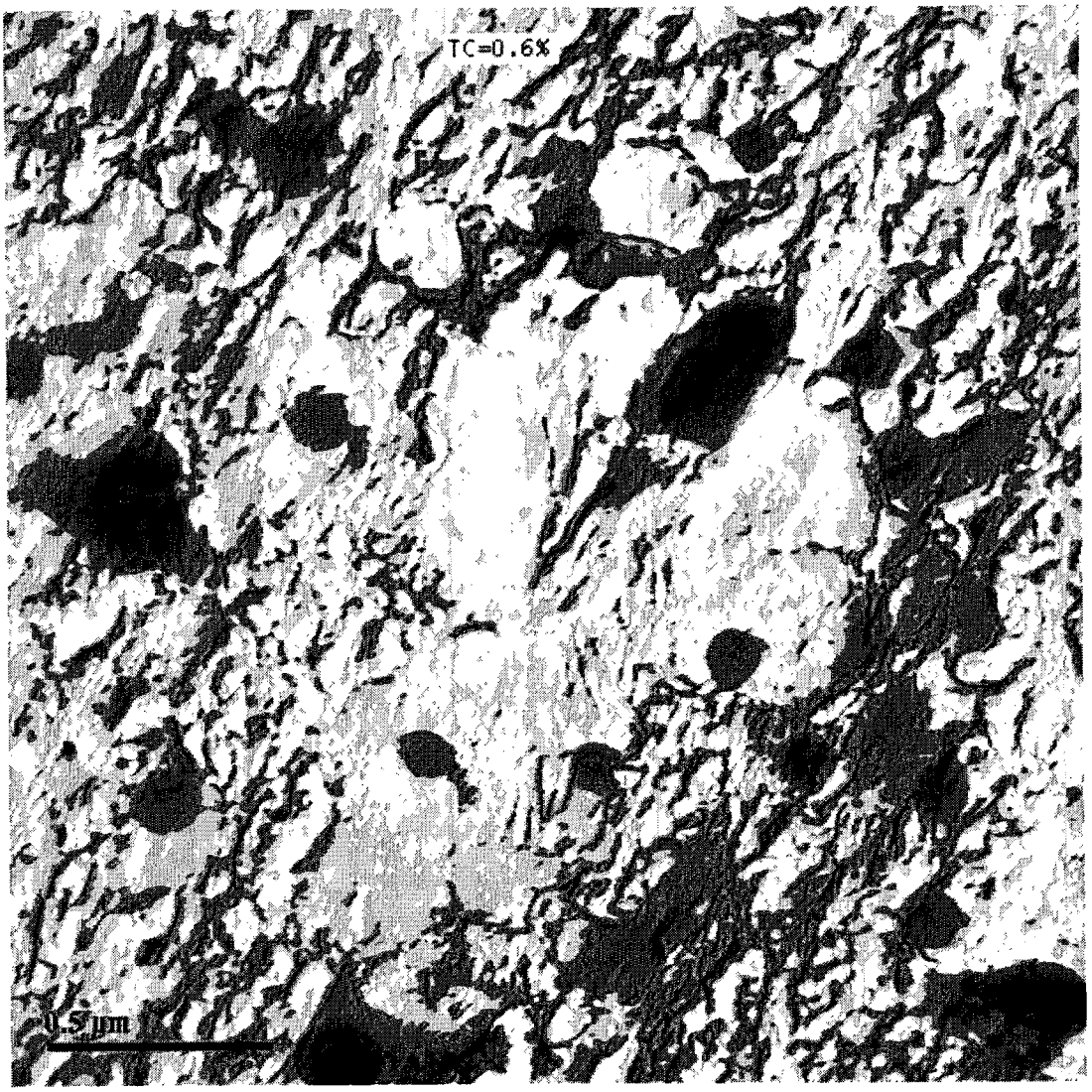

Figure 9.9 Microstructure of coating color with 0.6% of total charge of inhibitor.

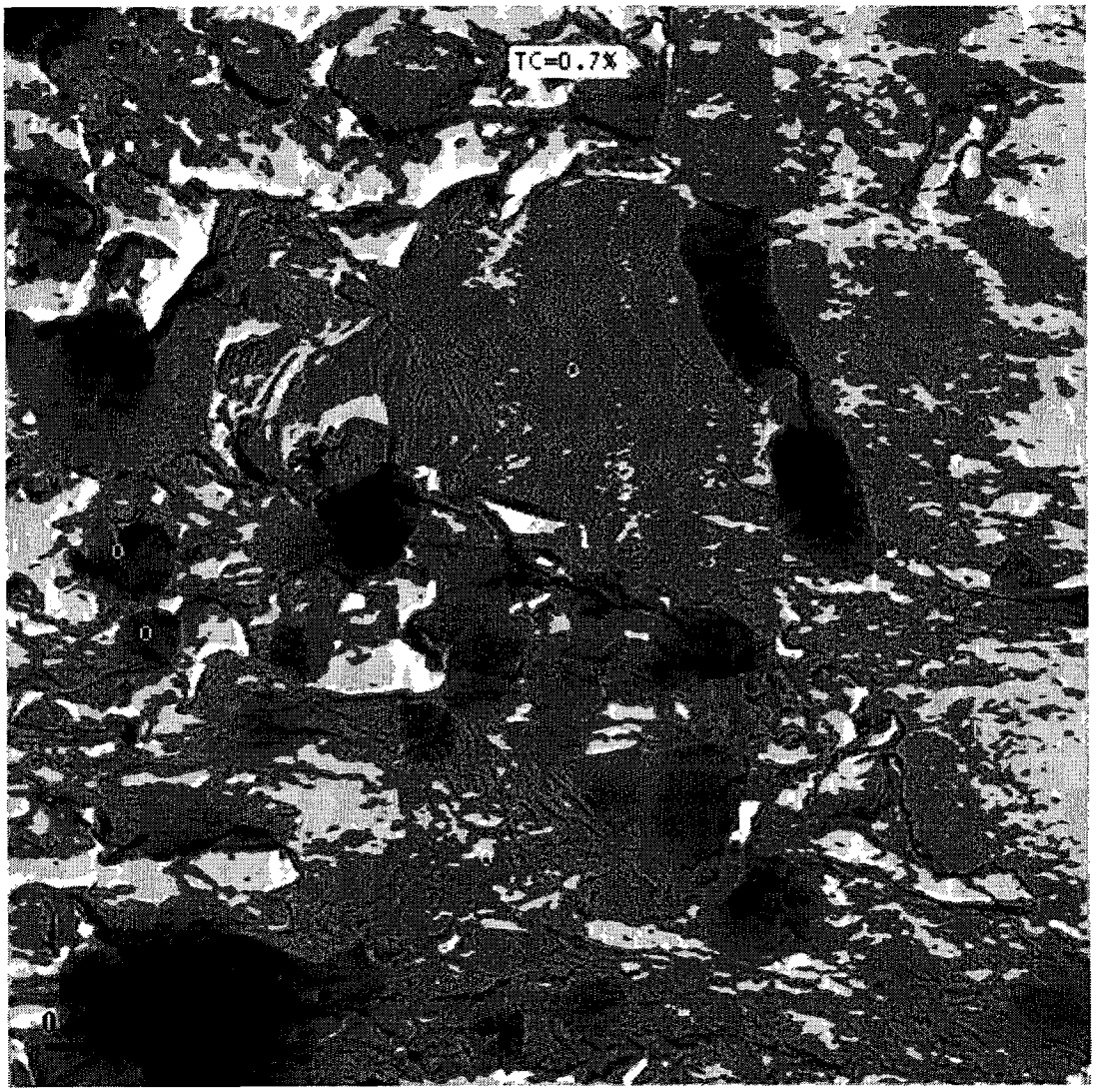

Figure 9.10 Microstructure of coating color with 0.7% of total charge of inhibitor.

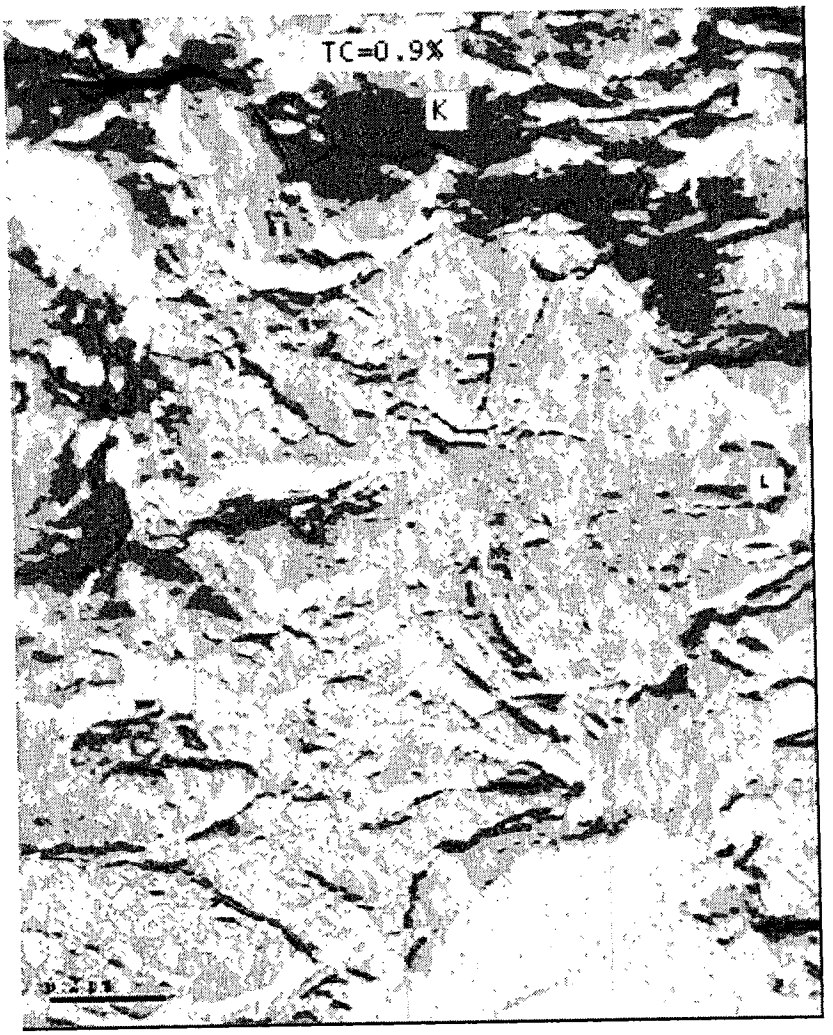

Figure 9.11 Microstructure of coating color with 0.9% of total charge of inhibitor.

Figures 9.11 and 9.12 show the micrograph of coating color with high concentration, 0.9% and 1% of inhibitor addition. The presence of inhibitor and the invisibility of pigment and latex suggest that inhibitors encapsulate pigment in suspension.

The inhibitors tend to increase the aggregation between the particles. It can be concluded that increasing the concentration of the inhibitor leads to increase in the adsorption on the pigment particles. Therefore, the aggregation between particles increases. Also, the ultrastructure of colloidal coating color dispersion is the result of complex interactions between the submicroscopic plate-like and aragonite mineral particles and the inhibitors.

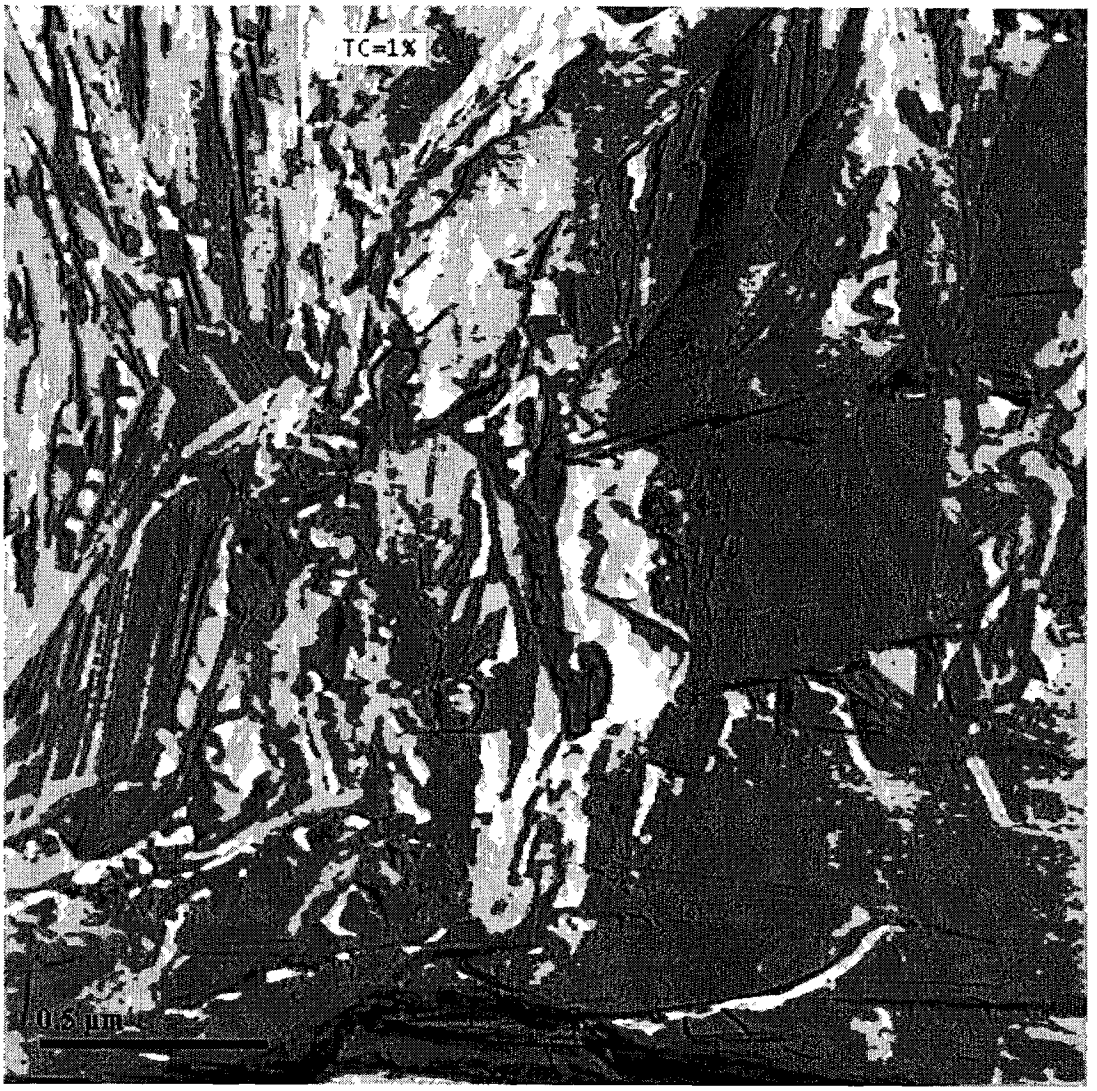

Figure 9.12 Microstructure of coating color with 1% of total charge of inhibitor.

Figure 9.13 Microstructure of coating color with 0.6% w. of radical scavenger.

Aqueous suspension of 0.6% w. of radical scavenger was observed. TEM image is in Figure 9.13. Many particles are bridged, possibly with radical scavenger. The image provides observation of the monomodal spheres

(latex). The explanation may be that the radical scavenger encapsulates pigment in suspension.

With these examples we have demonstrated that high magnification freeze-etching- transmission electron microscopy (TEM) provides new access to microstructures in coating pigments, binders, inhibitors and formulations. Also, high magnification-TEM is used to visualize directly components in both dilute and concentrated coating pigments in order to deduce component interaction and agglomeration.

On the other hand, the objective of this discussion has been to demonstrate the capability of freeze-etching replica technique in preserving the original structure of colloidal dispersions. The cryotechnique discussed has important applications in different fields dealing with the interaction between colloidal particles.

Chapter Ten

Simulation of Paper Coating Color in the Nip of Metering Size Press

In a paper coater, a thin layer of a highly pigmented coating color is applied on a paper web running at very high speed (1200m/min) between two contra-rotating rolls covered with an elastomeric layer. For a set of operating conditions and coating color formulations, undesirable phenomena like color spitting and coating ribs may be triggered in the application nip during the coating process. These runnability problems can be partially eliminated by an optimal choice of the metering rod diameter and transfer roll cover [132]. However, for better understanding of the flow patterns in the coating nip should shed light on some of the potential sources of these problems, such as vortex formation.

10.1 Problem Description

The problem to be considered is shown schematically in Figure 10.1. It deals with the flow through the nip of a metering size press. The flow enters and exits at a tangential velocity of 20 m/s between two rollers each with a diameter of 80 cm. The rollers length is 80 cm and the gap between them is 0.006cm. In the upper and bottom part of the domain the angular velocity is 314 rad /s which corresponds to a linear velocity of 20 m/s at the surfaces. The field consists of a single subdomain.

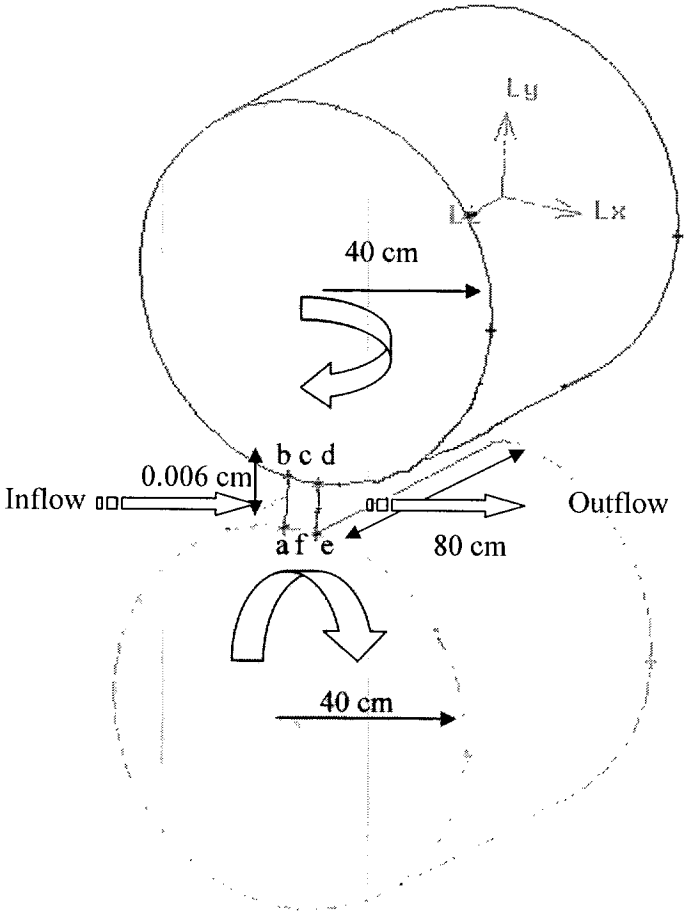

Figure 10.1 The geometry of metering size press.

Previous studies [129] focused on the region of the metering nip without considering the forces of inertia. We consider the forces of inertia. Our interest is in studying the flow in the application nip to reveal its hydrodynamic characteristics. Our numerical calculations are based on the commercial software Polyflow. Figure 10-2 shows the program structure. We focus on the following points:

- Use Polymat section of the software to fit our experimental data to a rheological model (Appendix E).
- Reveal the location of the vortices in the nip of the metering size press and calculate the vorticity as a function of the position in the nip (x,y,z).
- Calculate the shear rate, inelastic stress, stream function and the viscosity as a function of the position in the nip (x,y,z).
- Compare the solutions between two cases, case I (consider the problem as time-dependent problem, inertia taken into account) and case II (consider the problem as evolution problem).

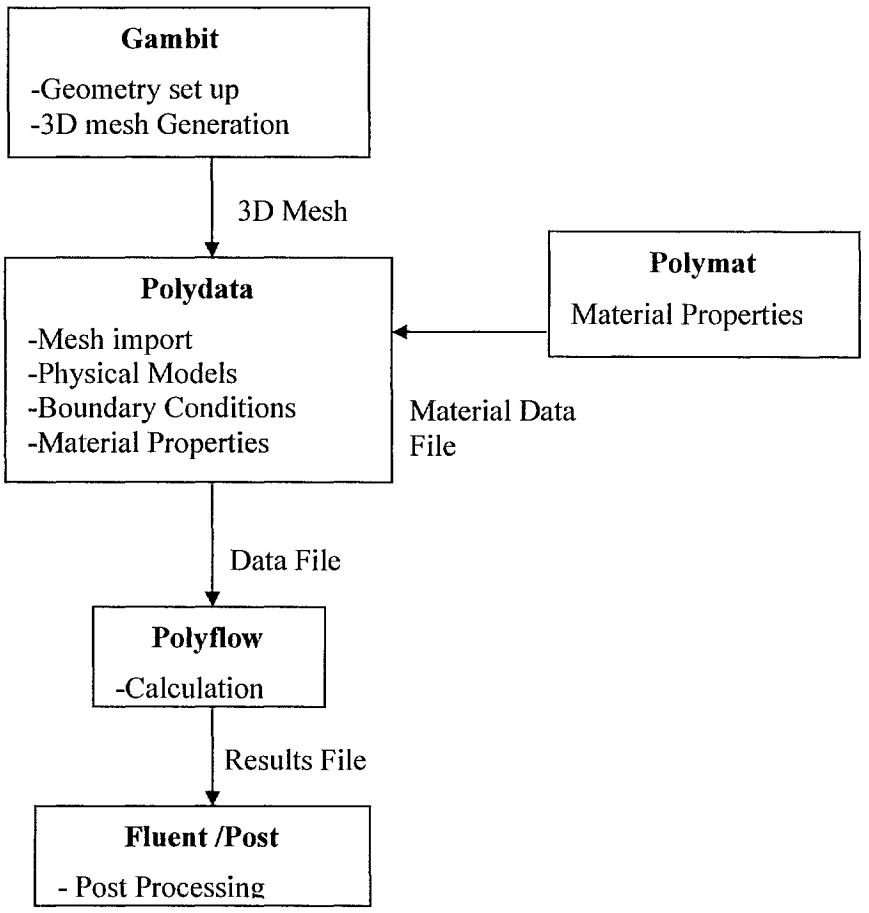

Figure 10.2 Program Structure.

10-2 Governing Equations

10-2-1 The conservation laws

The conservation laws for viscid fluid flows are described by:

The continuity equation is

$$\frac{\partial \rho}{\partial t} + \nabla.(\rho V) = 0 \qquad (1)$$

Density is considered as a variable and computed using the mass conservation.

The momentum equation (Navier-Stokes equation) is

$$\rho \frac{DV}{Dt} + \nabla P = \nabla \tau_{ij} \qquad (2)$$

where τ_{ij} is the stress tensor. Since P is the pressure and all the external body forces are neglected.

Equation of state : $\rho = \rho (P,T)$ where T is constant

$P = \rho R T$

where :

ρ = mass density
u, υ, w = velocity components in x, y, and z directions , respective ly
t = time
$V = u\,\hat{i} + \upsilon\,\hat{j} + w\,\hat{k}$
$\nabla = \hat{i}\,(\partial/\partial x) + \hat{j}(\partial/\partial y) + \hat{k}(\partial/\partial z)$

There are five equations for the five unknowns ρ, u, v, w, P.

10-2-2 Vorticity-Stream Function Formulation

Fluid rotation is defined as the average angular velocity of any two mutually perpendicular line elements of a fluid particle. For three-dimensional flow, the rotation vector is a three components vector given by:

$$\omega = \omega_x \mathrm{i} + \omega_y \mathrm{j} + \omega_z \mathrm{k} \qquad (3)$$

where ω x, ω y, ω z are the rotations about x, y, and z axis, respectively, and are defined by

$$\omega_x = \frac{1}{2}\left(\frac{\partial w}{\partial y} - \frac{\partial y}{\partial z}\right),\ \omega_y = \frac{1}{2}\left(\frac{\partial u}{\partial z} - \frac{\partial w}{\partial x}\right),\ \omega_z = \frac{1}{2}\left(\frac{\partial \upsilon}{\partial \mathrm{x}} - \frac{\partial u}{\partial y}\right)$$

In vector rotation we have

$$2\omega = \nabla \times \mathrm{V}$$

Therefore, the vorticity can be defined as:

$$\zeta = 2\omega = \nabla \times \mathrm{V} \qquad (4)$$

The action of viscous forces in a flow field develops rotation. Hence any viscous flow is a rotational flow with $\omega \neq 0$ [131]. Only the action of shearing stress can produce rotationality.

Two-dimensional flow can be characterized by introducing a stream function $\psi(\mathrm{x}, \mathrm{y})$. The stream function relates the concept of streamlines to the principle of mass conservation. For a two dimensional flow, the stream function:

$$\rho \mathrm{u} = \frac{\partial \psi}{\partial \mathrm{y}} \text{ and } \rho \upsilon = -\frac{\partial \psi}{\partial x} \qquad (5)$$

10-2-3 Non-Newtonian Inelastic Model

The flow phenomena observed with Non-Newtonian fluids cannot be predicted by only the Navier-Stokes equations. Non-Newtonian behavior has many facets as the shear rate dependence of the shear viscosity. Therefore, non-Newtonian inelastic flows should be characterized by different models. In this work the Carreau-Yasuda model is used.

The Carreau-Yasuda law for inelastic flows is

$$\eta = \eta_\infty + (\eta_0 - \eta_\infty)\left[1 + (\lambda\dot{\gamma})^a\right]^{\frac{n-1}{a}} \qquad (6)$$

where: η_0 = zero-shear-rate viscosity.

η_∞ = infinite-shear-rate viscosity.

λ = natural time (i.e., inverse of the shear rate which the fluid changes from Newtonian to power-law behavior).

a = index that controls the transition from the Newtonian plateau to the power-law region.

n = power-law index, which is a property of a given material.

The addition of the exponent a allows for control of the transition from the Newtonian plateau to the power-law ($\eta = K(\lambda\dot{\gamma})^{n-1}$) region. A low value (a<1) lengthens the transition, and a high value (a>1) results in an abrupt transition.

The results of using the regression technique to calculate the material properties are shown in Table 10-1.

Table 10-1 material properties of coating color using Carreau-Yasuda model

Material properties	η_o	η_∞	λ	n	a
Coating color	0.15	0	0.002817	0.5	2
Coating with 0.6% of inhibitors	0.3	0	0.002817	0.5	2
Coating with 1% of inhibitors	0.7	0	0.002817	0.5	2

It can be noticed that the material properties are the same for different coating colors.

10-3 Boundary Conditions

The boundary sets of the problem are also shown in Figure 10-3.

The conditions at the boundaries of the domain are (the points (x,y,z) of the geometry can be seen in Appendix- A10-1) :

-Boundary 1: vt (tangential velocity) = 20 m/s (abgl).

-Boundary 2: vt = 20 m/s (edij).

-Boundary 3: angular velocity = 314 rad/s (bghidc).

-Boundary 4: angular velocity = 314 rad/s (alkjef).

-Boundary 5: plane of symmetry axis (abcdef).

-Boundary 6: plane of symmetry axis (lghijkl).

- The density = 0.00125 kg/m^3 .

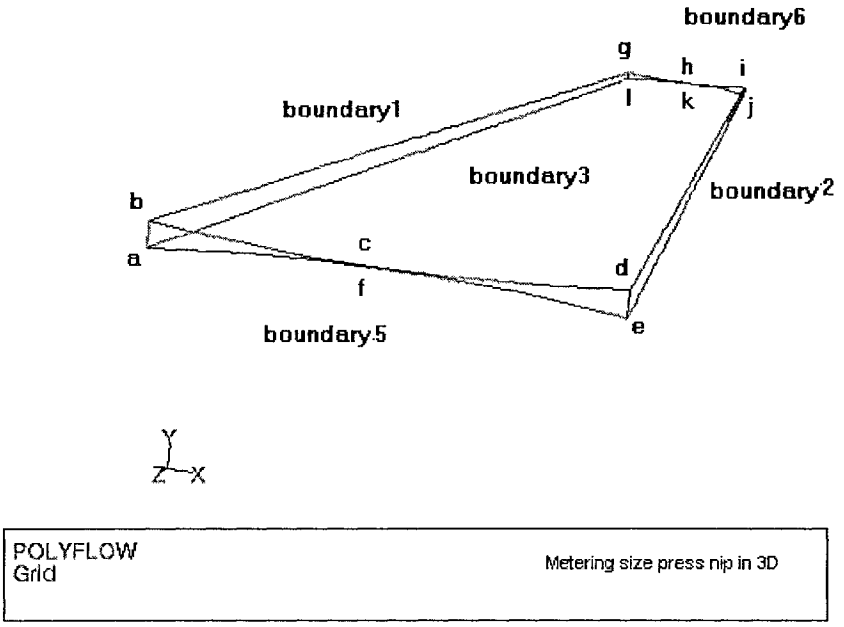

Figure 10-3 Boundaries and sub domain.

10-4 Finite Element Solution

The finite element mesh is displayed in Figure 10-4. As we see, a full 3D finite element mesh is built for the coating color in the application nip. For the flow in the nip, the need of volume elements can be understood for geometrical reasons; the most important ingredient however remains the proper description of the inner nip face. 3D elements are also needed in order to properly identify some directions along which boundary conditions apply. Typically, the geometry involves some planes of symmetry.

As seen in Figure 10-4, the mesh topology involves one sub-domain, 2240 elements and 4830 nodes. However, it was imperative to study stream function in 2D as shown in Figure 10-4.

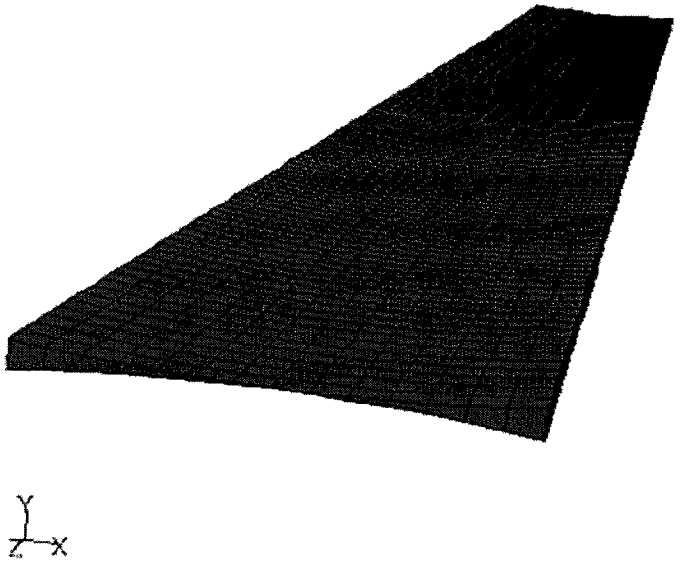

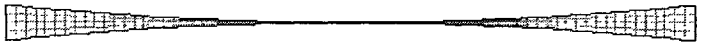

POLYFLOW
Grid, 2D

280
elements

Figure 10-4. Finite element mesh in 3D and 2D.

In three dimensions, we used hexahedron elements with all faces map-able and mesh is matching with spacing 0.5. In two dimensions, we used triangle elements with all faces pave and mesh is matching with spacing 0.1.

10-4-1 Time-Marching Scheme

In this work, a finite element solution procedure using implicit Euler method is applied to solve those equations for 3D, Non –Newtonian inelastic flow. Most of the partial differential equations that describe fluid flows are nonlinear. The non-linear algebraic equations corresponding to the implicit Euler method is obtained:

$$\frac{1}{\Delta t} M(X_{n+1} - X_n) + K X_{n+1} + F_{n+1} = 0 \qquad (7)$$

subject to initial conditions of the type

$$X(t_0) = X_0 \qquad (8)$$

X is the vector of nodal unknowns such as velocity, pressure or inelastic stress. The matrices M and K are the mass and stiffness matrices (variable coefficients), which may depend on the unknown vector X. The vector F corresponds to the volumetric forcing function and the boundary conditions. The above equations 7 & 8 are solved by a time-stepping procedure. Polyflow calculates a solution at a discrete set of times t_n, defined by

$$X_n = X(t_n) \qquad (9)$$

$$t_n = t_{n-1} + \Delta t_n \qquad (10)$$

Where the subscript n refers to the time step.

10-4-1-1 Internal Solution Strategies of Time-Marching Scheme

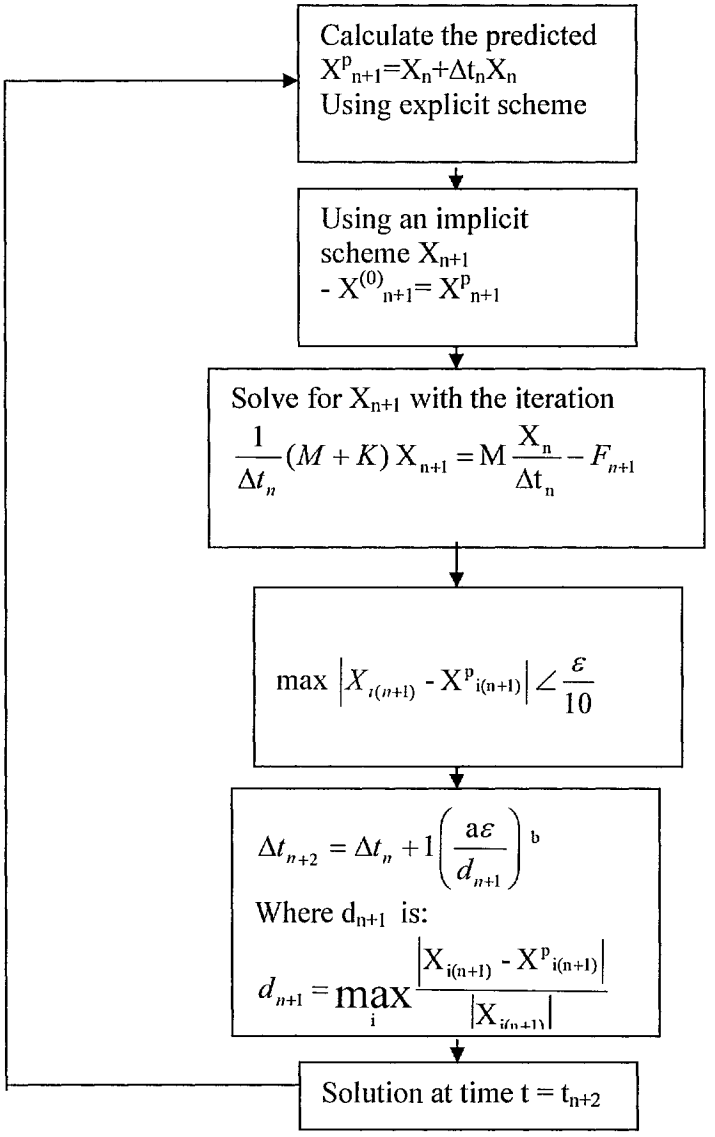

Figure 10-5 Time-marching Iterative solution algorithm

Where X^{p}_{n+1} is the predicted value, X_{n+1} is the corrected value, the coefficient a and b are equal to1 because the implicit Euler method is a first

order method, d_{n+1} is the maximum relative difference between the predicted and corrected value of X_{n+1}, $X_{i(n+1)}$ is the ith component in the vector X_{n+1}. ϵ is a relative tolerance of the error in X_{n+1} by comparison with the exact solution $X(t_{n+1})$.

The set up of the time-stepping procedure:

- Initial time step = 0
- Maximum time step = 1
- $\Delta t = 0.01$
- Min $\Delta t = 0.0001$
- Max $\Delta t = 0.25$
- ε (tolerance for time marching) = 0.001

During the transient scheme no step has failed. The number of iterations was 18 (Appendix E can show the iterations solution)

10-4-2 Evolution Scheme

Evolution is a tool to solve non-linear flow problems. The solution of the nonlinear problem is surrounded by a domain of convergence. The way to solve a nonlinear problem is to begin with a solution to a simpler problem. From this solution, we then solve a sequence of problems of increasing non-linearity, using the solution of one problem as the initial condition for the subsequent problem. Ultimately, the sequence should lead to the solution.

10-4-2-1 Internal Solution Strategies of evolution Scheme

In our problem, the velocity of the roller is found to be the largest responsible for the non-linear nature of the problem. For evolution scheme, the procedure should be followed as in Figure 10-6.

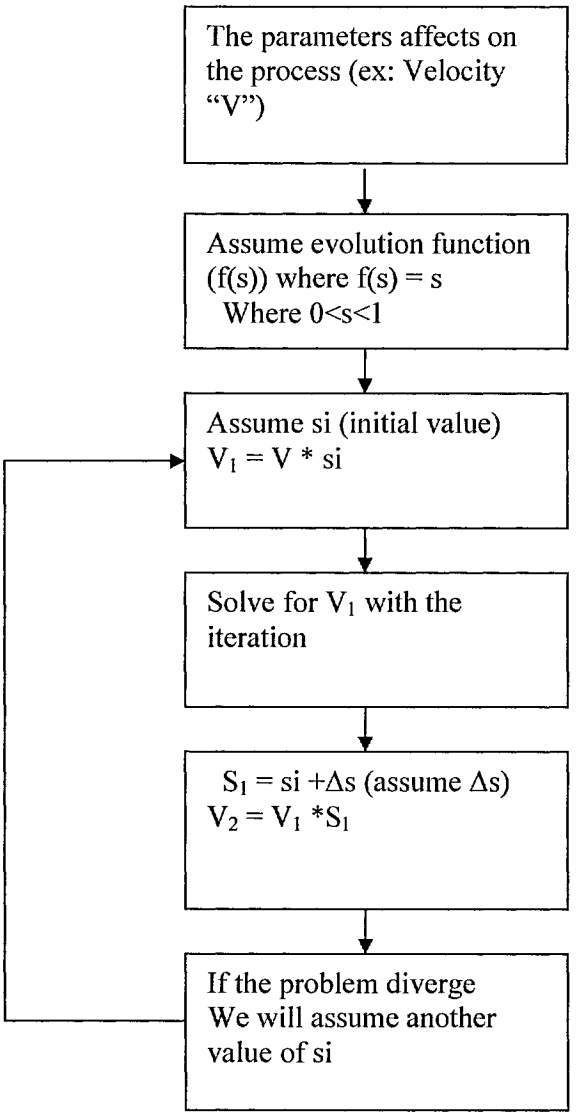

Figure 10-6 Evolution Iterative solution algorithm

10-5 Solution Examples

Figure 10-7 shows streamline patterns drawn along the application nip. For rotational flows, streamlines are spaced further apart as the distance from the centerline increases. It is noticed that there is difference in stream function lines using two different methods time-marching scheme and evolution. The velocity is higher using time-marching scheme than evolution scheme. Figure 10-8 reveals the direction of the velocity in both solutions (time-marching scheme and evolution scheme). The stream function distributions along the application nip are shown in Figure 10-9. The stream function reaches a maximum value at the center of the application nip

The vortex lines are shown in Figure 10-10. The formation of three vortices at the inlet, outlet and the center of the application nip are shown using time-marching scheme (taking inertia into account). The value of vorticity experienced significant increase for the vortex in the center, in calculations obtained from time-marching scheme (Figure 10-11b). It is known [133] that one of the characteristics of film-splitting is the formation of vortices. This is true for the case when both rolls move with the same speed, where the vortices are equal in size and are symmetrical around the stagnation line passing through the application nip center.

These vortices increase in size with inertia. When the speed of rolls increases, the vortices break up and cause misting, particularly for liquids with low viscosity. Figure 10-12 shows the shear rate as a function of the location. Using evolution scheme, the shear rate has the highest value at the center of the nip. However, using time-marching scheme, the variation in shear rate is slightly significant comparing to the variation in shear rate using evolution scheme. Numerical results for the viscosity of coating color are presented in Table 2.

Table 10-2 The viscosity value using two different schemes.

	Evolution	Time-marching scheme
Location at the Geometry (cm)	$vis\cos ity \times 10^{-9}$ (pas)	Viscosity (pas)
-3.5	6.44	3.16
-2.5	6.05	0.72
-1.5	2.42	3.4
-0.5	0.401	63.4
1.5	1.47	3.46
2.5	3.36	0.72
3.5	6.08	3.16

One of the interesting results of the numerical simulation is displayed in Figure 10-14. The figure shows variations of local values of viscosity and vorticity along the nip axis. First, one can notice from Table 10-2 that the values of local viscosity, calculated to the ratio of stress to shear rate, are quite realistic in the time-marching scheme. The qualitative changes along

the nip access are quite similar for viscosity and vorticity. This confirms that the strength in vortex rotation provoked higher frictional forces.

The flow characteristics vary with the relative strength of the viscous and inertia forces. Therefore, higher viscosities and speed induce formation of rips.

Previous results show that the flow in the application nip is time-dependent. Non-Newtonian flow is non-linear system and complex, it can't be solved only by Navier Stokes Equations, it needs model to identify the material properties. The evolution scheme is controlled by convergence of the iteration scheme, while time-marching scheme is controlled by the convergence and the accuracy of the time integral technique. Numerical 3D simulation of the flow in the coating nip taking inertia forces into consideration depicts vortex formations on the surface of the coater's rolls.

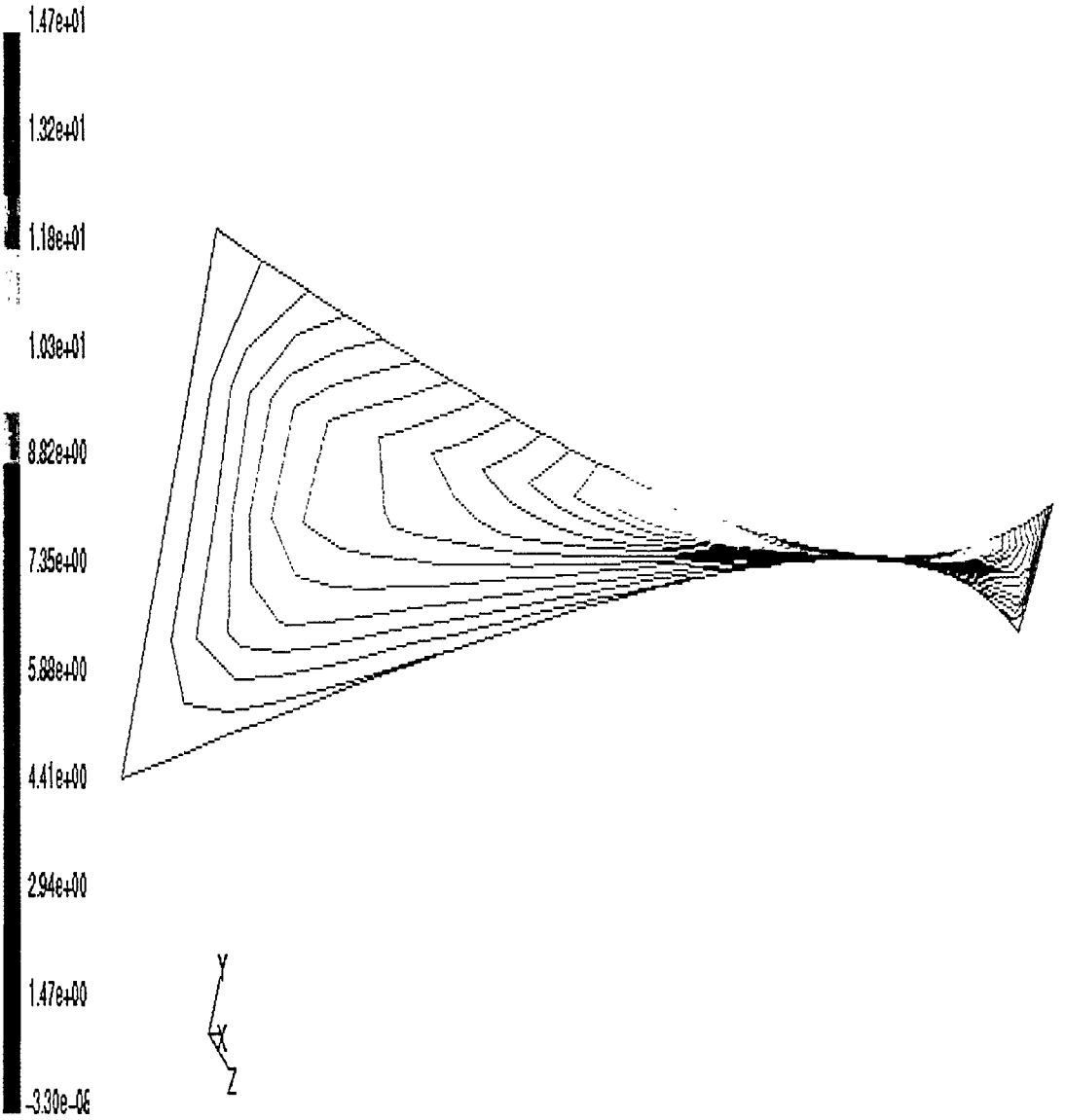

POLYFLOW
Contours of stream function Time-Marching Scheme (a)

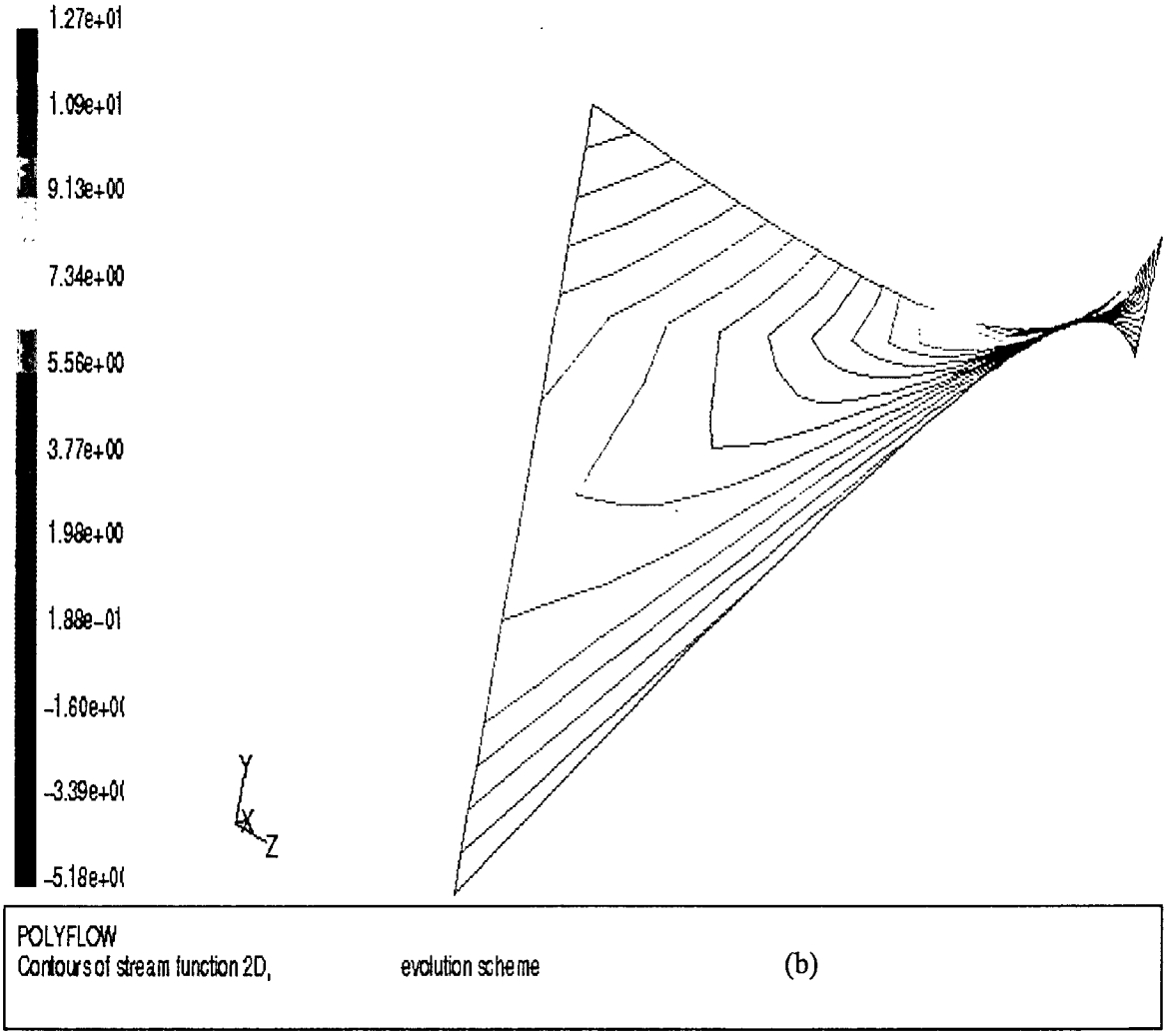

Figure 10-7 velocity colored by stream function using (a) time-marching scheme and (b) evolution scheme.

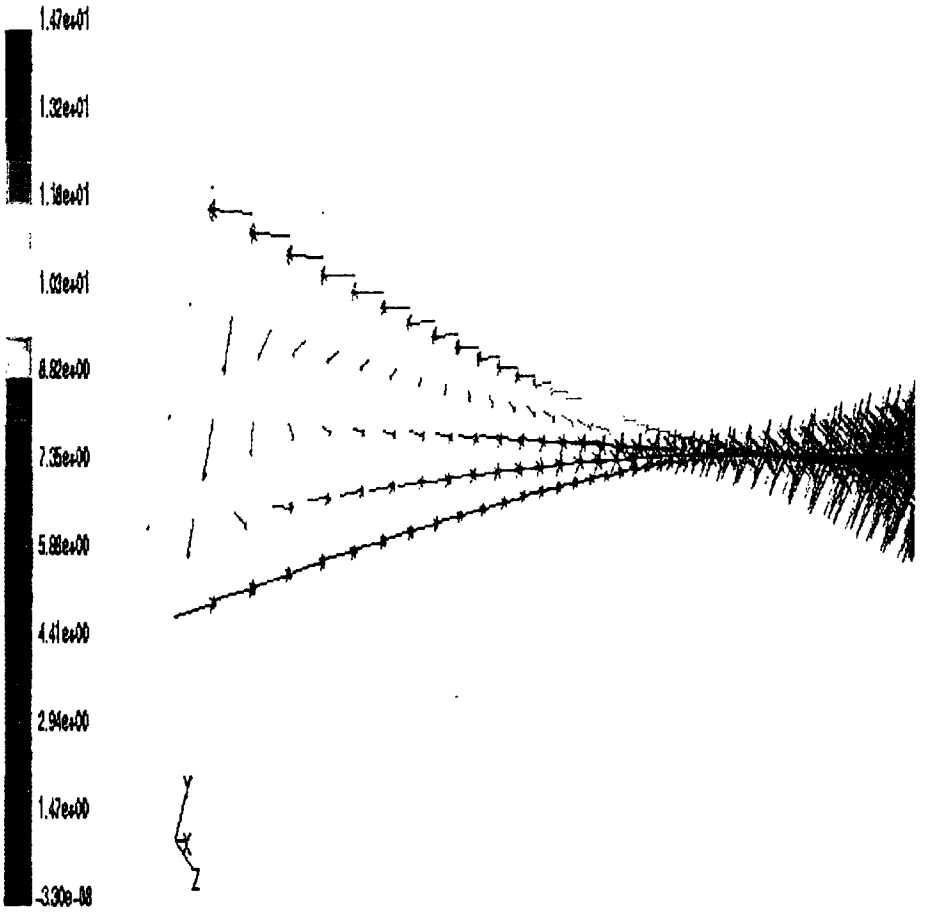

POLYFLOW
velocity Colored By stream function, time-marching scheme (a)

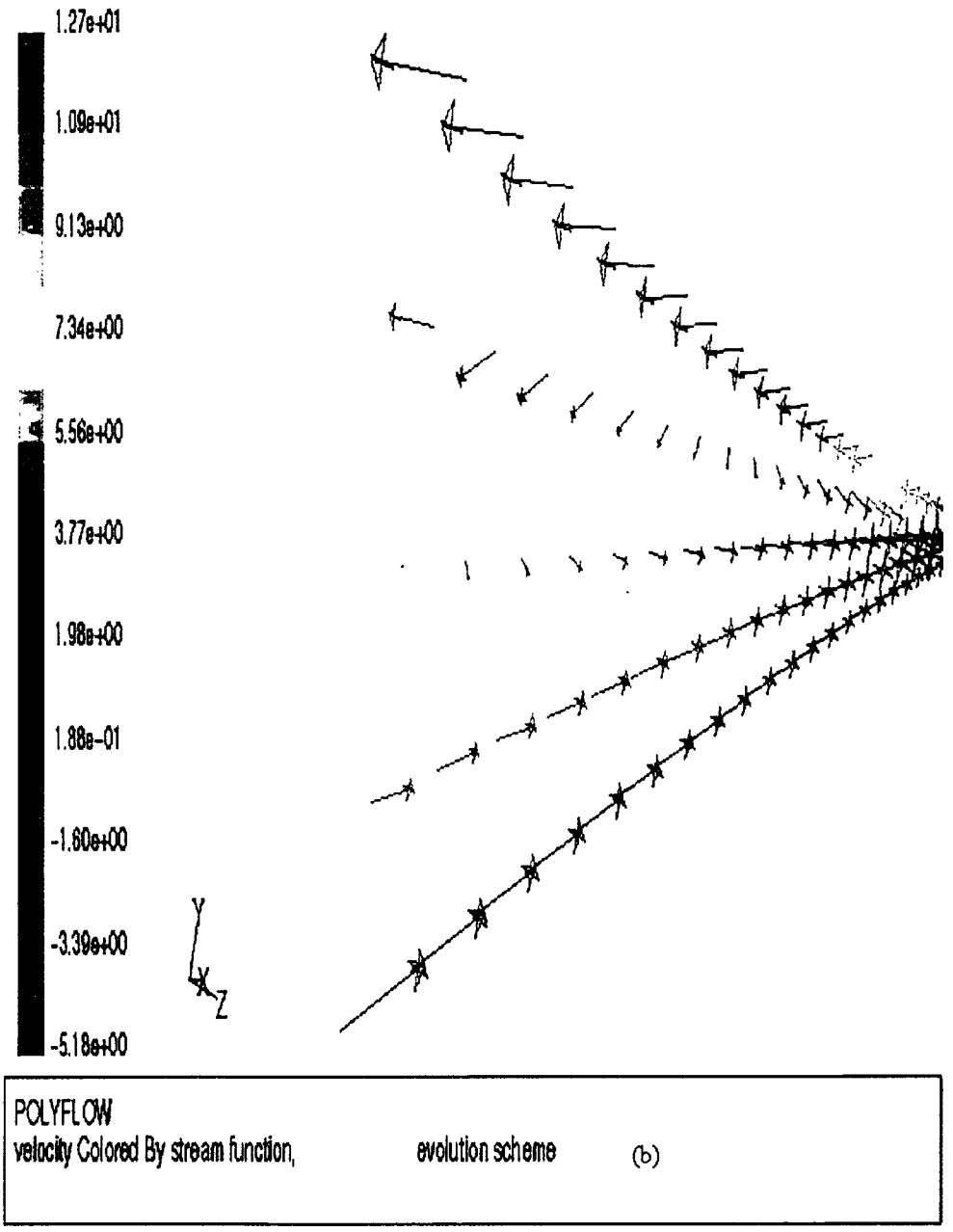

Figure 10-8. contour of the vorticity (a) evolution scheme, (b) time-marching scheme.

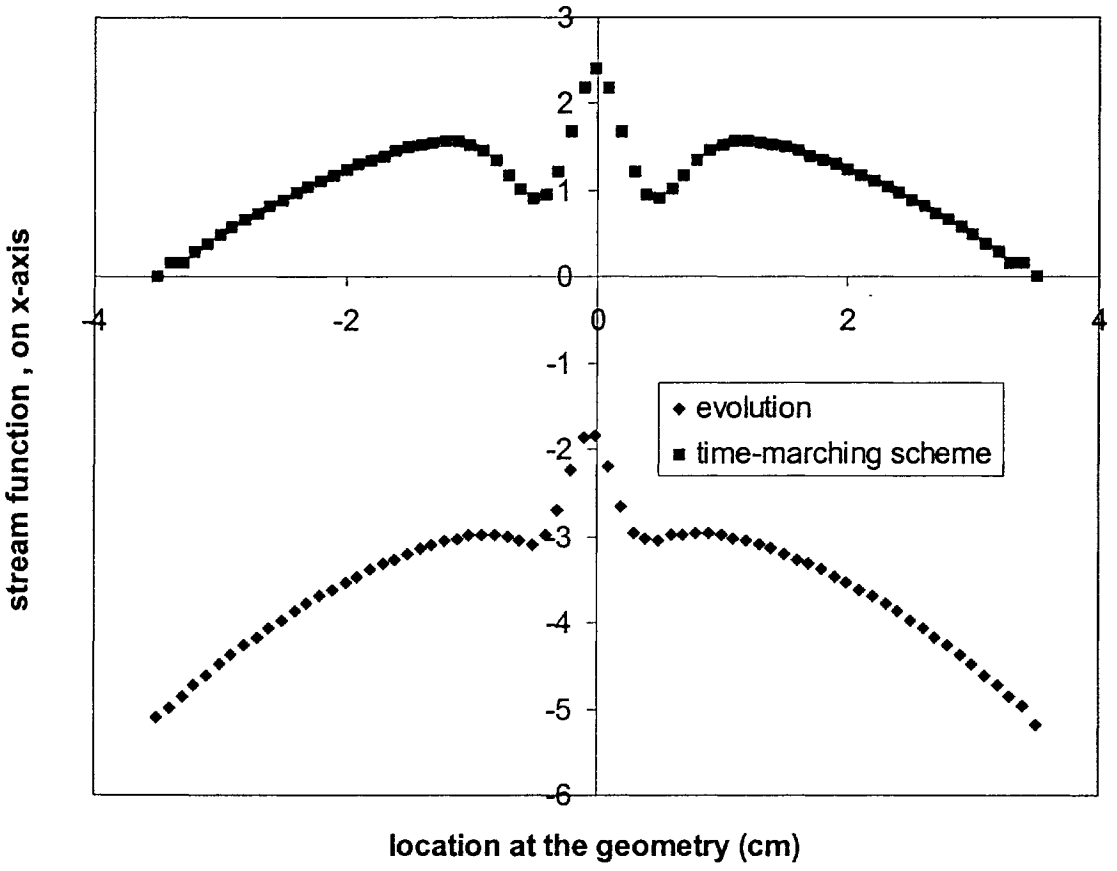

Figure 10-9 stream function distribution along the application nip.

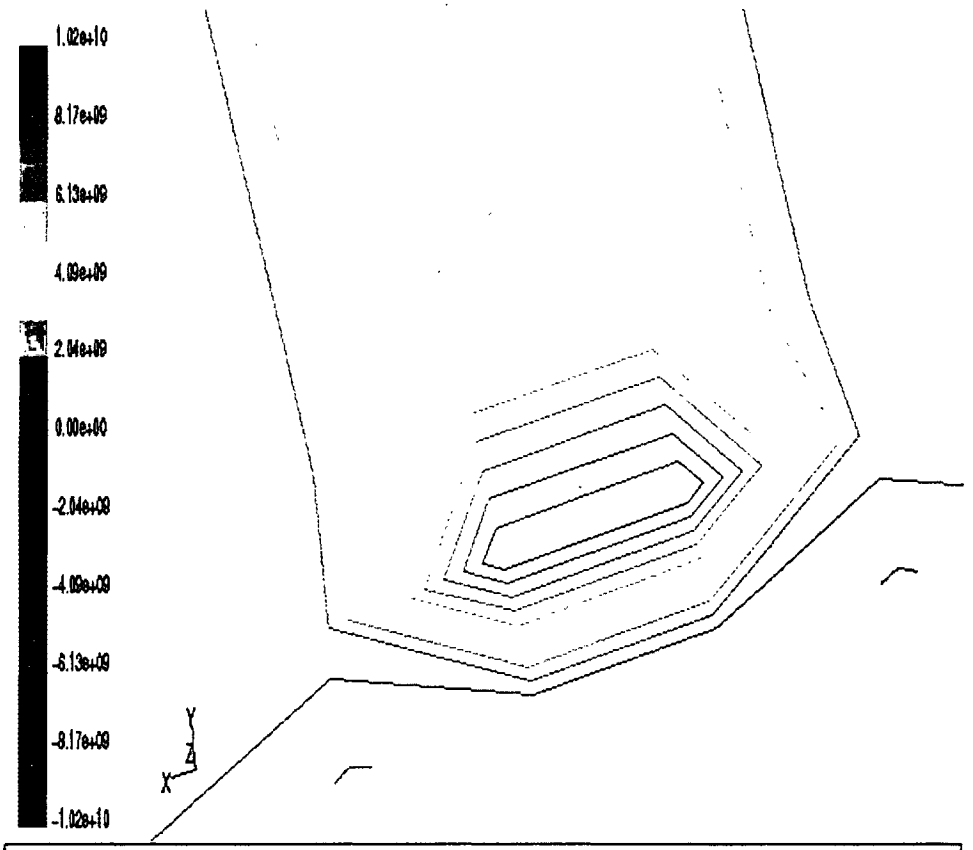

PCLYFLOW
Contours of Vorticas, evolution scheme (a) boundary 4

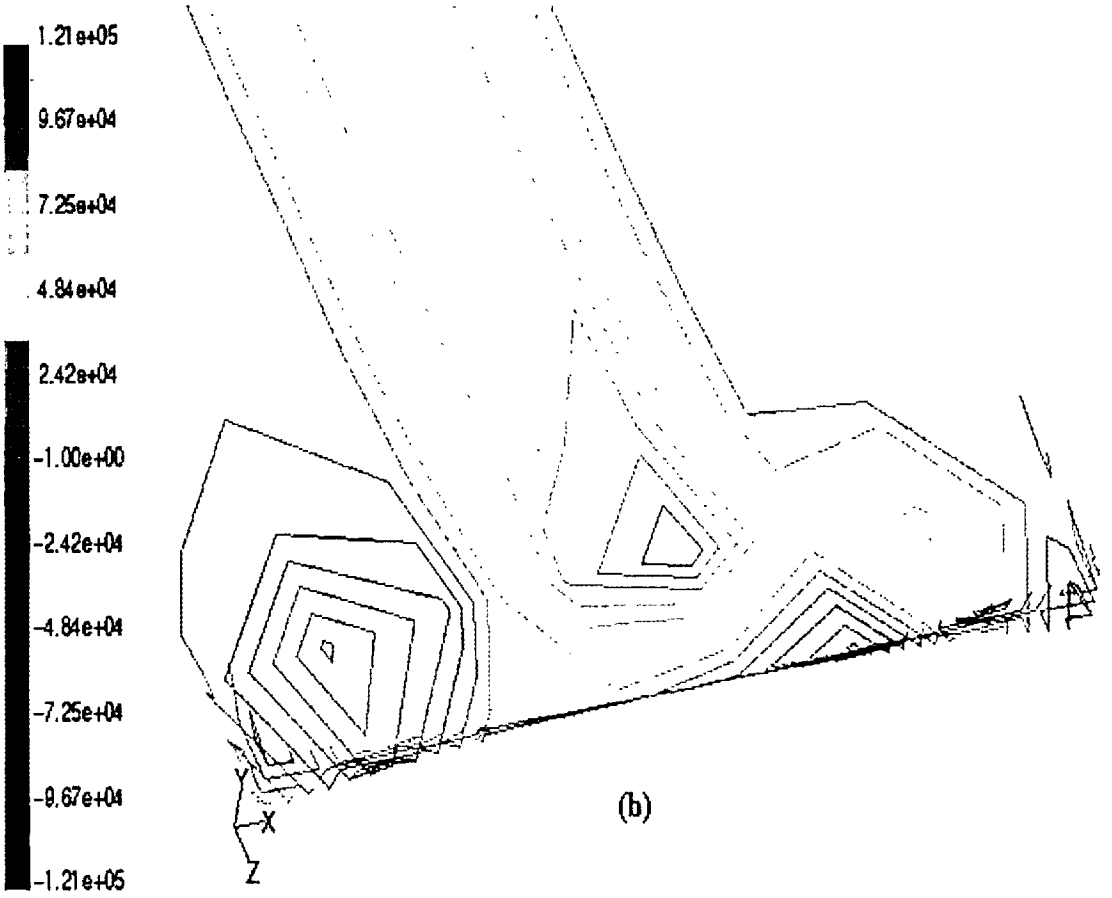

Vortices at boundary 4
Time-marching scheme

Figure 10-10 Vortices lines along the application nip.

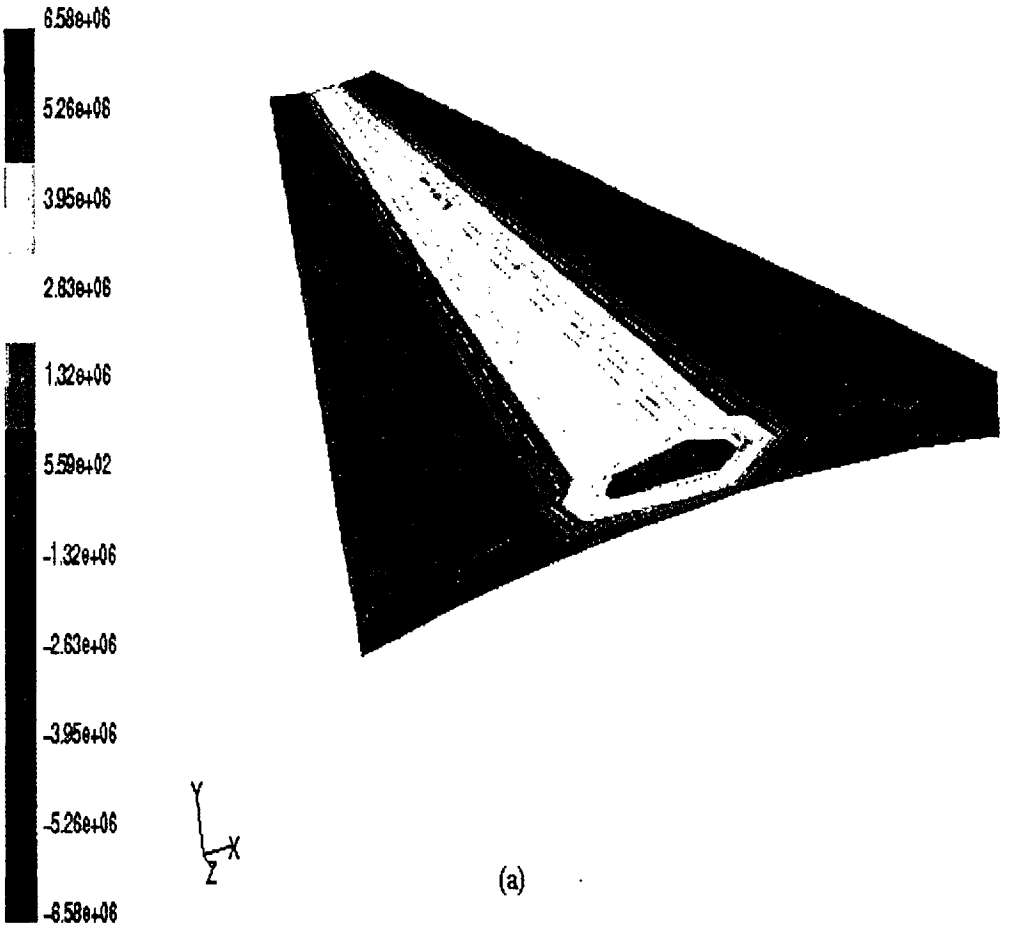
6.58e+06
5.26e+06
3.95e+06
2.63e+06
1.32e+06
5.59e+02
-1.32e+06
-2.63e+06
-3.95e+06
-5.26e+06
-6.58e+06
Y
X
Z

(a)

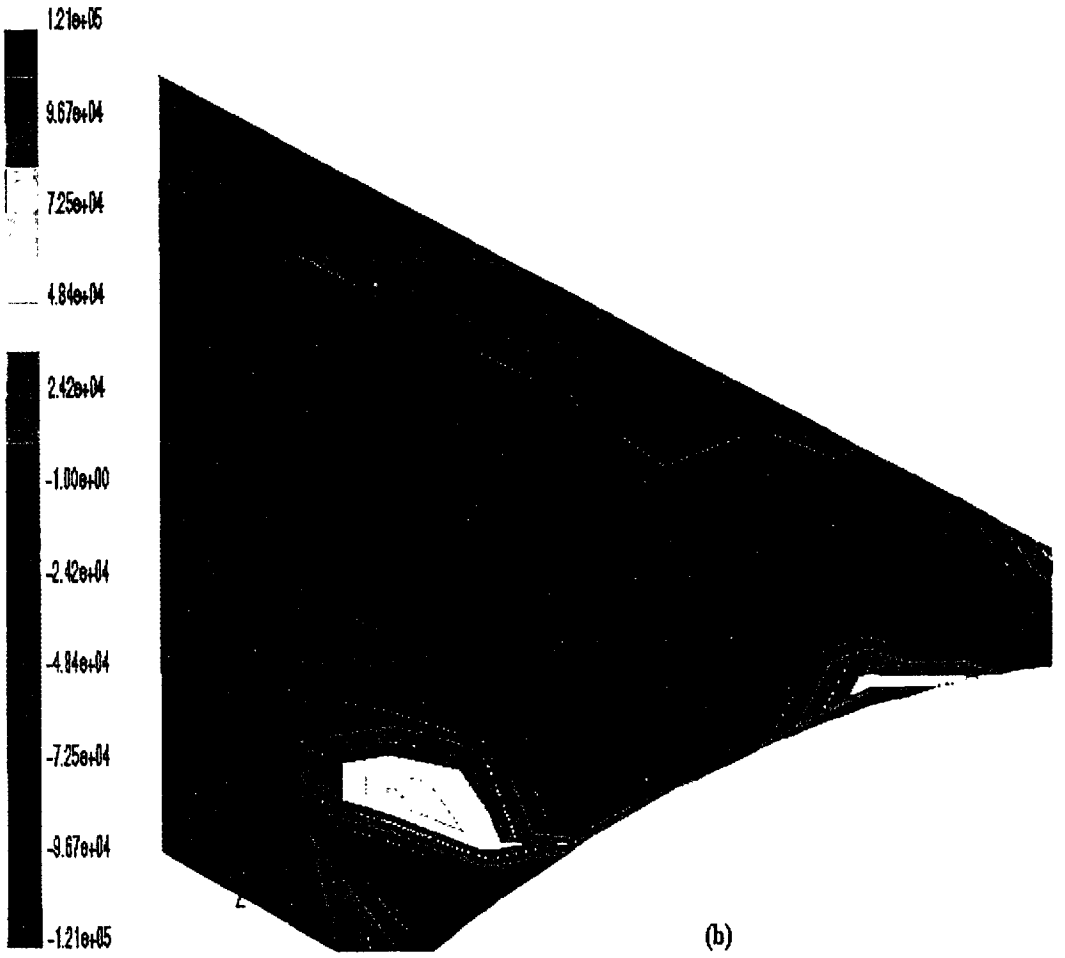

Figure 10-11 Contour of Vortices along the application nip (a) evolution scheme, (b) time-marching scheme.

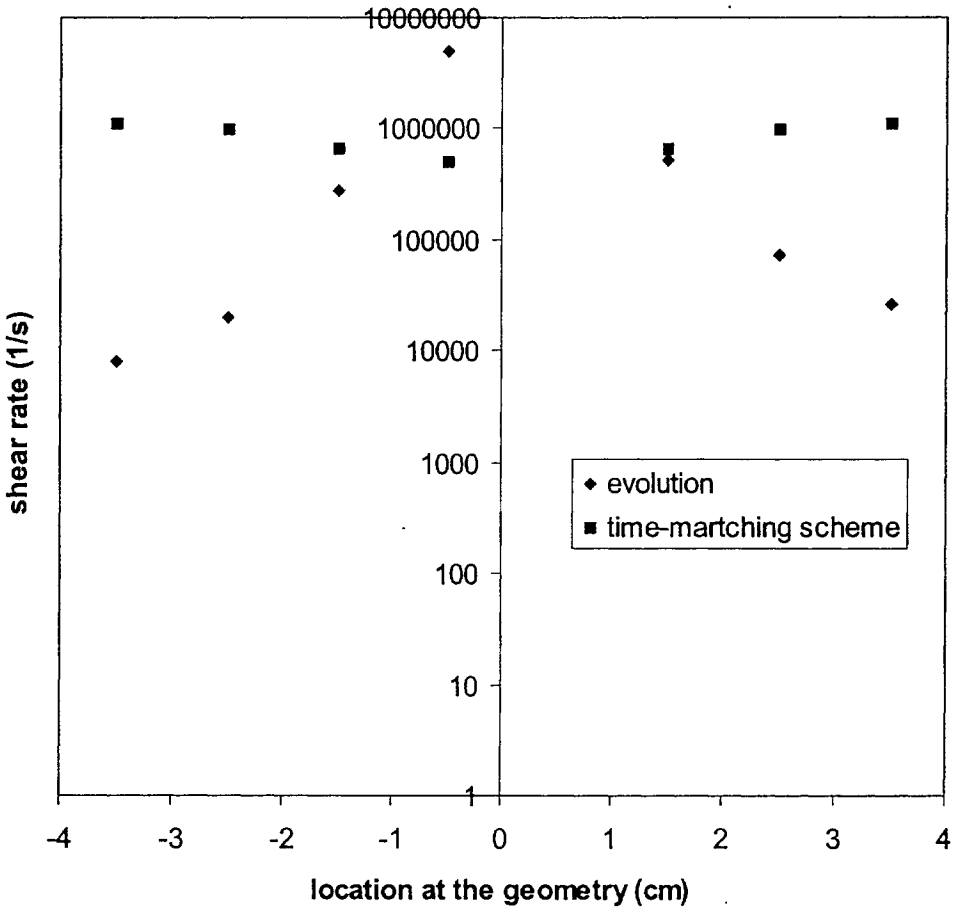

Figure 10-12. Shear rate as a function of the distance along application nip.

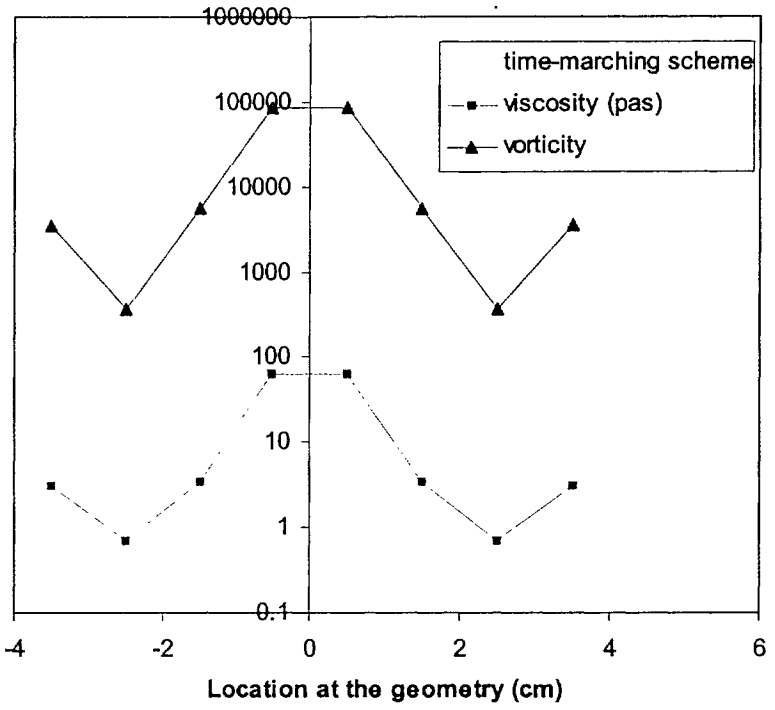

Figure 10-13. The viscosity-vorticity variation as a function of the geometry location.

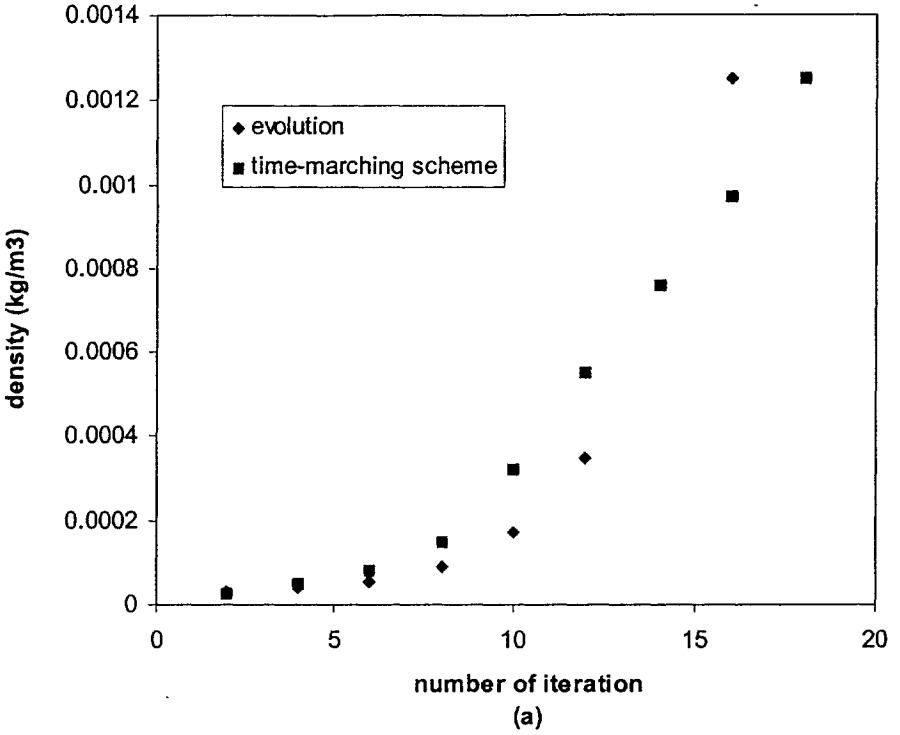
0.0014
0.0012
0.001
0.0008
0.0006
0.0004
0.0002
0
density (kg/m3)
evolution
time-marching scheme
0
5
10
15
20
number of iteration

(a)

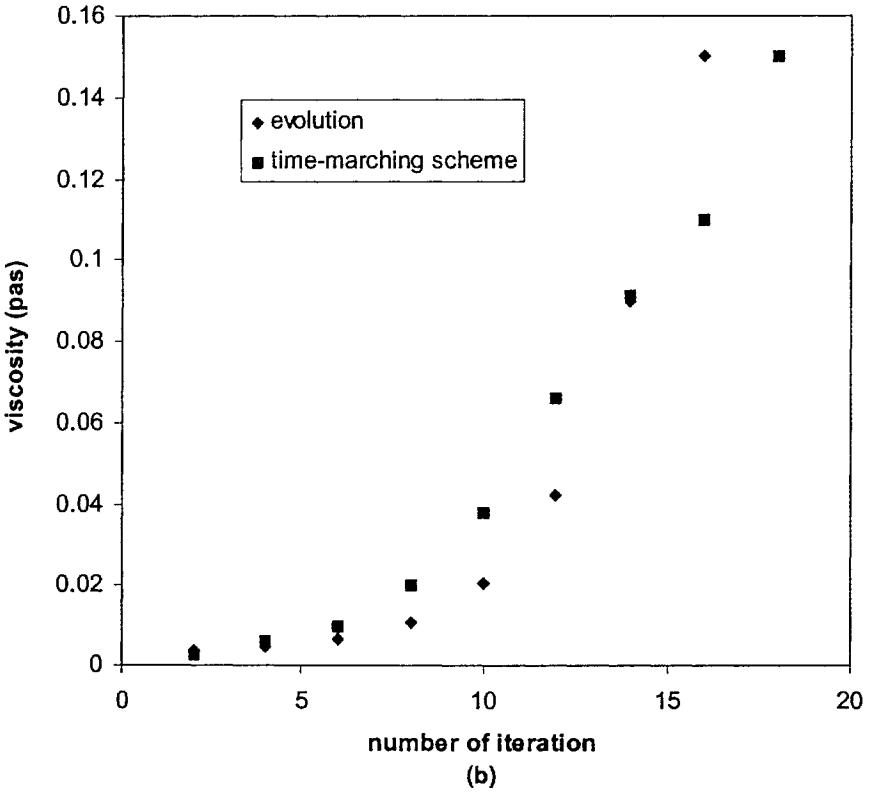
0.16
0.14
0.12
0.1
0.08
0.06
0.04
0.02
0
viscosity (pas)
evolution
time-marching scheme
0
5
10
15
20
number of iteration

(b)

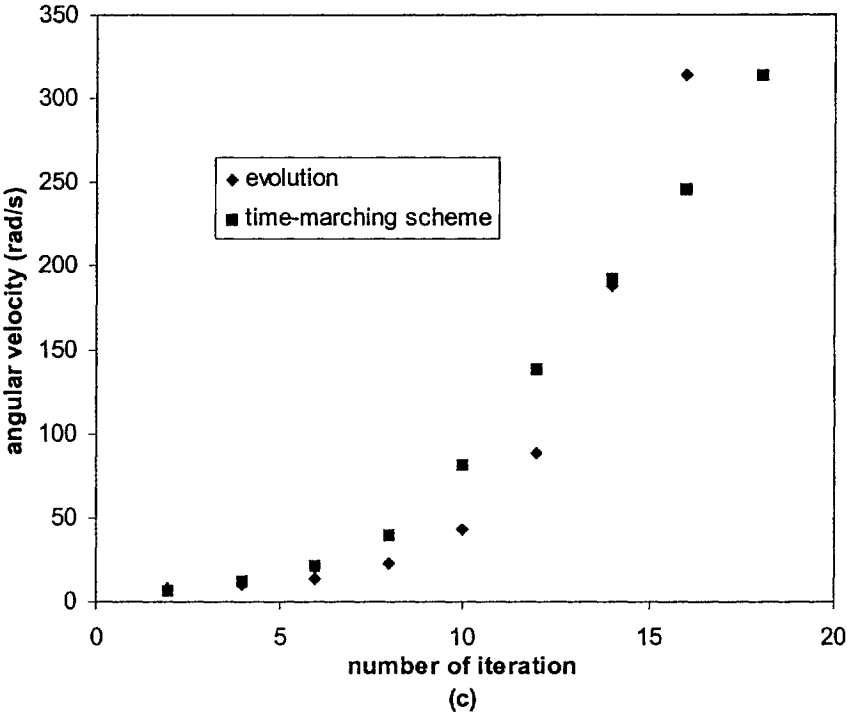

Figure 10-14. Convergence history for (a) density, (b) viscosity, (c) angular velocity.

Chapter Eleven

CONCLUSIONS

Among the operating parameters, the total concentration of inhibitors or total charge proved to have the largest effect of brightness stability or longer in time yellowing inhibition. The rheology of RS is Newtonian. The Ulrta-violet absorber (tin 1130) is an extremely viscous shear-thinning thixotropic material. Water-retention studies show that inhibitors increase water loss, with more water penetrating the paper web. Zeta potential measurements revealed the repulsive forces between pigment and inhibitor particles. RS adsorbs on ground calcium carbonate GCC and disrupts interactions between kaolinite particles. UVA adsorbs on particles of kaolinite and GCC. The inhibitors increase the viscosity, thixotropy, and elasticity of the original coating formulation. A study of pre-shear reveals decrease in viscosity, while inhibitors concentration under pre-shear increases viscosity and elasticity. Transmission Electron Microscopy shows the microstructure of increasing agglomerations with added inhibitors. Numerical 3D simulation of the flow in the coating nip taking inertia forces into consideration depicts vortex formations on the surface of the coater's rolls.

Application Factors

- The yellowing inhibition is most sensitive to total inhibitor charge. This sensitivity strongly depends on the ratio of RS/UVA, but is similar at different coat weights.

- A higher coat weight leads to a better yellowing inhibition while this trend remains the same at various inhibitor charge and ratio.
- The ratio of radical scavenger and UV absorber affects the yellowing inhibition mainly through its interaction with the total inhibitor charge. A higher RS/UVA ratio should be used to get better inhibition at a lower inhibitor charge, while a lower RS/UVA ratio is preferred at a higher inhibitor charge.
- At a low inhibitor charge or low RS/UVA ratio, inhibitors have negligible effect on initial brightness. However, a high RS/UVA ratio decreases initial brightness at a high inhibitor charge. The initial brightness drop due to inhibitors is less at a higher coat weight.

Rheological Properties

- We can conclude that RS is a simple Newtonian liquid, with water-like viscosity, while UV absorber (tin1130), which is hydrophobic polymer, is a shear-thinning thixotropic liquid, and is considerably more viscous. On the other hand, the inhibitors increase the viscosity of coating colors.

- Transient shear stress response determines that the coating formulation including inhibitors shows time independence of the shear stress. The thixotropy test results confirm that the RS and UVA increase the thixotropic behavior of coating formulations.

- The results of the frequency sweep indicate that the elastic behavior is more significant than the viscous behavior over the entire range of frequencies for all coating formulations. Phase angle is less than 30° for all coating formulations used in this study, which indicates that the elastic character of the color including inhibitors is more pronounced than the viscous character. The higher modulus of coating color containing inhibitor is due to strong particle-particle interaction and due to bridging between particle and micelle. Also, there is no rebuild of coating color with or without inhibitor for short period of time and the structure of coating color changes directly proportional to time.

- The effect of total charge of inhibitor on the rheological properties of coating colors shows that the viscosity of coating formulation increases with increasing the total charge. Above a critical shear rate, the viscosity increases (shear thickening). On the other hand, the thixotropic behavior of coating formulations increases with increasing the total charge. The total charge of coating formulation has no effect on the visco-elasticity behavior while decreasing the frequency of coating formulation transforms the visco-elasticity from linear to nonlinear.

Pre-shear

- The steady shear viscosity for coating colors depends on the concentration of added inhibitors. The viscous and elastic moduli of coating colors increase with increasing concentration of inhibitors, which is related to strong interaction between the particles.

➢

Water Retention

➢ Dewatering of coating colors during coating applications affects the coater runnability and the final paper properties. The coating color containing inhibitor has less water retention. Also, The coating color with low total charge has the strongest water holding capability decreasing with increasing total charge.

Surface Potentials

➢ We conclude that the inhibitor affects the interfacial properties. The surface potential of kaolinite and ground calcium carbonate particles depends on the inhibitor used. The surface potential of ground calcium carbonate and kaolinite particles, which is sensitive for the stability of coating colors depends on the concentration of inhibitors. The surface potential of kaolinite and ground calcium carbonate particles increases significantly when adding inhibitors. The surface potential of ground calcium carbonate particles is higher than that of kaolinite particles.

Ultra-Structure

➢ The ultra-structure of coating color dispersion is the result of complex interaction between the pigment and the inhibitor. The aggregation between coating components and inhibitor increases with the concentration of inhibitor. The concentration of inhibitor influences the size and shape of dispersed particles.

Numerical Simulation

- Since coating color is a visco-elastic suspension, the best model fit the experimental results of coating color behavior is KBKZ, which is an integral visco-elastic model (Appendix F).

- The flow in the coating nip is successfully simulated using 3D model, including forces of inertia at 1200 meters/ minute.

- Our 3D numerical simulation using the Carreau inelastic model, reveals vortex formations in the application nip of metering size press. Coating color is time dependent flow. The vortices are one of the parameter that has large effect on the coating process and cause defects on paper surface.

RECOMMENDATIONS

This thesis covered different types of experiments. The numerical part demonstrates the coating color in application nip using Non-Newtonian inelastic model taken into account the inertia.

However, my recommendations for the future work are as follows:

- Develop rheological model between total charge and the viscosity.
- Numerically solve the problem of visco-elastic flow using different geometries of coaters.
- Expand the study to include different coating formulations used in industry and different inhibitor systems.
- Expand the study of the correlation between the microstructure and the rheological properties of coating formulations.

References

1. Jan C. Walter "The coating Processes", Tappi Atlanta, 1993.
2. G.A. Smook "Handbook for Pulp & Paper Technologists", Tappi Technology Park/Atlanta, GA, USA, 1989
3. Pierre Lepoutre "Structure and Performance of pigmented Coatings: What Do We Know", international paper and Coating Chemistry Symposium, 1996.
4. Yohannes Chonde, John Roper, Pekka S. "A Review of Wet Coating Structure: Pigment/Latex/Cobinder Interaction and Its Impact on Rheology and Runnability" Tappi, Atlanta, Ga. USA. 1995.
5. Fadat, G., Rigdahl, M., Nordic Pulp Paper Research Journal, " Viscoelastic Properties of CMC/Latex Coating Colours", 1:30-38, 1987.
6. Nolan, P., Van den Akker, J.A., and Wink, W.A., "The Fading of Groundwood by Light. II. The physical Mechanism of Fading." Paper Trade J., (1945), 121(11), 101-105.
7. Davidson, R.S., "The Photodegradation of Some Naturally Occuring Polymers." J. Photochem. Photobiol. B:Biology, (1996), 33, 3-25.
8. 8- Heitner, C., ed. Light-Induced Yellowing of Wood-Containing Papers, An evaluation of the Mechanism. Photochemistry of Lignocellulosic Materials, Eds. C. Heitner and J.C. Scaiano. 1993, Washington, DC. 2-25.
9. 9- Leary, G.J., "Recent Progress in Understanding and Inhibiting the Light-Induced Yellowing of Mechanical Pulps." J. Pulp Paper Sci., (1994), 20(6), J154-J160.

10. Forsskahl, I., "Towards An Understanding of the Photoyellowing of Pulps and Papers." Trends in Photochem., (1994), 3, 503-520.
11. Lin, S.Y. and Kringstadt, K.P., "Stabilization of Lignin and Lignin Model Compounds to Photogradation." Tappi, (1970), 53 (9), 1675-1677.
12. Francis, R.C., Dence, C.W., Alexander, T.C., Agnemo, R., and Omori, S., "Photostabilization of Thermomechanical pulps by Alkylation and Borohydride Reduction." Tappi, (1991), 74(12), 127-133.
13. Paulsson, M. and Ragauskus, A.J.,"Chemical Modification of Lignin Rich Paper, Part 8. Effect of light source on the accelerated light-induced yellowing of untreated and acetylated high-yield pulps. "Nord. Pulp Pap. Res. J., (1998), 13, 132-142.
14. Schmidt, J.A. and Heitner, C., "Light Induced Yellowing of Mechanical Pulp: Effect of methylation, $NaBH_4$ reduction and ascorbic acid on chromophore formation." J. Wood Chem. Tech., (1991), 11, 397-418.
15. Pan, X., Harvey, L.C., and Ragauskas, A.J.,"Brightness Reversion f Mechanical Pulps. Part VI: Cooperative photostabilization approaches for high yield pulps." J. Pulp Paper Sci., (1996), 22(4), J135-J140.
16. Paulsson, M. and Ragauskus, A.J.,"Chemical Modification of Lignin Rich Paper, Part 7: Photostabilizing high-brightness aspen CTMP by combining various classes of additives and acetylation." Nord. Pulp Pap. Res. J., (1998), 13, 124-131.
17. Trichet, V., Grelier, S., Castellan, A., Choudry, H., and Davidson, R.S. "Attempt to Photostabilize Paper Made from High-yield Pulp by Application of UV Screens in Conjunction with Thiols."J. Photochem. Photobiol. A:Chem., (1996), (95),181-188.

18. D. Violet, P.F., Nourmamode, A., Colombo, N., and Zhu, J.H.,"photochemical Brightness Reversion of Peroxide Bleached Mechanical Pulp in the Presence of Various Additives." Cell. Chem. Technol., (1990), 24(2), 225-235.

19. Cook, C.M., Pan, X., and Ragauskas, A.J., "Brightness Reversion of Mechanical Pulps. VII: Photostabilization Studies of Thiol Additives for Lignocellulosic Materials." J. Wood Chem. Technol., (1996), 16, 327-345.

20. Cole, B.J.W. and Sarkanen, K.V., "Bleaching and Brightness Stabilization of High Yield Pulps by Sulfur Containing Compounds." Tappi, (1987), 70(11), 117-122.

21. Wang, J., Heitner, C., and Manley, R.S.J., "The Photodegradation of Milled Wood Lignin. Part II: The effect of inhibitors." J. Pulp Paper Sci., (1996), 22(2), J8-J63.

22. Davidson, R.S., Dunn, L.A., Castellan, A., Colombo, N., Nourmamode, A., and Zhu, Z.H., "A Study of the Photoyellowing of Paper made from Bleached Pulp." J. Wood Chem. Technol., (1991), 11, 419-437.

23. Pan, x. AND Ragauskas, A., "Brightness Reversion of Mechanical Pulps. Part 3: Mechanistic Studies of Mercapto-stabilizers for High Brightness Mechanical Pulps." J. Wood Chem. Technol., (1995), 15, 135-152.

24. Castellan, A., Noutary, C., and Davidson, R.S.,"Attempt to Photostabilize Paper made from High-yield Pulp by Application of UV Screens Containing Groups to Aid Their Compatibility with Cellulose and Lignin." J. Photochem. Photobiol. A. Chem., (1994), (84), 311-316.

25. McGarry, P., Heitner, C., Schmidt, J., Seltzer, R., Cunkle, G., Wolf, J.-P., and Nelson, R., "Inhibition of Pulp and Paper Yellowing using Nitroxides and other Coadditives", International Patent EP98/04381, (1998).

26. R.A. Leask, M.J. Kocurek "Pulp and Paper Manufacture", Volume 2, McGraw-Hill, 1987.

27. Cockram, R.A., "CTMP in Fine Papers", Intl. Mech. Pulping Conf., Helsinki, 2:20-24 (1989).

28. P.McGarry, c. Heitner, J. Schmidt, R. Seltzer, G.Cunkle and J.P.Wolf "Hindered Nitroxide:Anew Yellowing Inhibitor for Mechanical Pulps", Journal of Pulp and Paper Science:26,59-66, Feb.2000.

29. HU, T.Q., Leary, G. and Wong, D., "A New Approach Towards the Yellowing Inhibition of Mechanical Pulps. Part I: Selective Removal of α-Hydroxyl and α-Carbonyl Groups in Liginin Model Compounds", Holzforschung 53:43-48 (1999).

30. Tschirner, U. and Dence, C., "Attempts to Photostabilize Norway Spruce TMP by Chemical Modification", Paperi ja Puu 4:338-346 (1988).

31. Heitner, C.,"Inhibition of Light Induced Yellowing of Lignin-Containing Paper" in Photochemistry of Lignocellulosic Materials, C. Heitner and J.C. Scaiano, Eds., Am. Chem. Soc., Washington, DC, 192-204 (1993).

32. Leary, G.J., "Recent Progress in Under-standing and Inhibiting the Light-Induced Yellowing of Mechanical Pulps", J. Pulp Paper Sci. 20:154 (1994).

33. Nolan, P.A.,"The Fading of Groundwood by Light. V. Inhibition of Fading Through the Use of Ultraviolet Absorbing Compounds", Paper Trade J. 121(20):219(1945).

34. Castellan, A., Noutary, C. and Davidson, R.S.,"Attempts to Photostabilize Paper Made from High-Yield Pulp by Application of UV Screens Containing Groups to Aid Their Compatibility with Cellulose and Lignin", J. Photochem. Photobiol. A: Chem. 84:311-316(1994).

35. Barclay, L.R.C., XI, F, and Norris, J.Q.,"Antioxidant Properties of Phenolic Lignin Model Compounds", J. Wood Chem. Tech. 17:73-90 (1997).

36. Schmidt, J.A., Rye, C.S. and Gurnagul, N.,"Lignin Inhibits Auto-Oxidative Degradation of Cellulose", Polym. Deg. Stab. 49(2):291 (1995).

37. Paoli, M.-A.D. and Furlan, L.T.,"Sugar Cane Bagasse-Lignin as Photo-Stabilizer for Butadiene Rubber", Polym. Deg. Stab. 11:327-337 (1985).

38. Catignani, G.L. and Carter, M.E.,"Antioxidant Properties of Lignin", J. Food Sci. 47:1745 (1982).

39. Cook, C.M., Pan, X. and Ragauskas, A.J.,"Brightness Reversion of Mechanical Pulps VII: Photostabilization Studies of Thiol Additives for Lignocellulosic Materials", J. Wood Chem. Technol. 16(3):327(1996).

40. Cole, B.J.W. and Sarkanen, K.V.,"Bleaching and Brightness Stabilization of High Yield Pulps by Sulfur Containing Compounds", Tappi 70:117 (1987).

41. Agnemo, A.R., "Paper and a Mthod of Paper Manufacture", Intl. Patent WO92/09745 (1992).

42. Pan, X. and Ragauskas, A.J.,"Brightness Reversion of Mechanical Pulps. Part IV: A Study on the Action of Thiols and Disulphides on Hardwood BCTMP", J. Pulp Paper Sci. 21:25 (1995).

43. Trichet, V., Grelier, S., Castellan, A., Choudry, H. and Davidson, R.S., "Attempt to Photostabilize Paper Made from High-Yield Pulp by Application

of UV Screens in Conjunction with Thiols", J. Photochem. Photobiol. A:Chem. 95:181-188 (1996).

44. Pan, X., Harvey, L.C. and Ragauskas, A.J.,"Brightness Reversion of Mechanical Pulps. Part VI: Cooperative Photostabilization Approaches for High Yield Pulps", J. Pulp Paper Sci. 22:135-140 (1996).
45. Petit-Conil, M., Choudens, C.D., Castellan, A., Grelier, S. and Davidson, R.S.," Prevention of the Photoyellowing of High-Yield Pulps Using Ternary Mixtures Containing a UV Screen, a Polyethylene Oxide Dithiol and Sucrose", J. Pulp Paper Sci. 24(6): 167 (1998).
46. Heitner, C., in Photochemistry of Lignocellulosic Materials (C. Heitner and J. C. Scaiano, Eds.) ACS, Washington, 1993, 192-204.
47. Malik, J.S., Kline, J.E, Tappi Conference Proceedings 1992, "A study of the Effects of Water Soluble Polymers on Water Holding and Binder Migration Tendencies of Coatings," Tappi Press, Atlanta, pp. 105-113, 1992.
48. Ghosh, T., Lavoie, P. A. and Carreau, P. J., Tappi Journal, 80(11), 186, 1997.
49. J. Li, P. A. Tanguy and P.J.Carreau "Effect of Thickener Structure on Paper Coating Color Properties", J. of Colloid Poym Sci 279:872-878 (2001).
50. Walen-shaw, M.J., Gautman, N., Tappi Coating Conference Proceedings 1990,"A Model for the Colloidal and Rheological Characteristics of Clay, Latex, CMC Formulations," Tappi Press, Atlanta, p.371 (1990).
51. Sheehan, J.G., Whalen-Shaw, M., Tappi Coating Conference Proceedings 1990,"High Magnification Cryo SEM of Wet Coating Microstructure," Tappi Press, Atlanta, p.77 (1990).

52. Buscall, R., McGowan, R.J., Faraday Discussions of the Chemical Society,"Sedimentation and Viscous Flow of a Weakly Flocculated Concentrated Dispersion," 76:277 (1983).

53. McGenity, P.M., Gane, P.A.C., Husband, J.C., Engley, M.S., Tappi Coating Conference Proceedings 1992,"Effects of Interactions between Coating Color Components and Rheology, Water Retention and Runnability," Tappi Press, Atlanta, pp. 133-145 (1992).

54. Salminen, P., Fors, S., Tappi Coating Conference Proceedings 1992, "Fundamental Approaches for Optimizing Fibre Coverage in Blade Coating," Tappi Press, Atlanta, P. 7 (1992).

55. Larrondo, L.E., Lepoutre, P., Tappi Coating Conference Proceedings 1990," Approaches for Characterizing Interactions in Paper Coating Colors," Tappi Press, P.43 (1990).

56. Howard A. Barnes, Harry Schimanski and Derek Bell, Applied Rheology: 9, 2, 69-76, 1999.

57. Kevin R. Hase, Douglas W. "Kaolin Pigment-Latex Interactions During Coating" Proceedings of the 1994 Tappi Coating Conference, Tappi Press, 1994.

58. Chaffey CE Coll Polym Sci Nr 255:691, 1977.

59. Eklund D Cell Chem Techn 9:299, 1975.

60. U. Eriksson, G. Engstrom " Viscosity of some clay-based coating colors at high shear rates" Rheol Acta 29:352-359, 1990.

61. Paul-Andre Lavoie, Tamal Ghosh "The Rheology of Coating Colors: A comprehensive A approach", International Paper and Coating Chemistry Symposium, 253-257, 1996.

62. Christopher w. Macosko," Rheology Principles, Measurements, and Applications", VCH Publishers, Inc, 1994.

63. Barnes, H.A, JNNFM, 70 (1/2), 1-33 (1997).

64. Roger I. Tanner,"Engineering Rheology", British Library Cataloguing in Publication, 1988.

65. Nick G. Triantafillopoulos, "Paper Coating Viscoelasticity and Its Significant in Blade Coating", Tappi, GA, (1996).

66. Howard A. Barnes "A Handbook of Elementary Rheology", University of Wales, Institute of Non-Newtonian, Fluid Mechanics, Aberystwyth, 2000.

67. Johan Gullichsen, Hannu Paulapuro, "Pigment Coating and Surface Sizing of Paper" Published in cooperation with the Finish Paper Engineers, Association and Tappi, Copyright (c) 2000 by Fapet Oy. Helsinki, Finland.

68. Florence Yziquel, Michel Moan, Pierre J. Carreau, Philippe A. Tanguy, "Nonlinear Viscoelastic Behavior of Paper Coating Colors" Nordic Pulp and Paper Research Journal, 14:37-47 (1999).

69. Hirsch, G., Papier 32 (10A):66 (1978).

70. P. Lepoutre and D.Lord, J. Coll. Interf. Sci., 134, 66, (1990).

71. C.L. Garey, R.M. Leekley and J.D. Hultman, Tappi. 58:5, 79 (1975).

72. P. Louptre : Tappi. 59:12,70 (1976).

73. D.G.Bartell : Pulp Paper Can., 77:7,65 (1976).

74. A.J.Herbet, N. Gautam and M. Whalen-Shaw: Proc. Tappi Coating Conf., p.431 (1990).

75. Beazley, K.M. and Climpson, M., Tappi53(12):2227(1970).

76. Windle, W. and Beazley, K.M., Wochbl. Papierfabr. 101(10):332(May31,1973).

77. Hirsch, G., Papier 32 (10A):66 (1978).

78. Ubrich, J.-M. and Joanicot, M., Wochenbl. Papierfabr. 119(19):778(1991).

79. Letzelter, P. and Eklund, D., Tappi J. 76(5):63(1993);76(6):93(1993).

80. Johan Gullichsen, Hannu Paulapuro, "Pigment Coating and Surface Sizing of Paper" Published in cooperation with the Finish Paper Engineers, Association and Tappi, Copyright (c) 2000 by Fapet Oy. Helsinki, Finland.

81. U.Eriksson, M.Rigdahl"Differences in Consolidation Behaviour and Properties of Kaolin-Based Coating Layers Induced by CMC and Starch, Tappi Journal, 19-30, 1993.

82. Heiser, E. J. and Cullen, D. W., Tappi 48(8):80A (1965).

83. Krishnagopalan, A. and Simard, G.L., Tappi 59(12): 96(1976).

84. Michael J. Whalen-Shaw, " Binder Migration In Paper and Paperboard Coatings" Tappi Press, Atlanta, Georgia (1993).

85. Nissan, A.H., Proc. Tech. Sec. P.M.A. 30:96 (1949).

86. Michael J. Whalen-Shaw, "Binder Migration in Paper and Paperboard Coating", Tappi Press, Atlanta, Georgia, 1993.

87. Drew Myers, "Surfaces, Interfaces, and Colloids Principles and Applications", Second Edition, Published in Canada, Copyright by John Wiley & Sons, 1999.

88. Goodwin, J. W. and Hughes, R.W., in Technology for Waterborne Coatings, ed. Glass, J.E., ACS Symposium Series, 663, pp95-125 (1997).

89. Hawe, M., Nordic Pulp and Paper Research Journal, 1, 188 (1993).

90. Fadat, G., Nordic Pulp and Paper Research Journal, 1, 191 (1993).

91. Fitch, R.M., Polymer Colloids, Academic Press, New York (1997).

92. E. Fourcade, F. Bertrand, O. Reglat, P.A. Tanguy "Finite elemnt analysis of fluid-solid interaction in the metering nip of a metering size press" computer methods in applied mechanics and engineering, 174(1999) 235-245.

93. Huang D.K., Tappi Blade Coating Seminar, Tappi pree, Atlanta, GA, 1986.

94. Yohannes Chonde, John Roper, " A Review of Wet Coating Structure: Pigment/Latex/Cobinder Interaction and Its Impact on Rheology and Runnability", Tappi Coating Proceedings, Tappi Press Atlanta, p:57-62, 1995.

95. John A. Roper, Pekka Salminen, Robert Urscheler "Studies of Orange Peel Formation in High-Speed Film Coating" Tappi J. 82(1) 231-238(1999).

96. Nick G. Triantafillopoulos, Malcolm K. Smith, "Troubleshooting Rheology Problems in Metered Size Press" Tappi, MSPF II, New Orleans (1998).

97. Jarnstrom, L., G. Strom and P. Stenius, "The adsorpion of dispersing and thickening polymers and their effect on the rheology of coating colors" in "proc. Tappi Coating Conf.", Tappi, Atlanta, GA (1987), pp. 123-132.

98. Van Olphen, H. "An Introduction to clay colloid chemistry", 2nd ed., John Willey and sons, New York, NY (1977).

99. Whalen-Shaw, M., "Coating Structure Part I: A Mechanistic View", Tappi Coating Conference (1989).

100- Bachmann, L. and W.W. Schmitt, "Improved Cryofixation Applicable to Freeze Etching" Proc. Nat. Acad. Sci. USA 68 (9) pp.2149-2152, September, 1971.

101- John G. Sheehan, Michael Whalen, "HIGH-magnification Cryo-SEM of Wet Coating Microstructures", Tappi Coating Conference, 1990.

102- Hall, C.E.: Low temperature replica method for electron microscopy. J. Appl. Phys. 21, 61-62 (1950).

103- Merryman, H.T.:Replication of frozen liquids by vacuum evaporation. J.Appl. Phys. 21, 68 (1950).

104- Steere, R.L.: Electron microscopy of structural detail in frozen biological specimens. J.Biophys. Biochem. Cytol. 3, 45-60 (1957).

105- Greener, J. and Middleman, S., "Reverse Roll Coating of Purely Viscous Liquids", Ind. Eng. Chem. Fundam, 20(1):63-66 (1981).

106- Kang, Y.T. and Liu, T.J.,"Minimum Film Thickness for Reverse Roll Coating", Chem. Eng. Sci. Short Comm, 46(11): 2958-2960 (1991).

107- Coyle, D. J., Macosko, C.W. and Scriven, L. E., "The Fluid Dynamics of Reverse Roll Coating", AICHE J, 36(2):161-174 (1990).

108- Coyle, D. J., Macosko, C.W. and Scriven, L. E.,"A Simple Model of Reverse Roll Coating", Ind. Eng. Chem. Res., 29 (7):1416-1419 (1990).

109- Coyle, D. J., Macosko, C.W. and Scriven, L. E., "Reverse Roll Coating of non-Newtonian Liquids" J. Rheol., 34 (5):615-637 (1990).

110- Fourcade, E., Bertrand, F., Reglat, O. and Tanguy, P.A.,"Finite Element Analysis of Fluid-Solid Interaction in the Metering Nip of a metering size Press", Comp. Meth. In Appl. Mech and Eng., 174:235-245 (1999).

111- Poranen, J. and Niemisto, A.,"Experimental and Theoretical Study for Metering Size Press", Tappi Advanced Coating Fundamental Symp". Proc., Toronto, 159-161 (1999).

112- Pitts, E. and Greiller, J. "The Flow of Thin Liquid Films Between Rollers", J. Fluiid Mech. 11, 33, (1961).

113- Savage, M.D." Mathematical Models for Coating Processes", J. Fluid Mech. 117,443, (1982).

114- Coyle, D.J. "The Fluid Mechanics of Roll Coating:Steady Flows, Stability, and Rheology", Ph.D. Thesia, University of Minnesota.

115- Coyle, D.J. "Forward Roll Coating With Deformable Rolls", Chem. Eng Sci. 43, 2673 (1988a).

116- Van Olphen, H.,"Clay Colloid Chemistry," 2nd ed. Wiley, New York/London/Sydney/Toronto, 1977.

117- Heath, D., and Tadros, Th. F., J. Colloid Interface Sci. 93, 307 (1983).

118- Yariv, S., and Cross, H.,"Geochemistry of Colloidal Systems for Earth Scientists." Springer-Verlag, Berlin/Heidelberg/New York, 1979.

119- Brandenburg, U., and Lagaly, G., Appl. Clay Sci. 3, 263 (1988).

120- Guven, N., and Pease, R.W., Clays Clay Miner. 23, 187 (1975).

121- Gard, J.A. (Ed),"The Electron-Optical Investigation of Clays," Mineralogical Society Monograph 3. Mineralogical Society, London, 1971.

122- Grim, R.E., and Guven, N.,"Developments in Sedimentology," Vol. 24. Elsevier, Amsterdam/Oxford/New York, 1978.

123- Sudo, T., Shimoda, S., Yotsumoto, H., and Aita, S.,"Developments in Sedimentology," Vol. 31. Kodansha, Tokyo, and Elsevier, Amsterdam/Oxford/ New York, 1981.

124- Smart, P., and Tovey, N. K.,"Electron Microscopy of Soils and Sediments: Techniques." Calderon Press, Oxford, 1982.

125- Weiss, A., and Frank, R., z. Naaturforsch. B 16, 141 (1961).

126- Honigmann, B., Ber. Bunsenges. Phys. Chem. 71, 239 (1967).

127- Robards, A. W., and Sleytr, U.B.,"Practical Methods in Electron Microscopy"(A.M.Glauert, Ed.), Vol. 10. Elsevier, Amsterdam/New York/Oxford, 1986.

128- Bachmann, L., in"Cryotechniques in Biological Electron Microscopy" (R. A. Steinbrecht and K. Zierold, Eds.), Chap. 9, p. 192. Springer-Verlag, Berlin /Heidelberg /New York, 1987.

129- S. Alonso, O. Reglat, F. Bertrand, L. Choplin and P.A.Tanguy,"Process Viscosity in Reverse Roll Coating", Journal Trans IchemE, 79:128-136 (2001).

130- Nolan, P., van den Akker, J. A. and Wink, W. A., "The Fading of Groundwood by Light. II. The Physical Mechanism of Fading", *Paper Trade J.* 121(11):101-105 (1945).

131- H.R. valentine, Applied Hydrodynamics, Butterworth, London, 1959.

132- Stranger, K.M.:The film press-a versatile coating system Paper age 31(5):12-16 (1995).

133- Coyle, D.J., Macosko, C.V., Scriven, L.E.,"Liquid Flow in Formal Coating", Tappi coating Conference Proceedings, Tappi Press, Atlanta, p.161, 1983.

APPENDIX

APPENDIX A

A.1 Fifteen coating formulations have been prepared to study the factors (total charge, RSUVA and coat weight).

Table A.1 Coating formulations with different concentration of inhibitors.

AC control color		(A4)=(A6)=(A8)			
Chemical name	**S.C. (%)**	**Parts**	**Mass**	**Mass**	
				110.00	
				g Covercarb	
S.C. of coating color:		**30%**			
Covercarb	71.6	80	111.73	110.00	
Astraplate	70	20	28.57	28.13	
Penford Gum 280	20	6	30.00	29.54	
Acronal S728	49.4	12	24.29	23.91	
KZCote	100	0.5	0.50	0.49	***192.07***
Srerocoll BL	100	0.1	0.10	0.10	
Water			200.14	197.04	
Total Mass		**118.6**		**389.21**	

A4=A6=A8 are equal in components but different in coat weight where A4 has coat weight 4 g/m^2,

A6 has coat weight 6 g/m^2 and A8 has coat weight 8 g/m^2.

		(B)			
Chemical name	**S.C. (%)**	**Parts**	**Mass**	**Mass 110.00 g Covercarb**	
S.C. of coating color:		**30%**			
Covercarb	71.6	80	111.73	110.00	
Astraplate	70	20	28.57	28.13	
Penford Gum 280	20	6	30.00	29.54	
Acronal S728	49.4	12	24.29	23.91	
KZCote	100	0.5	0.50	0.49	***192.07***
Tinuvin 1130	87	9.5869	11.02	10.85	
PAX-2067	30	2.3967	7.99	7.87	
Srerocoll BL	100	0.1	0.10	0.10	
Water			221.08	217.65	
Total Mass		**130.5836**	**435.28**	**428.53**	

		(B4)			
Chemical name	**S.C. (%)**	**Parts**	**Mass**	**Mass 110.00 g covercarb**	
S.C. of coating color:		**30%**			
Covercarb	71.6	80	111.73	110.00	
Astraplate	70	20	28.57	28.13	
Penford Gum 280	20	6	30.00	29.54	
Acronal S728	49.4	12	24.29	23.91	
KZCote	100	0.5	0.50	0.49	***192.07***
Tinuvin 1130	87	3.575866	4.11	4.05	
PAX-2067	30	14.30346	47.68	46.94	
Srerocoll BL	100	0.1	0.10	0.10	
Water			207.95	204.72	
Total Mass		**136.47933**	**454.93**	**447.88**	

(B4I)					
Chemical name	**S.C. (%)**	**Parts**	**Mass**	**Mass**	
				110.00	
S.C. of coating color:		**30%**			
Covercarb	71.6	80	111.73	110.00	
Astraplate	70	20	28.57	28.13	
Penford Gum 280	20	6	30.00	29.54	
Acronal S728	49.4	12	24.29	23.91	
KZCote	100	0.5	0.50	0.49	***192.07***
Tinuvin 1130	87	1.15623	1.33	1.31	
PAX-2067	30	8.960784	29.87	29.41	
Srerocoll BL	100	0.1	0.10	0.10	
Water			202.66	199.52	
Total Mass		**128.717**	**429.06**	**422.41**	

(B4II)					
Chemical name	**S.C. (%)**	**Parts**	**Mass**	**Mass**	
				110.00	
S.C. of coating color:		**30%**			
Covercarb	71.6	80	111.73	110.00	
Astraplate	70	20	28.57	28.13	
Penford Gum 280	20	6	30.00	29.54	
Acronal S728	49.4	12	24.29	23.91	
KZCote	100	0.5	0.50	0.49	***192.07***
Tinuvin 1130	87	8.0936	9.30	9.16	
PAX-2067	30	2.0234	6.74	6.64	
Srerocoll BL	100	0.1	0.10	0.10	
Water			217.81	214.44	
Total Mass		**128.717**	**429.06**	**422.41**	

	(B4III)				
Chemical name	**S.C. (%)**	**Parts**	**Mass**	**Mass**	
				110.00	
S.C. of coating color:		**30%**			
Covercarb	71.6	80	111.73	110.00	
Astraplate	70	20	28.57	28.13	
Penford Gum 280	20	6	30.00	29.54	
Acronal S728	49.4	12	24.29	23.91	
KZCote	100	0.5	0.50	0.49	***192.07***
Tinuvin 1130	87	0.63814	0.73	0.72	
PAX-2067	30	2.552585	8.51	8.38	
Srerocoll BL	100	0.1	0.10	0.10	
Water			201.53	198.41	
Total Mass		**121.7907**	**405.97**	**399.68**	

		(B6)			
Chemical name	**S.C. (%)**	**Parts**	**Mass**	**Mass**	
				110.00	
S.C. of coating color:		**30%**			
Covercarb	71.6	80	111.73	110.00	
Astraplate	70	20	28.57	28.13	
Penford Gum 280	20	6	30.00	29.54	
Acronal S728	49.4	12	24.29	23.91	
KZCote	100	0.5	0.50	0.49	***192.07***
Tinuvin 1130	87	2.0234	2.33	2.29	
PAX-2067	30	8.0936	26.98	26.56	
Srerocoll BL	100	0.1	0.10	0.10	
Water			204.56	201.39	
Total Mass		**128.717**	**429.06**	**422.41**	

	(B4II)				
Chemical name	**S.C. (%)**	**Parts**	**Mass**	**Mass**	
				110.00	
S.C. of coating color:		**30%**			
Covercarb	71.6	80	111.73	110.00	
Astraplate	70	20	28.57	28.13	
Penford Gum 280	20	6	30.00	29.54	
Acronal S728	49.4	12	24.29	23.91	
KZCote	100	0.5	0.50	0.49	***192.07***
Tinuvin 1130	87	8.0936	9.30	9.16	
PAX-2067	30	2.0234	6.74	6.64	
Srerocoll BL	100	0.1	0.10	0.10	
Water			217.81	214.44	
Total Mass		**128.717**	**429.06**	**422.41**	

	(B4III)				
Chemical name	**S.C. (%)**	**Parts**	**Mass**	**Mass**	
				110.00	
S.C. of coating color:		**30%**			
Covercarb	71.6	80	111.73	110.00	
Astraplate	70	20	28.57	28.13	
Penford Gum 280	20	6	30.00	29.54	
Acronal S728	49.4	12	24.29	23.91	
KZCote	100	0.5	0.50	0.49	***192.07***
Tinuvin 1130	87	0.63814	0.73	0.72	
PAX-2067	30	2.552585	8.51	8.38	
Srerocoll BL	100	0.1	0.10	0.10	
Water			201.53	198.41	
Total Mass		**121.7907**	**405.97**	**399.68**	

		(B6I)			
Chemical name	**S.C. (%)**	**Parts**	**Mass**	**Mass**	
				110.00	
S.C. of coating color:		**30%**			
Covercarb	71.6	80	111.73	110.00	
Astraplate	70	20	28.57	28.13	
Penford Gum 280	20	6	30.00	29.54	
Acronal S728	49.4	12	24.29	23.91	
KZCote	100	0.5	0.50	0.49	***192.07***
Tinuvin 1130	87	2.0234	2.33	2.29	
PAX-2067	30	8.0936	26.98	26.56	
Srerocoll BL	100	0.1	0.10	0.10	
Water			204.56	201.39	
Total Mass		**128.717**	**429.06**	**422.41**	

		(B6II)			
Chemical name	**S.C. (%)**	**Parts**	**Mass**	**Mass**	
				110.00	
S.C. of coating color:		**30%**			
Covercarb	71.6	80	111.73	110.00	
Astraplate	70	20	28.57	28.13	
Penford Gum 280	20	6	30.00	29.54	
Acronal S728	49.4	12	24.29	23.91	
KZCote	100	0.5	0.50	0.49	***192.07***
Tinuvin 1130	87	2.5525	2.93	2.89	
PAX-2067	30	0.63814	2.13	2.09	
Srerocoll BL	100	0.1	0.10	0.10	
Water			205.71	202.52	
Total Mass		**121.7906**	**405.97**	**399.68**	

(B6III)					
Chemical name	**S.C. (%)**	**Parts**	**Mass**	**Mass**	
				110.00	
S.C. of coating color:		**30%**			
Covercarb	71.6	80	111.73	110.00	
Astraplate	70	20	28.57	28.13	
Penford Gum 280	20	6	30.00	29.54	
Acronal S728	49.4	12	24.29	23.91	
KZCote	100	0.5	0.50	0.49	***192.07***
Tinuvin 1130	87	2.0433	2.35	2.31	
PAX-2067	30	15.83597	52.79	51.97	
Srerocoll BL	100	0.1	0.10	0.10	
Water			204.60	201.43	
Total Mass		**136.4793**	**454.93**	**447.88**	

(B6IIII)					
Chemical name	**S.C. (%)**	**Parts**	**Mass**	**Mass**	
				110.00	
S.C. of coating color:		**30%**			
Covercarb	71.6	80	111.73	110.00	
Astraplate	70	20	28.57	28.13	
Penford Gum 280	20	6	30.00	29.54	
Acronal S728	49.4	12	24.29	23.91	
KZCote	100	0.5	0.50	0.49	***192.07***
Tinuvin 1130	87	2.0234	2.33	2.29	
PAX-2067	30	8.0936	26.98	26.56	
Srerocoll BL	100	0.1	0.10	0.10	
Water			204.56	201.39	
Total Mass		**128.717**	**429.06**	**422.41**	

B6IIIII					
Chemical name	**S.C. (%)**	**Parts**	**Mass**	**Mass**	
				110.00	
S.C. of coating color:		**30%**			
Covercarb	71.6	80	111.73	110.00	
Astraplate	70	20	28.57	28.13	
Penford Gum 280	20	6	30.00	29.54	
Acronal S728	49.4	12	24.29	23.91	
KZCote	100	0.5	0.50	0.49	***192.07***
Tinuvin 1130	87	14.30346	16.44	16.19	
PAX-2067	30	3.575866	11.92	11.73	
Srerocoll BL	100	0.1	0.10	0.10	
Water			231.38	227.79	
Total Mass		**136.4793**	**454.93**	**447.88**	

(B6IIIIII)					
Chemical name	**S.C. (%)**	**Parts**	**Mass**	**Mass**	
				110.00	
S.C. of coating color:		**30%**			
Covercarb	71.6	80	111.73	110.00	
Astraplate	70	20	28.57	28.13	
Penford Gum 280	20	6	30.00	29.54	
Acronal S728	49.4	12	24.29	23.91	
KZCote	100	0.5	0.50	0.49	***192.07***
Tinuvin 1130	87	0.364655	0.42	0.41	
PAX-2067	30	2.82607	9.42	9.27	
Srerocoll BL	100	0.1	0.10	0.10	
Water			200.93	197.82	
Total Mass		**121.7907**	**405.97**	**399.68**	

(B8)					
Chemical name	**S.C. (%)**	**Parts**	**Mass**	**Mass**	
				110.00	
S.C. of coating color:		**30%**			
Covercarb	71.6	80	111.73	110.00	
Astraplate	70	20	28.57	28.13	
Penford Gum 280	20	6	30.00	29.54	
Acronal S728	49.4	12	24.29	23.91	
KZCote	100	0.5	0.50	0.49	***192.07***
Tinuvin 1130	87	8.09366	9.30	9.16	
PAX-2067	30	2.0234	6.74	6.64	
Srerocoll BL	100	0.1	0.10	0.10	
Water			217.81	214.44	
Total Mass		**128.7171**	**429.06**	**422.41**	

(B8I)					
Chemical name	**S.C. (%)**	**Parts**	**Mass**	**Mass**	
				110.00	
S.C. of coating color:		**30%**			
Covercarb	71.6	80	111.73	110.00	
Astraplate	70	20	28.57	28.13	
Penford Gum 280	20	6	30.00	29.54	
Acronal S728	49.4	12	24.29	23.91	
KZCote	100	0.5	0.50	0.49	***192.07***
Tinuvin 1130	87	3.5758	4.11	4.05	
PAX-2067	30	14.30346	47.68	46.94	
Srerocoll BL	100	0.1	0.10	0.10	
Water			207.95	204.72	
Total Mass		**136.4793**	**454.93**	**447.88**	

(B8II)

Chemical name	S.C. (%)	Parts	Mass	Mass	
				110.00	
S.C. of coating color:		40%			
Covercarb	71.6	80	111.73	110.00	
Astraplate	70	20	28.57	28.13	
Penford Gum 280	20	6	30.00	29.54	
Acronal S728	49.4	12	24.29	23.91	
KZCote	100	0.5	0.50	0.49	*192.07*
Tinuvin 1130	87	1.156	1.33	1.31	
PAX-2067	30	8.96078	29.87	29.41	
Srerocoll BL	100	0.1	0.10	0.10	
Water			95.40	93.92	
Total Mass		128.7168	321.79	316.80	

(B8III)

Chemical name	S.C. (%)	Parts	Mass	Mass	
				110.00	
S.C. of coating color:		40%			
Covercarb	71.6	80	111.73	110.00	
Astraplate	70	20	28.57	28.13	
Penford Gum 280	20	6	30.00	29.54	
Acronal S728	49.4	12	24.29	23.91	
KZCote	100	0.5	0.50	0.49	*192.07*
Tinuvin 1130	87	0.638	0.73	0.72	
PAX-2067	30	2.5525	8.51	8.38	
Srerocoll BL	100	0.1	0.10	0.10	
Water			100.04	98.49	
Total Mass		121.7905	304.48	299.76	

VERIFICATION (verifi3)					
Chemical name	**S.C. (%)**	**Parts**	**Mass**	**Mass**	
				110.00	
S.C. of coating color:		**40%**			
Covercarb	71.6	80	111.73	110.00	
Astraplate	70	20	28.57	28.13	
Penford Gum 280	20	6	30.00	29.54	
Acronal S728	49.4	12	24.29	23.91	
KZCote	100	0.5	0.50	0.49	***192.07***
Tinuvin 1130	87	1.763658	2.03	2.00	
PAX-2067	30	3.089867	10.30	10.14	
Srerocoll BL	100	0.1	0.10	0.10	
Water			101.11	99.55	
Total Mass		**123.4535**	**308.63**	**303.85**	

VERIFICATION (verifi2)					
Chemical name	**S.C. (%)**	**Parts**	**Mass**	**Mass**	
				110.00	
S.C. of coating color:		**40%**			
Covercarb	71.6	80	111.73	110.00	
Astraplate	70	20	28.57	28.13	
Penford Gum 280	20	6	30.00	29.54	
Acronal S728	49.4	12	24.29	23.91	
KZCote	100	0.5	0.50	0.49	***192.07***
Tinuvin 1130	87	2.316034	2.66	2.62	
PAX-2067	30	11.58017	38.60	38.00	
Srerocoll BL	100	0.1	0.10	0.10	
Water			94.78	93.31	
Total Mass		**132.4962**	**331.24**	**326.11**	

VERIFICATION (verifi1)					
Chemical name	**S.C. (%)**	**Parts**	**Mass**	**Mass**	
				110.00	
S.C. of coating color:		**40%**			
Covercarb	71.6	80	111.73	110.00	
Astraplate	70	20	28.57	28.13	
Penford Gum 280	20	6	30.00	29.54	
Acronal S728	49.4	12	24.29	23.91	
KZCote	100	0.5	0.50	0.49	***192.07***
Tinuvin 1130	87	1.848795	2.13	2.09	
PAX-2067	30	6.470783	21.57	21.23	
Srerocoll BL	100	0.1	0.10	0.10	
Water			98.41	96.88	
Total Mass		**126.9196**	**317.30**	**312.38**	

A.2 Whiteness

Whiteness is a comprehensive term used to express the visual impact of near white surfaces by means of the single value. Numerous equations have been developed to this end, but CIE (Commission Internationale de l'Eclairage). Whiteness is the most common in practical use. Whiteness is the most common in practical use. Whiteness is also used to denote a more comprehensive expression of color by use of the CIE color coordinates L*, a*, and b* (or CIELAB). Three reflectance figures L*, a*, and b* are calculated from measurements made using a standard D65 light source. The coordinates a* and b* measure color. Positive figures for a* express redness, negative figures greenness, and positive figures for b* express yellowness, negative

figures blueness. L* is a percentage which measures luminance on a scale where black is zero and pure white is 100% (figure A.1). One can measure color coordinates as well as brightness with the same instrument.

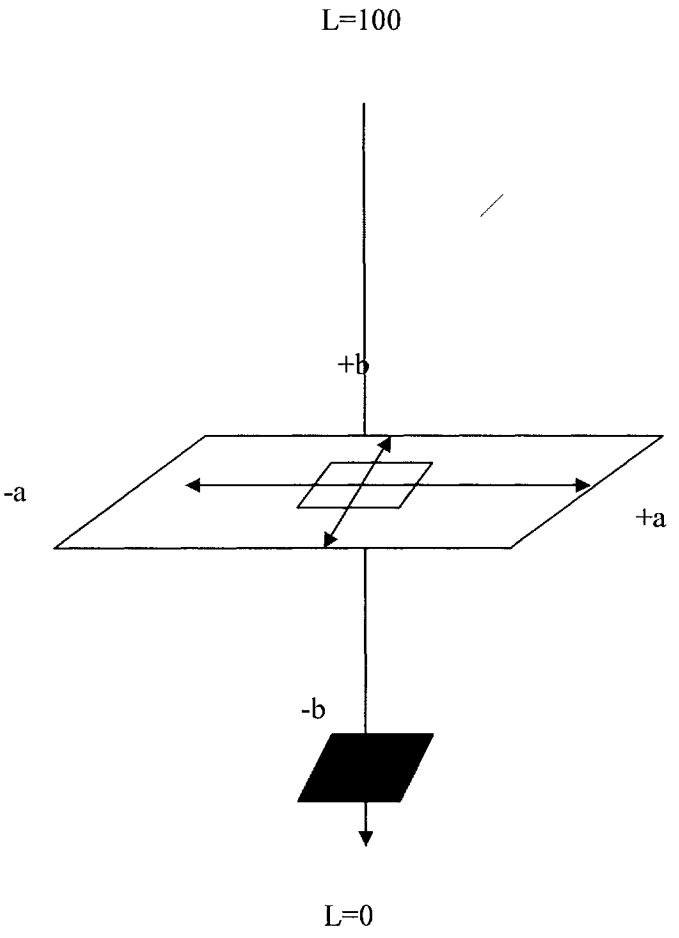

Figure A.1. CIELAB color space.

Figure A.2 b* as a function of time for different coating formulation which have been identified in section A.1. Figure A.3 L* as a function of time for different coating formulation.

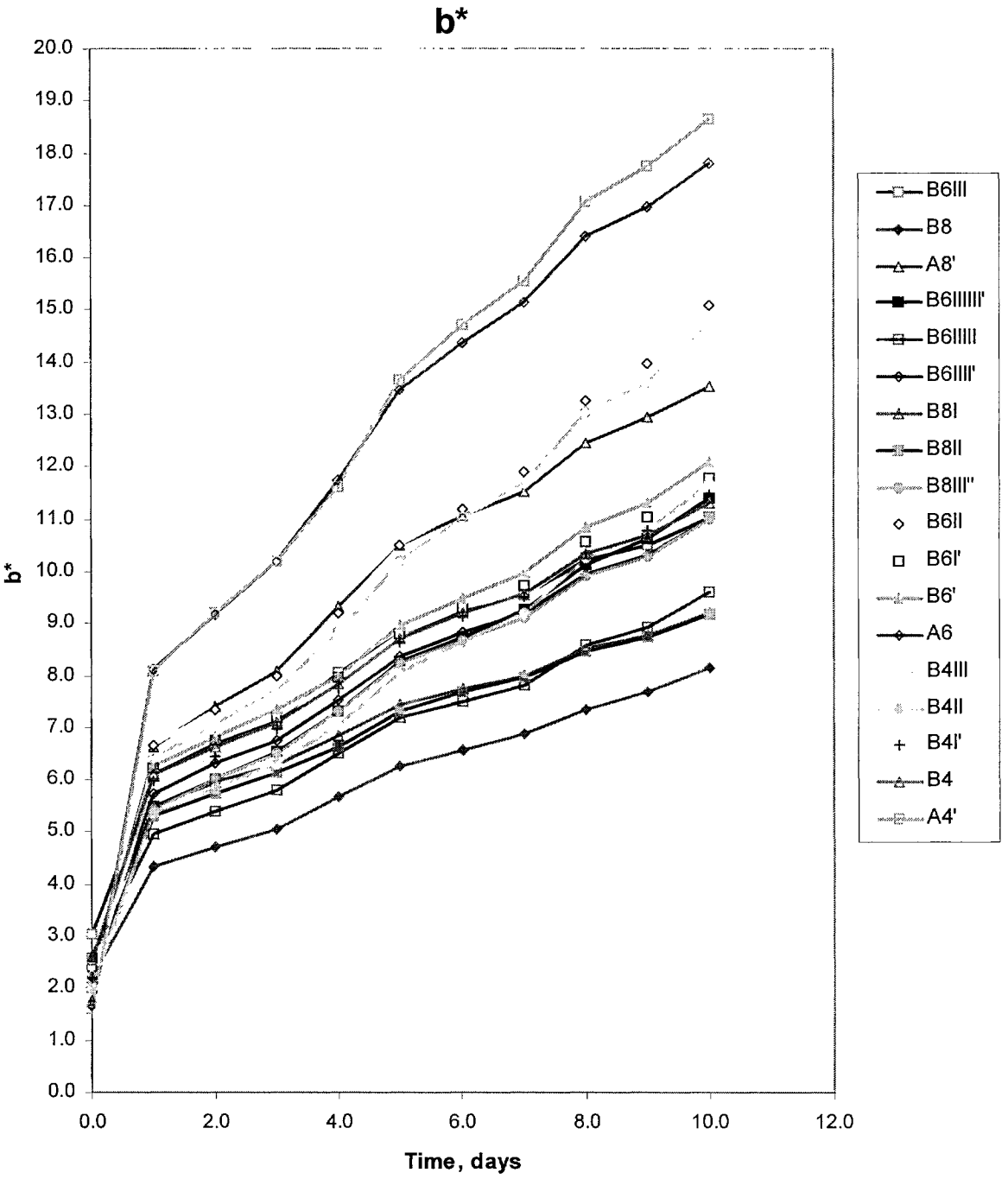

Figure A.2. b* as a function of time for different coating formulation

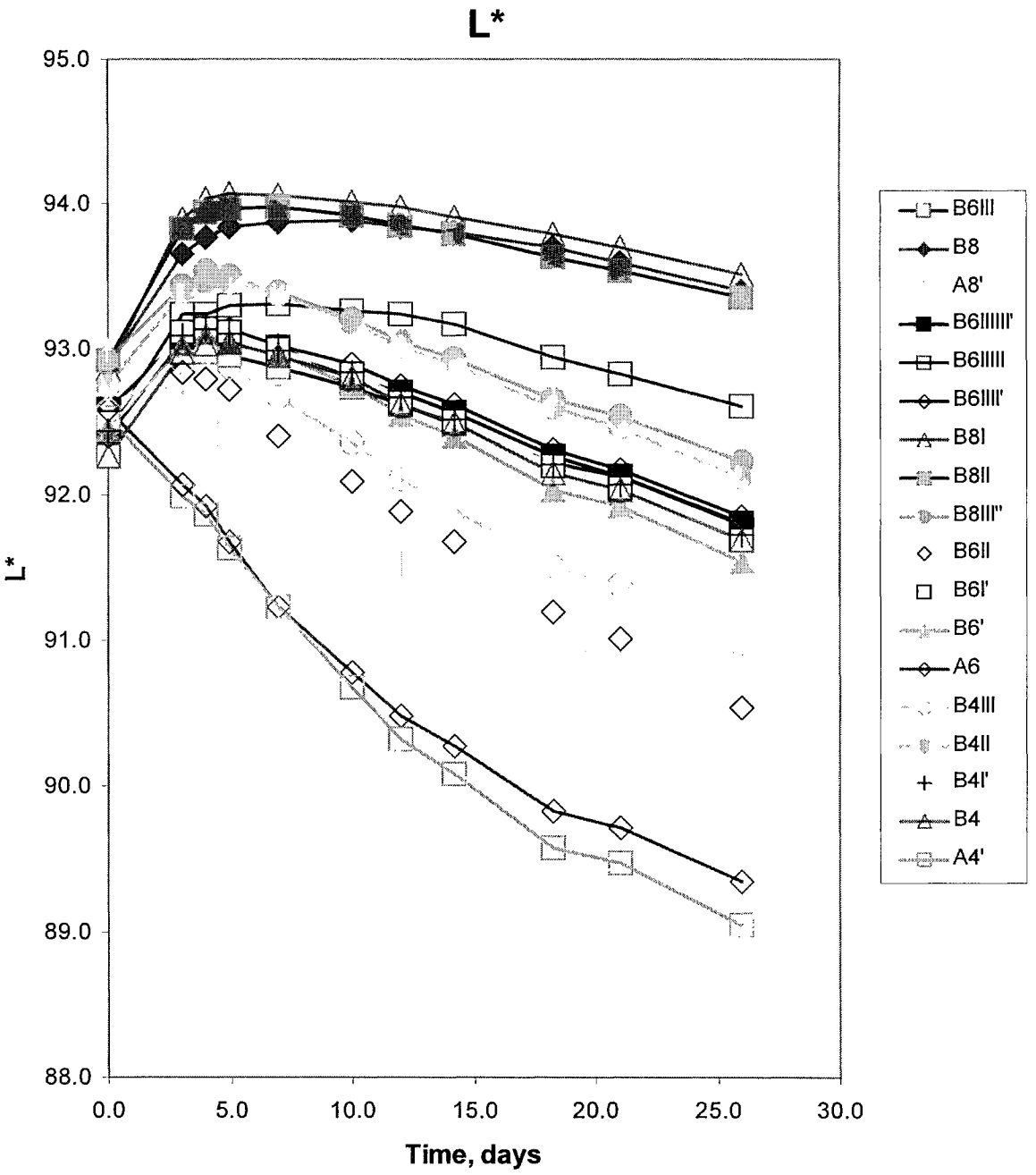

Figure A.3. L* as a function of time for different coating formulation

A.3 Analysis Summary of statistical model

Analysis Summary of statistical model for samples have been kept for 24 days in the light box.

Dependent variable : PC

Independent variables:

Coat weight
Coat weight * Coat weight
Coat weight *RSUVA
Coat weight * Tcharge
RSUVA
RSUVA *RSUVA
RSUVA * Tcharge
Tcharge
Tcharge * Tcharge

Table A.2 Multiple Regression Analysis for samples kept for 24 days in light box.

Dependent variable: PC			
Parameter	Estimate	Standard Error	T Statistic
Constant	6.4383	3.13392	2.05439
Coatweight	2.24941	1.04309	2.1565
Coat weight*coatweight	-0.251659	0.0863698	-2.91374
RS/UVA*RS/UVA	-.0647758	0.0147286	-4.39797
RSUVA*Tcharge	0.779913	0.186423	4.18357
Tcharge	-13.4448	2.73164	-4.9219`
Tcharge*Tcharge	5.15988	2.15924	2.38967

Table A.3 Analysis of Variance

Source	Sum of Squares	Degree of freedom	Mean Square	F-Ratio	P-Value
Model	56.4048	6	9.40079	21.25	0.0002
Residual	3.53903	8	0.442379		

The R-squared value provides a measure of how much of the variability in the observed response values can be explained by the experimental factors.

The residuals are the difference between the predicted and observed values. In particular, Residual = error in prediction = observed value - predicted value

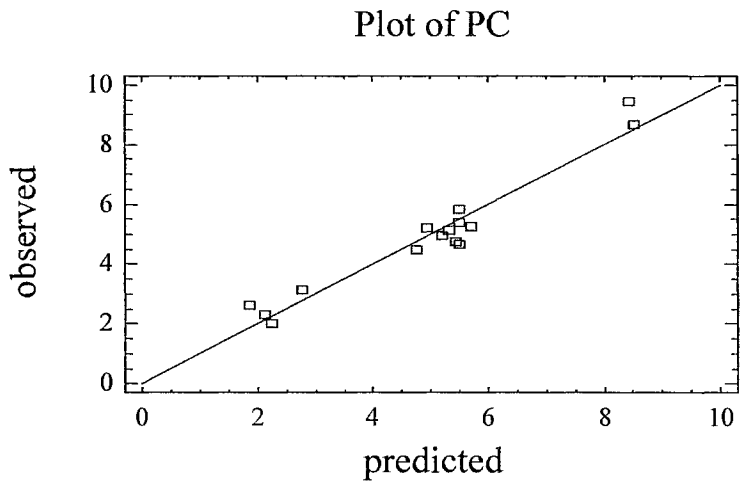

Figure A.4 Plot of predicted versus observed values for the reduced model for 24 days.

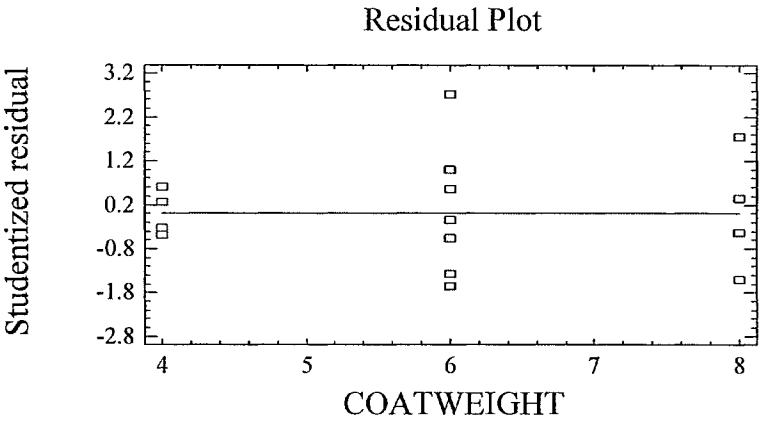

Figure A.5 Plot of residuals versus Total charge for reduced model.

A.4 A response surface plot for PC and is used for numerical optimization:

A) Response surface at coat weight = $4g/m^2$

```
Surface Plotting

PC:  6.4383 + 2.24941*4 - 0.251659*4*4 -0.0647758*y*y +
0.779913*y*x - 13.4448*x +5.15988*x*x
```

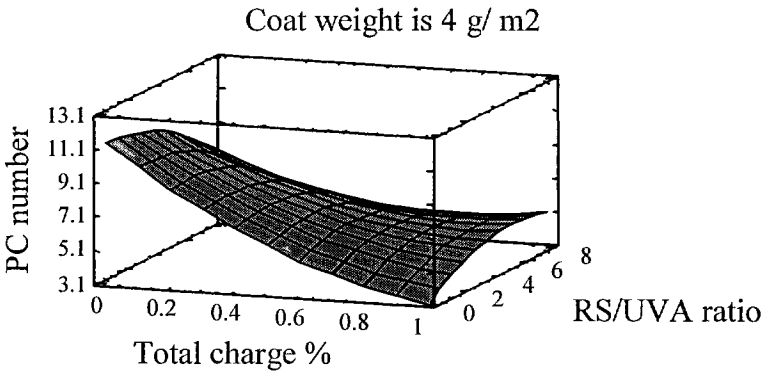

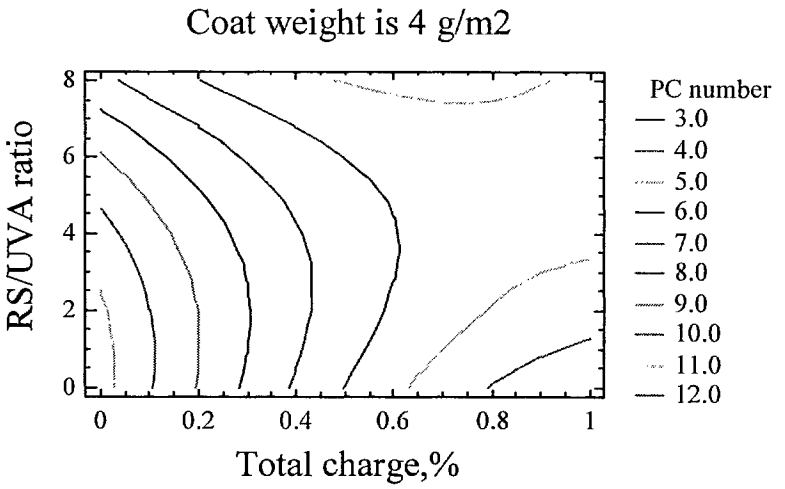

Figure A.6 PC as a function of RSUVA at coat weight = 4 g/m^2

B) Response surface at coat weight = 8 g/m^2

```
Surface Plotting


PC:  6.4383 + 2.24941*8 - 0.251659*8*8 -0.0647758*Y*Y +
0.779913*Y*X - 13.4448*X +5.15988*X*X
```

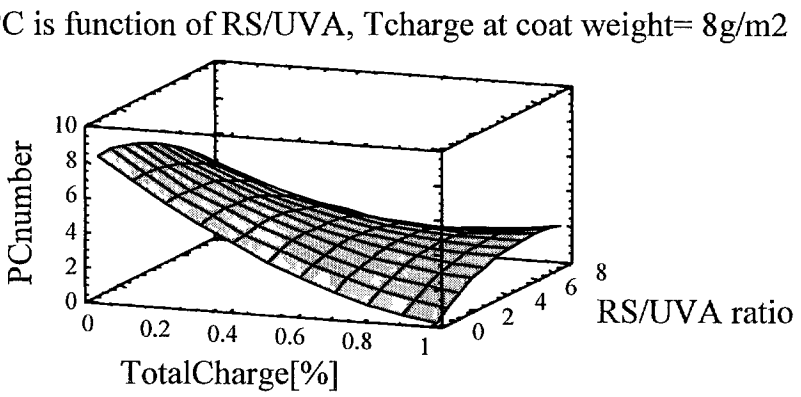

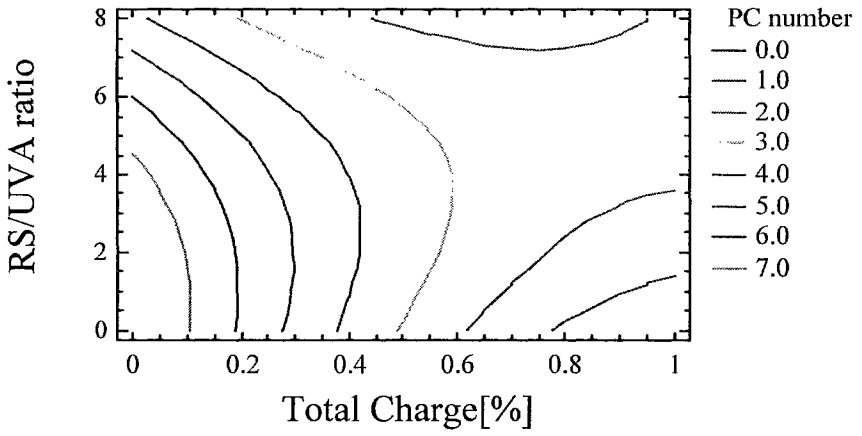

Figure A.7. PC as a function of RSUVA at coat weight = 8 g/m^2

C) Response surface at total charge = 0.2 %

```
Surface Plotting

PC: 6.4383 + 2.24941*Y - 0.251659*Y*Y -0.0647758*X*X +
0.779913*X*0.2 - 13.4448*0.2 +5.15988*0.2*0.2
```

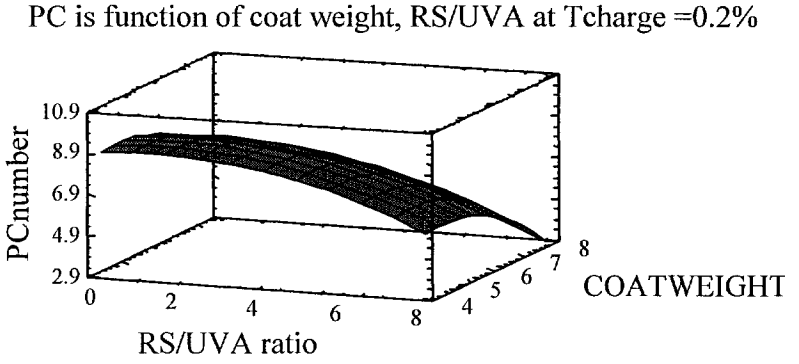

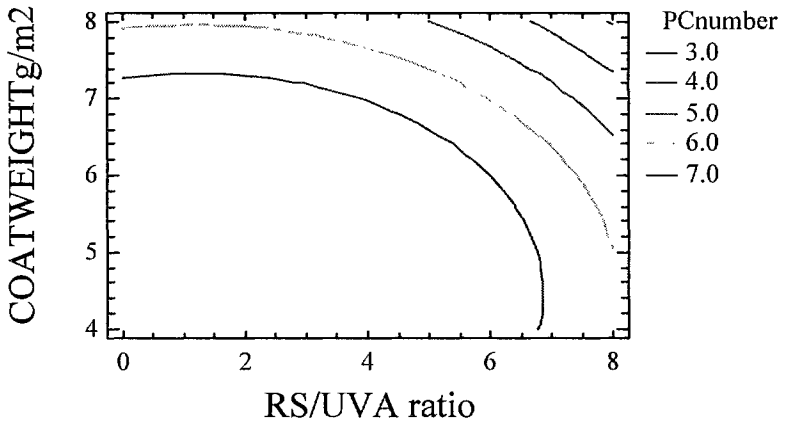

Figure A.8 PC as a function of RSUVA and coat weight at total charge = 0.2%

D) Response surface at total charge = 1 %

Surface Plotting after 24 days

PC= 6.4383 + 2.24941*Y - 0.251659*Y*Y -0.0647758*X*X + 0.779913*X*1 - 13.4448*1 +5.15988*1*1

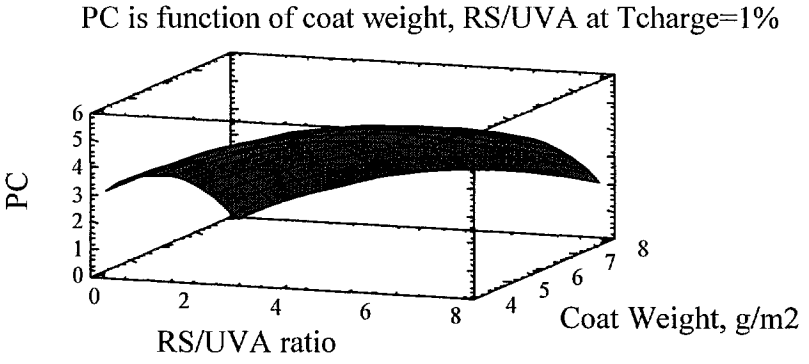

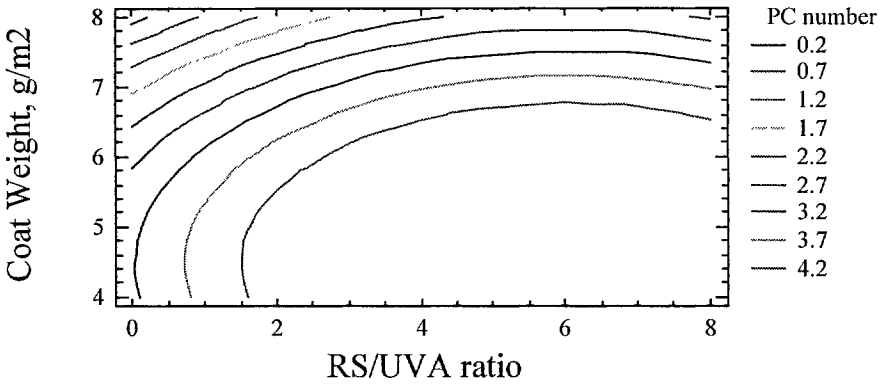

Figure A.9. PC as a function of RSUVA and coat weight at total charge = 1%

A.5 Response Surface Model of Initial Brightness As A Function of Tcharge and RS/UVA

The model which is used to characterize initial brightness as a function of coat weight, total charge and RS/UVA is a second order polynomial model. The output shows the results of fitting a multiple linear regression model to describe the relationship between initial brightness and independent variables.

The R- Squared statistic indicates that the model as fitted explains 0.906541 of the variability in Brightness.

Table A.4 Multiple Regression Analysis.

Dependent variable: PC

Parameter	Estimate	Standard Error	T Statistic
Constant	86.2833	1.2239	70.4989
Coatweight	-2.28562	0.422356	-5.4116
Coatweight*coatweight	0.195804	0.0349113	5.60861
Coat weight*RSUVA	0.0243079	0.00614002	3.95892
RSUVA*Tcharge	-0.340657	0.04799	-7.0985

Table A.5 Analysis of Variance

Source	Sum of Squares	Degree of freedom	Mean Square	F-Ratio	P-Value
Model	7.06181	4	1.76545	24.25	00.0
Residual	0.728028	10	0.0728028		

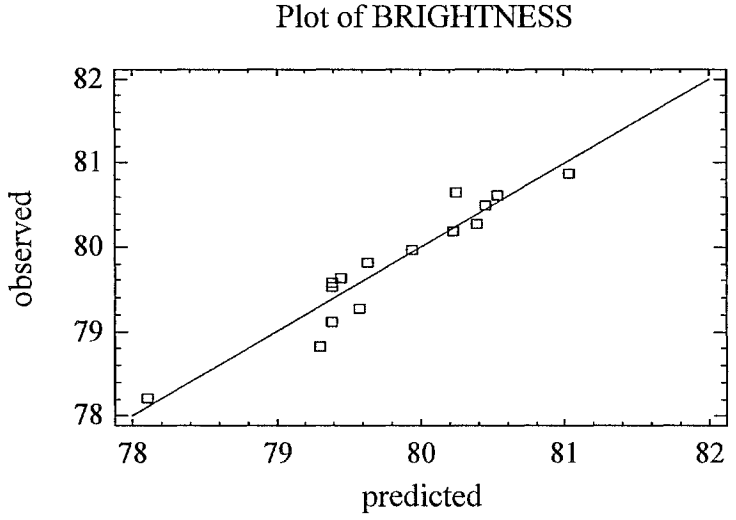

Figure A.10 Plot of predicted versus observed values for the reduced model.

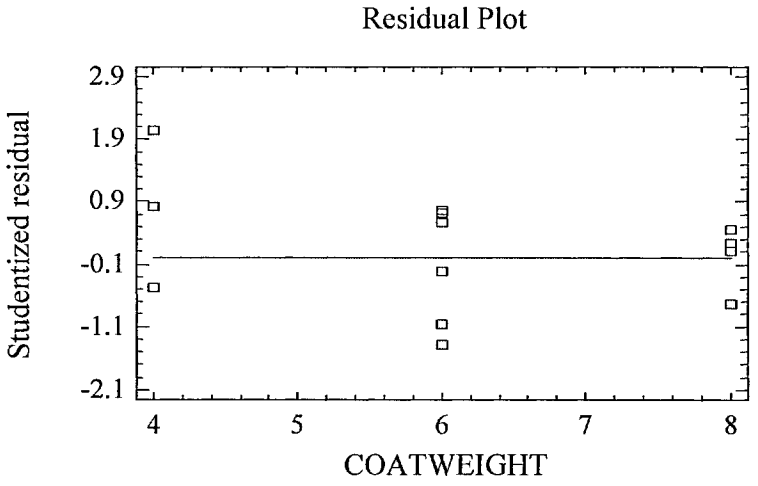

Figure A.11 Plot of residuals versus coat weight for reduced model.

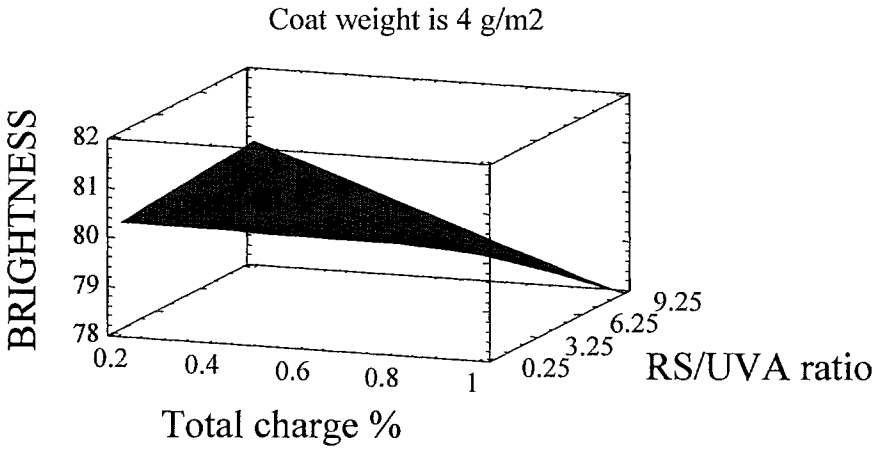

Figure A.12 This response surface plot represents the response brightness at coat weight = 4 g/m^2

.

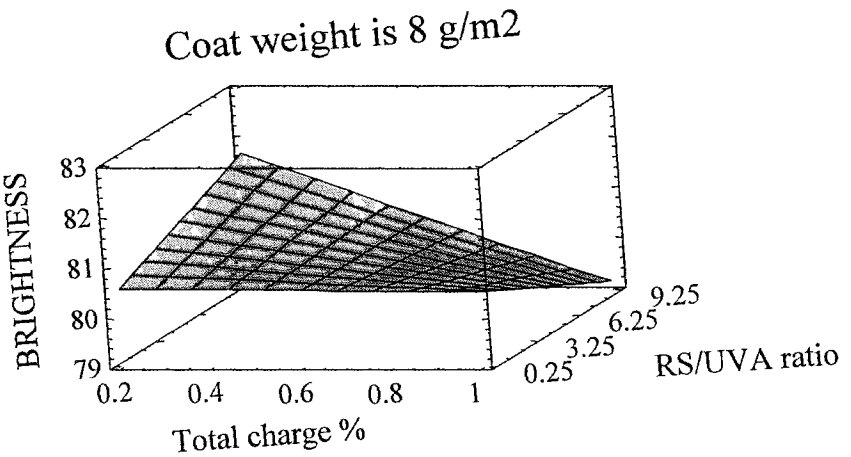

Figure A.13 This response surface plot represents the response brightness at coat weight = 8 g/m^2

APPENDIX B

B.1 Chemical Structure of inhibitor

These are the chemical structures of two inhibitors we tried.

The radical scavenger that we are used is hydroxylamine salt

And The UV-Absorber is a benzo-tri-aldol type UV-absorber, dispersed in 300 MW polyethylene glycol.

Our intended use of these inhibitors was fairly straightforward.

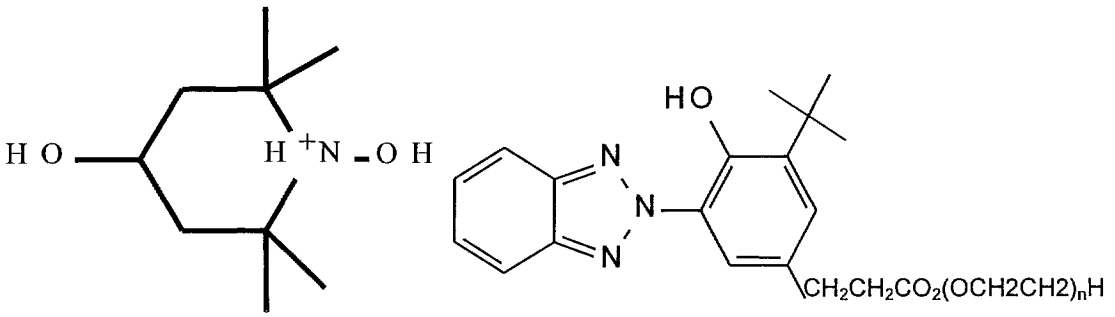

+ counter ion

Radical Scavenger **UV absorber**

Figure B. Chemical Structure of Radical Scavenger and Ultraviolet Absorber.

APPENDIX C

C. Coating formulation

Table C Coating formulation without inhibitor, with UVA, with RS and with RS&UVA.

Coating formulation with Radical Scavenger:

Chemical name	S.C. (%)	Parts	Mass	Mass
				200.00
				g Covercarb
S.C. of coating color:		55%		
Covercarb	71.6	80	111.73	200.00
Astraplate	70	20	28.57	51.14
Penford Gum 280	20	6	30.00	53.70
Acronal S728	49.4	12	24.29	43.48
KZCote	100	0.5	0.50	0.90
Tinuvin 1130	87	0	0.00	0.00
PAX-2067	30	8.97	29.90	53.52
Srerocoll BL	100	0.1	0.10	0.18
Water			6.85	12.26
Total Mass		127.57	231.95	415.18

Coating formulation with UVabsorber:

Chemical name	S.C. (%)	Parts	Mass	Mass 200.00 g Covercarb
S.C. of coating color:		**55%**		
Covercarb	71.6	80	111.73	200.00
Astraplate	70	20	28.57	51.14
Penford Gum 280	20	6	30.00	53.70
Acronal S728	49.4	12	24.29	43.48
KZCote	100	0.5	0.50	0.90
Tinuvin 1130	87	1.157	1.33	2.38
PAX-2067	30	0	0.00	0.00
Srerocoll BL	100	0.1	0.10	0.18
Water			21.22	37.98
Total Mass		**119.757**	**217.74**	**389.75**

Coating formulation with total charge 0.6% of Uvabsorber and Radical Scavenger:

Chemical name	S.C. (%)	Parts	Mass	Mass 200 g Covercarb
S.C. of coating color:		**55%**		
Covercarb	71.6	80	111.73	200.00
Astraplate	70	20	28.57	51.14
Penford Gum 280	20	6	30.00	53.70
Acronal S728	49.4	12	24.29	43.48
KZCote	100	0.5	0.50	0.90
Tinuvin 1130	87	1.157	1.33	2.38
PAX-2067	30	8.97	29.90	53.52
Srerocoll BL	100	0.1	0.10	0.18
Water			7.62	13.65
Total Mass		**128.727**	**234.05**	**418.95**

Coating formulation with total charge 0.2% of Uvabsorber and Radical Scavenger:

Chemical name	S.C. (%)	Parts	Mass	Mass 200.00 g Covercarb
S.C. of coating color:		**55%**		
Covercarb	71.6	80	111.73	200.00
Astraplate	70	20	28.57	51.14
Penford Gum 280	20	6	30.00	53.70
Acronal S728	49.4	12	24.29	43.48
KZCote	100	0.5	0.50	0.90
Tinuvin 1130	87	0.365	0.42	0.75
PAX-2067	30	2.83	9.43	16.89
Srerocoll BL	100	0.1	0.10	0.18
Water			16.40	29.35
Total Mass		**121.795**	**221.45**	**396.39**

Coating formulation with total charge 1% of Uvabsorber and Radical Scavenger:

Chemical name	S.C. (%)	Parts	Mass	Mass 100.00 g Covercarb
S.C. of coating color:		**55%**		
Covercarb	71.6	80	111.73	100.00
Astraplate	70	20	28.57	25.57
Penford Gum 280	20	6	30.00	26.85
Acronal S728	49.4	12	24.29	21.74
KZCote	100	0.5	0.50	0.45
Tinuvin 1130	87	2.04	2.34	2.10
PAX-2067	30	15.849	52.83	47.28
Srerocoll BL	100	0.1	0.10	0.09
Water			0.07	0.06
Total Mass		**136.489**	**250.44**	**224.14**

APPENDIX D

D. Coating Formulations with 0.1%, 0.3%, 0.5%, 0.7% and 0.9% of inhibitors.

Coating formulation with total charge 0.1% of UVabsorber and Radical Scavenger, RS/UVA= 4:

Table D. Coating Formulations with 0.1%, 0.3%, 0.5%, 0.7% and 0.9% of inhibitors.

Chemical name	S.C. (%)	Parts	Mass	Mass 100.00 g Covercarb
S.C. of coating color:		55%		
Covercarb	71.6	80	111.73	100.00
Astraplate	70	20	28.57	25.57
Penford Gum 280	20	6	30.00	26.85
Acronal S728	49.4	12	24.29	21.74
KZCote	100	0.5	0.50	0.45
Tinuvin 1130	87	0.315	0.36	0.32
PAX-2067	30	1.26	4.20	3.76
Srerocoll BL	100	0.1	0.10	0.09
Water			18.74	4.19
Total Mass		120.175	199.83	178.85

Coating formulation with total charge 0.3% of UVabsorber and Radical Scavenger, RS/UVA= 4:

Chemical name	S.C. (%)	Parts	Mass	Mass 100.00 g Covercarb
S.C. of coating color:		55%		
Covercarb	71.6	80	111.73	100.00
Astraplate	70	20	28.57	25.57
Penford Gum 280	20	6	30.00	26.85
Acronal S728	49.4	12	24.29	21.74
KZCote	100	0.5	0.50	0.45
Tinuvin 1130	87	0.97	1.11	1.00
PAX-2067	30	3.884	12.95	11.59
Srerocoll BL	100	0.1	0.10	0.09
Water			15.2	3.4
Total Mass		123.454	209.33	187.35

Coating formulation with total charge 0.5% of UVabsorber and Radical Scavenger, RS/UVA= 4:

Chemical name	S.C. (%)	Parts	Mass	Mass
				100.00
				g Covercarb
S.C. of coating color:		55%		
Covercarb	71.6	80	111.73	100.00
Astraplate	70	20	28.57	25.57
Penford Gum 280	20	6	30.00	26.85
Acronal S728	49.4	12	24.29	21.74
KZCote	100	0.5	0.50	0.45
Tinuvin 1130	87	1.66	1.91	1.71
PAX-2067	30	6.655	22.18	19.85
Srerocoll BL	100	0.1	0.10	0.09
Water			11.47	2.57
Total Mass		126.915	219.36	196.32

Coating formulation with total charge 0.7% of UVabsorber and Radical Scavenger, RS/UVA= 4:

Chemical name	S.C. (%)	Parts	Mass	Mass
				100.00
				g Covercarb
S.C. of coating color:		55%		
Covercarb	71.6	80	111.73	100.00
Astraplate	70	20	28.57	25.57
Penford Gum 280	20	6	30.00	26.85
Acronal S728	49.4	12	24.29	21.74
KZCote	100	0.5	0.50	0.45
Tinuvin 1130	87	2.46	2.83	2.53
PAX-2067	30	9.59	31.97	28.61
Srerocoll BL	100	0.1	0.10	0.09
Water			7.56	1.69
Total Mass		130.65	230.06	205.90

Coating formulation with total charge 0.9% of UVabsorber and Radical Scavenger, RS/UVA= 4:

Chemical name	S.C. (%)	Parts	Mass	Mass
				100.00
				g Covercarb
S.C. of coating color:		55%		
Covercarb	71.6	80	111.73	100.00
Astraplate	70	20	28.57	25.57
Penford Gum 280	20	6	30.00	26.85
Acronal S728	49.4	12	24.29	21.74
KZCote	100	0.5	0.50	0.45
Tinuvin 1130	87	3.17	3.64	3.26
PAX-2067	30	12.69	42.30	37.86
Srerocoll BL	100	0.1	0.10	0.09
Water			3.33	2.98
Total Mass		134.46	244.47	218.80

APPENDIX E

E.1 Microstructure of coating color

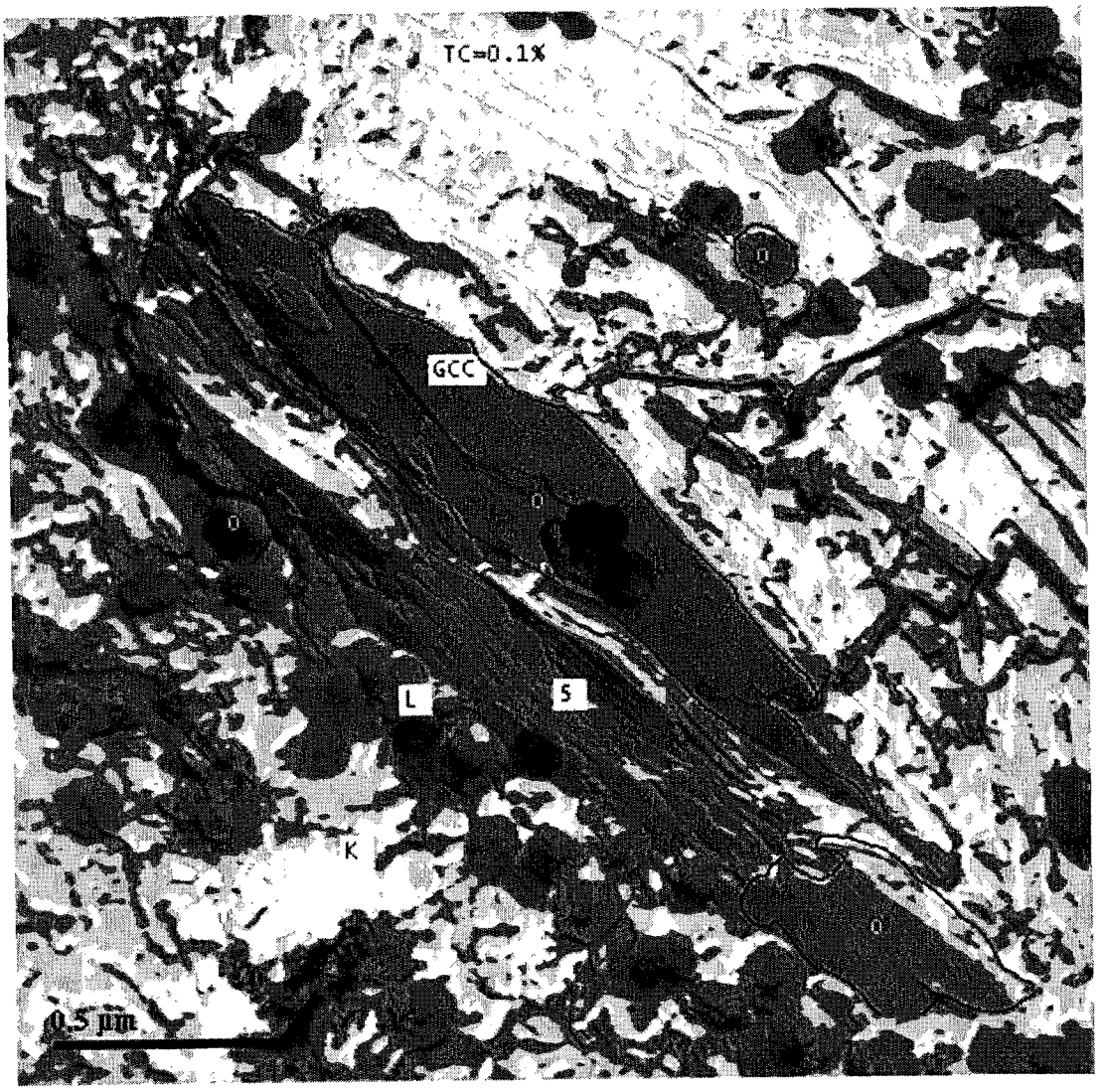

Figure AE.1 Coating formulation with total concentration 0.1% of inhibitors

Figure AE.2 Coating formulation with total concentration 0.1% of inhibitors

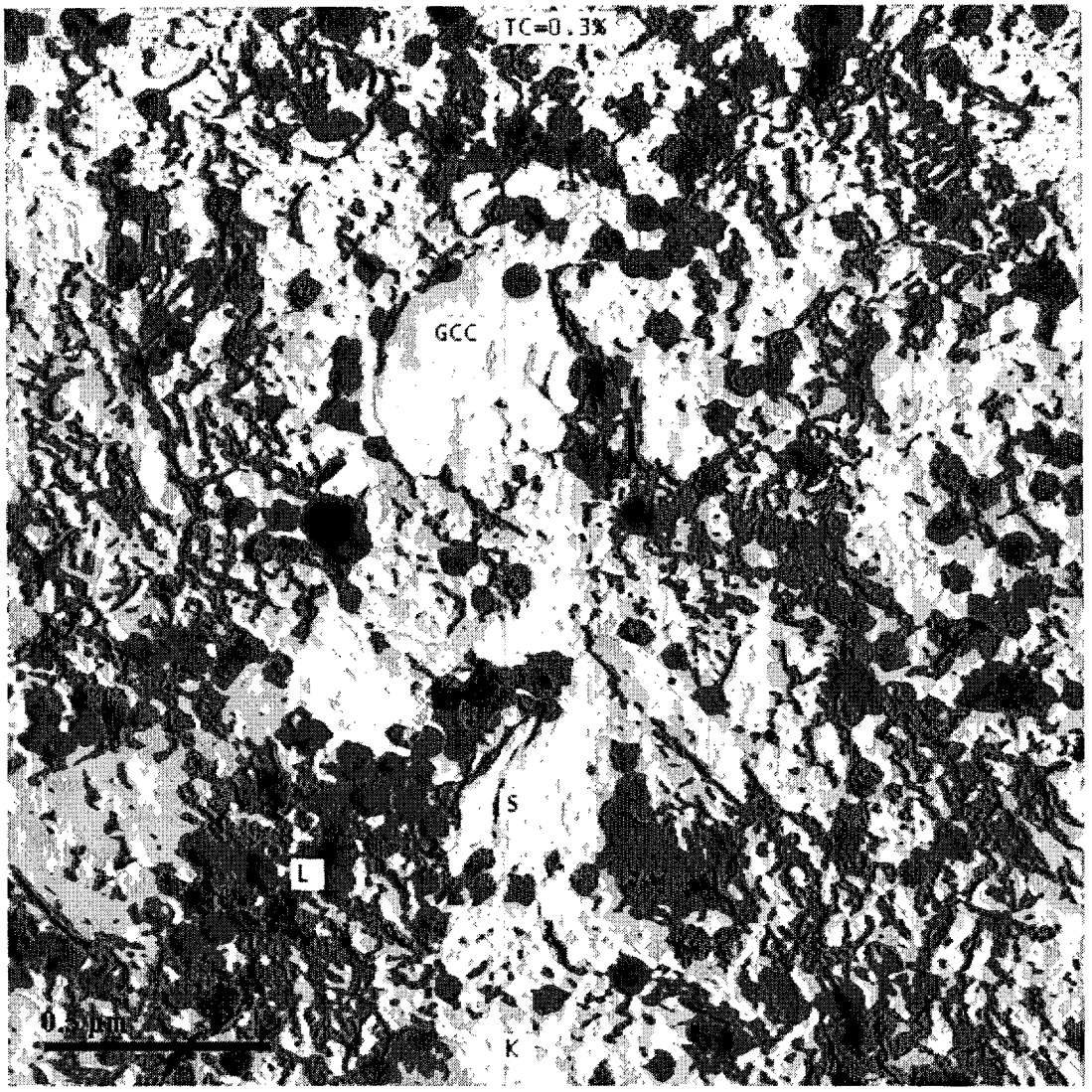

Figure AE.3. Coating formulation with total concentration 0.3% of inhibitors

Figure AE.4. Coating formulation with total concentration 0.3% of inhibitors.

Figure AE.5. Coating formulation with total concentration 0.3% of inhibitors

Figure AE.6. Coating formulation with total concentration 0.6% of inhibitors

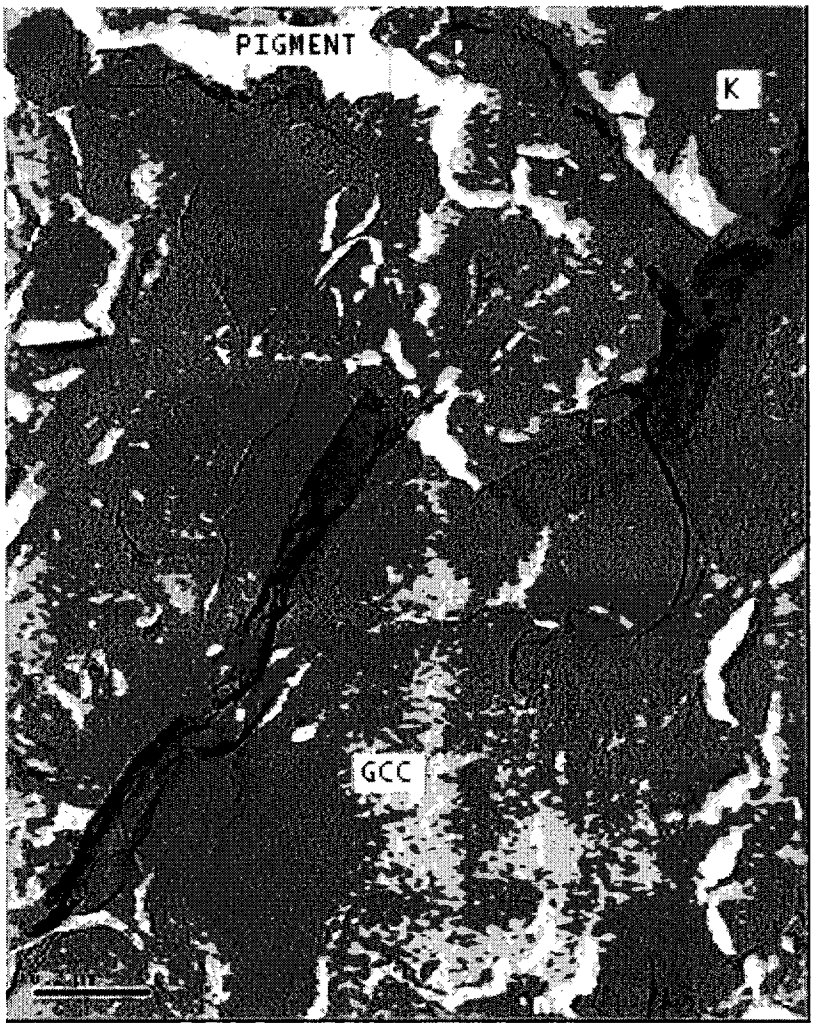

Figure AE.7. Mixture of ground calcium carbonate and kaolinite.

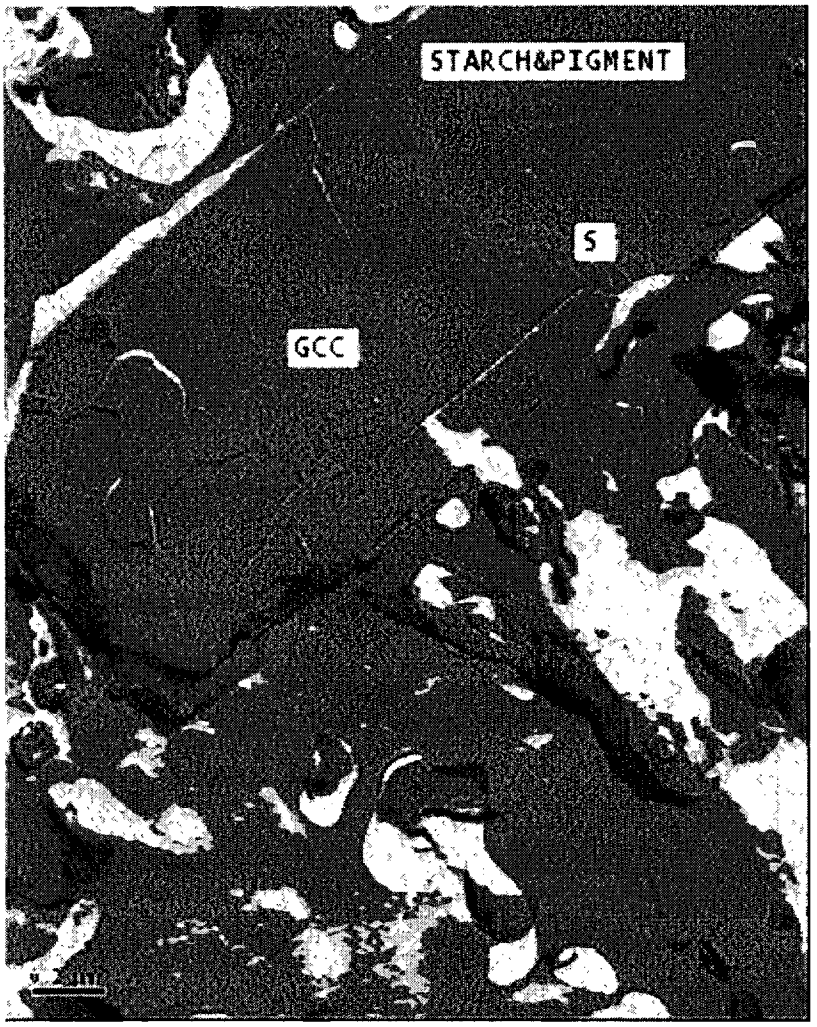

Figure AE.8. Mixture of ground calcium carbonate, kaolinite and starch.

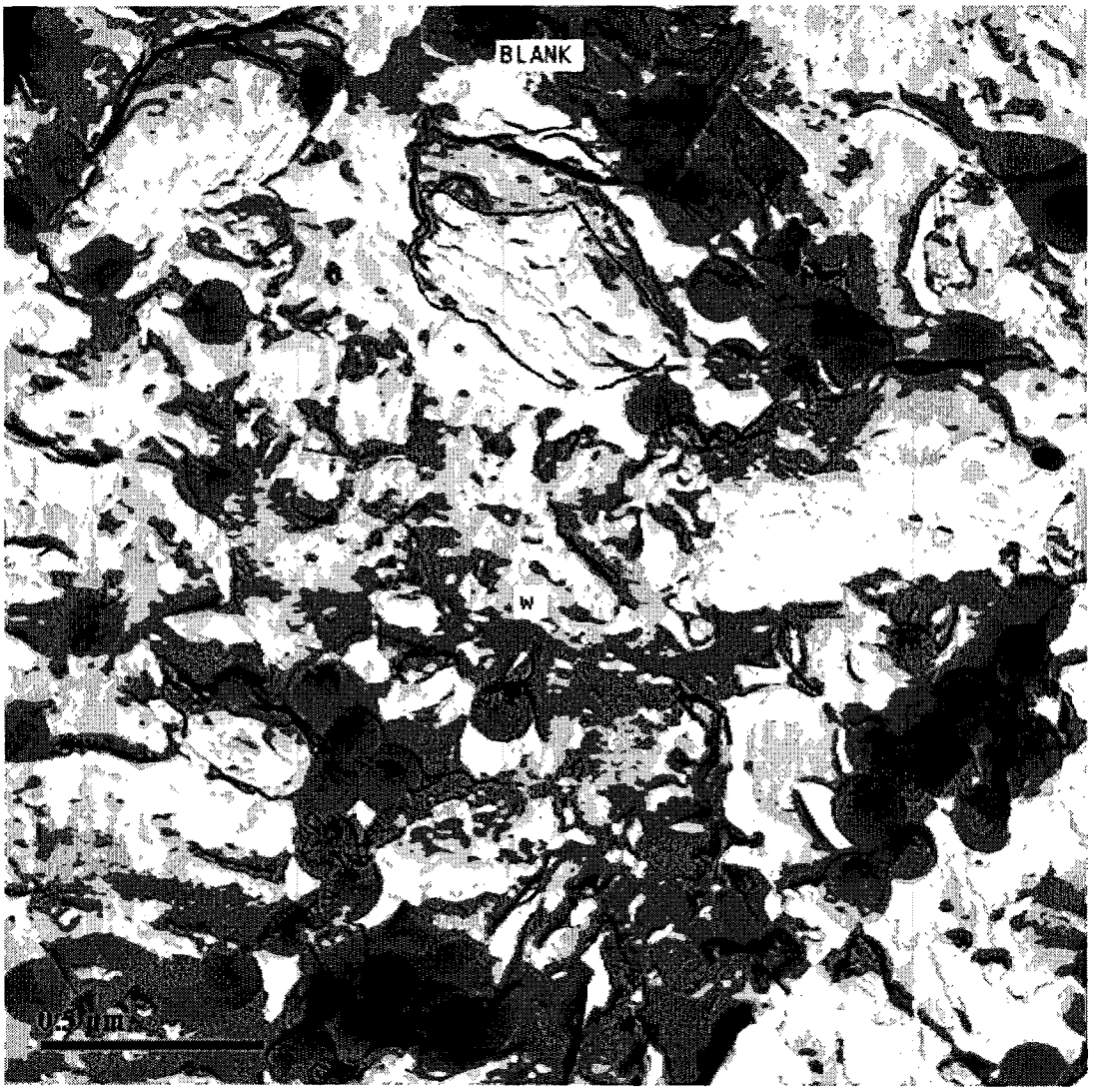

Figure AE.9. Coating formulation without inhibitor.

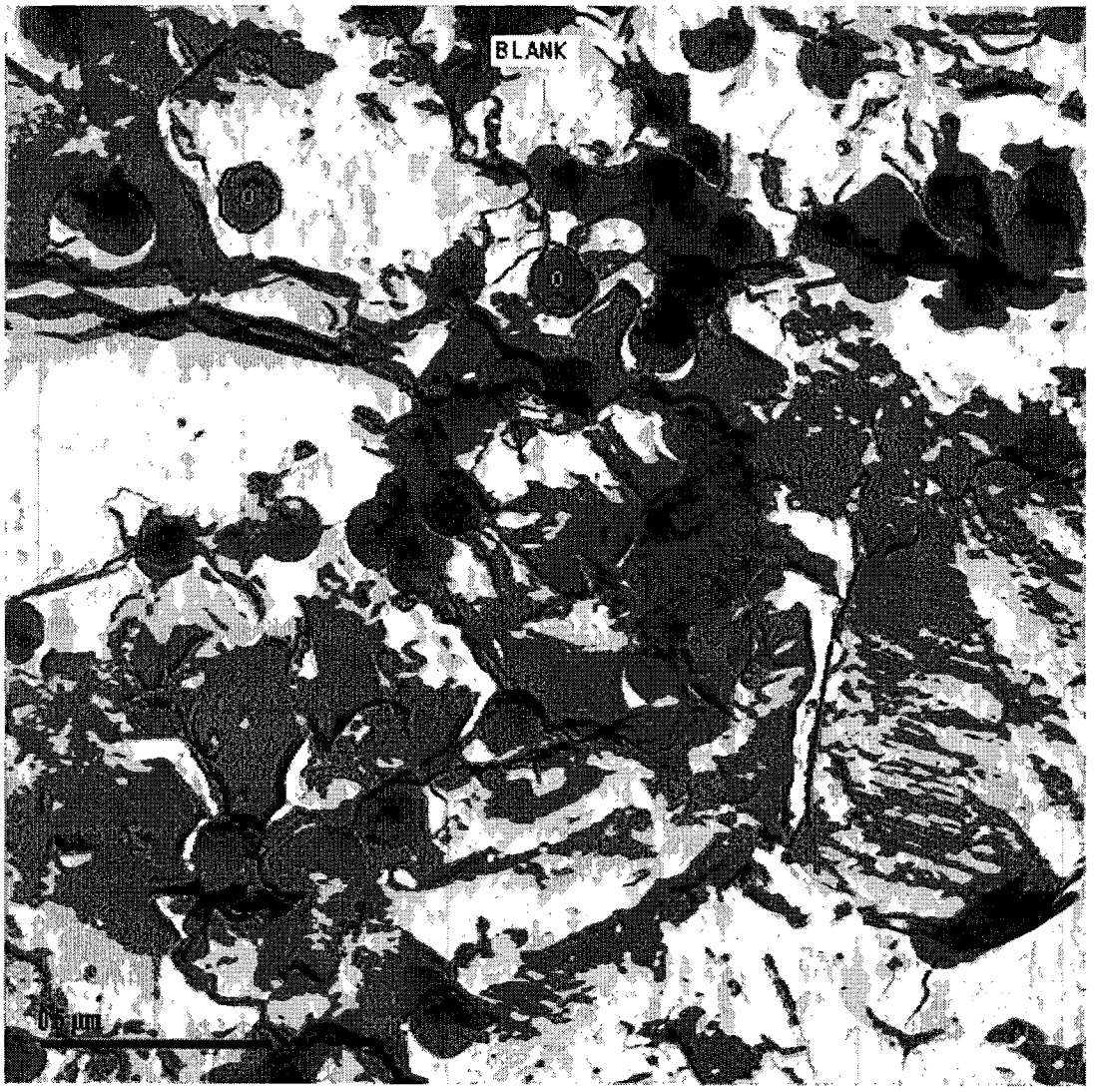

Figure AE.10. Coating formulation without inhibitors

Figure AE.11. Coating formulation without inhibitors

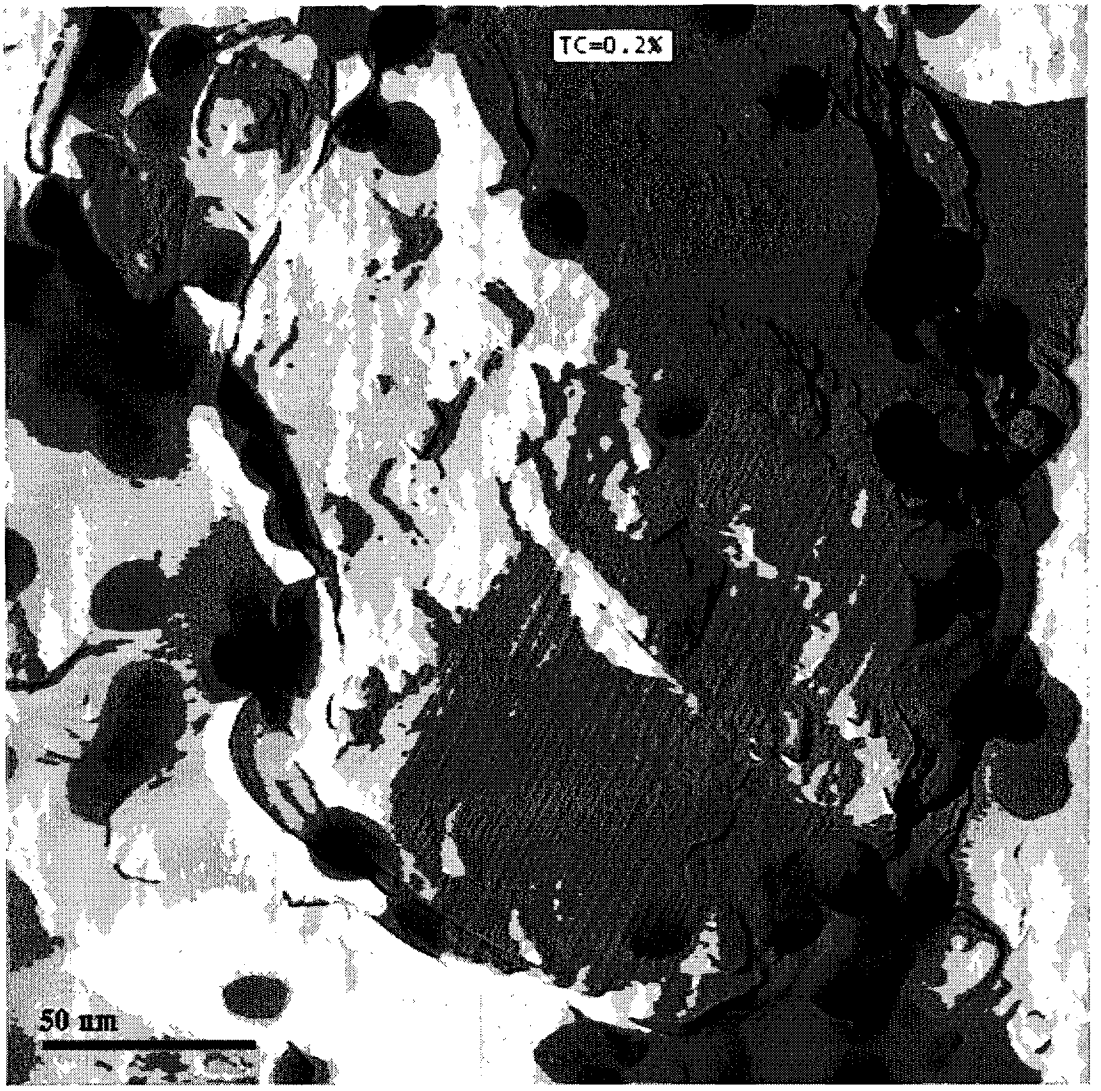

Figure AE.12. Coating formulation with total concentration 0.2% of inhibitors

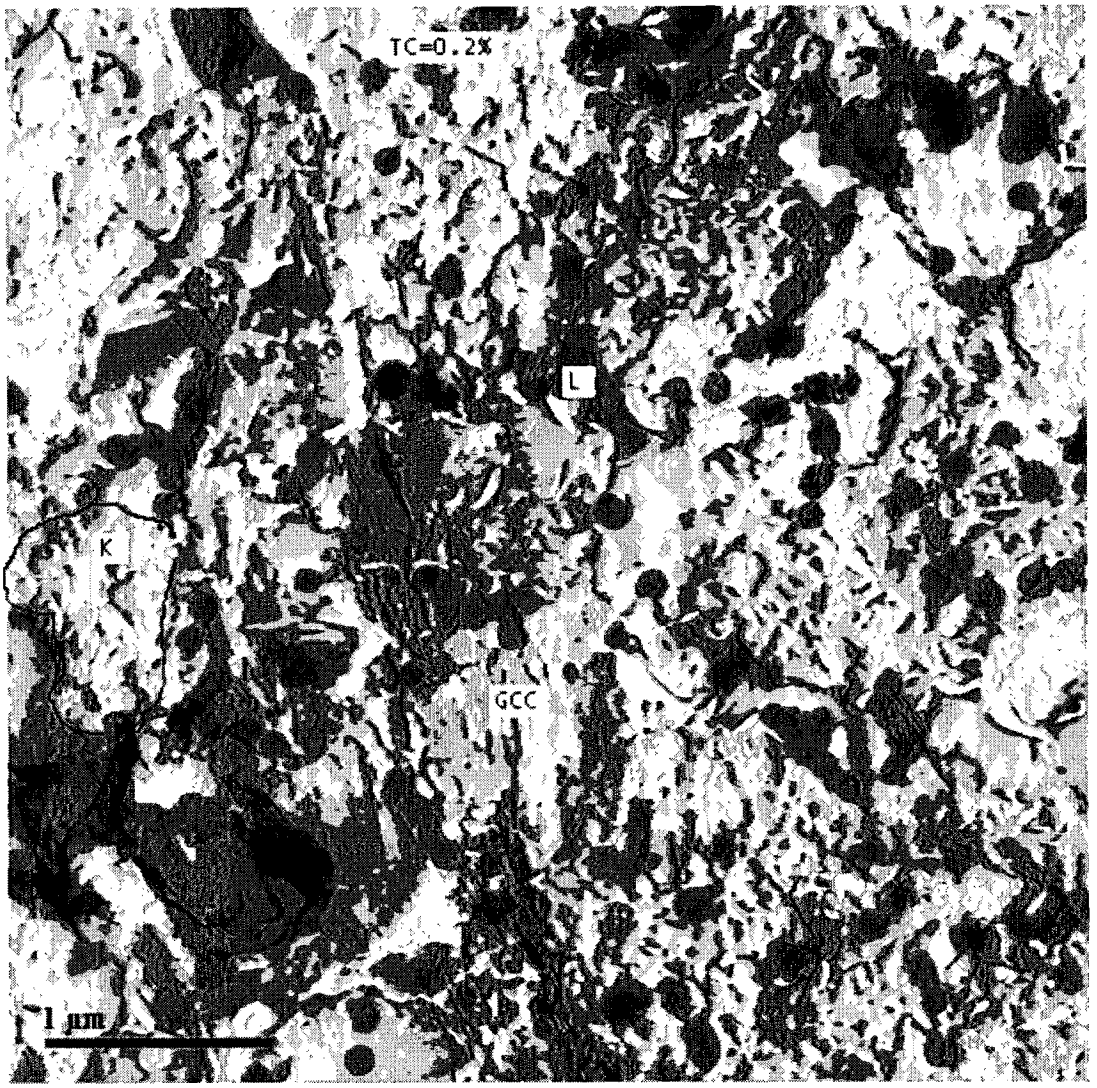

Figure AE.13. Coating formulation with total concentration 0.2% of inhibitors

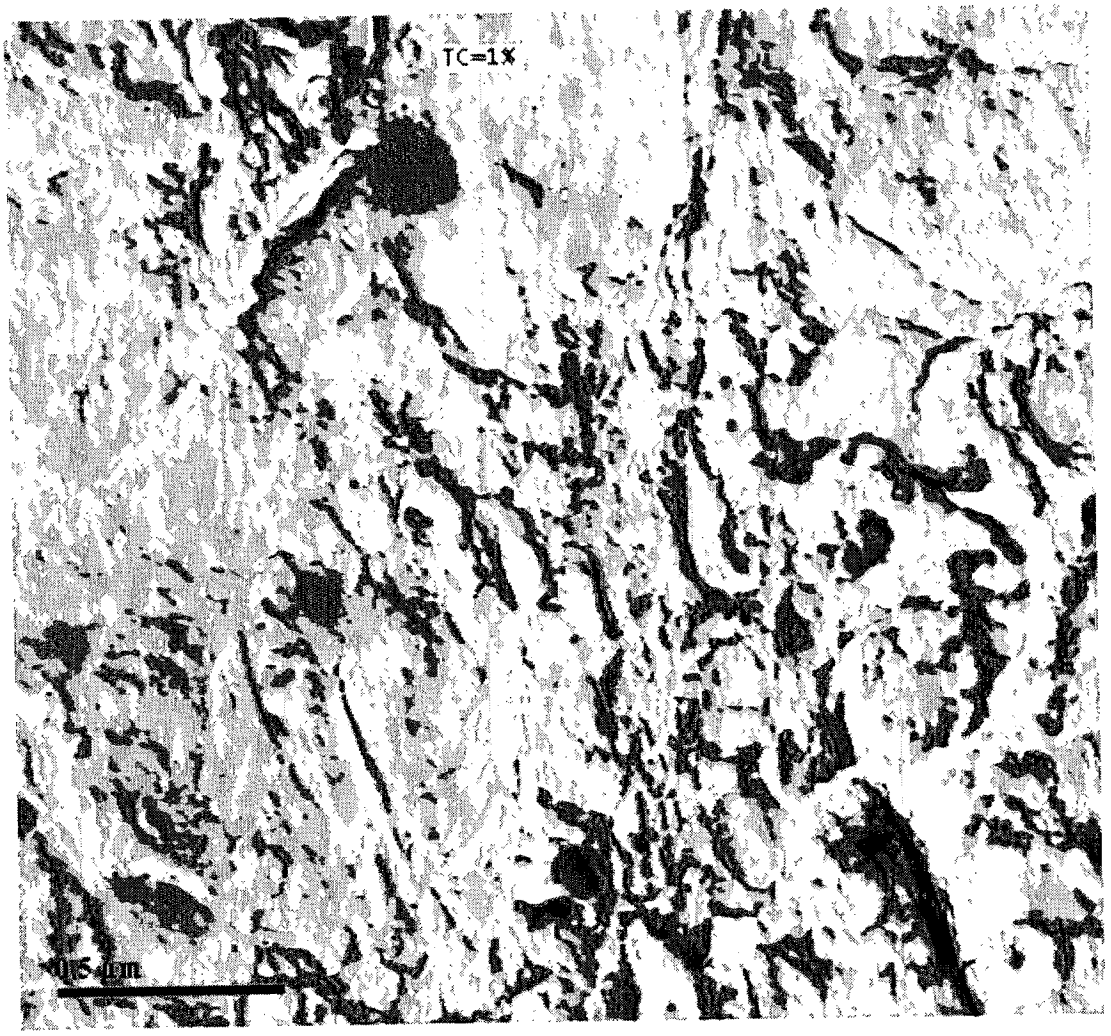

Figure AE.14. Coating formulation with total concentration 1% of inhibitors

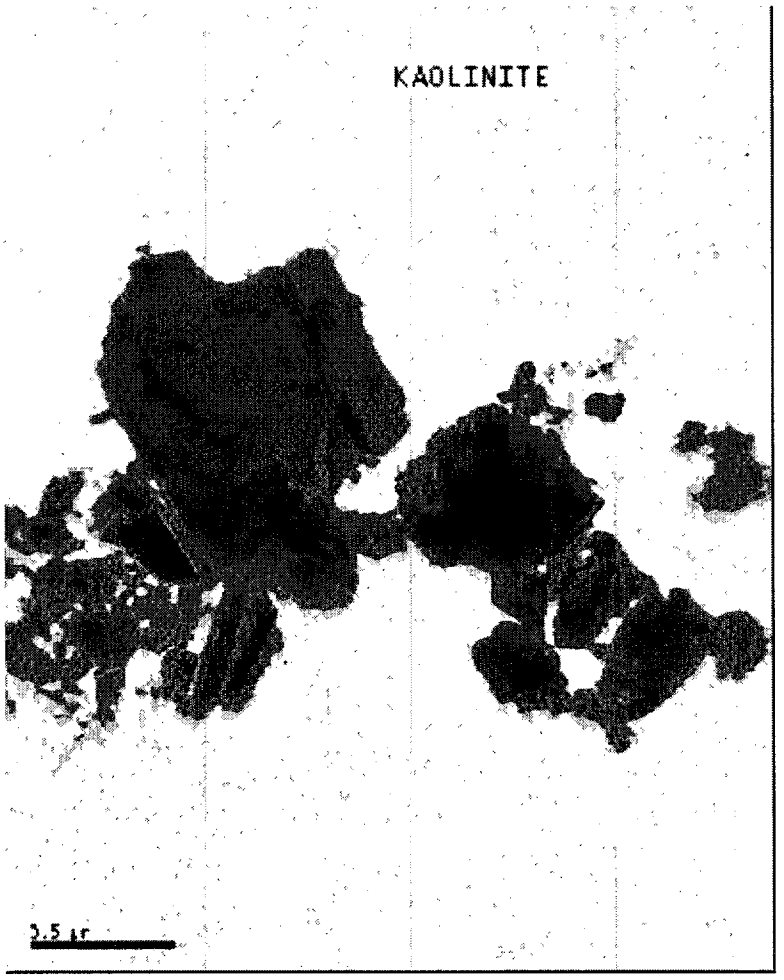

Figure AE.15. kaolinite crystals.

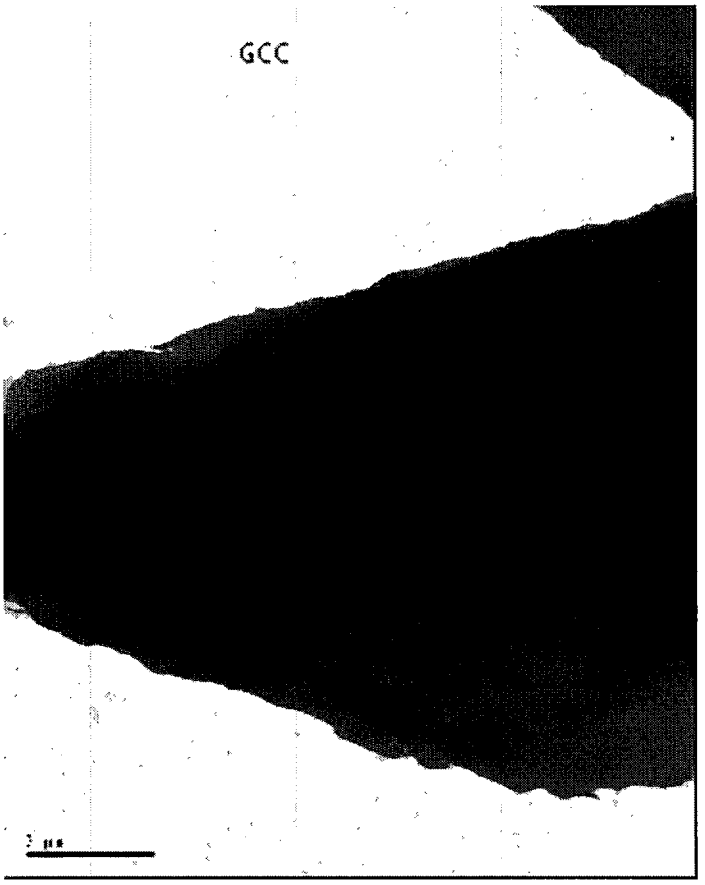

Figure AE.16. Ground calcium carbonate.

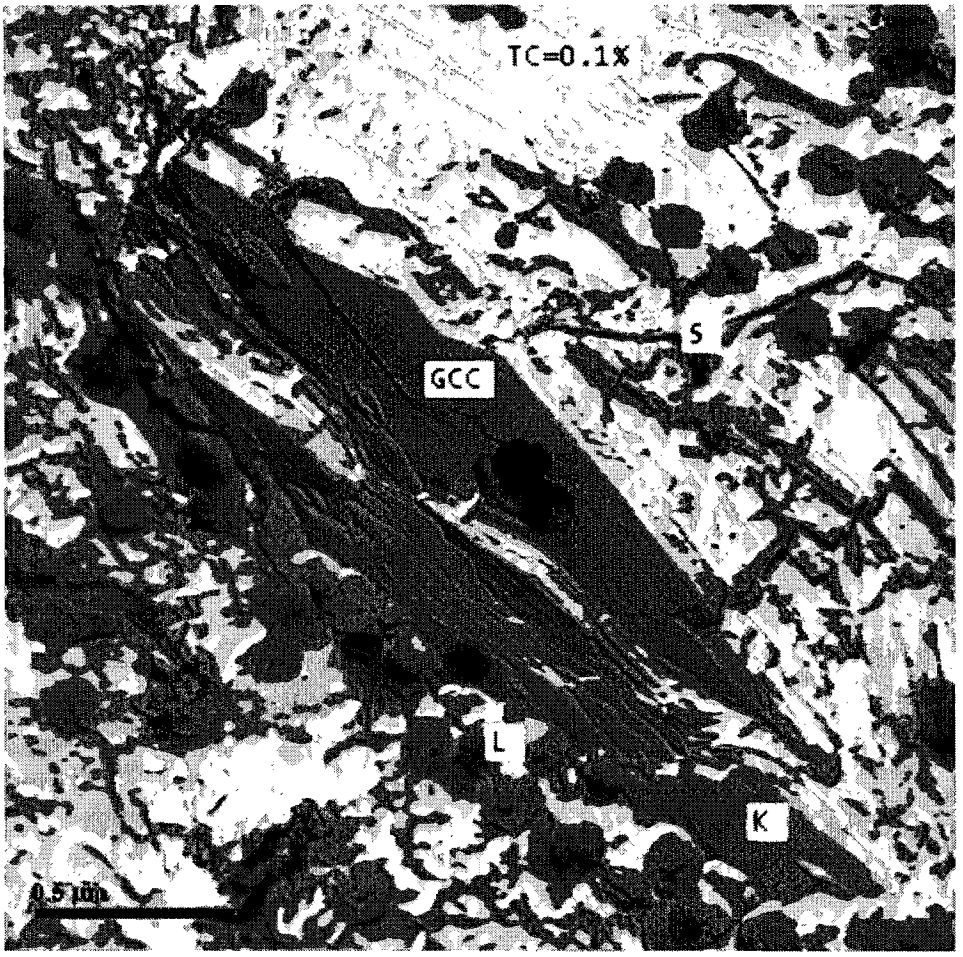

Figure AE.17. Coating formulation with 0.1% of inhibitors.

Figure AE.18. Coating formulation with 0.9% of inhibitors.

APPENDIX F

F-1 The points of the Geometry

The points in figure 10-3 shows the values in x, y and z axis, these points are:

a = (-3.5,39.8,0), b = (-3.5,-39.8,0), c = (0,-40,0), d = (3.5,-39.8,0),
e = (3.5,39.8,0), f = (0,40,0), g = (-3.5,-39.8,80), h = (0,-39.8,80),
i = (3.5,-39.8,80), j = (3.5,39.8,80), k = (0,39.8,80), l = (-3.5,39.8,80).

F-2 Curve Fitting of Experimental Results

POLYMAT preprocessor is used for material property analysis based on experimental. The result of the POLYMAT calculation is material property data that is passed to POLYDATA through a material data file. Since coating color is viscoelastic material, therefore, our interest was to find out the best viscoelastic model fit the experimental data of coating color.

Here we present a quantitative fitting of KBKZ model to the experimental data of coating color without inhibitor and coating colors with 0.6% and 1%. The data show that the solution is shear thinning at low shear rate.

The curve fitting shows that the KBKZ is the best model can fit the experimental data. Where KBKZ model is an integral viscoelastic model.

The KBKZ model provides additional accuracy by including a damping function in its constitutive equations.the KBKZ model can calculate the extra stress tensor (T) which is = T_1 +T_2.

Where T_1 is computed from:

$$\mathbf{T}_1 = \frac{1}{1-\theta}\int_0^{\infty}\sum_{i=1}^{N}\frac{\eta_k}{\lambda_i^2}\exp\left(\frac{-s}{\lambda_i}\right)H(I_1,I_2)\left[C_t^{-1}(t-s)+\theta C_t(t-s)\right]ds$$

(1)

and T_2 is computed from Equation:

(2) $\mathbf{T}_2 = 2\eta_2\mathbf{D}$

where D is the rate-of-deformation tensor and η_2 is the viscosity factor for the Newtonian (i.e., purely-viscous) component of the extra-stress tensor. The viscosity ratio r_η is defined as η_2 /η. The relationship of η_1 and η_2 to η is expressed by

$$\eta_1 = (1-r_\eta)\eta \quad (4)$$

and

$$\eta_2 = r_\eta\eta \quad (5)$$

In Equation (1), i is the index of the relaxation mode and θ is a scalar parameter that controls the ratio of the normal-stress differences:

$$\frac{N_2}{N_1} = \frac{\theta}{1-\theta} \quad (6)$$

and **H** is the damping function.

The Papanastasiou-Scriven-Macosko (PSM) model computes **H** from

$$H = \frac{\alpha}{\alpha + I - 3} \quad (7)$$

where α is a material parameter that primarily influences the shear-thinning behavior. The default value for α is 1, which may be unrealistic for many fluids, due to the large possible range of this parameter. The Papanastasiou-Scriven-Macosko (PSM) has a reversible and an irreversible function type. The irreversible PSM model allows H only to decrease.

I is computed from

$$I = \beta I_1 + (1 - \beta) I_2 \qquad \textbf{(8)}$$

I_1 and I_2 are the scalar invariants of the Cauchy-Green strain tensor:

$$I_1 = \mathrm{tr}\left(C_t^{-1}\right) \qquad \textbf{(9)}$$

$$I_2 = \mathrm{tr}(C_t) \qquad \textbf{(10)}$$

C_t = Cauchy-Green strain tensor.

t = current time

s = metric for time integrals

β is a material parameter that influences only the elongational behavior of the material. Table F reveals the material properties of different coating colors. It can be noticed the effect of inhibitors on the properties of coating color.

Table F Material Properties

Material properties	α	β	Partial viscosity	Relaxation time
Coating color	0.0013	0	52.5	0.01
Coating with 0.6% of inhibitors	8.91	0	0.092	0.01
Coating with 1% of inhibitors	15.7	0	2.65	0.01

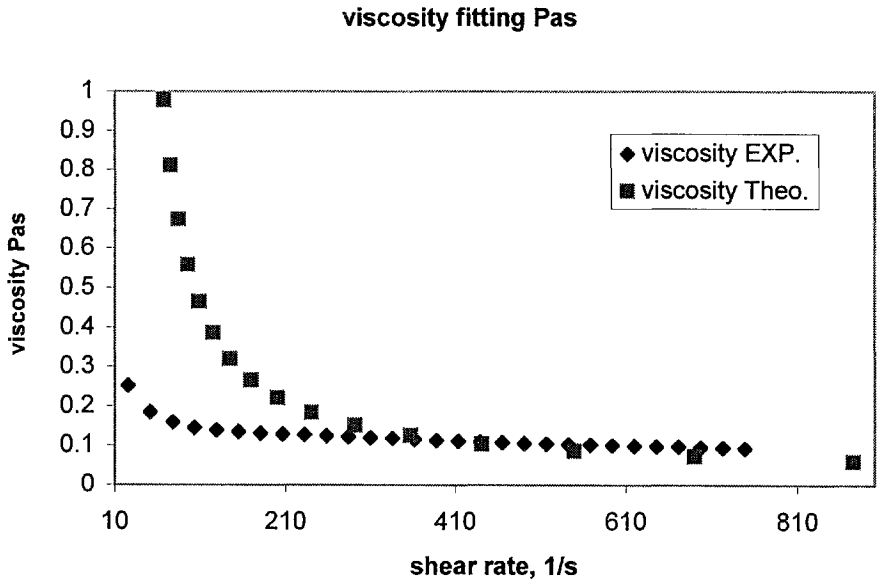

(a)

Figure AF.a shows that the viscosity of coating color which has been obtained from the simulation match the experimental data after specific shear rate. While the loss modulus from the experiments match the results obtained from the simulation as seen in Figure AF.b. On the other hand, it is observed that there is a slight variation between the storage modulus obtained from the experimental data and the storage modulus values from the simulation, as shown in figure AF.c

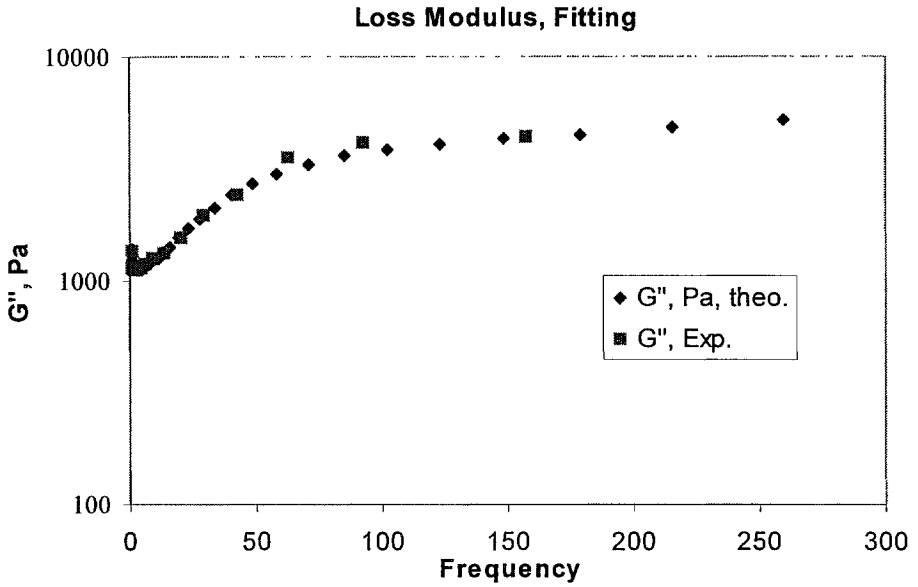

(b)

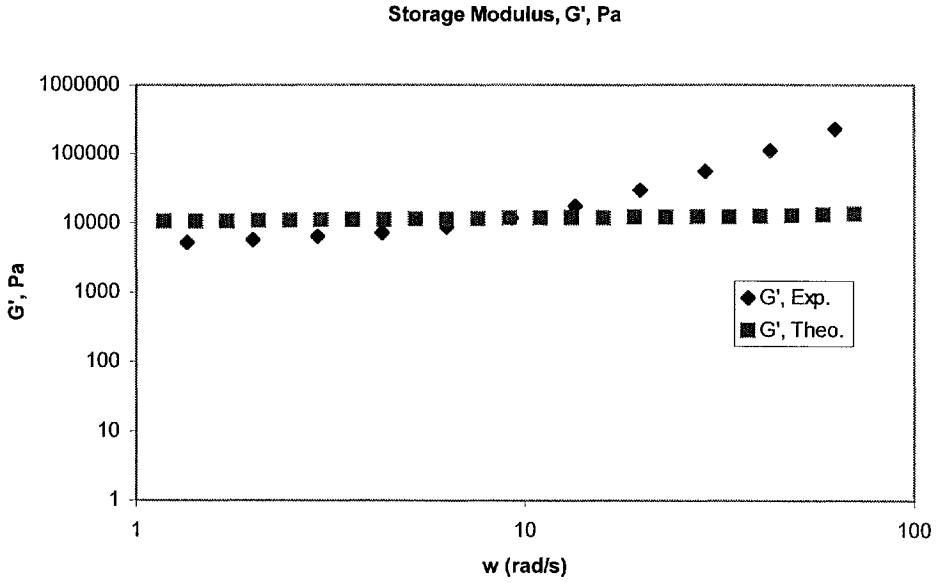

(c)

Figure AF.1 Plot of computed and experimental curves. (a) viscosiy, (b) loss modulus, (c) storage modulus.

The inhibitors appear to have a pronounced effect on viscosity and on elastic modulus of the coating color suspension. Elastic modulus increases with inhibitor containing suspensions. Despite the effect of elastic modulus behavior on coating process, however, calculation the extra stress tensor considering coating color as viscoelastic material can not be solved because:

- The big difference in dimensions of the geometry, between the application nip (0.006 cm) and the diameter of the roller (80 cm).
- Therefore, the number of elements in y-direction on the inlet and outlet was one.
- From polyflow requirements, the Weissenberg number shouldn't exceed 6 which is very small comparing to high speed used in the nip.

Therefore, the elasticity has been neglected and we concentrate on the viscosity using Non-Newtonian inelastic model (Carreau-Yasuda).

F-3 Numerical Methods

The iteration steps between Time-marching scheme and Evolution scheme for 3D

Evolution scheme:

Navier-Stokes 3D

Support : S1.

Output Fields : VELOCITIES

PRESSURE

Navier-Stokes 3D

isothermal flow problem

generalized newtonian fluid

newton-raphson iteration for viscosity law

viscosity function : visc = F(g)

shear-rate dependence of the viscosity : F(g)

viscosity law : Carreau-Yasuda :

F(g) = (fac-facinf) * (1 + (l*g)**a)**((n-1)/a) + facinf

fac = 1.50000E-01 , facinf = 0.00000E+00

l = 2.81700E-03 , n = 5.00000E-01

a = 2.00000E+00

specific mass : ro = 1.25000E-03

gravity field neglected

inertia terms neglected in momentum equation

****

* SOLVERS *

****

===> Starting Evolution

at Sinit = 0.2500000E-01

==========

****

*** Starting Step 1 ***

****

Parameter density = 3.125000000000000E-005

Parameter fac = 3.750000000000000E-003

Parameter omega = 1.250000000000000

Convergence assumed : Rel. var. LT 0.1000000E-03

*** Step size information : ***

==========

S = 0.2500000E-01, step # 1

dSnew = 0.1500000E-02

tests = 0.2068856E-05

****

*** Starting Step 2 ***

****

Parameter density = 3.312500000000001E-005

Parameter fac = 3.975000000000000E-003

Parameter omega = 1.325000000000000

*** Step size information : ***

==========

S = 0.2650000E-01, step # 2

dSnew = 0.2250000E-02

tests = 0.5103151E-04

****

*** Starting Step 3 ***

****

Parameter density = 3.593750000000001E-005

Parameter fac = 4.312500000000000E-003

Parameter omega = 1.437500000000000

*** Step size information : ***

==========

S = 0.2875000E-01, step # 3

dSnew = 0.3375000E-02

tests = 0.5156813E-05

****

*** Starting Step 4 ***

****

Parameter density = 4.015625000000001E-005

Parameter fac = 4.818750000000001E-003

Parameter omega = 1.606250000000000

*** Step size information : ***

==========

S = 0.3212500E-01, step # 4

dSnew = 0.5062500E-02

tests = 0.1752515E-04

****

*** Starting Step 5 ***

****

Parameter density = 4.648437500000002E-005

Parameter fac = 5.578125000000001E-003

Parameter omega = 1.859375000000001

*** Step size information : ***

==========

S = 0.3718750E-01, step # 5

dSnew = 0.7593750E-02

tests = 0.6340076E-04

****

*** Starting Step 6 ***

****

Parameter density = 5.597656250000002E-005

Parameter fac = 6.717187500000002E-003

Parameter omega = 2.239062500000001

*** Step size information : ***

==========

S = 0.4478125E-01, step # 6

dSnew = 0.1139063E-01

tests = 0.1774522E-07

****

*** Starting Step 7 ***

****

Parameter density = 7.021484375000002E-005

Parameter fac = 8.425781250000002E-003

Parameter omega = 2.808593750000001

*** Step size information : ***

==========

S = 0.5617188E-01, step # 7

dSnew = 0.1708594E-01

tests = 0.2746303E-06

****

*** Starting Step 8 ***

****

Parameter density = 9.157226562500002E-005

Parameter fac = 1.098867187500000E-002

Parameter omega = 3.662890625000001

*** Step size information : ***

==========

S = 0.7325781E-01, step # 8

dSnew = 0.2562891E-01

tests = 0.2756237E-05

****

*** Starting Step 9 ***

****

Parameter density = 1.236083984375000E-004

Parameter fac = 1.483300781250000E-002

Parameter omega = 4.944335937500001

*** Step size information : ***

==========

S = 0.9888672E-01, step # 9

dSnew = 0.3844336E-01

tests = 0.6479189E-05

```
************************************
***   Starting Step    10    ***
************************************
 Parameter density      =   1.716625976562500E-004
 Parameter fac          =   2.059951171875000E-002
 Parameter omega        =       6.866503906250002
 *** Step size information : ***
==============================
S    = 0.1373301E+00, step #    10
dSnew = 0.5766504E-01
tests = 0.1202532E-04
************************************
***   Starting Step    11    ***
************************************
 Parameter density      =   2.437438964843751E-004
 Parameter fac          =   2.924926757812501E-002
 Parameter omega        =       9.749755859375002
*** Step size information : ***
==============================
S    = 0.1949951E+00, step #    11
dSnew = 0.8649756E-01
tests = 0.8009260E-04
************************************
***   Starting Step    12    ***
************************************
 Parameter density      =   3.518658447265625E-004
 Parameter fac          =   4.222390136718750E-002
 Parameter omega        =       14.074633789062501
*** Step size information : ***
==============================
S    = 0.2814927E+00, step #    12
dSnew = 0.1297463E+00
tests = 0.2570039E-04
```

```
************************************
***   Starting Step     13     ***
************************************
 Parameter density      =   5.140487670898438E-004
 Parameter fac          =   6.168585205078125E-002
 Parameter omega        =      20.561950683593754
 *** Step size information : ***
==============================
S     = 0.4112390E+00, step #     13
dSnew = 0.1946195E+00
tests = 0.4625238E-06


************************************
***   Starting Step     14     ***
************************************
 Parameter density      =   7.573231506347657E-004
 Parameter fac          =   9.087877807617188E-002
 Parameter omega        =      30.292926025390628
*** Step size information : ***
==============================
S     = 0.6058585E+00, step #     14
dSnew = 0.2500000E+00
tests = 0.2478917E-05
************************************
***   Starting Step     15     ***
************************************
 Parameter density      =   1.069823150634766E-003
 Parameter fac          =   1.283787780761719E-001
 Parameter omega        =      42.792926025390628
```

*** Step size information : ***

==========

S = 0.8558585E+00, step # 15

dSnew = 0.1441415E+00

tests = 0.1387784E-05

****

*** Starting Step 16 ***

****

Parameter density = 1.250000000000000E-003

Parameter fac = 1.500000000000000E-001

Parameter omega = 50.000000000000000

*** Step size information : ***

==========

S = 0.1000000E+01, step # 16

dSnew = 0.2162122E+00

tests = 0.7446864E-05

===> Sfin has been reached. Stop.

==========

Time-marching scheme:

Navier-Stokes 3D

Output Fields : VELOCITIES

PRESSURE

newton-raphson iteration for viscosity law

viscosity function : visc = F(g)

shear-rate dependence of the viscosity : F(g)

viscosity law : Carreau-Yasuda :

F(g) = (fac-facinf) * (1 + (l*g)**a)**((n-1)/a) + facinf

fac = 1.50000E-01 , facinf = 0.00000E+00

l = 2.81700E-03 , n = 2.00000E+00

a = 5.00000E-01

specific mass : ro = 1.25000E-03

gravity field neglected

inertia terms taken into account in momentum equation

```
************************
*      SOLVERS      *
************************
 ===> Starting Time marching
      at t-ini =  0.0000000E+00
 ==================================
************************************
***   Starting Step     1     ***
************************************
 Parameter density       =   1.250000000000000E-005
 Parameter fac           =   1.500000000000000E-003
 Parameter omega         =   5.000000000000000E-001
 Convergence assumed : Rel. var. LT  0.1000000E-03

*** time step information : ***
================================
t     = 0.1000000E-01, step #     1
dtnew = 0.1000000E-01
tests = 0.2000000E+02
************************************
***   Starting Step     2     ***
************************************
 Parameter density       =   2.500000000000000E-005
 Parameter fac           =   3.000000000000000E-003
 Parameter omega         =       1.000000000000000

*** time step information : ***
================================
```

```
t    = 0.2000000E-01, step #     2
dtnew = 0.1000000E-01
tests = 0.1000000E+01
************************************
***   Starting Step     3     ***
************************************
 Parameter density      =   3.750000000000000E-005
 Parameter fac          =   4.500000000000000E-003
 Parameter omega        =       1.500000000000000
*** time step information : ***
==================================
t    = 0.3000000E-01, step #     3
dtnew = 0.1000000E-01
tests = 0.1203371E-02
************************************
***   Starting Step     4     ***
************************************
 Parameter density      =   5.000000000000000E-005
 Parameter fac          =   6.000000000000000E-003
 Parameter omega        =       2.000000000000000
 *** time step information : ***
==================================
t    = 0.4000000E-01, step #     4
dtnew = 0.1075772E-01
tests = 0.1728181E-02
************************************
***   Starting Step     5     ***
************************************
 Parameter density      =   6.344715495228832E-005
 Parameter fac          =   7.613658594274599E-003
 Parameter omega        =       2.537886198091533
*** time step information : ***
==================================
t    = 0.5075772E-01, step #     5
```

dtnew = 0.1613659E-01

tests = 0.7384034E-03

****

*** Starting Step 6 ***

****

Parameter density = 8.361788738072081E-005

Parameter fac = 1.003414648568650E-002

Parameter omega = 3.344715495228832

*** time step information : ***

==========

t = 0.6689431E-01, step # 6

dtnew = 0.2420488E-01

tests = 0.6526193E-03

****

*** Starting Step 7 ***

****

Parameter density = 1.138739860233695E-004

Parameter fac = 1.366487832280435E-002

Parameter omega = 4.554959440934782

*** time step information : ***

==========

t = 0.9109919E-01, step # 7

dtnew = 0.3630732E-01

tests = 0.7213310E-03

****

*** Starting Step 8 ***

****

Parameter density = 1.592581339873427E-004

Parameter fac = 1.911097607848112E-002

Parameter omega = 6.370325359493706

*** time step information : ***

==========

t = 0.1274065E+00, step # 8

dtnew = 0.5446098E-01

tests = 0.8495437E-03

****

*** Starting Step 9 ***

****

Parameter density = 2.273343559333023E-004

Parameter fac = 2.728012271199627E-002

Parameter omega = 9.093374237332091

*** time step information : ***

==========

t = 0.1818675E+00, step # 9

dtnew = 0.7767654E-01

tests = 0.9831531E-03

****

*** Starting Step 10 ***

****

Parameter density = 3.244300277307940E-004

Parameter fac = 3.893160332769528E-002

Parameter omega = 12.977201109231759

*** time step information : ***

==========

t = 0.2595440E+00, step # 10

dtnew = 0.9213328E-01

tests = 0.1421598E-02

****

*** Starting Step 11 ***

****

Parameter density = 4.395966233922289E-004

Parameter fac = 5.275159480706747E-002

Parameter omega = 17.583864935689157

*** time step information : ***

==========

t = 0.3516773E+00, step # 11

dtnew = 0.9111836E-01

tests = 0.2044802E-02

****

*** Starting Step 12 ***

****

Parameter density = 5.534945743742762E-004

Parameter fac = 6.641934892491314E-002

Parameter omega = 22.139782974971045

*** time step information : ***

==========

t = 0.4427957E+00, step # 12

dtnew = 0.8117853E-01

tests = 0.2519761E-02

****

*** Starting Step 13 ***

****

Parameter density = 6.549677424830928E-004

Parameter fac = 7.859612909797113E-002

Parameter omega = 26.198709699323715

*** time step information : ***

==========

t = 0.5239742E+00, step # 13

dtnew = 0.8881727E-01

tests = 0.1670773E-02

****

*** Starting Step 14 ***

****

Parameter density = 7.659893341890312E-004

```
 Parameter fac          =   9.191872010268373E-002
 Parameter omega        =      30.639573367561248
*** time step information : ***
==========================
t    = 0.6127915E+00, step #    14
dtnew = 0.8060349E-01
tests = 0.2428383E-02
**********************************
***   Starting Step    15    ***
**********************************
 Parameter density      =   8.667437003754752E-004
 Parameter fac          =   1.040092440450570E-001
 Parameter omega        =      34.669748015019010

*** time step information : ***
==========================
t    = 0.6933950E+00, step #    15
dtnew = 0.9053189E-01
tests = 0.1585384E-02

**********************************
***   Starting Step    16    ***
**********************************
 Parameter density      =   9.799085581897013E-004
 Parameter fac          =   1.175890269827641E-001
 Parameter omega        =      39.196342327588049

*** time step information : ***
==========================
t    = 0.7839268E+00, step #    16
dtnew = 0.1255047E+00
tests = 0.1040671E-02

**********************************
```

```
***   Starting Step     17     ***
************************************
 Parameter density       =   1.136789372695258E-003
 Parameter fac           =   1.364147247234309E-001
 Parameter omega         =      45.471574907810314

*** time step information : ***
==============================
t     = 0.9094315E+00, step #     17
dtnew = 0.9056850E-01
tests = 0.3866568E-02
************************************
***   Starting Step     18     ***
************************************
 Parameter density       =   1.250000000000000E-003
 Parameter fac           =   1.500000000000000E-001
 Parameter omega         =      50.000000000000000

*** time step information : ***
==============================
t     = 0.1000000E+01, step #     18
dtnew = 0.9081095E-01
tests = 0.1989335E-02
===> tfin has been reached. Stop.
==================================
```

During the transient scheme no step has failed.

F-4 Stream Function in 2D.

```
Time-marching scheme:
************************
*                      *
*     PROBLEMS         *
*                      *
************************
Stream function
          Output Fields : STREAM FUNCTION
Navier-Stokes 2D

    newton-raphson iteration for viscosity law

    viscosity function : visc = F(g)

    shear-rate dependence of the viscosity  : F(g)
     viscosity law : Carreau-Yasuda :
     F(g) = (fac-facinf) * (1 + (l*g)**a)**((n-1)/a) + facinf
       fac   = 1.50000E-01 ,  facinf = 0.00000E+00
       l     = 2.81700E-03 ,  n      = 2.00000E+00
       a     = 5.00000E-01

    specific mass : ro    = 1.25000E-03
    gravity field neglected
    inertia terms taken into account in momentum equation

************************
*                      *
*  Boundary Conditions *
*                      *
************************


 Vn Vs imposed   support      :      (S1*B1).
          For comp. 1   :  2.0000000E+01

          For comp. 2   :     Zero Value
 Vn Vs imposed
          Support      :      (S1*B2).
```

```
            For comp. 1  :  2.0000000E+01

            For comp. 2  :    Zero Value


V = Cart.Veloc. support     :      (S1*B3).
            For comp. 1  :     Identity
            For comp. 2  :     Identity


V = Cart.Veloc.
            Support      :     (S1*B4).
            For comp. 1  :     Identity
            For comp. 2  :     Identity

===> Starting Time marching
     at t-ini =  0.0000000E+00
 ====================================
**************************************
***   Starting Step      1     ***
**************************************
 Parameter density       =   1.250000000000000E-005
 Parameter fac           =   1.500000000000000E-003
 Parameter angular velocit =   5.000000000000000E-001
 Parameter angular velocit =  -5.000000000000000E-001

************************
*     SOLVER       *
*                  *
************************
 Preprocessors
            Type of Evolu.:      Implicit


Nb. of active elements :    280
Nb. of sub-parts ..... :      1

Iteration   1

Frontal method information :
 Minimal pivot      : 0.1000000E+01
 Maximal pivot      : 0.2000000E+01
 Relative var. of field  CART_VELOCITIES  0.1000000E+01
************************
*     SOLVER       *
*                  *
************************
Iteration   1
```

```
Frontal method information :
 Minimal pivot      : 0.2424114E-04
 Maximal pivot      : 0.6010139E+00
 Relative var. of field  VELOCITIES     0.1000000E+01
 Relative var. of field (PRESSURE       0.1000000E+01)

Iteration  2
Frontal method information :
 Minimal pivot      : 0.6090621E-06
 Maximal pivot      : 0.1741637E+02
 Relative var. of field  VELOCITIES     0.1160617E+00
 Relative var. of field (PRESSURE       0.9550778E+00)


Iteration  3

Frontal method information :
 Minimal pivot      : 0.5981237E-06
 Maximal pivot      : 0.1669862E+02
 Relative var. of field  VELOCITIES     0.2011986E-01
 Relative var. of field (PRESSURE       0.1942954E-01)


Iteration  4

Frontal method information :
 Minimal pivot      : 0.5977216E-06
 Maximal pivot      : 0.1679704E+02
 Relative var. of field  VELOCITIES     0.1470760E-02
 Relative var. of field (PRESSURE       0.5321253E-03)


Iteration  5

Frontal method information :
 Minimal pivot      : 0.5977140E-06
 Maximal pivot      : 0.1680106E+02
 Relative var. of field  VELOCITIES     0.1001814E-04
 Relative var. of field (PRESSURE       0.2869849E-05)
Convergence assumed : Rel. var. LT  0.1000000E-03
Relative var. of field  STREAM FUNCTION  0.1000000E+01
Flow rate =  0.0000000E+00  on (S1*B1).
Flow rate =  0.0000000E+00  on (S1*B2).
Flow rate =  0.6661338E-15  on (S1*B3).
Flow rate =  0.1387779E-15  on (S1*B4).


*** time step information : ***
==============================
t    = 0.1000000E-01, step #     1
```

```
dtnew = 0.1000000E-01, okincr :  T
tests = 0.1690257E+04

************************************
***  Starting Step     2     ***
************************************
 Parameter density       =  2.500000000000000E-005
 Parameter fac           =  3.000000000000000E-003
 Parameter angular velocit =       1.000000000000000
 Parameter angular velocit =      -1.000000000000000
Relative var. of field  CART_VELOCITIES  0.4408449E-07
Convergence assumed : Rel. var. LT  0.1000000E-03

Iteration   1

Frontal method information :
 Minimal pivot      : 0.8859446E-07
 Maximal pivot      : 0.1111251E+03
 Relative var. of field  VELOCITIES      0.1118214E-01
 Relative var. of field (PRESSURE        0.8441317E+00)


Iteration   2

Frontal method information :
 Minimal pivot      : 0.8858733E-07
 Maximal pivot      : 0.1107773E+03
 Relative var. of field  VELOCITIES      0.2226753E-02
 Relative var. of field (PRESSURE        0.1263684E-03)


Iteration   3

Minimal pivot      : 0.8858727E-07
 Maximal pivot      : 0.1107810E+03
 Relative var. of field  VELOCITIES      0.6493963E-04
 Relative var. of field (PRESSURE        0.5299482E-07)
Convergence assumed : Rel. var. LT  0.1000000E-03
 Relative var. of field  STREAM FUNCTION  0.4466711E-02
 Flow rates
Flow rate =  0.0000000E+00  on (S1*B1).
Flow rate =  0.0000000E+00  on (S1*B2).
Flow rate =  0.1443290E-14  on (S1*B3).
Flow rate = -0.2636780E-15  on (S1*B4).

*** time step information : ***
==============================
t     = 0.2000000E-01, step #     2
dtnew = 0.1000000E-01,
tests = 0.1096037E-01
```

```
************************************
***   Starting Step     3     ***
************************************
 Parameter density       =   3.750000000000000E-005
 Parameter fac           =   4.500000000000000E-003
 Parameter angular velocit =       1.500000000000000
 Parameter angular velocit =      -1.500000000000000


Iteration   1

Frontal method information :
 Minimal pivot      : 0.2788197E-07
 Maximal pivot      : 0.3490166E+03
 Relative var. of field  VELOCITIES      0.3717438E-02
 Relative var. of field (PRESSURE        0.5890612E+00)


Iteration   2

Frontal method information :
 Minimal pivot      : 0.2788199E-07
 Maximal pivot      : 0.3489806E+03
 Relative var. of field  VELOCITIES      0.3678596E-02
 Relative var. of field (PRESSURE        0.2665379E-06)


Iteration   3

Frontal method information :
 Minimal pivot      : 0.2788199E-07
 Maximal pivot      : 0.3489806E+03
 Relative var. of field  VELOCITIES      0.1537998E-03
 Relative var. of field (PRESSURE        0.2318098E-08)


Iteration   4

Frontal method information :
 Minimal pivot      : 0.2788199E-07
 Maximal pivot      : 0.3489806E+03
 Relative var. of field  VELOCITIES      0.1627017E-05
 Relative var. of field (PRESSURE        0.5916535E-11)
Convergence assumed : Rel. var. LT  0.1000000E-03

 Relative var. of field  STREAM FUNCTION  0.1369988E-02
 Flow rates
```

```
Flow rate =  0.0000000E+00  on (S1*B1).
Flow rate =  0.0000000E+00  on (S1*B2).
Flow rate =  0.3330669E-14  on (S1*B3).
Flow rate = -0.1387779E-15  on (S1*B4).


*** time step information : ***
==============================
t    = 0.3000000E-01, step #     3
dtnew = 0.1000000E-01,
tests = 0.9257568E-03

************************************
***   Starting Step     4     ***
************************************
 Parameter density       =   5.000000000000000E-005
 Parameter fac           =   6.000000000000000E-003
 Parameter angular velocit =       2.000000000000000
 Parameter angular velocit =      -2.000000000000000


Iteration   1

Frontal method information :
 Minimal pivot      : 0.1213237E-07
 Maximal pivot      : 0.7984587E+03
 Relative var. of field  VELOCITIES      0.2444493E-02
 Relative var. of field (PRESSURE       0.4113319E+00)


Iteration   2

Frontal method information :
 Minimal pivot      : 0.1213237E-07
 Maximal pivot      : 0.7984414E+03
 Relative var. of field  VELOCITIES      0.2231807E-02
 Relative var. of field (PRESSURE       0.4471958E-07)


Iteration   3

Frontal method information :
 Minimal pivot      : 0.1213237E-07
 Maximal pivot      : 0.7984414E+03
 Relative var. of field  VELOCITIES      0.3033262E-03
 Relative var. of field (PRESSURE       0.1917959E-08)


Iteration   4
```

```
Frontal method information :
 Minimal pivot      : 0.1213237E-07
 Maximal pivot      : 0.7984414E+03
 Relative var. of field  VELOCITIES      0.7383797E-05
 Relative var. of field (PRESSURE        0.1747224E-10)
Convergence assumed : Rel. var. LT  0.1000000E-03

 Relative var. of field  STREAM FUNCTION  0.6931697E-03
 Flow rates

Flow rate =  0.0000000E+00  on (S1*B1).
Flow rate =  0.0000000E+00  on (S1*B2).
Flow rate =  0.5662137E-14  on (S1*B3).
Flow rate = -0.4579670E-15  on (S1*B4).

*** time step information : ***
==============================
t    = 0.4000000E-01, step #     4
dtnew = 0.1500000E-01
tests = 0.2487597E-03

************************************
***   Starting Step     5     ***
************************************
 Parameter density       =  6.875000000000000E-005
 Parameter fac           =  8.250000000000000E-003
 Parameter angular velocit =       2.750000000000000
 Parameter angular velocit =      -2.750000000000000

Iteration  1

Frontal method information :
 Minimal pivot      : 0.4788515E-08
 Maximal pivot      : 0.2015424E+04
 Relative var. of field  VELOCITIES      0.4679843E-02
 Relative var. of field (PRESSURE        0.4195191E+00)


Iteration  2

Frontal method information :
 Minimal pivot      : 0.4788515E-08
 Maximal pivot      : 0.2015401E+04
 Relative var. of field  VELOCITIES      0.4025123E-02
 Relative var. of field (PRESSURE        0.4834290E-07)


Iteration  3

Frontal method information :
```

```
 Minimal pivot      : 0.4788515E-08
 Maximal pivot      : 0.2015401E+04
 Relative var. of field  VELOCITIES     0.6465617E-03
 Relative var. of field (PRESSURE       0.3682564E-08)


Iteration   4

Frontal method information :
 Minimal pivot      : 0.4788515E-08
 Maximal pivot      : 0.2015401E+04
 Relative var. of field  VELOCITIES     0.2269100E-04
 Relative var. of field (PRESSURE       0.6709991E-10)
Convergence assumed : Rel. var. LT  0.1000000E-03

 Relative var. of field  STREAM FUNCTION  0.6527215E-03
Flow rates

Flow rate =  0.0000000E+00  on (S1*B1).
Flow rate =  0.0000000E+00  on (S1*B2).
Flow rate = -0.2609024E-14  on (S1*B3).
Flow rate =  0.6938894E-17  on (S1*B4).

*** time step information : ***
==============================
t     = 0.5500000E-01, step #     5
dtnew = 0.2250000E-01,
tests = 0.1525094E-03

************************************
***   Starting Step     6     ***
************************************
 Parameter density       =   9.687500000000000E-005
 Parameter fac           =   1.162500000000000E-002
 Parameter angular velocit =       3.875000000000000
 Parameter angular velocit =      -3.875000000000000

Iteration   1

Frontal method information :
 Minimal pivot      : 0.1746358E-08
 Maximal pivot      : 0.5509925E+04
 Relative var. of field  VELOCITIES     0.6399046E-02
 Relative var. of field (PRESSURE       0.4618182E+00)


Iteration   2

Frontal method information :
 Minimal pivot      : 0.1746358E-08
```

```
 Maximal pivot      : 0.5509884E+04
 Relative var. of field  VELOCITIES      0.4995719E-02
 Relative var. of field (PRESSURE        0.4353520E-07)


Iteration   3

Frontal method information :
 Minimal pivot      : 0.1746358E-08
 Maximal pivot      : 0.5509884E+04
 Relative var. of field  VELOCITIES      0.1781814E-02
 Relative var. of field (PRESSURE        0.8555046E-08)


Iteration   4

Frontal method information :
 Minimal pivot      : 0.1746358E-08
 Maximal pivot      : 0.5509884E+04
 Relative var. of field  VELOCITIES      0.2371090E-03
 Relative var. of field (PRESSURE        0.2687110E-09)


Iteration   5

Frontal method information :
 Minimal pivot      : 0.1746358E-08
 Maximal pivot      : 0.5509884E+04
 Relative var. of field  VELOCITIES      0.4357300E-05
 Relative var. of field (PRESSURE        0.5865111E-11)
Convergence assumed : Rel. var. LT  0.1000000E-03

 Relative var. of field  STREAM FUNCTION  0.6947876E-03
 Flow rates

Flow rate =  0.0000000E+00  on (S1*B1).
Flow rate =  0.0000000E+00  on (S1*B2).
Flow rate = -0.1101896E-13  on (S1*B3).
Flow rate = -0.7285839E-16  on (S1*B4).


*** time step information : ***
==============================
t     = 0.7750000E-01, step #     6
dtnew = 0.3375000E-01
tests = 0.1131316E-03


**********************************
***    Starting Step      7     ***
```

```
************************************
 Parameter density       =  1.390625000000000E-004
 Parameter fac           =  1.668750000000000E-002
 Parameter angular velocit =      5.562500000000000
 Parameter angular velocit =     -5.562500000000000

 Iteration  1

 Frontal method information :
  Minimal pivot      : 0.5993611E-09
  Maximal pivot      : 0.1601841E+05
  Relative var. of field  VELOCITIES     0.1275812E-01
  Relative var. of field (PRESSURE       0.4932213E+00)


 Iteration  2

 Frontal method information :
  Minimal pivot      : 0.5993611E-09
  Maximal pivot      : 0.1601834E+05
  Relative var. of field  VELOCITIES     0.9344687E-02
  Relative var. of field (PRESSURE       0.6241579E-07)


 Iteration  3

 Frontal method information :
  Minimal pivot      : 0.5993611E-09
  Maximal pivot      : 0.1601834E+05
  Relative var. of field  VELOCITIES     0.2946521E-02
  Relative var. of field (PRESSURE       0.8769695E-08)


 Iteration  4

 Frontal method information :
  Minimal pivot      : 0.5993611E-09
  Maximal pivot      : 0.1601834E+05
  Relative var. of field  VELOCITIES     0.9516809E-03
  Relative var. of field (PRESSURE       0.3283510E-09)


 Iteration  5

 Frontal method information :
  Minimal pivot      : 0.5993611E-09
  Maximal pivot      : 0.1601834E+05
  Relative var. of field  VELOCITIES     0.2546775E-03
  Relative var. of field (PRESSURE       0.4057985E-10)
```

```
Iteration   6

Frontal method information :
 Minimal pivot       : 0.5993611E-09
 Maximal pivot       : 0.1601834E+05
 Relative var. of field  VELOCITIES      0.5104020E-05
 Relative var. of field (PRESSURE        0.2627423E-11)
Convergence assumed : Rel. var. LT  0.1000000E-03

 Relative var. of field  STREAM FUNCTION  0.6584911E-03
Flow rates

Flow rate =  0.0000000E+00  on (S1*B1).
Flow rate =  0.0000000E+00  on (S1*B2).
Flow rate =  0.1366962E-13  on (S1*B3).
Flow rate = -0.9697104E-15  on (S1*B4).

*** time step information : ***
==============================
t     = 0.1112500E+00, step #     7
dtnew  = 0.5062500E-01,
tests  = 0.7620899E-04

************************************
***    Starting Step      8      ***
************************************
 Parameter density       =   2.023437500000000E-004
 Parameter fac           =   2.428125000000000E-002
 Parameter angular velocit =        8.093750000000000
 Parameter angular velocit =       -8.093750000000000

Iteration   1

Frontal method information :
 Minimal pivot       : 0.1966918E-09
 Maximal pivot       : 0.4873220E+05
 Relative var. of field  VELOCITIES      0.1162560E-01
 Relative var. of field (PRESSURE        0.5157113E+00)


Iteration   2

Frontal method information :
 Minimal pivot       : 0.1966918E-09
 Maximal pivot       : 0.4873209E+05
 Relative var. of field  VELOCITIES      0.7228178E-02
 Relative var. of field (PRESSURE        0.7451792E-07)
```

```
Iteration  3

Frontal method information :
 Minimal pivot      : 0.1966918E-09
 Maximal pivot      : 0.4873209E+05
 Relative var. of field  VELOCITIES     0.3258213E-02
 Relative var. of field (PRESSURE       0.1831880E-07)


Iteration  4

Frontal method information :
 Minimal pivot      : 0.1966918E-09
 Maximal pivot      : 0.4873209E+05
 Relative var. of field  VELOCITIES     0.1310935E-02
 Relative var. of field (PRESSURE       0.7755492E-09)


Iteration  5

Frontal method information :
 Minimal pivot      : 0.1966918E-09
 Maximal pivot      : 0.4873209E+05
 Relative var. of field  VELOCITIES     0.3575480E-03
 Relative var. of field (PRESSURE       0.1428851E-09)


Iteration  6

Frontal method information :
 Minimal pivot      : 0.1966918E-09
 Maximal pivot      : 0.4873209E+05
 Relative var. of field  VELOCITIES     0.4161362E-04
 Relative var. of field (PRESSURE       0.7429685E-11)
Convergence assumed : Rel. var. LT  0.1000000E-03

 Relative var. of field  STREAM FUNCTION  0.5623529E-03
Flow rates
Flow rate =  0.0000000E+00  on (S1*B1).
Flow rate =  0.0000000E+00  on (S1*B2).
Flow rate =  0.1428718E-13  on (S1*B3).
Flow rate =  0.5715914E-15  on (S1*B4).


*** time step information : ***
==============================
t     = 0.1618750E+00, step #     8
dtnew = 0.7593750E-01,
tests = 0.5776746E-04
```

```
************************************
***  Starting Step     9    ***
************************************
 Parameter density       =  2.972656250000000E-004
 Parameter fac           =  3.567187500000000E-002
 Parameter angular velocit =      11.890625000000000
 Parameter angular velocit =     -11.890625000000000


Iteration  1

Frontal method information :
 Minimal pivot      : 0.6251185E-10
 Maximal pivot      : 0.1531584E+06
 Relative var. of field  VELOCITIES     0.2835060E-01
 Relative var. of field (PRESSURE       0.5314328E+00)


Iteration  2

Frontal method information :
 Minimal pivot      : 0.6251185E-10
 Maximal pivot      : 0.1531582E+06
 Relative var. of field  VELOCITIES     0.2070014E-01
 Relative var. of field (PRESSURE       0.2282484E-06)


Iteration  3

Frontal method information :
 Minimal pivot      : 0.6251184E-10
 Maximal pivot      : 0.1531582E+06
 Relative var. of field  VELOCITIES     0.4985386E-02
 Relative var. of field (PRESSURE       0.2566510E-07)


Iteration  4

Frontal method information :
 Minimal pivot      : 0.6251184E-10
 Maximal pivot      : 0.1531582E+06
 Relative var. of field  VELOCITIES     0.2216018E-02
 Relative var. of field (PRESSURE       0.7611381E-09)


Iteration  5

Frontal method information :
 Minimal pivot      : 0.6251183E-10
 Maximal pivot      : 0.1531582E+06
```

```
 Relative var. of field  VELOCITIES      0.1013702E-02
 Relative var. of field (PRESSURE        0.1908650E-09)


Iteration  6

Frontal method information :
 Minimal pivot       : 0.6251184E-10
 Maximal pivot       : 0.1531582E+06
 Relative var. of field  VELOCITIES      0.4013266E-03
 Relative var. of field (PRESSURE        0.3315931E-10)


Iteration  7

Frontal method information :
 Minimal pivot       : 0.6251184E-10
 Maximal pivot       : 0.1531582E+06
 Relative var. of field  VELOCITIES      0.3062978E-04
 Relative var. of field (PRESSURE        0.4966457E-11)
Convergence assumed : Rel. var. LT  0.1000000E-03

 Relative var. of field  STREAM FUNCTION  0.4424137E-03
Flow rates

Flow rate =  0.0000000E+00  on (S1*B1).
Flow rate =  0.0000000E+00  on (S1*B2).
Flow rate =  0.8108098E-14  on (S1*B3).
Flow rate = -0.2445526E-14  on (S1*B4).

*** time step information : ***
==============================
t     = 0.2378125E+00, step #     9
dtnew  = 0.1139063E+00
tests  = 0.4446848E-04

************************************
***    Starting Step     10     ***
************************************
 Parameter density       =   4.396484375000000E-004
 Parameter fac           =   5.275781249999999E-002
 Parameter angular velocit =       17.585937500000000
 Parameter angular velocit =      -17.585937500000000

Iteration  1

Frontal method information :
 Minimal pivot       : 0.1942648E-10
 Maximal pivot       : 0.4924500E+06
 Relative var. of field  VELOCITIES      0.3438585E-01
```

Relative var. of field (PRESSURE 0.5422479E+00)

Iteration 2

Frontal method information :
Minimal pivot : 0.1942648E-10
Maximal pivot : 0.4924497E+06
Relative var. of field VELOCITIES 0.1982011E-01
Relative var. of field (PRESSURE 0.7785901E-07)

Iteration 3

Frontal method information :
Minimal pivot : 0.1942649E-10
Maximal pivot : 0.4924497E+06
Relative var. of field VELOCITIES 0.7731716E-02
Relative var. of field (PRESSURE 0.4853114E-07)

Iteration 4

Frontal method information :
Minimal pivot : 0.1942648E-10
Maximal pivot : 0.4924497E+06
Relative var. of field VELOCITIES 0.3833565E-02
Relative var. of field (PRESSURE 0.1973834E-08)

Iteration 5

Frontal method information :
Minimal pivot : 0.1942649E-10
Maximal pivot : 0.4924497E+06
Relative var. of field VELOCITIES 0.2068352E-02
Relative var. of field (PRESSURE 0.3179013E-09)

Iteration 6

Frontal method information :
Minimal pivot : 0.1942647E-10
Maximal pivot : 0.4924497E+06
Relative var. of field VELOCITIES 0.8457012E-03
Relative var. of field (PRESSURE 0.1281706E-09)

Iteration 7

```
Frontal method information :
 Minimal pivot      : 0.1942648E-10
 Maximal pivot      : 0.4924497E+06
 Relative var. of field  VELOCITIES     0.1777341E-03
 Relative var. of field (PRESSURE       0.2609365E-10)


Iteration  8

Frontal method information :
 Minimal pivot      : 0.1942648E-10
 Maximal pivot      : 0.4924497E+06
 Relative var. of field  VELOCITIES     0.7589740E-05
 Relative var. of field (PRESSURE       0.5327402E-12)
Convergence assumed : Rel. var. LT  0.1000000E-03

 Relative var. of field  STREAM FUNCTION  0.3189022E-03

Flow rates

Flow rate =  0.0000000E+00  on (S1*B1).
Flow rate =  0.0000000E+00  on (S1*B2).
Flow rate =  0.1305032E-13  on (S1*B3).
Flow rate = -0.2974400E-14  on (S1*B4).


*** time step information : ***
==============================
t    = 0.3517187E+00, step #    10
dtnew = 0.1708594E+00,
tests = 0.3002147E-04


************************************
***   Starting Step    11    ***
************************************
 Parameter density      =   6.532226562500000E-004
 Parameter fac          =   7.838671875000000E-002
 Parameter angular velocit =      26.128906250000000
 Parameter angular velocit =     -26.128906250000000


Iteration  1

Frontal method information :
 Minimal pivot      : 0.5944436E-11
 Maximal pivot      : 0.1608451E+07
 Relative var. of field  VELOCITIES     0.5237059E-01
 Relative var. of field (PRESSURE       0.5496092E+00)
```

Iteration 2

Frontal method information :
Minimal pivot : 0.5944442E-11
Maximal pivot : 0.1608451E+07
Relative var. of field VELOCITIES 0.3273890E-01
Relative var. of field (PRESSURE 0.5980440E-07)

Iteration 3

Frontal method information :
Minimal pivot : 0.5944436E-11
Maximal pivot : 0.1608451E+07
Relative var. of field VELOCITIES 0.1114501E-01
Relative var. of field (PRESSURE 0.3486544E-07)

Iteration 4

Frontal method information :
Minimal pivot : 0.5944427E-11
Maximal pivot : 0.1608451E+07
Relative var. of field VELOCITIES 0.5345315E-02
Relative var. of field (PRESSURE 0.1304018E-08)

Iteration 5

Frontal method information :
Minimal pivot : 0.5944443E-11
Maximal pivot : 0.1608451E+07
Relative var. of field VELOCITIES 0.2384195E-02
Relative var. of field (PRESSURE 0.5375653E-09)

Iteration 6

Frontal method information :
Minimal pivot : 0.5944436E-11
Maximal pivot : 0.1608451E+07
Relative var. of field VELOCITIES 0.1061249E-02
Relative var. of field (PRESSURE 0.1508732E-09)

Iteration 7

Frontal method information :
Minimal pivot : 0.5944428E-11

```
 Maximal pivot      : 0.1608451E+07
 Relative var. of field  VELOCITIES      0.5367262E-03
 Relative var. of field (PRESSURE        0.3392283E-10)


Iteration   8

Frontal method information :
 Minimal pivot      : 0.5944437E-11
 Maximal pivot      : 0.1608451E+07
 Relative var. of field  VELOCITIES      0.7202090E-04
 Relative var. of field (PRESSURE        0.1386774E-10)
Convergence assumed : Rel. var. LT  0.1000000E-03

 Relative var. of field  STREAM FUNCTION  0.2128317E-03
Flow rates

Flow rate =  0.0000000E+00  on (S1*B1).
Flow rate =  0.0000000E+00  on (S1*B2).
Flow rate =  0.4177995E-13  on (S1*B3).
Flow rate = -0.4655889E-14  on (S1*B4).



*** time step information : ***
==============================
t    = 0.5225781E+00, step #    11
dtnew  = 0.2500000E+00,
tests  = 0.1858798E-04



************************************
***   Starting Step    12    ***
************************************
 Parameter density       =   9.657226562500000E-004
 Parameter fac           =   1.158867187500000E-001
 Parameter tnat          =   2.176352578125000E-003
 Parameter angular velocit =      38.628906250000000
 Parameter angular velocit =     -38.628906250000000


Iteration   1

Frontal method information :
 Minimal pivot      : 0.1844139E-11
 Maximal pivot      : 0.5182820E+07
 Relative var. of field  VELOCITIES      0.6805859E-01
 Relative var. of field (PRESSURE        0.5460647E+00)
```

Iteration 2

Frontal method information :
Minimal pivot : 0.1844144E-11
Maximal pivot : 0.5182820E+07
Relative var. of field VELOCITIES 0.5262405E-01
Relative var. of field (PRESSURE 0.3702481E-06)

Iteration 3

Frontal method information :
Minimal pivot : 0.1844138E-11
Maximal pivot : 0.5182820E+07
Relative var. of field VELOCITIES 0.1402150E-01
Relative var. of field (PRESSURE 0.8528948E-07)

Iteration 4

Frontal method information :
Minimal pivot : 0.1844142E-11
Maximal pivot : 0.5182820E+07
Relative var. of field VELOCITIES 0.7012911E-02
Relative var. of field (PRESSURE 0.3383021E-08)

Iteration 5

Frontal method information :
Minimal pivot : 0.1844138E-11
Maximal pivot : 0.5182820E+07
Relative var. of field VELOCITIES 0.3655580E-02
Relative var. of field (PRESSURE 0.1213894E-08)

Iteration 6

Frontal method information :
Minimal pivot : 0.1844139E-11
Maximal pivot : 0.5182820E+07
Relative var. of field VELOCITIES 0.2001974E-02
Relative var. of field (PRESSURE 0.5571911E-09)

Iteration 7

Frontal method information :
Minimal pivot : 0.1844136E-11

```
 Maximal pivot      : 0.5182820E+07
 Relative var. of field  VELOCITIES      0.8415375E-03
 Relative var. of field (PRESSURE        0.1796430E-09)


Iteration  8

Frontal method information :
 Minimal pivot      : 0.1844133E-11
 Maximal pivot      : 0.5182820E+07
 Relative var. of field  VELOCITIES      0.4286891E-03
 Relative var. of field (PRESSURE        0.2185430E-10)


Iteration  9

Frontal method information :
 Minimal pivot      : 0.1844150E-11
 Maximal pivot      : 0.5182820E+07
 Relative var. of field  VELOCITIES      0.7261497E-04
 Relative var. of field (PRESSURE        0.6647018E-11)
Convergence assumed : Rel. var. LT  0.1000000E-03

 Relative var. of field  STREAM FUNCTION  0.1250461E-03
 Flow rates

Flow rate =  0.0000000E+00  on (S1*B1).
Flow rate =  0.0000000E+00  on (S1*B2).
Flow rate = -0.1151351E-12  on (S1*B3).
Flow rate =  0.1730868E-13  on (S1*B4).

*** time step information : ***
==============================
t    = 0.7725781E+00, step #    12
dtnew = 0.2274219E+00,
tests = 0.1059289E-04

**********************************
***   Starting Step    13    ***
**********************************
 Parameter density       =   1.250000000000000E-003
 Parameter fac           =   1.500000000000000E-001
 Parameter tnat          =   2.817000000000000E-003
 Parameter angular velocit =      50.000000000000000
 Parameter angular velocit =     -50.000000000000000


Iteration  1

Frontal method information :
```

Minimal pivot : 0.8513746E-12
Maximal pivot : 0.1122433E+08
Relative var. of field VELOCITIES 0.7220735E-01
Relative var. of field (PRESSURE 0.3867697E+00)

Iteration 2

Frontal method information :
Minimal pivot : 0.8513766E-12
Maximal pivot : 0.1122435E+08
Relative var. of field VELOCITIES 0.4503729E-01
Relative var. of field (PRESSURE 0.2763726E-05)

Iteration 3

Frontal method information :
Minimal pivot : 0.8513820E-12
Maximal pivot : 0.1122433E+08
Relative var. of field VELOCITIES 0.1450059E-01
Relative var. of field (PRESSURE 0.3220161E-07)

Iteration 4

Frontal method information :
Minimal pivot : 0.8513850E-12
Maximal pivot : 0.1122433E+08
Relative var. of field VELOCITIES 0.7217560E-02
Relative var. of field (PRESSURE 0.2797149E-08)

Iteration 5

Frontal method information :
Minimal pivot : 0.8513782E-12
Maximal pivot : 0.1122433E+08
Relative var. of field VELOCITIES 0.3495766E-02
Relative var. of field (PRESSURE 0.5997700E-09)

Iteration 6

Frontal method information :
Minimal pivot : 0.8513848E-12
Maximal pivot : 0.1122433E+08
Relative var. of field VELOCITIES 0.1600840E-02
Relative var. of field (PRESSURE 0.2988003E-09)

Iteration 7

```
Frontal method information :
 Minimal pivot      : 0.8513849E-12
 Maximal pivot      : 0.1122433E+08
 Relative var. of field  VELOCITIES      0.8212829E-03
 Relative var. of field (PRESSURE        0.6308247E-10)

Iteration  8
Frontal method information :
 Minimal pivot      : 0.8513863E-12
 Maximal pivot      : 0.1122433E+08
 Relative var. of field  VELOCITIES      0.3889610E-03
 Relative var. of field (PRESSURE        0.2967121E-10)

Iteration  9

Frontal method information :
 Minimal pivot      : 0.8513800E-12
 Maximal pivot      : 0.1122433E+08
 Relative var. of field  VELOCITIES      0.2880537E-04
 Relative var. of field (PRESSURE        0.3190656E-11)
Convergence assumed : Rel. var. LT  0.1000000E-03
 Relative var. of field  STREAM FUNCTION  0.4164969E-04
Flow rate =  0.0000000E+00  on (S1*B1).
Flow rate =  0.0000000E+00  on (S1*B2).
Flow rate = -0.9188754E-14  on (S1*B3).
Flow rate =  0.7091501E-14  on (S1*B4).
*** time step information : ***
==================================
t     = 0.1000000E+01, step #    13
dtnew  = 0.2500000E+00,
tests  = 0.3753897E-05
===> tfin has been reached. Stop.
==================================
During the transient scheme no step has failed.
```